**Defined Culture Environments Create an Improved Human Intestinal Organoid Model
System to Study Intestinal Development**

by

Meghan M. Capeling

A dissertation submitted in partial fulfillment
of the requirements for the degree of
Doctor of Philosophy
(Biomedical Engineering)
in the University of Michigan
2022

Doctoral Committee:

        Associate Professor Jason R. Spence, Chair
        Assistant Professor Idse Heemskerk
        Professor Linda Samuelson
        Professor Lonnie Shea

Meghan M. Capeling

mmcapeli@umich.edu

ORCID iD: 0000-0003-0310-123X

Acknowledgements

I would like to thank my thesis advisor, Jason Spence, for your help and support throughout the past five years. You have helped me learn and grow as a scientist while providing critical feedback that has helped shape my project, and empathy and guidance when experiments haven't worked as planned. Thank you to my committee members, Dr. Lonnie Shea, Dr. Linda Samuelson, and Dr. Idse Heemskerk, for asking hard questions and offering insight and suggestions to help drive my project forward. Most importantly, thank you to all members of the Spence lab, both past and current, for kindness, support, and collaboration throughout my time in graduate school. It has been such a joy working with you all and I cannot thank you enough for all of the help and guidance that I have received.

Table of Contents

List of Tables

List of Figures

Abstract

Organoids are small, stem cell-derived culture systems that mimic aspects of the structure and function of the organs they are modelled after. Thus, organoids provide a 3D model for studying human development and disease in a complex human-derived *in vitro* system, and offer advantages over traditionally utilized 2D *in vitro* cell culture platforms or *in vivo* animal models. Intestinal organoids have been well characterized and used for over a decade to model intestinal pathologies and advance our understanding of intestinal biology. However, intestinal organoid models have been limited by a reliance on commercial basement membrane extracellular matrix (ECM) products such as Matrigel which introduce experimental variability, limit experimental control, and are unsuitable for downstream clinical applications due to their xenogeneic origin. Additionally, current intestinal organoids are relatively immature and do not contain many of the key cell types found in the human intestine. In particular, a serosal mesothelium, the outermost layer of the intestine that provides a protective boundary for the gut, has not been observed within previous *in vitro* intestinal cell models. In this dissertation, I describe improved culture methods for pluripotent stem cell-derived human intestinal organoids (HIOs) that eliminate reliance on Matrigel and more faithfully recapitulate the organization of the human small intestine. HIOs contain both epithelial and mesenchymal compartments, which enables the formation of a supportive niche within the organoid. Thus, HIOs can be cultured in bioinert environments, including unmodified alginate hydrogels and even suspension culture. Alginate and suspension

culture provide simple, cost-effective culture systems for HIOs that offer increased experimental control and decreased variability compared to Matrigel. My studies demonstrate that alginate and suspension culture are effective replacements for Matrigel to support the HIO epithelium, as HIOs cultured in alginate and suspension give rise to expected intestinal epithelial cell types. Additionally, HIOs cultured in bioinert conditions (alginate or suspension) form an organized outer mesenchymal layer that closely resembles the human intestine. Strikingly, HIOs cultured in alginate and suspension form an outer serosal mesothelium that has not been previously observed in Matrigel HIOs. This serosa formation is enhanced in suspension culture compared to alginate. I characterized HIO-serosa to demonstrate that it is molecularly and functionally similar to human intestinal serosal mesothelium. I then utilized suspension HIOs as a model to investigate serosal development and identified roles for Hedgehog (HH) and WNT signaling in human intestinal serosa formation and patterning. Overall, this work provides improved, defined culture methods for human intestinal organoids that better recapitulate the native human intestine for enhanced studies of intestinal development and disease modelling.

Chapter 1 : Introduction

Portions of this chapter have been published:

1.1 Intestine Overview

The human small intestine is a structurally and functionally complex organ that serves to absorb nutrients, secrete waste, coordinate nutrient levels, and provide a barrier for gut microbes. To fulfill these roles, the intestinal epithelium contains absorptive enterocytes which take in nutrients, as well as secretory cells including goblet, Paneth, and enteroendocrine cells [1]. The small intestinal epithelium is organized into finger-like villus projections which maximize surface area for nutrient absorption. Crypt regions in between the villi contain Paneth cells as well as intestinal stem cells that frequently regenerate intestinal epithelial cell types. This inner mucosal (epithelial) layer of the gut is surrounded by mesenchymal cells in three outer layers: submucosa, muscularis propria, and serosa [2]. Interactions between the epithelium, smooth muscle, and enteric nervous system drive mechanical functions to enable mixing and movement of luminal contents [1]. Given the diverse cell types and functionality of the gut, intestinal disorders including irritable bowel syndrome, fecal incontinence, malabsorption, and inflammatory bowel disease are common health concerns [1].

Historically, studies on intestinal development have been limited by animal models, with chick and mouse models used most commonly. Chick embryos are inexpensive and easy to manipulate, but pose challenges for tissue-specific genetic manipulation. Mouse models are typically more expensive and time-consuming to work with, but are effective as tools for modulating gene expression [3]. However, there are stark differences in intestinal development and physiology between chick and mouse. Notably, villus patterning in the chick is initiated by mechanical deformation of the epithelium caused by formation of the outer muscularis layers. Villus development in the mouse, on the other hand, is prompted by Hedgehog signaling involving crosstalk between the epithelium and Hedgehog-responsive mesenchymal clusters in the sub-epithelial space [4]. Human villus development appears to be more similar to mouse villus development as it does not depend on muscle formation [5]. These species-specific differences highlight a need for more representative human model systems. Animal models are not always an accurate representation of human physiology, making human *in vitro* systems a useful alternative to study human development and pathology.

For many years, studies focusing on the human GI tract as opposed to animal models have relied on 2D cell lines and primary tissue explants [6]. However, cell lines cultured in 2D do not recapitulate the 3D architecture of the GI tract, and immortalization techniques limit their efficacy in studying development and disease [7].Primary explant cultures, on the other hand, better recapitulate the 3D environment and tissue complexity of the GI tract, but can only be cultured over short periods *in vitro* [8-10].

In recent years, organoid model systems have eliminated many of these issues by providing long-term 3D culture systems for studying the GI tract *in vitro*. Organoids are

3D organ-like tissues that partially recapitulate structural and functional aspects of the organs after which they are modeled [11-18], and can broadly include tissue-derived epithelial-only organoids (enteroids) [19-22], tissue-derived epithelial and mesenchymal organoids [23, 24], and organoids derived from human pluripotent stem cells (hPSCs) [12, 25, 26]. In particular, human intestinal organoids (HIOs) derived from hPSCs are a useful tool to study intestinal development [27-34], evaluate gut-microbe interactions [35], and model chronic health conditions such as Crohn's disease and inflammatory bowel disease [1].

In this introduction, I review systems used to model the human intestine *in vitro*. I provide background for the work outlined in this thesis, which describes improved models of the developing human intestine that can be utilized to study development of the intestinal mesenchyme and serosal mesothelium. This work focuses on *in vitro* systems that mimic human intestinal development with implications for studies on homeostasis/disease in the adult, and thus this overview briefly discusses intestinal development as well as adult intestinal homeostasis and injury. I then highlight *in vitro* models of the human intestine as compared to animal models, including immortalized cell lines, primary tissue-based models, and finally organoid models derived from human pluripotent stem cells. I also highlight ways in which bioengineering approaches have been used to create improved organoid model systems as an introduction to the approaches described in this thesis. Throughout this overview I evaluate benefits and drawbacks of these current model systems and examine future directions in the field.

1.2 Human, Mouse, and Chick Intestinal Development

Development of the intestine begins at gastrulation, during which the three germ layers (endoderm, mesoderm, and ectoderm) are specified. The small intestine will ultimately contain cells from all three germ layers, but is primarily considered an endodermal organ as the intestinal epithelium is derived from the endoderm. Early mesendodermal cells ingress through the primitive streak during gastrulation and are exposed to the TBF-β related growth factor Nodal, specifying endodermal fate [36]. The resulting endodermal sheet covered by mesoderm undergoes morphogenetic movements that result in an epithelial gut tube surrounded by mesoderm, which occurs by E9 in the mouse [3, 4, 37]. As the gut tube is forming, it is patterned along the anterior-posterior axis into distinct regions that give rise to multiple organs. The small intestine arises from the midgut, while the large intestines arise from the hindgut [37]. Region-specific identities are patterned in response to secreted morphogens including members of the FGF, WNT, BMP, and retinoic acid signaling pathways [1]. WNT signaling in particular plays a large role in patterning the intestinal endoderm during mid- and hindgut development by inducing expression of the intestine-specific transcription factor CDX2 [3, 38]. The CDX2+ gut tube forms a simple pseudostratified epithelium by E9.5 in the mouse. This epithelium along with the surrounding mesenchyme rapidly proliferates from E9.5 to E13.5 in mice, or approximately 3-7 weeks in humans, to promote elongation and increased circumferential area of the developing gut. WNT and FGF play a large role in intestinal development during this time [3, 37].

The mesenchyme of the early intestine develops along with the epithelium. Intestinal mesenchyme is derived from splanchnic mesoderm, which arises from the lateral plate mesoderm and is adjacent to the developing intestinal epithelium. The mesenchyme gives rise to multiple cell types critical for intestinal function, including fibroblasts and smooth muscle [1]. The mesenchyme begins differentiating into smooth muscle surrounding the epithelium at around E11 in the mouse and proceeds in a proximal to distal manner. HH signaling from the epithelium contributes to smooth muscle formation, resulting in defined muscle layers of the muscularis propria and muscularis mucosae that aid in peristalsis [3, 39, 40].

In addition to development of the smooth muscle layers, the splanchnic mesoderm gives rise to the serosal mesothelium of the developing intestine [41-43]. The serosa is the outermost layer of the intestine that arises from a resident population of mesenchymal progenitors [41, 42]. The developing mouse gut is surrounded by mesothelial cells at E11.5 [44]. These mesothelial cells from the serosa then contribute to the developing mesenchyme and give rise to vascular smooth muscle. Endothelial sprouts are present in the mouse gut by E9.5 [45] and reach the surface of the gut by E13.5. These sprouts become associated with vascular smooth muscle derived from mesothelial cells undergoing EMT by E16.5 to produce mature vasculature [44]. The serosa additionally contributes to other cell types in the developing intestinal mesenchyme and thus plays a large role in intestinal development [44, 46]. Little is currently known about the mechanism by which the serosal mesothelium develops or differentiates into mesenchymal cell types, but Hedgehog signaling has been implicated in mesothelial development of the lung and intestine [47, 48], while BMP and FGF

signaling play a role in mesothelial development of the heart [49, 50]. The serosal mesothelium will be a key topic in later chapters of this dissertation.

Intestinal development additionally requires contribution from the ectoderm as migrating vagal neural crest cells contribute to the enteric nervous system (ENS). Vagal neural crest cells are present in the developing mouse gut by E9. These cells colonize the myenteric region between the developing muscularis layers and later invade the submucosa. By E14, the neural crest cells form neurons that continue to develop into a mature ENS throughout embryonic development and postnatally [3]. RET/GDNF signaling plays a large role in establishing the enteric nervous system of the gut [51]. The resulting ENS coordinates peristaltic movements of the smooth muscle layers to aid in digestion.

As these developments in the mesenchyme and ENS are taking place, the epithelium exists as a flat pseudostratified layer. At around E14 in the mouse, the epithelium begins reorganizing into columnar intestinal epithelium in a proximal-to-distal manner [37]. The epithelium initiates organization into villi, or finger-like projections that help to increase the absorptive surface area of the gut, at E14.5 in the mouse which corresponds to day 51-54 in the human [3, 4, 37, 52]. The specific mechanism of human villus formation is not completely understood, but Hedgehog and PDGF signaling between the epithelium and mesenchyme play a large role in this process [4, 52]. Villus formation is complete by around E16.5 in the mouse, or about 10 weeks in the human [37]. Following villus formation, epithelial cells undergo differentiation into mature intestinal epithelial cell types, including secretory and absorptive cells, starting at E16.5 in the mouse [3]. The epithelium additionally undergoes morphogenetic changes

resulting in the formation of epithelial invaginations - crypts of Lieberkühn or simply

crypts - at the base of the villi. Intestinal stem cells as well as secretory Paneth cells

reside at the base of the crypts. While crypts do not emerge until after birth in mice,

crypts arise with the development of Paneth cells in humans at around week 20 of

gestation [3, 53]. This highlights a key difference between mouse and human intestinal

development, prompting the need for realistic *in vitro* models of human development.

See Figure 1-1 for a schematic overview of early intestinal developmental events.

1.3 Adult Intestine Homeostasis and Disease

The dynamic series of events that take place in early intestinal development

enables the gut to fulfill many important roles in the adult. Small intestinal functions,

including nutrient absorption, waste secretion, and protection against external factors,

are carried out by diverse cell types which are functionally arranged into four layers

throughout the gut. In this section I highlight the cell types and function of each layer of

the adult intestine, including disease states and pathologies associated with these cell

types. See Figure 1-2 for a schematic overview of layers in the human small intestine.

Mucosa

The innermost layer of the intestine, the mucosa, is comprised of the intestinal

epithelium and surrounding lamina propria and muscularis mucosa [2]. The small

intestinal epithelium is organized into villi - fingerlike projections of the intestinal wall that

contain differentiated cell types, and crypts – invaginations into the intestinal wall. The

crypts contain proliferative LGR5+ crypt-base columnar cells which act as intestinal

stem cells (ISCs) that fuel epithelial self-renewal, interspersed with Paneth cells that

protect the crypt-base columnar cells [54] and secrete antimicrobial compounds including α-defensins and lysozyme [55]. ISCs at the crypt base are capable of differentiating into all intestinal epithelial cell types by first giving rise to transit amplifying cells that proliferate and differentiate into mature epithelial cell types. The transit amplifying cells migrate upward from the crypt base toward the villi. As more transit amplifying cells emerge, the existing cells differentiate and migrate to the villi as mature cell types that continue migrating to the villus tip where they are sloughed off into the lumen [54], with a total lifespan of 3-5 days [56]. Paneth cells are an exception as they migrate downward to the crypt upon differentiation [54]. Mature intestinal epithelial cell types include Paneth cells, enterocytes that absorb nutrients and water, goblet cells that secrete mucins, Tuft cells – chemosensory cells that play a role in immune response, enteroendocrine cells that secrete hormones, and M cells that play a role in antigen uptake [57, 58].

The epithelium is surrounded by mesoderm-derived lamina propria and muscularis mucosa, which are mesenchymal layers still considered to be part of the mucosa. The lamina propria is a thin layer of connective tissue and lymph nodes between the epithelium and outer muscularis mucosa [2] that contains mesenchymal cell types including fibroblasts, myofibroblasts, pericytes of the vasculature, smooth muscle cells of the lymphatic lacteal, and mesenchymal stem cells [59, 60], as well as immune cells including macrophages, lymphocytes, plasma cells, mast cells, and granulocytes [61]. These cell types play a role in supporting the intestinal stem cell niche, regulating immune response, and maintaining epithelial homeostasis in pathological states such as inflammatory bowel disease [60].

The surrounding muscularis mucosa, a thin layer of smooth muscle, enables the mucosa to fold and move [62]. Additionally, the muscularis mucosa contains sub-epithelial mesenchymal cells expressing PDGFRA/F3/DLL1. These sub-epithelial cells produce NRG1, a member of the EGF family, to support the ISC niche [63]. Dysregulation of the intestinal mucosa, including establishment of a leaky mucosal barrier triggered by an immune response, can contribute to inflammatory bowel disease [64].

Submucosa

The next layer of the gut is the submucosa, which surrounds the adjacent mucosa. The submucosa provides support for movement and contractions of the gut wall. This layer contains a multitude of mesenchymal, immune, and neuronal cells including inflammatory cells, lymphatics, ganglion cells, and autonomic nerve fibers. Vasculature is embedded within the submucosa, and arteries and veins branch in this region [2]. Decellularized small intestinal submucosa is commonly used for wound healing and tissue repair applications as it provides a bioactive 3D microenvironment [65, 66]. Fibrosis or muscularization of the submucosa may contribute to the onset of Crohn's disease [67].

Muscularis Propria

Surrounding the submucosa lies the muscularis propria, which includes the inner circular muscle layer, intermuscular space, and outer longitudinal muscle layer [2]. Both muscularis layers of the small intestine are comprised of smooth muscle cells. The

intermuscular space between the two muscularis layers is home to the myenteric plexus, a combination of autonomic nerve fibers and ganglion clusters. Contractions of the muscularis propria, coordinated by neural and hormonal events, lead to peristaltic movements that propel luminal contents through the gut during digestion [2]. Smooth muscle contractions are autonomous and largely driven by intracellular Ca^{2+} signaling as well as intrinsic pacemaker cells known as interstitial cells of Cajal (ICCs) [68]. ICCs are embedded within the smooth muscle layers and become electrically coupled to smooth muscle cells. These cells generate a rhythmic electrical current that causes slow waves in membrane potential and acts as a pacemaker for gut motility [69]. Smooth muscle cells form electrical and mechanical junctions with surrounding cells to coordinate contractions [68]. Injury or disease affecting smooth muscle can lead to chronic intestinal pseudo-obstruction which is characterized by inefficient peristalsis [70]. Additionally, absence of an enteric nervous system in the distal bowel causes Hirschsprung's disease, which is often fatal [71].

Serosa

The outermost layer of the intestine, the serosal mesothelium or serosa, is a single cell layer of mesothelial cells on a basement membrane with underlying connective tissue [2, 72]. The primary function of the serosa is to create a frictionless, lubricating surface that protects the gut from physical damage and prevents it from adhering to other organs or the body wall. Mesothelial cells of the serosa form tight junctions with each other to aid in their protective function, and are lined with microvilli that retain a film of glycosaminoglycans, particularly hyaluronan, to create lubrication

and protect against abrasion [72, 73]. The serosa additionally plays a role in cell and fluid transportation across serosal cavities, inflammation and tissue repair, antigen presentation, and fibrinolysis [73]. Pathologies associated with the serosal mesothelium include fibrosis, serosal adhesions that are common after abdominal surgery, mesothelioma, and peritoneal sclerosis [72, 74-76]. These diseases involve epithelial to mesenchymal transitions (EMT) of mesothelial cells that mimic EMT progression during mesothelial development [77].

1.4 A Need for Human Intestinal Models

Intestinal diseases including those mentioned in the previous section as well as fecal incontinence, nutritional malabsorption, and irritable bowel syndrome are common health concerns [1]. Additionally, most oral drugs are absorbed in the small intestine, which leads to drug side effects targeting the intestine such as duodenal ulcers, diarrhea, and colitis [78, 79]. In order to study these diseases, develop treatment methodologies, and examine the intestinal effects of oral drugs, model systems that accurately represent human physiology are imperative. Mouse models have significantly advanced our understanding of intestinal physiology, disease progression, and development. However, there are key differences between the GI tract in mouse and humans that make mouse models non-ideal. For example, mice have a non-glandular forestomach that is not found in humans. In the human intestine, the mucosa is organized into circular folds known as plicae circularis while the mouse mucosa is smooth, which may cause differences in microbiota composition. Further, the composition and architecture of villi differs between mice and humans [80]. These differences make it difficult to draw concrete conclusions about intestinal development

from mouse models or to accurately predict how a drug will impact the human intestine based on its impact on the mouse intestine.

Multiple *in vitro* model systems of the human intestine currently exist, and can be broadly divided into those that contain only epithelial elements, and those that contain both epithelial and mesenchymal elements. Examples of both model types will be described in the following sections. Within these human *in vitro* intestinal models, there exists a tradeoff between simplicity and realism (Figure 1-3). Complex 3D models that more accurately mimic the native tissue may provide additional scientific insights, but can be more challenging and expensive to work with. Given these challenges, reductionist human models that offer enough complexity to yield meaningful results may be ideal.

1.5 Epithelial-Only *in vitro* Models of the Human Intestine

Immortalized Cell Lines

Immortalized cell lines derived from colorectal cancer cells were some of the earliest *in vitro* models of the human intestine. The most widely utilized intestinal cell lines are Caco-2, T84, and HT-29 [81]. Caco-2 cells are derived from colonic adenocarcinoma and form confluent monolayers with small intestinal enterocyte-like characteristics in culture. These cells have advanced studies on intestinal absorption and transport processes as they form both tight junctions and microvilli, and express transporters and enzymes that are typical of enterocytes [6, 81, 82]. T84 and HT-29 cells do not form a tight barrier but instead phenotypically resemble goblet cells and produce mucus [81]. Immortalized cell lines are inexpensive, easy to culture, and, as they are cancer-derived, are highly proliferative. These cell lines are thus useful for basic studies as well as high-

throughput drug screens. However, cancer-derived cells are not always physiologically relevant to study normal, healthy tissue, and 2D cell-culture models do not recapitulate the 3D architecture of the human intestine (Figure 1-3). Additionally, immortalized intestinal cell lines are unable to differentiate into all of the epithelial cell types of the native intestine, which contains multiple epithelial cell types working in conjunction [83]. Further, immortalized cell lines can acquire mutations over time in culture that are often ignored and can skew experimental results.

More recent studies using Caco-2 cells have increased physiological relevance by culturing polarized monolayers on permeable transwell inserts. These inserts provide access to both the apical and basolateral surface for studies on permeability and transport [82, 84], and more closely mimic native ECM compared to tissue culture plastic which is significantly stiffer than the microenvironment faced by cells *in vivo*. To better mimic human tissue, Some studies have included immortalized Caco-2 cells in 3D organotypic cultures [85] or co-cultured with mesenchymal cell types [86]. Caco-2 cells have additionally been utilized in organ-on-a-chip models to mimic the 3D structure of the intestinal environment [87, 88], and to examine the effects of shear forces, contractile motion, and microbes that occur *in vivo* [89, 90]. While the 3D nature of these cultures increases complexity and resemblance to native tissue, non-immortalized primary cells may offer a more realistic model of human tissue.

Primary Intestinal Epithelial Monolayers

Researchers have developed systems to culture primary intestinal epithelial cells in monolayer systems to overcome drawbacks of working with immortalized cell lines.

Culturing primary intestinal epithelial cells may be more physiologically relevant compared to immortalized cell lines, especially since cells can be extracted from patients with intestinal diseases for disease modelling and drug screening, but primary cells have a finite lifespan in culture and thus limit experimental use (Figure 1-3). Additionally, these experiments depend on tissue donations, which is more challenging than having steady access to an immortalized cell line for experiments. [82, 83, 91]. Both primary intestinal epithelial cells and Caco-2 cells are often cultured as polarized monolayers on permeable transwell inserts, which provide access to both the apical and basolateral cell surface [82, 83]. This is an advantage compared to the 3D culture methods described below, in which the luminal surface is enclosed. Transwell inserts are often coated with a layer of ECM, which additionally makes the 2D culture system more physiologically relevant compared to culturing cells on traditional tissue culture plastic as ECM coating more closely mimics the cellular microenvironment. The cell types contained within primary epithelial cultures can be controlled by modifying the scaffold cells are cultured on to form differentiated cell types as well as proliferative progenitor cells [83].

Tissue-Derived Epithelial-Only Enteroids

As an alternative to primary epithelial monolayer culture, intestinal epithelial cells can be cultured as 3D organoids, or epithelial-only 'enteroids', that more closely mimic the 3D structure of the human intestine. While epithelial monolayers have been adapted to 3D culture conditions utilizing micromolded scaffolds that mimic the 3D architecture of crypts and villi [83, 92, 93], enteroids capture 3D structure with lower technical complexity. Intestinal enteroids are typically generated by isolating whole crypts or LGR5+ intestinal

stem cells from the crypts of donor tissue, and embedding them into droplets of a 3D ECM such as Matrigel. This laminin-rich Matrigel provides a 3D microenvironment to support enteroid growth in 3D and recapitulates the laminin-rich basement membrane of the intestinal stem cell niche (Figure 1-3) [20]. As enteroids are derived from intestinal stem cells, they can differentiate into multiple epithelial cell types, which is another advantage over immortalized cell lines that typically resemble only one cell type [94]. Enteroids are traditionally cultured in media supplemented with EGF, Wnt, Wnt agonists (R-spondin), and BMP inhibitors (Noggin) to mimic the signaling environment in the crypt, thus enabling the proliferation of intestinal epithelial cells in the absence of supportive mesenchyme [20].

Enteroids were first established using intestinal stem cells isolated from mice [20], and were later adapted to human tissue [95]. Mouse enteroids self-organize into budding crypt-like domains that contain intestinal stem cells and Paneth cells, as well as villus-like domains that contain differentiated enterocytes, goblet cells, and enteroendocrine cells. Human enteroids, on the other hand, do not form budding crypt-like domains separated from mature cell types in traditional culture conditions, and instead remain largely undifferentiated unless cultured in specialized media to promote differentiation [95]. This suggests that there may be species-specific differences between the intestinal stem cell niche in mouse and human, further prompting the need for improved human intestinal model systems.

Enteroids have advanced our understanding of intestinal biology and disease. In particular, enteroids have greatly contributed to studies on bacterial infections of the gut including *E. coli, Salmonella,* and *C. difficile* [96]. However, while the 3D nature of

enteroids increases their complexity and relevance to the native tissue, it eliminates access to the luminal surface. Additionally, 3D structures may alter or bend morphogen gradients, making it difficult to assess how signaling molecules play a role in tissue development [97]. This has prompted the more recent establishment of enteroid monolayers, in which crypts or established enteroids can be seeded as monolayers in 2D culture, thus enabling access to the apical epithelial surface. Enteroid monolayers are typically cultured in media containing the same factors used to promote enteroid growth: EGF, Noggin, and R-spondin [98]. These monolayers contain regions of both stem and differentiated cell types, and can be adapted for high-throughput screening [98, 99] or studies on host-pathogen interactions [100].

More recent studies have developed a protocol to access the apical surface of enteroids in 3D by reversing enteroid polarity [101, 102]. In this method, enteroids cultured in Matrigel can be transferred into suspension culture. The enteroids undergo a polarity reversal and adopt an apical-out morphology in the absence of ECM proteins, a process that is dependent on interactions with integrin. Polarity reversal in suspension culture has been demonstrated for epithelial-only enteroids isolated from all regions of the small intestine as well as the colon, and offers a model to study barrier integrity, nutrient uptake, and host-pathogen interactions in a 3D system without microinjection or dissociation of the cultures. However, enteroids cultured in suspension exhibit significantly decreased proliferation compared to ECM-based cultures, and are thus only useful for short-term experiments [101, 102].

Benefits and Drawbacks of Epithelial-Only Cultures

When selecting an intestinal model system for a particular study, there is a tradeoff between experimental tractability and resemblance to the native tissue. Epithelial-only cultures mimic the human intestinal epithelium to varying degrees. While 3D primary tissue-derived cultures may offer a more complete and realistic model compared to an immortalized cell line, cell lines are often easier to work with and persist for longer periods of time in culture while primary cells have a finite lifespan *in vitro*. However, even the most complex epithelial-only intestinal models fail to consider effects of the mesenchyme. The epithelium (mucosa) is only one of the four main layers of the intestine, and interactions between the epithelium and mesenchyme are critical in development, homeostasis, and disease [52, 103, 104]. Epithelial-mesenchymal crosstalk is especially critical in regulating the intestinal stem cell niche [63, 105]. Thus, many studies have focused efforts on the development of human intestinal models that contain both epithelial and mesenchymal cell types in order to more closely mimic the native tissue.

1.6 Epithelial and Mesenchymal *in vitro* Models of the Human Intestine

Mesenchymal cells have been co-cultured with epithelial cells to improve upon the physiologic relevance of epithelial monolayers and enteroids. In this section, I introduce complex intestinal model systems that are designed to include mesenchymal cells.

Tissue-Derived Epithelial and Mesenchymal Cultures

Early efforts to derive 3D cultures of primary intestinal epithelium focused on co-cultures with mesenchymal cells to recapitulate the intestinal stem cell niche. For example, small and large intestinal cells isolated from mice can be cultured in 3D using an air-liquid interface culture system where epithelial cells are cultured on a collagen gel

with primary intestinal myofibroblasts [24]. These cultures were sustained *in vitro* for over 30 days, and gave rise to differentiated intestinal epithelial cell types including goblet, enteroendocrine, and Paneth cells. Unlike enteroid culture systems [20], these co-cultures did not require exogenous growth factor supplementation of WNT or Notch due to endogenous support from the mesenchymal cells [24]. The presence of mesenchymal cells in these cultures has provided advantages for disease modeling, and air-liquid interface co-cultures have been used to model pathologies such as gastrointestinal cancer [106].

Models Derived from hPSCs

As an alternative to co-culture of intestinal epithelium with mesenchyme, intestinal organoids have additionally been developed from pluripotent stem cells in order to co-differentiate epithelium with mesenchyme. These hPSC-derived intestinal organoids, termed human intestinal organoids or HIOs, are formed through a directed differentiation approach that mimics intestinal development and produces organoids resembling early-stage human fetal intestine. HIOs are thus an ideal model for studying early human intestinal development [12, 26]. HIOs contain both an inner epithelium with differentiated intestinal epithelial cells including enterocytes, goblet cells, and enteroendocrine cells, as well as an outer mesenchymal layer (Figure 1-3). The formation of a mesenchymal layer within HIOs is due to the pluripotency of the hPSCs they are derived from as hPSCs can give rise to multiple cell lineages. On the other hand, enteroids are derived from tissue-specific intestinal stem cells that are incapable of differentiation into mesenchymal cell types.

This mesenchymal layer increases relevance to the human intestine, but HIOs are still relatively immature *in vitro* and lack some of the cell types of the native intestine including neurons [107], vasculature [108], microbiome [35], and a serosal mesothelium. However, HIOs can be transplanted into mice to produce more mature tissue for studies on later developmental events [109]. HIOs will be the model system of choice throughout this dissertation owing to their complexity and unique ability to offer insights into the early developmental crosstalk between epithelium and mesenchyme, and will be described in more depth in subsequent sections.

While HIOs are a preferred model system for many applications, they are not the only intestinal organoid system that contains both epithelium and mesenchyme. An alternate model system involves differentiation of hPSCs under xenogeneic conditions as opposed to culture on plates coated with Matrigel, which is derived from mouse-tumor cell ECM, and utilized throughout the HIO differentiation process [110]. These 'mini-guts' are formed by culturing pluripotent stem cells on circle-patterned glass coated with a cell attachment substrate, and brought through a differentiation protocol that is more intrinsic and less directed compared to HIO generation. Cells cultured using this protocol self-assemble into 3D cystic spheroids that bud off from the plate and contain differentiated epithelial cell types as well as smooth muscle cells and interstitial cells of Cajal [110]. However, these mini-guts are more experimentally challenging to generate and have been less well characterized than HIOs, making them a non-ideal model system.

Benefits and Drawbacks of Stem Cell-Derived in vitro Intestinal Model Systems

The epithelium is only one of the four main layers in the human intestine. Thus, models that include mesenchymal cells are preferable for experiments which favor complete representation of the human gut. However, as these systems are more complex, they require increased time and resources to maintain. For example, the differentiation process to bring pluripotent stem cells into mature human intestinal organoids takes about one month [12], whereas epithelial-only systems can be used for experiments upon formation of a confluent monolayer within days. While mesenchymal cells increase the complexity and relevance of epithelial model systems, there are many other components present in the native intestine including immune cells, neuronal cells, vasculature, and a microbiome that are often lacking in *in vitro* models, even organoids with both epithelium and mesenchyme such as HIOs. It is near impossible to accurately mimic all of the structural features of the native tissue; thus, there is no 'one size fits all' intestinal model, and a model system should be selected based on the particular question being asked.

1.7 Bioengineering 3D Environments to Increase Reproducibility and Clinical Use of Organoids

Regardless of the choice between epithelial-only enteroids vs. organoids containing epithelium and mesenchyme, one of the major challenges facing organoid research is reproducibility and limited control over the 3D self-organization process [111, 112]. Currently, the same experimental conditions may yield organoids with variations in cellular composition, architecture, size and shape that limit modeling of development and clinical translation [111]. A major cause of variation in organoid cultures is animal-derived ECM products such as Matrigel, which are standard for

culturing many organoid models including intestine, lung and liver [11, 12, 16, 18]. Natural ECMs limit reproducibility and control over organoid formation as they are prone to batch-to-batch variability, comprised of a poorly defined protein and growth factor composition, and cannot be easily modified to control biophysical and biochemical matrix properties. Additionally, animal-derived ECM limits clinical translation as it is a xenogeneic material and poses a risk for pathogen transfer [113].

To address these limitations, bioengineers are working to create well-defined systems for organoid culture. Given that both biochemical and mechanical/physical cues drive organogenesis [52, 97, 114, 115], it is important that matrix cues such as mechanical stiffness, degradability and adhesive ligand presentation can be independently modulated. This will maximize the ability to model the complex interplay between the physical environment, cell behavior, and organ formation using organoid models. Additionally, it is likely that each organ will require a unique biochemical and physical niche to support optimal development. Here, I discuss bioengineering strategies that have enhanced reproducibility, experimental control/precision, and clinical application of organoids. Organ-on-a-chip advances are not discussed here, and have been reviewed elsewhere [116, 117]. Future work may focus on combining organ-on-a-chip technologies with organoids to model crosstalk between organ systems.

Defined ECM-Mimetic Hydrogels

The importance of choosing an appropriate ECM or ECM-mimetic to control organoid properties was demonstrated in a study that compared tissue-derived intestinal epithelial organoids grown in floating collagen 1 gels with Matrigel-grown organoids [118].

In collagen, but not Matrigel, organoids aligned, fused and formed macroscopic hollow tubes with a single enclosed lumen and budding crypt-like domains, more closely resembling the native architecture of the intestine. Collagen gel contraction by organoids may enable tube formation. This study demonstrates that simply changing ECM constituents can increase control over organoid formation/organization and presents a system to model the intestine on a larger scale. These experiments were performed using mouse organoids, but the importance of the ECM environment on organoid behavior is applicable to human systems as well. Defined collagen 1 matrices have additionally been utilized to culture intestinal epithelial cells supplemented with Wnt3a to promote a repairing epithelial phenotype, further demonstrating the applicability of defined hydrogel systems [119].

Another recent study utilized defined fibrin hydrogels supplemented with adhesive cues to increase experimental control over epithelial organoid culture [120]. Experiments on mouse intestinal epithelial organoids in fibrin revealed that organoid formation depended on matrix properties, as increased stiffness or decreased access to the adhesive motif RGD reduced organoid formation. Supplementation with laminin, the major component of Matrigel, led to organoid yields in fibrin that were comparable to Matrigel. The fibrin/laminin hydrogel system was successfully applied to culture human epithelial organoids derived from small intestine, liver, and pancreas.

In addition to collagen and fibrin/laminin, a recent landmark study demonstrated that chemically defined polyethylene glycol (PEG) hydrogels could be used as an ECM replacement to culture intestinal epithelial organoids [121]. These hydrogels served as a synthetic ECM-mimetic to exert better control over growing organoids and to reduce

reliance on animal-derived matrices. By working with PEG, a biologically inert hydrogel possessing no inherent ability for cells to adhere or degrade the matrix unless otherwise modified, variables including matrix stiffness, degradation properties and adhesivity were independently modulated. In order to determine the effects of these properties on intestinal stem cell proliferation, organoid formation, and cellular differentiation, PEG hydrogels were modified with proteolytically degradable crosslinkers and cell-adhesive peptides. This work identified that while a stiff matrix was optimal for initial intestinal stem cell expansion, maintaining cells in a stiff matrix prohibited differentiation, suggesting that epithelial differentiation required a softer matrix. Based on these observations, a mechanically dynamic matrix was created to support stem cell expansion and then adapt to permit organoid differentiation. These dynamic hydrogels exhibited an initial stiffness optimized for stem cell expansion but were hydrolytically active and therefore able to soften over time to permit cellular differentiation by alleviating compressive forces. While these hydrogels were optimized using mouse intestinal epithelial organoids, the resulting matrices were successfully used to culture human intestinal epithelial organoids as well.

Recent work has also demonstrated that defined PEG hydrogels can be used to replace Matrigel for the culture of human pluripotent stem cell-derived intestinal (HIOs) and lung organoids (HLOs) [122]. PEG hydrogels were modulated to determine specific mechanical properties and adhesive ligand presentation that optimized HIO formation, thus identifying a stiffness range and adhesive motif (RGD) that supported HIO viability. HLOs were viable in PEG hydrogels optimized for HIO culture, but matrix properties such as stiffness and adhesive cues may need to be optimized for different organoid systems.

Additionally, PEG hydrogels served as an injection vehicle to deliver HIOs to injured mucosa, providing an *in situ* polymerized gel that improved HIO engraftment as compared to HIOs injected without a delivery vehicle.

Chemically defined PEG hydrogels have additionally been utilized to control organization of mouse pluripotent stem cells into neuroepithelial cysts, or organoids that mimic neural tube morphogenesis [123]. A high-throughput system was used to screen factors (mechanical properties, adhesive ligands and degradability) necessary for neuroepithelial morphogenesis in PEG hydrogels. This study utilized mouse organoids, but the methodology may be more broadly applicable to human systems as well. Notably, the ideal properties identified for neural tube morphogenesis did not match the properties tuned for intestinal development [121, 123], although differences may arise from comparison between human and mouse systems. Nonetheless, this suggests that using Matrigel as a "one size fits all" matrix for all organoid systems is suboptimal. Interestingly, neuroepithelial colonies in Matrigel exhibited more heterogeneous colony sizes and morphology as compared with colonies in PEG hydrogels, while a greater proportion of cysts in PEG became properly polarized as compared with Matrigel. This highlights the utility of defined matrices to increase reproducibility in organoid cultures.

Engineered Control Over Local Matrix Properties

While these defined matrices offer improved control over organoid formation, current hydrogel systems have largely focused on control over bulk properties and have not provided spatiotemporal control over local mechanical cues or signaling gradients. Recently, micromolded hydrogels were utilized to provide controlled positional

information to intestinal epithelial cells and guide organization of crypt/villus structures that mimic the structure of the native intestine [92]. In this system, human small intestine crypt fragments were cultured on collagen gels micromolded into crypt/villus domains, creating a pattern for cell growth with distinct luminal and basal fluid reservoirs that enabled spatial control over the local signaling environment by application of different media conditions on either side of the reservoir. This strategy produced intestinal epithelium arranged in proliferative crypt zones with differentiated villus domains based on the application of signaling gradients. A similar strategy has also been used to pattern crypts derived from human colonic epithelium [93]. While micromolded techniques enable control over the spatial organization and signaling environment of 3D cell culture systems, they do not promote the self-organization provided within organoid model systems to properly model development, especially since this system lacked a mesenchymal component. Future work may focus on development of dynamic hydrogels to spatiotemporally control matrix mechanical and biochemical properties in order to better control organoid development.

Interestingly, a recent study combined these two strategies of organoid self-assembly with bioengineered constructs to guide the formation of human brain organoids [124]. Fiber microfilaments comprised of poly(lactide-co-glycolide) (PLGA) were used as floating scaffolds to pattern embryoid bodies from hPSCs. This method enabled shaping of brain organoids from the inside at an early stage. By increasing the surface-area-to-volume ratio with these microfilament scaffolds, reproducible induction of neuroectoderm from micropatterned embryoid bodies was observed. Patterned embryoid bodies were then transferred to Matrigel droplets for expansion into engineered cerebral organoids, or

enCORs. This work demonstrates the potential for bioengineered micropatterned constructs to guide and control organoid self-assembly.

While bioengineering defined environments for organoid culture presents a promising approach to better control organoid development and increase reproducibility, there may still be uncontrollable elements in the differentiation process that are unrelated to the growth matrix. For example, recent work has revealed heterogeneity in hindgut spheroids, the precursor to HIOs, that contributes to inefficient organoid formation and may additionally contribute to variation in organoid phenotype [125]. Process engineering was used to develop a pipeline that sorted spheroids based on size and identified certain phenotypes predisposed for growth into HIOs in order to increase organoid yield from this selected population. This study demonstrated the necessity of controlling all aspects of organoid formation, and highlights methodology to engineer early aspects of HIO maturation.

1.8 The Future of *in vitro* Intestinal Model Systems

Significant progress has been made in developing *in vitro* intestinal models that mimic the native tissue while retaining experimental practicality. However, there are many limitations with current model systems. Among all systems described in this Chapter, common limitations include reliance on naturally derived 3D ECMs like Matrigel that limit experimental control and introduce variability and uncertainty, and immaturity of *in vitro* systems that fail to recapitulate the complex 3D architecture or diversity of cell types found within the human intestine *in vivo*.

For my thesis work, I have focused on developing improved *in vitro* models of the human intestine to address these issues. My work has focused on human intestinal

organoids (HIOs), which have traditionally been cultured in 3D droplets of Matrigel to support organoid growth and viability. I have developed two Matrigel-free culture systems for HIOs, alginate and suspension culture, described in Chapters 3 and 4, that increase experimental control, decrease experimental variability, and are simple, cost effective, and amenable to scale-up. Additionally, my work has focused on differentiation of additional cell types within the HIO including an outer serosal mesothelium (Chapter 4) to increase relevance to the native tissue.

1.9 Figures

E9.0: Epithelial gut tube surrounded by mesenchyme.

E9.5: Endothelial sprouts present. Vagal neural crest cells present

E9.5 - E10.5: CDX2+ epithelium forms simple pseudostratified epithelium

E13: Developing smooth muscle cells are arranged into layer of αSMA+ circular muscle

E11.5: Gut is surrounded by mesothelial cells

E11: Smooth muscle differentiation begins

E14: Pseudostratified epithelium becomes columnar. Neural crest cells form neurons. Longitudinal smooth muscle develops.

E14.5 - E16.5: Villus formation proceeds in a proximal to distal wave

E16.5: Epithelial cells differentiate into mature intestinal cell types. Mature vessels are present

Figure 1-1. Timeline of Early Intestinal Development

Schematic depicting early developmental events in the mouse gut, including epithelial and mesenchymal development and villus emergence. Human intestinal development follows a similar pattern, but along a longer timescale. Created with BioRender.com
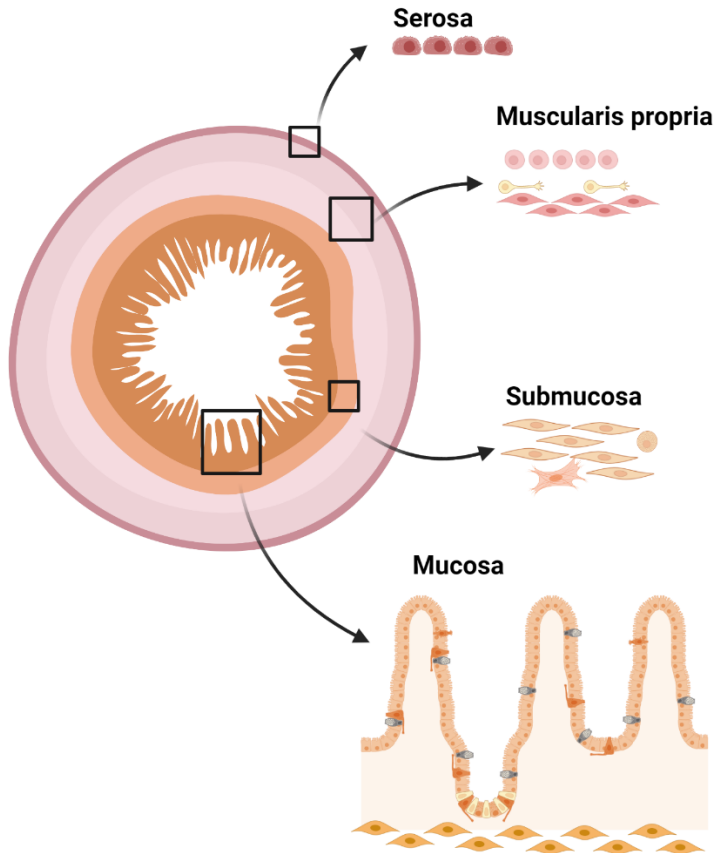
Figure 1-2. Layers of the Human Small Intestine
Schematic depicting the four main layers of the human small intestine (serosa, muscularis propria, submucosa, and mucosa). Created with BioRender.com
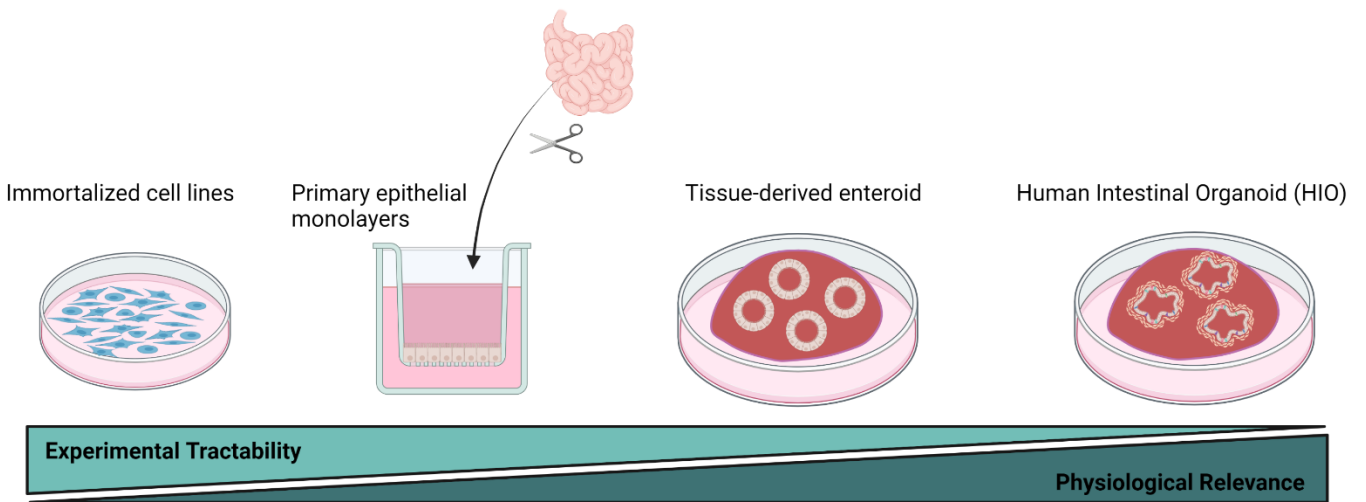
Figure 1-3. *In vitro* Models of the Human Intestine.

Representation of common *in vitro* intestinal model systems, organized by ranking of experimental tractability and physiological relevance. Use of primary cells, 3D culture, and inclusion of mesenchymal cells along with epithelial cells increase physiological relevance but pose technical challenges that make experiments more difficult. Created with BioRender.com.

1.10 References

1.   Wells, J.M. and J.R. Spence, *How to make an intestine.* Development, 2014. **141**: p. 752-760.

2.   Rao, J. and J. Wang, *Regulation of Gastrointestinal Mucosal Growth.* Morgan & Claypool Life Sciences, 2010.

3.   Chin, A.M., et al., *Morphogenesis and maturation of the embryonic and postnatal intestine.* Seminars in Cell & Developmental Biology, 2017. **66**: p. 81-93.

4.   Walton, K.D., et al., *Generation of intestinal surface: an absorbing tale.* Development, 2016. **143**(13): p. 2261–2272.

5.   Walton, K.D., et al., *Blueprint for an Intestinal Villus: Species-specific Assembly Required.* Wiley Interdiscip Rev Dev Biol., 2018. **7**(4): p. e317.

6.   Pageot, L., et al., *Human cell models to study small intestinal functions: recapitulation of the crypt-villus axis.* Microscopy Research and Technique, 2000. **49**(4): p. 394-406.

7.   Sambuy, Y., et al., *The Caco-2 cell line as a model of the intestinal barrier: influence of cell and culture-related factors on Caco-2 cell functional characteristics.* Cell Biology and Toxicology, 2005. **21**(1): p. 1-26.

8.   Evans, G., et al., *The development of a method for the preparation of rat intestinal epithelial cell primary cultures.* Journal of Cell Science, 1992. **101**(Pt 1): p. 219-231.

9.   Fukamachi, H., *Proliferation and differentiation of fetal rat intestinal epithelial cells in primary serum-free culture.* Journal of Cell Science, 1992. **103**: p. 511-519.

10.   Randall, K.J., J. turton, and J.R. Foster, *Explant culture of gastrointestinal tissue: a review of methods and applications.* Cell Biology and Toxicology, 2011. **27**: p. 267-284.

11.   Takebe, T., et al., *Vascularized and functional human liver from an iPSC-derived organ bud transplant.* Nature, 2013. **499**: p. 481-484.

12.   Spence, J.R., et al., *Directed differentiation of human pluripotent stem cells into intestinal tissue in vitro.* Nature, 2011. **470**(7332): p. 105-109.

13.   Eiraku, M., et al., *Self-organizing optic-cup morphogenesis in three-dimensional culture.* Nature, 2011. **472**(7341): p. 51-6.

14.   Lancaster, M., et al., *Cerebral organoids model human brain development and microcephaly.* Nature, 2013. **501**(7467): p. 373-9.

15.   Takasato, M., et al., *Directing human embryonic stem cell differentiation towards a renal-lineage generates a self-organizing kidney.* Nature Cell Biology, 2014. **16**: p. 118-126.

16.   Miller, A.J., et al., *In Vitro Induction and In Vivo Engraftment of Lung Bud Tip Progenitor Cells Derived from Human Pluripotent Stem Cells.* Stem Cell Reports, 2018. **10**(1): p. 101-119.

17.   Dye, B., et al., *A bioengineered niche promotes in vivo engraftment and maturation of pluripotent stem cell derived human lung organoids.* eLife, 2016.

18.   Dye, B., et al., *In vitro generation of human pluripotent stem cell derived lung organoids.* eLife, 2015.

19.   Jung, P., et al., *Isolation and in vitro expansion of human colonic stem cells.* Nature Medicine, 2011. **17**(10): p. 1225-1227.

20.   Sato, T., et al., *Single Lgr5 stem cells build crypt-villus structures in vitro without a mesenchymal niche.* Nature, 2009. **459**: p. 262-265.

21.   Yui, S., et al., *Functional engraftment of colon epithelium expanded in vitro from a single adult Lgr5+ stem cell.* Nature Medicine, 2012. **18**(4): p. 618-623.

22.   Sato, T., et al., *Long-term expansion of epithelial organoids from human colon, ademona, adenocarcinoma, and Barrett's epithelium.* Gastroenterology, 2011. **141**(5): p. 1762-1772.

23.   Li, X., et al., *Oncogenic transformation of diverse gastrointestinal tissues in primary organoid culture.* Nature MEdicine, 2014. **20**(7): p. 769-777.

24.   Ootani, A., et al., *Sustained in vitro intestinal epithelial culture within a Wnt-dependent stem cell niche.* Nature Medicine, 2009. **15**(6): p. 701-706.

25.   Forster, R., et al., *Human Intestinal Tissue with Adult Stem Cell Properties Derived from Pluripotent Stem Cells.* Stem Cell Reports, 2014. **2**(6): p. 838-852.

26.   McCracken, K., et al., *Generating human intestinal tissue from pluripotent stem cells in vitro.* Nature Protocols, 2011. **6**(12): p. 1920-1928.

27.   Singagoga, K.L. and J.M. Wells, *Generating human intestinal tissues from pluripotent stem cells to study development and disease.* The EMBO Journal, 2015. **34**(9): p. 1149-1163.

28.   Munera, J., et al., *Differentiation of Human Pluripotent Stem Cells into Colonic Organoids via Transient Activation of BMP Signaling.* Cell Stem Cell, 2017. **21**(1): p. 51-64.

29.   Tsai, Y.-H., et al., *In vitro patterning of pluripotent stem cell-derived intestine recapitulates in vivo human development.* Development, 2017. **144**(6): p. 1045-1055.

30.   Aurora, M. and J.R. Spence, *hPSC-derived lung and intestinal organoids as models of human fetal tissue.* Dev Biol., 2016. **420**(2): p. 230-238.

31.   Tsai, Y.-H., et al., *LGR4 and LGR5 Function Redundantly During Human Endoderm Differentiation.* Cel Mol Gastroenterol Hepatol., 2016. **2**(5): p. 648-662.

32.   Dedhia, P.H., et al., *Organoid Models of Human Gastrointestinal Development and Disease.* Gastroenterology, 2016. **150**(5): p. 1098-1112.

33.   Finkbeiner, S.R., et al., *Generation of tissue-engineered small intestine using embryonic stem cell-derived human intestinal organoids.* Biology Open, 2015. **4**(11): p. 1462-1472.

34.   Finkbeiner, S.R., et al., *Transcriptome-wide Analysis Reveals Hallmarks of Human Intestine Development and Maturation In Vitro and In Vivo.* Stem Cell Reports, 2015. **4**: p. 1140-1155.

35.   Hill, D.R., et al., *Bacterial colonization stimulates a complex physiological response in the immature human intestinal epithelium.* eLife, 2017. **6**.

36.   Noah, T.K., B. Donahue, and N.F. Shroyer, *Intestinal development and differentiation.* Experimental Cell Research, 2012. **317**(19): p. 2702-2710.

37.   Spence, J.R., R. Lauf, and N.F. Shroyer, *Vertebrate Intestinal Endoderm Development.* Developmental Dynamics, 2011. **240**(3): p. 501-520.

38.   Sherwood, R.I., et al., *Wnt signaling specifies and patterns intestinal endoderm.* Mechanisms of development, 2011. **128**(7-10): p. 387-400.

39.   McHugh, K.M., *Molecular Analysis of Gastrointestinal Smooth Muscle Development.* Journal of Pediatric Gastroenterology & Nutrition, 1996. **23**(4): p. 379-394.

40.   Huycke, T.R., et al., *Genetic and Mechanical Regulation of Intestinal Smooth Muscle Development.* Cell, 2019. **179**(1): p. 90-105.e21.

41.   Winters, N.I., R.T. Thomason, and D.M. Bader, *Identification of a novel developmental mechanism in the generation of mesothelia.* Development, 2012. **139**(16): p. 2926-2934.

42.   Winters, N.I., A.M. Williams, and D.M. Bader, *Resident progenitors, not exogenous migratory cells, generate the majority of visceral mesothelium in organogenesis.* Developmental Biology, 2014. **391**(2): p. 125-132.

43.   Winters, N.I. and D.M. Bader, *Development of the Serosal Mesothelium.* Journal of Developmental Biology, 2013. **1**: p. 64-81.

44.   Wilm, B., et al., *The serosal mesothelium is a major source of smooth muscle cells of the gut vasculature.* Development, 2005. **132**: p. 5317-5328.

45.   Hatch, J. and Y.-s. Mukouyama, *Spatiotemporal mapping of vascularization and innervation in the fetal murine intestine.* Developmental Dynamics, 2014. **244**(1): p. 56-68.

46.   Carmona, R., et al., *Cells Derived from the Coelomic Epithelium Contribute to Multiple Gastrointestinal Tissues in Mouse Embryos.* PLOS One, 2013. **8**(2): p. e55890.

47.   Dixit, R., X. Ai, and A. Fine, *Derivation of lung mesenchymal lineages from the fetal mesothelium requires hedgehog signaling for mesothelial cell entry* Development, 2013. **140**(21): p. 4398-4406.

48.   Kolterud, A., et al., *Paracrine Hedgehog signaling in stomach and intestine: new roles for hedgehog in gastrointestinal patterning.* Gastroenterology, 2009. **137**(2): p. 618-628.

49.   Kruithof, B.P.T., et al., *BMP and FGF regulate the differentiation of multipotential pericardial mesoderm into the myocardial or epicardial lineage.* Developmental Biology, 2006. **295**(2): p. 507-522.

50.   Schlueter, J., J. Manner, and T. Brand, *BMP is an important regulator of proepicardial identity in the chick embryo.* Developmental Biology, 2006. **295**(2): p. 546-558.

51.   Uesaka, T., et al., *Development of the intrinsic and extrinsic innervation of the gut.* Dev Biol., 2016. **417**(2): p. 158-167.

52.   Walton, K.D., et al., *Hedgehog-responsive mesenchymal clusters direct patterning and emergence of intestinal villi.* PNAS, 2012. **109**: p. 15817–15822.

53.   Kim, T.-H., S. Escudero, and R.A. Shivdasani, *Intact function of Lgr5 receptor-expressing intestinal stem cells in the absence of Paneth cells.* PNAS, 2012. **109**(10): p. 3932-3937.

54.   Gehart, H. and H. Clevers, *Tales from the crypt: new insights into intestinal stem cells.* Nature Reviews Gastroenterology & Hepatology, 2019. **16**: p. 19-34.

55. Gassler, N., *Paneth cells in intestinal physiology and pathophysiology.* World J Gastrointest Pathophysiol., 2017. **8**(4): p. 150-160.

56. Darwich, A.S., et al., *Meta-analysis of the turnover of intestinal epithelia in preclinical animal species and humans.* Drug Metab Dispos., 2014. **42**(12): p. 2016-2022.

57. Allaire, J.M., et al., *The Intestinal Epithelium: Central Coordinator of Mucosal Immunity.* Trends in Immunology, 2018. **39**(9): p. 677-696.

58. Gerbe, F., C. Legraverend, and P. Jay, *The intestinal epithelium tuft cells: specification and function.* Cell Mol Life Sci., 2012. **69**(17): p. 2907-2917.

59. Powell, D.W., et al., *Mesenchymal Cells of the Intestinal Lamina Propria.* Annu Rev Physiol., 2011. **73**: p. 213-237.

60. Roulis, M. and R.A. Flavell, *Fibroblasts and myofibroblasts of the intestinal lamina propfia in physiology and disease.* Differentiation, 2016. **92**(3).

61. Hunyady, B., E. Mezey, and M. Palkovits, *Gastrointestinal immunology: cell types in the lamina propria--a morphological review.* Acta Physiol Hung., 2000. **87**(4): p. 305-328.

62. Uchida, K. and Y. Kamikawa, *Muscularis mucosae — the forgotten sibling.* J. Smooth Muscle Res., 2007. **43**(5): p. 157-177.

63. Holloway, E.M., et al., *Mapping Development of the Human Intestinal Niche at Single-Cell Resolution.* Cell Stem Cell, 2021. **28**(3): p. 568-580.e4.

64. Coskun, M., *Intestinal Epithelium in Inflammatory Bowel Disease.* Front Med (Lausanne), 2014. **1**(24).

65. Cao, G., et al., *Small intestinal submucosa: superiority, limitations and solutions, and its potential to address bottlenecks in tissue repair.* Journal of Materials Chemistry B, 2019. **7**(33): p. 5038-5055.

66. Shi, L. and V. Ronfard, *Biochemical and biomechanical characterization of porcine small intestinal submucosa (SIS): a mini review.* Int J Burns Trauma. , 2013. **3**(4): p. 173-179.

67. Koukoulis, G., et al., *Obliterative muscularization of the small bowel submucosa in Crohn disease: a possible mechanism of small bowel obstruction.* Arch Pathol Lab Med., 2001. **125**(10): p. 1331-1334.

68. Sanders, K.M., et al., *Regulation of gastrointestinal motility—insights from smooth muscle biology.* Nat Rev Gastroenterol Hepatol., 2012. **9**(11): p. 633-645.

69. Thomson, L., et al., *1998.* Nature Medicine, Interstitial cells of Cajal generate a rhythmic pacemaker current. **4**(848-851).

70. Antonucci, A., et al., *Chronic intestinal pseudo-obstruction.* World J Gastroenterol., 2008. **14**(19): p. 2953–2961.

71. Heuckeroth, R.O., *Hirschsprung disease — integrating basic science and clinical medicine to improve outcomes.* Nat Rev Gastroenterol Hepatol., 2018. **15**: p. 152–167.

72. Mutsaers, S.E., *The mesothelial cell.* The International Journal of Biochemistry & Cell Biology, 2004. **36**(1): p. 9-16.

73. Mutsaers, S.E., *Mesothelial cells: Their structure, function and role in serosal repair.* Respirology, 2002. **7**: p. 171-191.

74. Dobbie, J., *Pathogenesis of peritoneal fibrosing syndromes (sclerosing peritonitis) in peritoneal dialysis.* Peritoneal Dialysis International, 1992. **12**(1): p. 14-27.

75. Bridda, A., et al., *Peritoneal Mesothelioma: A Review.* Medscape General Medicine, 2007. **9**(2): p. 32.

76. Tsai, J.M., et al., *Surgical adhesions in mice are derived from mesothelial cells and can be targeted by antibodies against mesothelial markers.* Sci Transl Med., 2018. **10**(469): p. eaan6735.

77. Koopmans, T. and Y. Rinkevich, *Mesothelial to mesenchyme transition as a major developmental and pathological player in trunk organs and their cavities.* Communications Biology, 2018. **1**(170).

78. Murakami, T., *Absorption sites of orally administered drugs in the small intestine.* Expert Opinion on Drug Discovery, 2017. **12**(12): p. 1219-1232.

79. Makins, R. and A. Ballinger, *Gastrointestinal side effects of drugs.* Expert Opin Drug Saf., 2003. **2**(4): p. 421-429.

80. Hugenholtz, F. and W.M. de Vos, *Mouse models for human intestinal microbiota research: a critical evaluation.* Cell Mol Life Sci., 2018. **75**(1): p. 149-160.

81. Jochems, P.G.M., et al., *Evaluating Human Intestinal Cell Lines for Studying Dietary Protein Absorption.* Nutrients, 2018. **10**(3): p. 322.

82. Noben, M., et al., *Human intestinal epithelium in a dish: Current models for research into gastrointestinal pathophysiology.* United European Gastroenterol J., 2017. **5**(8): p. 1073-1081.

83. Dutton, J.S., et al., *Primary Cell-Derived Intestinal Models: Recapitulating Physiology.* Trends Biotechnol., 2019. **37**(7): p. 744-760.

84. Váradi, J., et al., *Alpha-Melanocyte Stimulating Hormone Protects against Cytokine-Induced Barrier Damage in Caco-2 Intestinal Epithelial Monolayers.* PLOS One, 2017. **12**: p. e0170537.

85. Drummond, C.G., C.A. Nickerson, and C.B. Coyne, *A Three-Dimensional Cell Culture Model To Study Enterovirus Infection of Polarized Intestinal Epithelial Cells.* mSphere, 2015. **1**: p. e00030-15.

86. Darling, N.J., et al., *Bioengineering Novel in vitro Co-culture Models That Represent the Human Intestinal Mucosa With Improved Caco-2 Structure and Barrier Function.* Frontiers in Bioengineering and Biotechnology, 2020. **8**(992).

87. Costello, C.M., et al., *3-D Intestinal Scaffolds for Evaluating the Therapeutic Potential of Probiotics.* Mol. Pharmaceutics, 2014. **11**: p. 2030–2039.

88. Yu, J., et al., *In vitro 3D human small intestinal villous model for drug permeability determination.* Biotechnology and Bioengineering, 2012. **109**: p. 2173-8.

89. Shah, P., et al., *A microfluidics-based in vitro model of the gastrointestinal human–microbe interface.* Nature Communications, 2016. **7**.

90. Hyun Jung Kim, et al., *Contributions of microbiome and mechanical deformation to intestinal bacterial overgrowth and inflammation in a human gut-on-a-chip.* PNAS, 2016. **113**: p. E7-E15.

91. Graves, C.L., et al., *A method for high purity intestinal epithelial cell culture from adult human and murine tissues for the investigation of innate immune function.* J Immunol Methods., 2014. **414**: p. 20-31.

92. Wang, Y., et al., *A microengineered collagen scaffold for generating a polarized crypt-villus arhcitecture of human small intestinal epithelium.* Biomaterials, 2017. **128**: p. 44-55.

93. Wang, Y., et al., *Formation of Human Colonic Crypt Array by Application of Chemical Gradients Across a Shaped Epithelial Monolayer.* Cellular and Molecular Gastroenterology and Hepatology, 2018. **5**: p. 113–130.

94. Yoo, J.-H. and M. Donowitz, *Intestinal enteroids/organoids: A novel platform for drug discovery in inflammatory bowel diseases.* World J Gastroenterol., 2019. **25**(30): p. 4125–4147.

95. Sato, T., et al., *Long-term Expansion of Epithelial Organoids From Human Colon, Adenoma, Adenocarcinoma, and Barrett's Epithelium.* Gastroenterology, 2011. **141**(5): p. 1762-1772.

96. Ranganathan, S., et al., *Research in a time of enteroids and organoids: how the human gut model has transformed the study of enteric bacterial pathogens.* Gut Microbes, 2020. **12**(1).

97. Shyer, A.E., et al., *Bending Gradients: How the Intestinal Stem Cell Gets Its Home.* Cell, 2015. **161**: p. 569–580.

98. Thorne, C.A., et al., *Enteroid Monolayers Reveal an Autonomous WNT and BMP Circuit Controlling Intestinal Epithelial Growth and Organization.* Developmental Cell, 2018. **44**.

99. Sanman, L.E., et al., *Generation and Quantitative Imaging of Enteroid Monolayers.* Intestinal Stem Cells, 2020. **2171**: p. 99-113.

100. Roodsant, T., et al., *A Human 2D Primary Organoid-Derived Epithelial Monolayer Model to Study Host-Pathogen Interaction in the Small Intestine.* Front. Cell. Infect. Microbiol, 2020. **10**.

101. Co, J.Y., et al., *Controlling Epithelial Polarity: A Human Enteroid Model for Host-Pathogen Interactions.* Cell Reports, 2019. **26**: p. 2509–2520.

102. Co, J.Y., et al., *Controlling the polarity of human gastrointestinal organoids to investigate epithelial biology and infectious diseases.* Nature Protocols, 2021. **16**: p. 5171–5192.

103. Le Guen, L., et al., *Mesenchymal--epithelial interactions during digestive tract development and epithelial stem cell regeneration.* Cell Mol Life Sci., 2015. **72**: p. 3883–3896.

104. Li, C. and J.F. Kuemmerle, *The mechanisms that mediate the development of fibrosis in patients with Crohn's Disease.* Inflamm Bowel Dis., 2014. **20**: p. 1250-1258.

105. Pastuła, A. and J. Marcinkiewicz, *Cellular Interactions in the Intestinal Stem Cell Niche.* Arch Immunol Ther Exp (Warsz), 2019. **67**: p. 19-26.

106. Li, X., et al., *Oncogenic transformation of diverse gastrointestinal tissues in primary organoid culture.* Nature Medicine, 2014. **20**: p. 769–777.

107. Workman, M.J., et al., *Engineered human pluripotent-stem-cell-derived intestinal tissues with a functional enteric nervous system.* Nature Medicine, 2016. **23**: p. 49-59.

108. Holloway, E.M., et al., *Differentiation of Human Intestinal Organoids with Endogenous Vascular Endothelial Cells.* Developmental Cell, 2020. **54**(4): p. 516-528.e7.

109. Watson, C., et al., *An in vivo model of human small intestine using pluripotent stem cells.* 2014, 2014. **20**(11): p. 1310-1314.

110. Uchida, H., et al., *A xenogeneic-free system generating functional human gut organoids from pluripotent stem cells.* JCI Insight, 2017. **2**(1): p. e86492.

111. Huch, M., et al., *The hope and the hype of organoid research.* Development, 2017. **144**: p. 938–941.

112. Spence, J.R., *Taming the Wild West of Organoids, Enteroids, and Mini-Guts.* Cellular and Molecular Gastroenterology and Hepatology, 2018. **5**: p. 159–160.

113. Czerwinski, M. and J.R. Spence, *Hacking the Matrix.* Cell Stem Cell, 2017. **20**(1): p. 9-10.

114. Kurpios, N.A., et al., *The direction of gut looping is established by changes in the extracellular matrix and in cell:cell adhesion.* PNAS, 2008. **105**(25): p. 8499-8506.

115. Savin, T., et al., *On the growth and form of the gut.* Nature, 2011. **476**(57-62).

116. Ronaldson-Bouchard, K. and G. Vunjak-Novakovic, *Organs-on-a-Chip: A Fast Track for Engineered Human Tissues in Drug Development.* Cell Stem Cell, 2018. **22**: p. 310-324.

117. Zhang, B., et al., *Advances in organ-on-a-chip engineering.* Nature Reviews Materials, 2018. **3**: p. 257-278.

118. Sachs, N., et al., *Intestinal epithelial organoids fuse to form self-organizing tubes in floating collagen gels.* Development, 2017. **144**: p. 1107-1112.

119. Yui, S., et al., *YAP/TAZ-Dependent Reprogramming of Colonic Epithelium Links ECM Remodeling to Tissue Regeneration.* Cell Stem Cell, 2018. **22**(1): p. 35-49.

120. Broguiere, N., et al., *Growth of Epithelial Organoids in a Defined Hydrgel.* Advanced Materials, 2018. **30**(43): p. e1801621.

121. Gjorevski, N., et al., *Designer matrices for intestinal stem cell and organoid culture.* Nature, 2016. **539**: p. 560-564.

122. Cruz-Acuna, R., et al., *Synthetic hydrogels for human intestinal organoid generation and colonic wound repair.* Nature Cell Biology, 2017. **19**(11): p. 1326-1335.

123. Ranga, A., et al., *Neural tube morphogenesis in synthetic 3D microenvironments.* PNAS, 2016. **113**(44): p. E6831-E6839.

124.   Lancaster, M.A., et al., *Guided self-organization and cortical plate formation in human brain organoids.* Nature Biotechnology, 2017. **35**(659-666).

125.   Arora, N., et al., *A process engineering approach to increase organoid yield.* Development, 2017. **144**: p. 1128-1136.

Chapter 2 : Generation of Small Intestinal Organoids for Experimental Intestinal Physiology

Portions of this chapter have been published:

2.1 Introduction

In vitro models of human intestinal tissue have long played a vital role in diverse areas of research including pharmacology, metabolism, and immunology. Until recently this work relied on transformed colorectal carcinoma lines of widely varying pedigree and reproducibility. While these model systems have advanced permeability and absorption screening in drug discovery research [1], they are known for their unpredictable correlation with *in vivo* and clinical trial data [1]. Long-term culture of primary epithelial cells remained an elusive goal until break-through work demonstrating that Lgr5 + stem cells in the intestinal crypt could be isolated in culture and induced to differentiate into villus-like epithelial domains [2]. Other seminal work demonstrated that the underlying stromal cells were also amenable to long-term culture in concert with the epithelium [3]. Together, these studies defined the niche required to support and propagate intestinal stem cells, and facilitated rapid progress in a parallel body of

research on embryonic intestinal development that resulted in de novo differentiation of human intestinal epithelium and mesenchyme from pluripotent stem cells [4].

Both tissue-derived and pluripotent stem cell derived intestinal epithelial cultures form 3-dimensional structures containing differentiated epithelial cells and other cell types in vitro and are commonly referred to as "organoids." Simian and Bissel have published a comprehensive history of this term and the field of research that preceded the contemporary use of the term "organoid" [5]. The overarching, long-term goal of the field of organogenesis is the development of lab-grown tissues to replace aging or diseased structures in human patients [6]. A by-product of this effort has been the development of dramatically improved *in vitro* model systems for human intestinal development, pathophysiology, pharmacology and other areas of research. The application of these intestinal organoid technologies requires a thorough understanding of the unique properties of organoid systems and familiarity with their experimental uses.

This chapter will focus on defining a protocol for the generation of small intestinal organoid tissues derived from pluripotent stem cells as well as describe several related and alternative culture methodologies.

2.2 Applications of Intestinal Organoids

Medical Need

One of the primary applications of intestinal organoids is use for the medical field. Organoids can be used for translational purposes such as disease modeling, drug screening, or replacement tissue [7, 8]. Thus far, intestinal enteroids and organoids

have been used to study microvillus inclusion disease, multiple intestinal atresia, model epithelial to mesenchymal transitions implicated in intestinal fibrosis, as well as study basic aspects of intestinal bowel disease and Crohn's disease including mucosal integrity, apoptosis, and inflammatory cytokines [9-12]. Organoids have also been used to model cancer and screen for drug efficacy [8, 13-17]. Organoids additionally could serve as regenerative therapies by providing replacement tissue to repair damage by complementing/replacing the use of donor organs. If organoids are derived from the patient's own cells or tissue, this additionally removes the concern of immune response or tissue rejection. Previous studies have shown that intestinal organoids and enteroids engraft and mature in vivo when transplanted into immunocompromised mice, presenting a source of more mature intestinal tissue [18, 19]. Additionally, transplanted organoids have been shown to contribute to repair of intestinal injury [20, 21].

Research Need

Intestinal organoids present a tool to study human intestinal development and disease *in vitro* with a relevant 3D system that mimics the architecture of the native intestine *in vivo*. The organoid model system reduces reliance on animal model systems, enabling the study of human development and diseases in a human model system. They additionally provide a closer representation of the intestine over traditionally utilized 2D cell lines. HIOs in particular enable the study of epithelial-mesenchymal crosstalk due to the fact that they contain both an inner epithelium and outer supporting mesenchyme, presenting advantages both for understanding intestinal development and diseases impacting the mesenchyme.

Overview of Differentiation Protocol

Pluripotent stem cell derived intestinal organoids, referred to here as human intestinal organoids (HIOs), have emerged as a useful system to study co-development of epithelial and mesenchymal cells from a pluripotent state. HIOs are generated through a directed differentiation process in which pluripotent stem cells are first differentiated into definitive endoderm over 3 days. The definitive endoderm is then pushed toward a hindgut endoderm fate which results in the formation of 3D hindgut spheroids that spontaneously bud off from the 2D monolayer after 4–5 days. These hindgut spheroids will mature into HIOs over the course of approximately 4 weeks *in vitro.* The resulting HIOs contain an inner epithelium surrounded by mesenchyme that is thought to originate from incomplete definitive endoderm induction [4]. Overall, the differentiation process takes approximately 5 weeks from the time hPSCs are plated to mature HIOs.

2.3 Materials, Equipment and Reagents

Cell lines

We find that the H9 human embryonic stem cell line is a very reliable line for generating HIOs and is a good line to start with to optimize the protocol and ensure an efficient differentiation with robust spheroid generation. However, the protocol is robust across other cell lines and has been used with over 10 different human embryonic and induced pluripotent stem cell lines.

Cell Culture Plates

Nunclon® delta tissue culture dishes are critical for the proper adhesion of Matrigel droplets to the plasticware surface:

- 6-Well plate for human pluripotent stem cell (hPSC) maintenance and passaging (ThermoFisher Nunclon® Delta; cat. no. 140675).

- 24-Well plate for hPSC differentiation protocol (ThermoFisher Nunclon® Delta surface; cat. no. 142475).

Stem Cell Maintenance Culture

- mTeSR1 basal medium + 5 × supplement (STEMCELL technologies #85850). More recently, mTeSR Plus basal medium + 5 x supplement (STEMCELL technologies #100-0276) has been used as it is manufactured under cGMPs and growth-factor stabilized.

- Matrigel Growth Factor Reduced (GFR) Basement Membrane Matrix, LDEV-free (Corning cat. no. 354230)
    - Store concentrated aliquots in − 80 °C ready to dilute to 100 μg/mL concentration using cold DMEM/F12
    - Alternatively, use Corning® Matrigel hESC-Qualified Matrix, LDEV-free (Corning cat. # 354277)
    - Follow manufacture dilution factor for this Matrigel

- DMEM/F12 cell culture media (Thermo Fisher Cat no. 11320033 or Corning)

- o   Used for Matrigel and dispase dilution, and stem cell washing

- Dispase II Powder (Gibco™ 17105041), store 5 mg/mL aliquots dissolved in DMEM/F12 at − 20 °C

Spheroid Differentiation Culture

- Activin A (R&D Systems cat. no. 338-AC)

  - o   Reconstitute with 1 × PBS. Store 100 µg/mL aliquots at − 80 °C. To prepare for 3 days of endoderm differentiation on one 24-well plate, it may be convenient to store 37 µL aliquots

- Penicillin and Streptomycin (Gibco cat. no. 15140122)

- RPMI 1640 (Thermo Fisher cat. no. 11875093)

- Hyclone defined FBS (GE Healthcare SH3007003)

  - o   Prepare 1 mL or 10 mL aliquots. Store in − 80°C

- Purified human recombinant FGF4 protein (Sugawara et al., 2014)

  - o   Purified by using a modified protocol as described by Sugawara et al. (2014) and prepare 500 µg/mL (1:1000 dilution) in 1 × PBS aliquots, store at − 80°C

- Alternatively, recombinant human FGF-4 protein can be purchased (R&D Systems cat. no. 235-F4)

- CHIR99021 (Tocris cat. no. 4423 or APExBIO A3011)

  - o   To prepare 10 mM (1:5000 dilution) stock solution add 215 µL of DMSO to 10 mg of CHIR99021. Store at − 20 °C

HIO Differentiation Culture

- Advanced DMEM/F12 (Thermo Fisher cat. no. 12634-010)

- Matrigel basement membrane (Corning cat. no. 354234)

- Dilute with DMEM/F12 to 8 mg/mL

- B27 (Thermo Fisher cat. no. 17504044)

- GlutaMAX (Thermo Fisher cat. no. 35050061)

- HEPES 1 M buffer solution (Gibco cat. no. 15630-080 or Corning 25-060-CI)

- Penicillin and streptomycin (Gibco cat. no. 15140122)

- Epidermal growth factor (EGF) (R&D Systems cat no. 236-EG)

  o Reconstitute with 1 × PBS, prepare 100 µg/mL (1:1000 dilution) aliquots, store at − 80°C

- Purified Recombinant Human Noggin-FC Protein from Hek293 cells expressing Fc-tagged Noggin (Heijmans et al., 2013). This cell line is used to produce either purified Noggin protein or Noggin-conditioned medium

  o Purified by using Protein A Agarose Kit (KPL cat. no. 553-50-00). Prepare 100 µg/mL (1:1000 dilution) aliquots in 1 × PBS, or 10 mL aliquots of conditioned medium, store at − 80 °C

  o Alternatively, recombinant human noggin protein can be purchased (R&D Systems cat. no. 6057-NG). Prepare 100 µg/mL (1:1000 dilution) aliquots, store at − 80 °C

- Human R-Spondin1 conditioned medium from Cultrex HA-R-Spondin1-Fc 293 T Cells (R&D Systems cat. no. 3710-001-01). This cell line is used to produce

either R-Spondin 1-conditioned medium or purified recombinant human R-Spondin1 protein

- o Prepare 10 mL aliquots of conditioned medium, store at − 80 °C

- o Purified by using Protein A Agarose Kit (KPL cat. no. 553-50-00). Prepare 250 μg/mL aliquots in 1 × PBS (1:1000 dilutions), store at − 80 °C

- o Alternatively, recombinant human R-Spondin1 protein can be purchased (R&D Systems cat. no. 4645-RS). Prepare 500 μg/mL (1:1000 dilution) aliquots, store at − 80 °C

Recommended Culture Tools

- Pipettes and sterile tips, 10–1000 μL

- Dissecting microscope/stereoscope

- Labconco horizontal clean bench

- 15 cm Petri dish

- Scalpels

- 1 mL Syringe and size 30 gage (30G × 1″) needle

Routine Stem Cell Culture and Maintenance

- Human pluripotent stem cell line

- 6-Well cell culture plate

- mTeSR1 basal medium + 5 × supplement (STEMCELL Technologies #85850)

- Matrigel growth factor reduced (GFR) basement membrane matrix, LDEV-free (Corning cat. #354230)

- o Store aliquots in − 80 °C ready to dilute to 100 μg/mL concentration at volumes of 12 mL or 24 mL using cold DMEM/F12
- DMEM/F12 (Thermo Fisher cat. #11320033 or Corning 10092CV)
- Dispase II, Powder (Gibco™ 17105041)
- Store 5 mg/mL aliquots dissolved in DMEM/F12 at − 20 °C
- Cell scraper

2.4 Organoid Differentiation Protocol

Sterile Technique

As with all cell culture applications, use of sterile culture techniques is essential to the success of this organoid differentiation protocol. Use of a cell culture hood is essential. We recommend cleaning the work surface with 70% ethanol or isopropanol before and after use and UV treatment of the cell culture hood after use. See Phelan and May [22] for a review of general purpose aseptic cell culture techniques.

Routine Stem Cell Culture and Maintenance

This protocol describes passaging and maintenance of human pluripotent stem cell lines. The timing of stem cell passaging should be based on both confluence and density of the individual stem cell colonies. Colony density is a more important factor than overall confluence as dense colonies will begin to spontaneously differentiate around the edges.

1. When stem cells are ready for passaging based upon confluence and colony density (Figure 2-1D), prepare for passaging. Check for any signs of spontaneous differentiation

49

(easily noticed as white clusters especially around the center or edges of colonies). Scrape away differentiated spots with a pipette tip—they will be removed during washing.

2. Dilute GFR Matrigel to 100 µg/mL using cold DMEM/F12.

3. Add 1 mL per well of a 6-well plate

- Stem cells are maintained in 6-well plates.

4. Coat plate for at least 1 h at room temperature prior to passaging

- Matrigel-coated plates can be wrapped in parafilm and stored at 4 °C for up to 1 week for later use.

5. Warm dispase solution to room temperature and dilute to 0.2 mg/mL in pre-warmed DMEM/F12.

6. Add 1 mL diluted dispase to each well (6-well plate) that will be passaged. Place in the 37C° incubator for 10 min

- For stem cell maintenance, one well of a 6-well plate is passaged to an entire 6-well plate (1:6 dilution).

7. While waiting for the 10 min dispase treatment to pass, remove Matrigel coating from 6-well plate and add 1 mL of mTSER1 media to each.

8. After 10 min, aspirate dispase from the well and wash 3 × with pre-warmed DMEM/F12 media

- First wash with 2 mL, second wash with 1.5 mL and third wash with 1 mL of DMEM/F12 media.

9. Aspirate DMEM/F12 and add 3.5 mL mTSER1 media to each well for routine passaging. Keep in mind that each well will be used to seed a new 6-well plate, so one 6-well plate can be used to generate six additional 6-well plates (1:6 passaging ratio).

10. Use scraper to scrape the bottom of every well, making sure to scrape off everything on the plate.

11. Pipette cells and media vigorously 3–5 times using a 5 mL serological pipette to break up the colonies. Place tip of the pipette to the bottom of the well at a 90° angle to use shear force to break up the colonies.

12. Check under microscope to verify colony size (Figure 2-1A). Pipette again if needed. Use pipette to distribute/wash the bottom of the well to evenly distribute the colonies.

13. Split 1:6 by adding 0.5 mL of stem cells in mTeSR1 to each well of the Matrigel-coated 6-well plate.

14. Shake the plate back-to-back and side-to-side (~ 3 times) to evenly distribute the colonies and then place in the incubator.

15. Change media on the stem cells with fresh mTeSR every day by aspirating old medium and adding 1.5 mL warm mTeSR to each well of the 6-well plate:

- It is common to see some cell death (floating cells) the day after passaging (Figure 2-1B). Shake plate to lift dead cells from bottom before adding fresh media.

Note: For routine stem cell culture, cells will typically be ready for passaging 4–5 days after the last passage (Figure 2-1E).

Preparing and Plating Stem Cells for Differentiation

1. Prepare media stocks for Days 1–3 of differentiation.

- Day 1 basal Media (no dFBS): add 5 mL Pen/Strep (1%) to 500 mL RPMI 1640 media

- Day 2 basal Media (0.2% dFBS): add 1 mL Hyclone dFBS and 5 mL Pen/Strep (1%) to 500 mL RPMI 1640 500 mL media

- Day 3 basal Media (2% dFBS): add 10 mL Hyclone dFBS and 5 mL Pen/Strep (1%) to 500 mL RPMI 1640 media

Notes:

- Media can be prepared in advance for 500 mL stocks which can be stored at 4 °C for a few weeks to a month.

- Day 3 media is used throughout hindgut differentiation; therefore, it will be depleted more quickly relative to the Days 1–2 media.

2. Start with a 6-well plate of stem cells that are ready to passage (see previous section).

3. When cells are ready for passaging, coat a 24-well plate with Matrigel. Dilute GFR Matrigel to 100 µg/mL using cold DMEM/F12 (12 mL per 24-well plate), and coat a 24-well plate with 0.5 mL of cold Matrigel (cat. no. 354230) per well for differentiation.

4. Coat plate for at least 1 hour at room temperature prior to passaging

Matrigel-coated plates can be wrapped in parafilm and stored at 4 °C for up to 1 week for later use.

5. Aspirate Matrigel from each well. To ensure that the plate does not dry out prior to adding cells, it is best to aspirate the Matrigel during the dispase incubation step or after the cells have been washed with DMEM/F12.

6. Passage stem cells using dispase as described above (see steps 5–12 of the previous section). One well from the 6-well plate will be used to generate 6 wells of the 24-well plate. After dispase treatment and scraping/trituration of stem cell colonies, ensure stem cells/media are well mixed and passage 0.5 mL of stem cells/mTesR1 per well of the 24-well plate using a 5 mL serological pipette. For a complete 24-well plate, repeat using additional wells from the 6-well plate. A total of 4 wells from the 6-well plate will be used to seed an entire 24-well plate.

- Ensure that cells are well mixed before transferring to the 24-well plate so that each well receives approximately the same number of triturated pieces of stem cell colonies for efficient differentiation. Tap on the side of the 24-well plate several times to distribute colonies evenly. Check plate under a microscope before returning to the incubator to ensure that cells are evenly distributed throughout the well.

7. Let the plate sit in the incubator overnight. On the day after passaging, aspirate old media and add fresh mTeSR1 (0.5 mL per well in a 24-well plate). It is normal to see some cell death and floating debris.

8. On the second day after passaging, check cell confluence and colony size under a microscope. The plate should be around 70–80% confluent before starting endoderm differentiation (Figure 2-2A). Correct colony size and well confluency will typically arise 2 days after passaging, but the plate should be monitored closely to start endoderm differentiation at the correct time. Note: Plating density and colony size are major sources of variation in the directed differentiation process, and will lead to variable endoderm differentiation and spheroid production. Colony plating size (after trituration)

and density prior to differentiation should be optimized for each new hESC or iPSC line. For example, instead of a passage ratio of 1 well of a 6-well plate into 6 wells of a 24-well plate (1:6 ratio), ratios of 1:3, 1:6, 1:12 can be tested. Similarly, colony size can be tested by varying the amount of trituration prior to plating. Efficient differentiation can be assessed at the end of the endoderm differentiation stage (see next section) by immunostaining for FOXA2/SOX17 as previously described in detail [23, 24].

Human Definitive Endoderm Differentiation

9. Thaw one 37 µL aliquot of Activin-A (100 µg/mL stock).

10. Prepare Day 1 differentiation medium by adding 12 µL Activin-A to 12 mL of Day 1 basal media (100 ng/mL) in a 15 mL conical tube. The remainder of the aliquot can be stored in the 4 °C for the 3 days that Activin-A is needed.

11. Aspirate mTeSR1 and add 0.5 mL/well of warm Day 1 differentiation media in the 24-well plate. Leave the plate in the incubator for 24 h.

- Note the time that endoderm differentiation is started. It is important to change media at approximately the same time every day during endoderm differentiation.

12. On the second day of endoderm differentiation, check plate under microscope.

Note: It is normal to see cell death after 24 h of Activin-A because the media contains no serum. Attached cells can be best viewed after changing media, or using an inverted microscope (Figure 2-2B).

13. Prepare Day 2 differentiation medium by adding 12 µL Activin-A to 12 mL of Day 2 basal media (100 ng/mL).

14. Replace Day 1 differentiation media with warm Day 2 differentiation media (0.5 mL per well) approximately 24 h after Day 1 differentiation media was added. Leave the plate in the incubator for 24 h.

15. On the third day of endoderm differentiation, check plate under the microscope. Note: It is normal to see cell death (Figure 2-2C).

16. Prepare Day 3 differentiation medium by adding 12 µL Activin-A to 12 mL of Day 3 basal media (100 ng/mL).

17. Replace Day 2 differentiation media with warm Day 3 differentiation media (0.5 mL per well) approximately 24 h after Day 2 differentiation media was added. Leave the plate in the incubator for 24 h.

18. After 24 h (72 total hours of differentiation), check the plate under a microscope. Note: It is normal to see a slight amount of cell death. At this point the cells should have formed a flat monolayer (Figure 2-2D). Proceed to hindgut differentiation.

Hindgut Differentiation

19. Prepare hindgut differentiation medium: 500 ng/mL FGF4 (1:1000 dilution) and 2 µM CHIR99021 (1:5000 dilution) in Day 3 basal medium. For a 50 mL aliquot, add 50 µL FGF4 and 10 µL CHIR99021 to 50 mL of Day 3 basal medium. Note: The original intestinal organoid protocol utilized WNT3A rather than the small molecule CHIR99021 to activate Wnt signaling. Using CHIR99021 results in a significant cost savings compared to purchasing commercially available WNT3A. However, differences in the organization of epithelial and mesenchymal cells within the resulting spheroids have been noted when comparing CHIR99021 and WNT3A [25]. In our hands, either

molecule will generate hindgut spheroids that mature into HIOs that are indistinguishable.

20. Aspirate media and replace with warm hindgut differentiation media (0.5 mL/well) approximately 24 h after Day 3 endoderm differentiation media was added. Leave the plate in the incubator for 24 h. This step marks Day 1 of hindgut differentiation.

21. On Days 2–5 of hindgut differentiation, continue changing media every day and replace with fresh hindgut differentiation medium (0.5 mL/well). After the first day it is no longer as important to change media at the same time each day. During this process the monolayer should begin forming 3D structures (Figure 2-2E–J). Spheroids should emerge and can be collected beginning on the fifth day of treatment with FGF4/CHIR.

- Note: Spheroids collected on fifth day of differentiation are considered "Day 4 spheroids" as they result from the media change on Day 4 of FGF4/CHIR hindgut differentiation. Spheroids are typically collected between Days 5–7, resulting in Days 4–6 spheroids. Spheroids can be collected on later days as well, but will become patterned into distal rather than proximal small intestine.

Spheroid Collection

22. Prepare "Mini Gut" basal medium:

- 500 mL Advanced DMEM/F1
- 10 mL B27 supplement (1 ×)
- 5 mL GlutaMAX (1 ×)
- 5 mL Pen/Strep (100 U m−L− 1 penicillin; 100 µg mlL− 1 streptomycin)
- 7.8 mL HEPES buffer (15 mM)

Note: Mini Gut medium will last for at least 1 month at 4 °C.

23. Prepare EGF, Noggin, R-spondin (ENR) HIO growth medium

- 95 mL Mini Gut basal medium

- 5 mL R-spondin1-Fc conditioned medium (5%)

- 100 µL EGF (100 ng/mL)

- 100 µL purified Noggin-Fc (100 ng/mL)

Note: alternatively, ENR HIO growth media can be made with commercially purchased Noggin and R-Spondin. Prepare 100 mL MiniGut with 100 µL Recombinant Human R-spondin1 (500 ng/mL), 100 µL Recombinant Human Noggin (100 ng/mL) and 100 µL EGF (100 ng/mL). See materials section for product information.

24. On the fifth day of the differentiation, 3D hindgut spheroids (these are considered "Day 4 spheroids") should begin budding off from the monolayer and will be floating in the media (Figure 2-2H). Use a 1000 µL pipette tip to collect the floating spheroids from each well and transfer to 1.5 mL Eppendorf tubes (around 2–3 wells per tube). Alternatively, spheroids can be collected in a 15 mL conical tube but will take additional time to settle to the bottom.

- Use a stereoscope to ensure that all spheroids are collected. Avoid touching the bottom of the well and disturbing the monolayer. Optional: use the same media to wash the well and collect missed spheroids.

25. After collecting media containing spheroids from all wells, add fresh FGF4/CHIR differentiation media to each well (0.5 mL/well). Spheroid collection should be completed quickly (< 8 min) to avoid drying out the wells. Alternatively, collect 6 wells and add fresh medium back, repeat for the remaining wells.

26. Wait 10–30 min for the spheroids to settle to the bottom of the Eppendorf tubes.

27. After the spheroids have settled, collect spheroids from the bottom of each tube using a P-200 (it is not necessary to aspirate the excess media; collect spheroids from the bottom of the tube while collecting as little media as possible) and combine all spheroids into one new Eppendorf tube.

- To ensure collection of all of the spheroids, optionally wait another 10–30 min after the first collection and then collect any spheroids that were missed the first time to combine with the previously collected spheroids.

28. Assess the number of spheroids collected to determine the desired Matrigel seeding density. Counting the total number of spheroids is not necessary; an approximation by eye will suffice. Typically, about 100–200 spheroids are seeded per 50 µL droplet of Matrigel.

29. Wait 10–30 min to allow spheroids to settle into the bottom of the combined Eppendorf tube.

30. Remove as much media as possible from the Eppendorf tube containing spheroids using a P-1000 pipette tip.

31. Add the desired amount of Matrigel based on the number of spheroids. For example, if seeding an entire 24-well plate with 50 µL per well, 1200 µL are required. Gently pipette up and down using a wide bore P-1000 pipette tip (this can be achieved by cutting the end with a sterile scalpel or scissors) to obtain a homogenous mixture.

- Important: Matrigel must be kept on ice until droplets are formed in the 24-well plate. Place Matrigel and Eppendorf tubes containing spheroids on ice to prevent the Matrigel from solidifying.

- A lower density of spheroids in each droplet of Matrigel is preferred over a high density. If spheroids are seeded too densely, they will clump during HIO growth/development.

32. Collect 150 µL of Matrigel/spheroid mixture with a 200 µL pipette and divide the volume between six wells (1 row of a 24-well dish, with roughly 25 µL per droplet). Carefully place the Matrigel droplet in the center of the well. Work quickly as Matrigel/spheroids will begin to solidify as they warm up. Collect another 150 µL of Matrigel/spheroid mixture and distribute evenly on top of the existing six Matrigel droplets to form complete droplets of approximately 50 µL/well. This helps to maintain even distribution of spheroids between wells, and avoid spheroids settling to the bottom of the gel.

33. Repeat for remaining spheroids, until they have all been distributed.

34. Label the plates with:

- Cell line and passage number

- Day spheroids were collected (date)

Day of spheroid generation (d4, d5, or d6 spheroids)—this is important as studies show that spheroids collected at later time points (beyond Day 7) are patterned into more distal intestine [24].

35. Place plate in the incubator and wait 15–30 min for the Matrigel to solidify.

36. Add warm or room temperature ENR HIO growth media to spheroids encapsulated in Matrigel (500 µL/well).

37. On Days 6 and 7 of hindgut differentiation (Figure 2-2I and J), repeat steps 22–33 to collect Days 5 and 6 spheroids. Day 5 (Figure 2-2I) is typically the day of highest spheroid yield. After collecting Day 6 spheroids on Day 7 the plate can be discarded.

HIO Maintenance

38. Spheroids will grow slowly over the first few days in culture (Figure 2-3). Change media every 5–7 days depending on the condition of the media. Once spheroids start growing more rapidly, typically media changes are done every 3–4 days.

Spheroids will remain in the same Matrigel droplet for around 2 weeks until they begin to grow/expand into one another, spread onto the bottom of the plate, or accumulate debris in the lumen (Figure 2-4A). At this point, the HIOs will need to be passaged. Proceed to HIO passaging.

HIO Passaging

39. Using a wide bore P-1000 pipette tip (this can be achieved by cutting the end with a sterile scalpel or scissors), dislodge the Matrigel droplets from the dish and transfer to a 15 cm Petri dish. Matrigel may break into pieces during the transfer. Pipetting Matrigel/HIO several times may help to dislodge HIOs from the Matrigel. Add a volume (~ 5–10 mL) of DMEM/F12 to the dish so that HIOs do not dry out:

- Use a sterile scalpel and 1 mL syringe with an attached 30G × 1 needle to remove excess Matrigel from HIOs.

- Excess mesenchyme can also be removed from the HIOs at this time, but this is not a necessary step. Refer to Figure 2-4B—the inner epithelium of the HIO is

60

outlined in green, and is surrounded by mesenchyme. The loose outer

mesenchyme that is crawling away from the epithelium (outside of the red dotted

line) can be cut away.

- If HIOs are large and accumulating debris in the center as evidenced by a dark
  color (Figure 2-4A), cut the HIO in half or poke a hole into the center using the
  needle to release debris.

- Recommended Technique: Hold HIOs in place by piercing the HIO with the
  syringe/needle using your non-dominant hand. Using your dominant hand and a
  scalpel, cut away the mesenchyme and separate the HIOs that may have grown
  together. Large HIOs can also be cut in half.

40. Using a wide bore P-1000 pipette tip, collect and transfer HIOs to a new Petri dish

with fresh DMEM/F12 to wash away residual Matrigel and debris.

41. Collect HIOs in a 1.5 mL Eppendorf tube.

42. Re-embed in Matrigel following the protocol for embedding spheroids. HIOs should

be re-plated with approximately 10 HIOs per 50 µL per droplet.

43. Change media to fresh ENR every 3–4 days depending on media color. After

passaging, HIOs should have minimal accumulation in the lumen. Within a few days of

culture, the mesenchyme will begin to grow and spread (Figure 2-4C).

HIOs are typically considered mature for experimentation or analysis after

approximately 4 weeks in culture but can be maintained for over 60 days or more if

passaged as needed.

2.5 Application of HIOs, and Variations on HIO Culture

2.5.1 Culturing HIOs in Alginate Hydrogels

The gold standard for most organoid systems, including HIOs described here, includes culture in basement membrane-derived ECM products such as Matrigel. This reliance on Matrigel originates from the development of epithelial-only intestinal organoids (enteroids) which require support from the basement membrane to maintain epithelial cell viability. Matrigel provides both structural and biochemical support in the form of ECM proteins and a number of growth factors. While Matrigel is effective in supporting organoid growth, it is not an ideal matrix as it has a poorly defined composition with batch-to-batch variability, is difficult to modulate, exhibits limited potential for downstream clinical translation due to its xenogeneic source, and is cost-prohibitive for many applications.

These limitations have prompted investigations into defined hydrogels for organoid culture. Hydrogels are easily modulated with adhesive and degradable properties to match those exhibited in Matrigel, making them an ideal material for organoid culture. However, in the case of HIOs, we have shown that the mesenchyme surrounding the epithelium removes the need for a supportive ECM and that HIOs can be cultured in a bio-inert hydrogel, alginate [26]. HIO culture in alginate will be described in more detail in Chapter 3. Hindgut spheroids can be embedded directly into alginate hydrogels upon collection rather than embedding into Matrigel droplets. The resulting alginate-grown HIOs are nearly identical to Matrigel-grown HIOs both *in vitro* and after transplantation. This technique is significantly more cost-effective than Matrigel culture, and alginate-grown HIOs require less maintenance as the mesenchyme is unable to

62

invade the surrounding matrix. However, a lower percentage of spheroids will mature

into organoids when cultured in alginate as compared to Matrigel. Nonetheless, this

represents a cost-effective and well-defined alternative to Matrigel that avoids the

influence of poorly defined matrix components and growth factors.

Materials, Equipment and Reagents

1. 24-Well cell culture plate.

2. Hindgut spheroids as described above.

3. Microcentrifuge tubes.

4. 1 × cell-culture grade PBS.

5. Low-viscosity sodium alginate powder (Alfa Aesar, B25266).

6. Calcium chloride (Sigma-Aldrich, 449709).

7. Heating block.

Alginate Cleaning Protocol (Optional)

Un-purified alginate may exhibit endotoxin activity, which may affect downstream

experimental applications. We have not experienced significant decreases in HIO

viability using un-purified alginate as compared to purified alginate. This protocol is an

optional step to reduce endotoxin activity within the alginate.

1. Prepare 1% alginate solution in diH2O.

2. Dialyze with tubing that has 3500 Da molecular weight cutoff in diH2O for 3 days with

3–4 water changes at 4 °C.

3. Collect alginate solution in a beaker, add 5 g activated carbon (50–200 mesh) per 1 L

alginate solution, mix for 30 min, and then allow carbon to settle for 5 min.

4. Filter through a sterile bottle-top filter (0.22 mm) after pre-wetting with 5 mL diH2O.

5. Place sterile alginate solution in a new bottle that has the filter on top (weigh

beforehand if you want to know the alginate weight after drying).

6. Place sample in freezer overnight (− 80 °C).

7. Place samples on a lyophilizer until dry. Open attachment slowly not to break a filter

membrane.

Alginate Preparation

1. Prepare 2% (w/v) CaCl2 solution by dissolving CaCl2 in diH2O. Autoclave. This

solution is stable, so relatively large amounts can be prepared in advance.

2. Dissolve alginate in 1 × tissue culture grade PBS to the desired concentration in a

microcentrifuge tube. We have observed the best results in 1% alginate. Alginate may

degrade over time so prepare small volumes (1–2 mL) that will be used within 2 weeks

for best results.

3. Heat alginate solution to 98 °C on a heating block for 30 min. Heating helps to fully

dissolve the alginate and may promote sterility.

- Note: Alginate can be autoclaved or filtered to ensure sterility. However,

  autoclaving can decrease mechanical properties and filtration is difficult due to

  the viscosity of the solution. We have never observed contamination in heated

  alginate when cultured in media containing pen/strep.

4. Allow alginate to cool and then pipette up and down with a cut P-1000 pipette tip to

mix. If bubbles occur, briefly centrifuge to remove bubbles before mixing with spheroids.

- Alginate is viscous so cut pipette tips are more effective.

5. Collect hindgut spheroids in an Eppendorf tube as if embedding in Matrigel and remove as much media as possible.

6. Add appropriate volume of alginate solution to the tube containing spheroids for a density of approximately 50 spheroids per 45 μL alginate gel.

7. Add 5 μL droplets of 2% CaCl2 to the center of each well of a 24-well plate (Figure 2-1F). If the calcium droplets spread out, the alginate gel will not form properly.

8. Pipette up and down to evenly distribute spheroids in the alginate solution.

9. Using a cut P-200 pipette tip, transfer 45 μL of alginate with spheroids to one of the 5 μL droplets (Figure 2-1G).

- Alginate will gel quickly upon contact with calcium. For best results pipette the alginate with spheroids directly onto the calcium droplet without touching.

10. Repeat for the remainder of the spheroids.

11. Let the plate sit at room temperature for approximately 10 min without disturbing the gels to allow the alginate to polymerize (Figure 2-1H). Transfer to the 37 °C incubator for another 10 min to ensure the gels have solidified.

12. Add 500 μL of warm ENR to the top of each gel.

- Note: Alginate gels will typically float in the media and do not stick to the bottom of the plate like Matrigel does. Push gels down with a pipette tip to ensure that they are covered by media.

13. Change media as necessary. As alginate does not stick to the plate, do not aspirate media from the wells to avoid aspirating the gels. Remove media one well at a time using a P-1000.

HIO Maintenance in Alginate Hydrogels

14. HIOs cultured in alginate do not exhibit the mesenchymal spreading observed in Matrigel HIOs. However, they can accumulate debris in the center as well as dislodge from the alginate gels. Alginate HIOs can be passaged in a similar way as Matrigel HIOs by cutting away the alginate from the HIOs and cutting the HIOs in half as necessary.

2.5.2 Protocol to Isolate HIO-Derived Epithelium (HdE) or Mesenchyme from HIOs

An advantage of HIOs as a model system is that they contain an inner epithelium and outer mesenchyme with an architecture that mimics the architecture of the native intestine. However, in some cases it may be advantageous to study the epithelium and mesenchyme in separate contexts. HIO-derived epithelium (HdEs [27]), provide an intestinal epithelial model system derived from human pluripotent stem cells rather than relying on donor tissue. HdEs can be cultured separately to study the epithelium without extraneous effects from the mesenchyme. Alternatively, HdEs can be re-combined with HIO-derived mesenchyme using hanging drop co-culture methods to study the effects of mesenchymal cells on the epithelium.

Additional Equipment and Reagents

- Advanced Dulbecco's modified Eagle medium/F12 (ThermoFisher Scientific Cat. no. 12634010).
- L-WRN cell line conditioned media (ATCC CRL-3276, see Miyoshi & Stappenbeck, 2013 [28]).

- Collagen Type I (Sigma C55533-5MG).

See 'Materials, equipment and reagents' section for product information for materials common to other protocols in this chapter.

Generation of LWRN Complete Media

Note: Since the mesenchyme provides support for the epithelium, culture of the epithelium alone relies on a more complex media that possess additional factors. A detailed protocol for generating media for human epithelium-only organoids (also called enteroids) has been published [29], and is briefly outlined below.

1. Prepare 2 × basal media: 214 mL advanced Dulbecco's modified Eagle medium/F12, 5 mL GlutaMAX (Gibco, Japan) (100 ×, 200 mmol/L), 5 mL HEPES (100 ×, 1 mol/L), 5 mL N2 supplement (100 ×), 10 mL B27 supplement (50 ×), 5 mL penicillin/streptomycin (100 ×), 1 mL N-acetylcystine (500 mmol/L), and 5 mL nicotinamide (1 mol/L).

2. Combine basal media with conditioned media from L-WRNA cells containing Wnt3a, Rspondin3, and Noggin at a 1:1 ratio.

3. For the first 3 days of enteroid culture, prepare LWRN complete media containing TZV (2.5 µmol/L), SB431542 (100 nmol/L), and CHIR99021 (4 µmol/L).

Isolation of Epithelium and Mesenchyme from HIOs

1. Collect HIOs by dislodging them from Matrigel using a cut P-1000 pipette tip and transfer to a Petri dish. Try to get rid of Matrigel by pipetting up and down using the cut pipette tip.

2. Fill a Petri dish or one well of a 6-well tissue culture plate with 3 mL cold dispase and transfer HIOs to this dish.

3. Incubate HIOs in dispase for 30 min on ice.

4. After 30 min, remove as much dispase as possible and replace it with 3–5 mL of 100% FBS.

5. Incubate in FBS for 15 min on ice.

6. Add an equal volume (3–5 mL) of Advanced DMEM/F12 to the dish. Pipette up and down to break up the tissue. At this point the epithelium and mesenchyme can be picked up separately—the epithelium should settle to the bottom in fragments.

Mesenchyme Culture from HIOs

7. Prepare 20 µg Collagen Type I per cm2 (Sigma C55533-5MG) in 0.01 N acetic acid.

8. Coat a tissue culture plate with collagen for 2 h at 37 °C.

9. Plate can be used right away or stored at 4 °C.

10. Collect the HIO mesenchyme in a 15 mL conical tube.

11. Add 3–5 mL TrypLE to the tube.

12. Dissociate mesenchymal cells for 5–10 min at 37 °C. It is okay if cells are not fully dissociated.

13. Centrifuge for 5 min at 300 g.

14. Resuspend pelleted mesenchymal cells in ENR medium and culture on collagen 1 coated cell culture plate.

Generation of Epithelium-Only Organoids from HIOs (HdEs)

15. Collect epithelial fragments from the bottom of the dish (step 6) using a P-200 pipette. This is typically done by manually selecting epithelial pieces that have dissociated from the larger tissue pieces under a stereomicroscope in a Labconco horizontal clean bench.

16. Transfer epithelial pieces into a fresh Petri dish containing Advanced DMEM/F12 to rinse the tissue.

17. Transfer the epithelium and media into a 1.5 mL Eppendorf tube on ice and let the epithelium settle by gravity sedimentation to the bottom of the tube.

18. After the epithelium has settled to the bottom of the tube, gently remove the media with a P-200 pipette.

19. Add 55 µL ice cold Matrigel to the tube for each new culture well that you intend to seed and mix with epithelium.

20. Plate the Matrigel with epithelium in 50 µL droplets, one per well, in a 24-well plate.

21. Allow Matrigel to solidify in the hood for 3–5 min and transfer to 37 °C incubator.

22. Allow Matrigel to solidify for 15–30 min at 37 °C.

23. After the Matrigel has solidified, add 500 µL LWRN Complete media with TZV, SB431442, 4 µM CHIR, and 10 µM Y27632 media to each well.

24. Feed the cultures daily for the first 3 days with LWRN Complete media with TZV, SB431542 and CHIRON (4 µM).

25. After 3 days, feed every other day with LWRN complete media. It may take 1–2 weeks to establish enteroids.

Tissue Freezing and Storage

For short-term transportation of differentiated HIOs, including overnight shipment to another laboratory, we recommend manually removing the tissues from embedded Matrigel and transferring to a sterile 15 mL conical tube. Re-embed HIOs in an appropriate volume of Matrigel in the 15 mL tube such that they will not spread into each other during shipment. Add 37 °C ENR media. Seal the tube and ship at room temperature in a well-insulated container. Organoids shipped in this way will remain viable for up to 48 h providing that internal temperatures do not exceed 37 °C or fall below 4 °C.

For long-term storage, HIO cultures can be suspended in an organoid freezing media consisting of ENR + 20% DMSO and transferred to a "Mr. Frosty" container overnight at − 80 °C before transfer to liquid N2 according to the manufacturer's instructions.

Microbial Co-Culture

Among the unique applications of 3D human intestinal organoid tissues is the ability to form stable and prolonged symbioses with live microbes [30]. Multiple groups have demonstrated the microinjection of live microbial cultures into the luminal compartment of both tissue-derived and pluripotent stem cell derived human intestinal organoids [30-35]. At present, microinjection of intestinal organoids is a notably low-throughput technique, although recent protocols have attempted to standardize and simplify the approach and tools [33] and one report has demonstrated the use of automated systems to identify organoids tissues in culture, perform a precision microinjection, and screen the resulting co-cultures using advanced AI-guided imaging

70

[36]. Several groups have opted for an alternative approach of adapting 3D intestinal organoid cultures to 2-dimensional Transwell® scaffolds [37, 38], which allows for highly reproducible and high-throughput access to both the luminal and basolateral compartments but sacrifices the hypoxic and mucus rich microenvironment present in the luminal compartment of 3D organoids tissues [30]. Epithelium isolated from pluripotent stem-cell derived human intestinal organoids as described above can be readily adapted to 2D [30]. Emerging technologies are seeking to engineer luminal microenvironments that more closely mimic the native intestinal niche in these 2D Transwell® systems [39, 40]. At present, one of the principle advantages of pluripotent stem cell derived intestinal organoid systems over other in vitro co-culture systems is the ability to form long-term stable symbioses with commensal microbes [30]. See Capeling et al. 2020 for a protocol describing preparations specific to microinjection of live microbes and their maintenance in human intestinal organoid co-cultures [41].

2.6 Pros and Cons of Pluripotent Stem Cell Derived Intestinal Organoids

Pros	Cons
HIOs form a luminal microenvironment that can harbor live microorganisms	HIOs have an enclosed epithelial lumen, making it difficult to access the apical epithelial surface for experimentation
HIOs model early stages of human intestinal development including co-	HIOs are subject to some heterogeneity both between batches and within one batch

development of epithelium and mesenchyme	
The combination of epithelium and mesenchyme enables HIOs to be cultured in more defined, bio-inert matrices	HIOs are currently not cost-effective for large scale-up
HIOs can be transplanted into immunocompromised mice to generate more mature intestinal tissue	HIOs lack key intestinal cell types (vasculature, neuronal cells, lymphatic and immune cells) and are immature prior to transplantation

2.7 Troubleshooting and Optimization

Problem: No spheroids are formed

Solution:

- Pay close attention to the starting condition of the cells prior to endoderm induction—too low or too high density can result in no spheroid formation
- Check all reagents for integrity and ensure that proper doses and timing are applied
- Restart cultures with early passage PSCs
- Verify expression of intestinal transcription factors CDX2, KLF5, or SOX9

Problem: 3D organoids are small, dense masses even after many days in culture

Solution:

- Reduce the density of spheroid cultures and separate small 3D cysts from other tissues at the earliest possible time

- Remove as much excess Matrigel as possible when re-plating dense spheroid cultures

- Additional 3D cysts are unlikely to develop after ~ 6 weeks in culture

- In some cases, 3D cyst formation may be inefficient and it may be necessary to culture a large excess of spheroids to generate a small number of large 3D cysts suitable for microinjection applications. This may vary greatly between batches and may be dependent on the number of culture passages applied to the pluripotent stem cell progenitor cultures

2.8 Related Techniques

As with any emerging model system, the full range of capabilities and experimental applications for pluripotent stem cell derived human intestinal organoid cultures remains to be explored. Modifications to the protocol presented here have resulted in the generation of other hindgut lineage tissues, including gastric organoids, lung organoids [42-45], and colonic organoids [46, 47]. Recently, methods for generating epithelium-only human intestinal organoids from induced pluripotent stem cell progenitors were also described [48]. Many of the principles described in the present protocol will also apply to those tissues and interested readers are advised to carefully review those manuscripts for modifications to the growth factor regimen described above.

2.9 Ethical Considerations and Standards

Pluripotent stem cell derived organoids may be generated from embryonic stem cells or induced pluripotent stem cells, with either source producing comparable end tissues [4]. Embryonic stems cells have tremendous proliferative potential and do not require genetic reprogramming. However, working with embryonic stem cells may present legal or ethical limitations in some jurisdictions or institutions [49]. In general, use of embryonic stem cells lines in the United States is limited to only NIH-approved cell lines. Investigators are prevented by law from using US Government funds in research that may cause harm to a human embryo. This effectively restricts the generation of new ES cell lines to non-federally funded research. By contrast, induced pluripotent stem cells are typically generated from non-embryonic human tissues such as skin fibroblasts. Although the specific restrictions regarding the use of embryonic cells generally do not apply to induced pluripotent stem cells, human subjects' protections may apply to the source material. The collection of human tissues for the generation of induced pluripotent stem cells usually requires Informed Consent from donors and IRB oversight. In particular, Informed Consent must address the risks associated with the generation of novel induced pluripotent stem cells lines which may be propagated in perpetuity and/or shared with other labs as a biological resource or as genetic sequence data. These risks include the risk of exposing the inherent unique genetic identifiers contained in DNA. These identifiers could potentially be associated with the human subject donors by medical researchers or public DNA profiling services, resulting in a loss of privacy and possibly other unforeseen risks.

2.10 Conclusions

The procedures described in this Chapter will result in the generation of 3D intestinal tissue derived from pluripotent stem cells. For the sake of convenience, we have also included a basic overview of our procedures for pluripotent stem cell culture and maintenance. For a more detailed discussion of that technique, thorough protocols are highly recommended [50, 51]. We have also presented several useful adjunct protocols for modification of the intestinal organoid differentiation system, including the alternate method of substituting defined alginate matrices for Matrigel, methods for tissue freezing and long-term storage, and methods for sub-culturing the separate epithelial and mesenchymal populations produced during directed differentiation. Finally, we have included a protocol for the generation of intestinal organoid and microbial co-cultures, a key application of pluripotent stem cell derived human intestinal organoids. Application of these adjunct protocols may require modification depending upon the specific experimental requirements and laboratory setup.

2.11 Figures
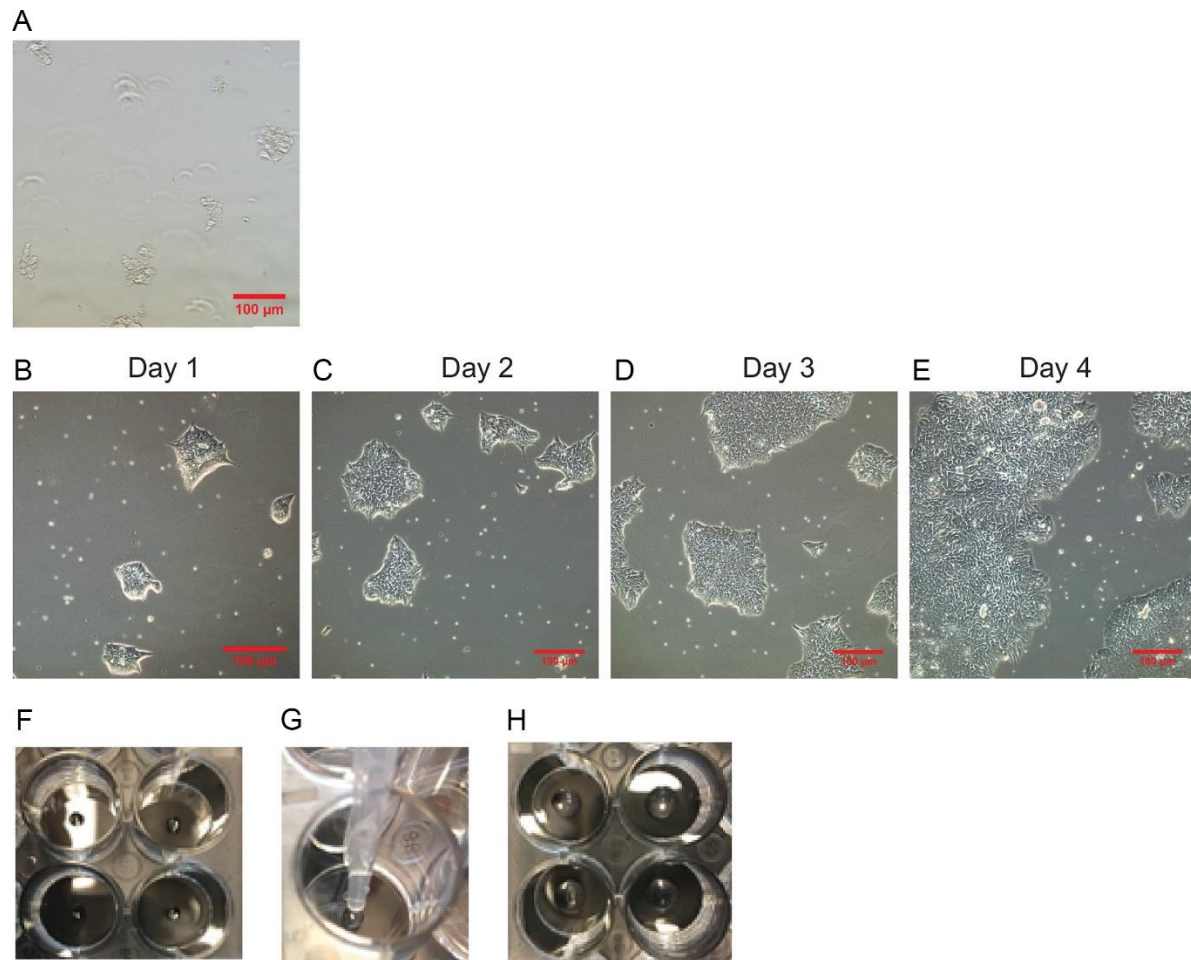
Figure 2-1. Stem Cell Culture and HIO Embedding in Alginate.

(A) Stem cell colonies immediately after passaging. Scale bar = 100 µm. (B–E) Representative images of hPSCs on days 1–4 after passaging. Cell colonies are small on Day 1 with dead cells floating. By Day 4, the colonies have expanded in size and are ready to be passaged. Scale bar = 100 µm. (F–H) Alginate droplets for HIO culture. Spheroids or HIOs can be embedded in alginate hydrogels as a replacement to Matrigel by depositing 5 µL droplets of CaCl2 onto the tissue culture plate and adding 45 µL of alginate directly onto the calcium.
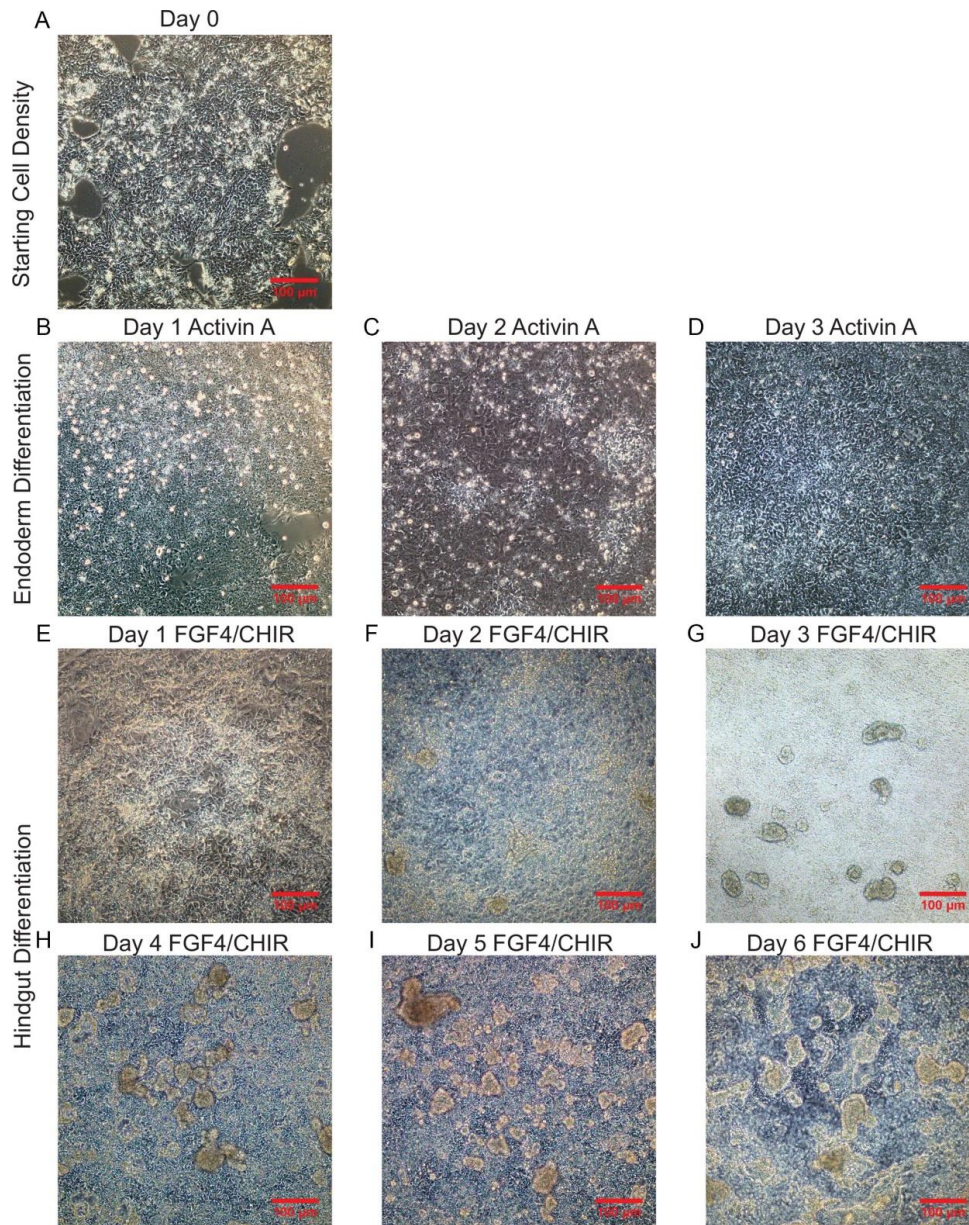
Figure 2-2. hPSCs are Differentiated into Hindgut Spheroids.

(A) hPSCs in a 24-well plate, cultured in mTeSR1 2 days after passaging. Image shown is representative of an ideal starting cell density immediately prior to switching to endoderm differentiation conditions. Scale bar = 100 μm. (B–D) Representative images of hPSCs treated with Activin A throughout three-day definitive endoderm induction. Images depict cells on the day after initial treatment, where Day 1 Activin A represents the cells after treatment with Activin A for 1 day, etc. Scale bar = 100 μm. (F–J) Representative images of cells throughout hindgut differentiation into spheroids. Images depict cells on the day after initial treatment, where Day 1 FGF4/CHIR represents the cells after treatment with FGF4/CHIR for 1 day, etc. Scale bar = 100 μm.
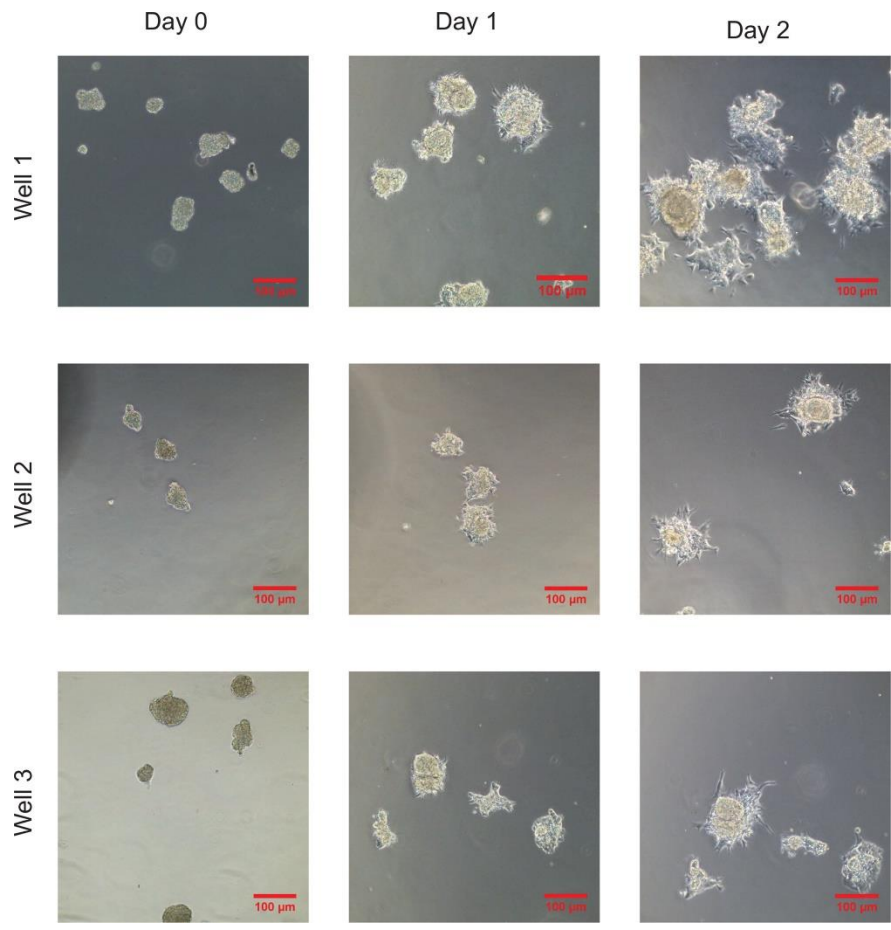
Figure 2-3. Hindgut Spheroids Grow and Spread in Matrigel

Hindgut spheroids embedded in Matrigel droplets for 3 days. Spheroids increase in size and develop an expanded mesenchyme in culture. Scale bar = 100 µm.
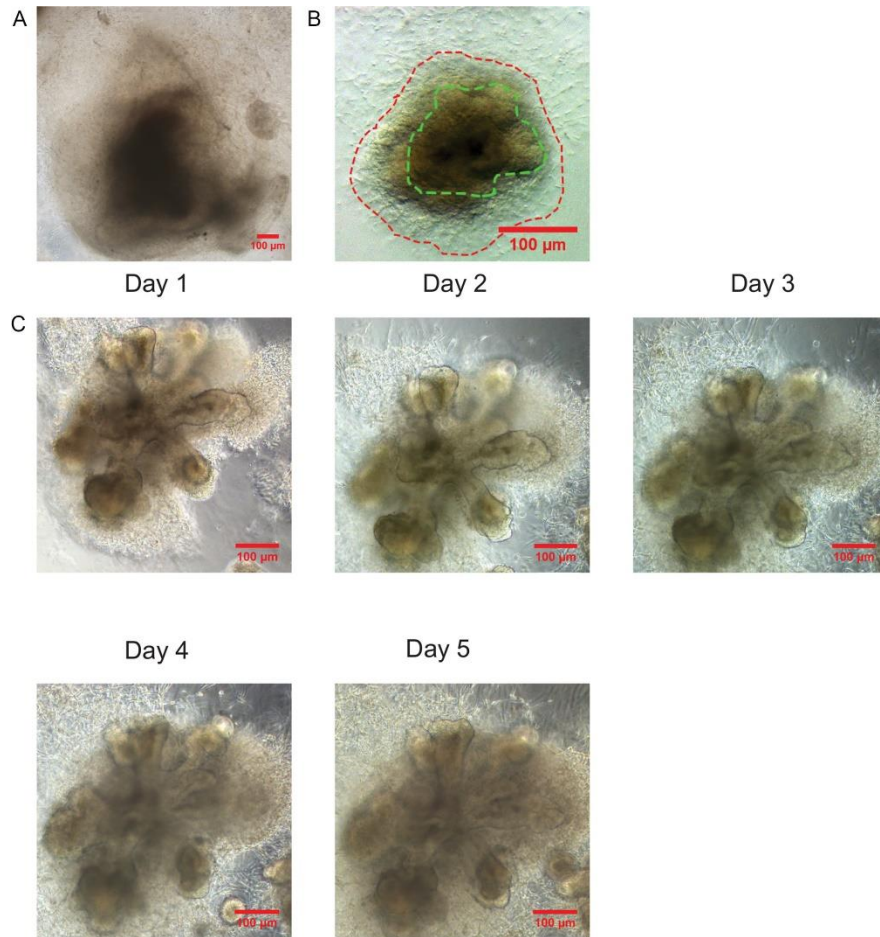
Figure 2-4. HIOs Require Passaging for Continued Maintenance.

(A) Representative image of an HIO prior to passaging. This HIO has developed a dark, debris-filled lumen as well as an outer mesenchyme that is spreading into nearby HIOs. Passaging is required to release luminal contents and cut away the spreading mesenchyme. Scale bar = 100 μm. (B) Outlined epithelium and mesenchyme in an HIO. The epithelium is on the inside of the HIO (outlined in green) and is surrounded by mesenchyme. The loose, outer mesenchyme outside of the red dotted line can be cut away during passaging. Scale bar = 100 μm. (C) An HIO after passaging depicted for 5 days. Immediately after passaging the lumen is not full of debris and the mesenchyme is maintained to the immediate vicinity of the HIOs. By 5 days after passaging, the mesenchyme has begun to spread but the lumen is still relatively light in color, indicating that passaging is not yet required. Scale bar = 100 μm.

2.12 References

1.   Balimane, P.V. and S. Chong, *Cell culture-based models for intestinal permeability: a critique.* Drug Discov Today, 2005. **10**(5): p. 335-343.

2.   Sato, T., et al., *Single Lgr5 stem cells build crypt-villus structures in vitro without a mesenchymal niche.* Nature, 2009. **459**: p. 262-265.

3.   Ootani, A., et al., *Sustained in vitro intestinal epithelial culture within a Wnt-dependent stem cell niche.* Nature Medicine, 2009. **15**(6): p. 701-706.

4.   Spence, J.R., et al., *Directed differentiation of human pluripotent stem cells into intestinal tissue in vitro.* Nature, 2011. **470**(7332): p. 105-109.

5.   Simian, M. and M.J. Bissell, *Organoids: A historical perspective of thinking in three dimensions.* J Cell Biol., 2017. **216**(1): p. 31-40.

6.   Takebe, T. and J.M. Wells, *Organoids by design.* Science, 2019. **364**(6444): p. 956-959.

7.   Dedhia, P.H., et al., *Organoid Models of Human Gastrointestinal Development and Disease.* Gastroenterology, 2016. **150**(5): p. 1098-1112.

8.   Drost, J. and H. Clevers, *Translational applications of adult stem cell-derived organoids.* Development, 2017. **144**(6): p. 968-975.

9.   Bigorgne, A., et al., *TTC7A mutations disrupt intestinal epithelial apicobasal polarity.* Journal of Clinical Investigation, 2014. **124**(1): p. 328-337.

10.   Grabinger, T., et al., *Ex vivo culture of intestinal crypt organoids as a model system for assessing cell death induction in intestinal epithelial cells and enteropathy.* Cell Death & Disease, 2014. **15**.

11.   Hahn, S., et al., *Organoid-based epithelial to mesenchymal transition (OEMT) model: from an intesitnal fibrosis perspective.* Scientific Reports, 2017. **7**.

12.   Wiegerinck, C., et al., *Loss of syntaxin 3 causes variant microvillus inclusion disease.* Gastroenterology, 2014. **147**(1): p. 65-68.

13.   Crespo, M., et al., *Colonic organoids derived from human induced pluripotent stem cells for modeling colorectal cancer and drug testing.* Nature Medicine, 2017. **23**: p. 878-884.

14.   Fujii, M., et al., *A Colorectal Tumor Organoid Library Demonstrates Progressive Loss of Niche Factor Requirements during Tumorigenesis.* Cell Stem Cell, 2016. **18**(6): p. 827-838.

15. Li, X., et al., *Oncogenic transformation of diverse gastrointestinal tissues in primary organoid culture.* Nature MEdicine, 2014. **20**(7): p. 769-777.

16. Nadauld, L., et al., *Metastatic tumor evolution and organoid modeling implicate TGFBR2 as a cancer driver in diffuse gastric cancer.* Genome Biology, 2014. **15**(8): p. 428.

17. Van de Wetering, M., et al., *Prospective derivation of a living organoid biobank of colorectal cancer patients.* Cell, 2015. **161**(4): p. 933-945.

18. Watson, C., et al., *An in vivo model of human small intestine using pluripotent stem cells.* Nature Medicine, 2014. **20**: p. 1310-1314.

19. Yui, S., et al., *Functional engraftment of colon epithelium expanded in vitro from a single adult Lgr5+ stem cell.* Nature Medicine, 2012. **18**(4): p. 618-623.

20. Cruz-Acuna, R., et al., *Synthetic hydrogels for human intestinal organoid generation and colonic wound repair.* Nature Cell Biology, 2017. **19**(11): p. 1326-1335.

21. Fordham, R., et al., *Transplantation of expanded fetal intestinal progenitors contributes to colon regeneration after injury.* Cell Stem Cell, 2013. **13**(6): p. 734-744.

22. Phelan, K. and K.M. May, *Mammalian Cell Tissue Culture Techniques.* Curr Protoc Mol Biol., 2017. **117**: p. A.3F.1-A.3F.23.

23. McCracken, K.W., et al., *Modelling human development and disease in pluripotent stem-cell-derived gastric organoids.* Nature, 2014. **516**(7531): p. 400-404.

24. Tsai, Y.-H., et al., *LGR4 and LGR5 Function Redundantly During Human Endoderm Differentiation.* Cel Mol Gastroenterol Hepatol., 2016. **2**(5): p. 648-662.

25. Arora, N., et al., *A process engineering approach to increase organoid yield.* Development, 2017. **144**: p. 1128-1136.

26. Capeling, M., et al., *Nonadhesive Alginate Hydrogels Support Growth of Pluripotent Stem Cell-Derived Intestinal Organoids.* Stem Cell Reports, 2019. **12**(2): p. 381–394.

27. Finkbeiner, S.R., et al., *Transcriptome-wide Analysis Reveals Hallmarks of Human Intestine Development and Maturation In Vitro and In Vivo.* Stem Cell Reports, 2015. **4**(6): p. 1140-1155.

28. Miyoshi, H. and T.S. Stappenbeck, *In vitro expansion and genetic modification of gastrointestinal stem cells in spheroid culture.* Nat Protoc., 2013. **8**(12): p. 2471-2482.

29. Tsai, Y.-H., et al., *A Method for Cryogenic Preservation of Human Biopsies and Subsequent Organoid Culture.* Cellular and Molecular Gastroenterology and Hepatology, 2018.

30. Hill, D.R., et al., *Bacterial colonization stimulates a complex physiological response in the immature human intestinal epithelium.* eLife, 2017. **6**.

31. Engevik, M.A., et al., *Loss of NHE3 alters gut microbiota composition and influences Bacteroides thetaiotaomicron growth.* Am J Physiol Gastrointest Liver Physiol., 2013. **305**(10): p. G697–G711.

32. Forbester, J.L., et al., *Interaction of Salmonella enterica Serovar Typhimurium with Intestinal Organoids Derived from Human Induced Pluripotent Stem Cells.* Infect Immun., 2015. **83**(7): p. 2926-34.

33. Hill, D.R., et al., *Real-time Measurement of Epithelial Barrier Permeability in Human Intestinal Organoids.* J Vis Exp., 2017. **130**: p. 56960.

34. Leslie, J., et al., *Persistence and toxin production by Clostridium difficile with human intestinal organoids result in disruption of epithelial paracellular barrier function.* Infection and Immunity, 2015. **83**(1).

35. Nickerson, K.P., et al., *Salmonella Typhi Colonization Provokes Extensive Transcriptional Changes Aimed at Evading Host Mucosal Immune Defense During Early Infection of Human Intestinal Tissue.* EBioMedicine, 2018. **31**: p. 92-109.

36. Williamson, I.A., et al., *A High-Throughput Organoid Microinjection Platform to Study Gastrointestinal Microbiota and Luminal Physiology.* Cell Mol Gastroenterol Hepatol., 2018. **6**(3): p. 301-319.

37. Ettayebi, K., et al., *Replication of human noroviruses in stem cell-derived human enteroids.* Science, 2016. **353**: p. 1387-1393.

38. Kolawole, A.O., et al., *Astrovirus replication in human intestinal enteroids reveals multi-cellular tropism and an intricate host innate immune landscape.* PLoS Pathog., 2019. **15**(10): p. e1008057.

39. Hinman, S.S., Y. Wang, and N.L. Allbritton, *Photopatterned Membranes and Chemical Gradients Enable Scalable Phenotypic Organization of Primary Human Colon Epithelial Models.* Anal Chem., 2019. **91**(23): p. 15240-15247.

40.   Kim, R., et al., *An in vitro intestinal platform with a self-sustaining oxygen gradient to study the human gut/microbiome interface.* Biofabrication, 2019. **12**(1): p. 015006.

41.   Capeling, M., et al., *Generation of small intestinal organoids for experimental intestinal physiology.* Methods Cell Biol., 2020. **159**: p. 143-174.

42.   Dye, B., et al., *In vitro generation of human pluripotent stem cell derived lung organoids.* eLife, 2015.

43.   Dye, B., et al., *A bioengineered niche promotes in vivo engraftment and maturation of pluripotent stem cell derived human lung organoids.* eLife, 2016.

44.   Miller, A.J., et al., *In Vitro Induction and In Vivo Engraftment of Lung Bud Tip Progenitor Cells Derived from Human Pluripotent Stem Cells.* Stem Cell Reports, 2018. **10**(1): p. 101-119.

45.   Miller, A.J., et al., *Generation of lung organoids from human pluripotent stem cells in vitro.* Nat Protoc., 2019. **14**: p. 518-540.

46.   Munera, J., et al., *Differentiation of Human Pluripotent Stem Cells into Colonic Organoids via Transient Activation of BMP Signaling.* Cell Stem Cell, 2017. **21**(1): p. 51-64.

47.   Tsai, Y.-H., et al., *In vitro patterning of pluripotent stem cell-derived intestine recapitulates in vivo human development.* Development, 2017. **144**(6): p. 1045-1055.

48.   Mithal, A., et al., *Generation of mesenchyme free intestinal organoids from human induced pluripotent stem cells.* Nature Communications, 2020. **11**.

49.   Murugan, V., *Embryonic Stem Cell Research: A Decade of Debate from Bush to Obama.* Yale J Biol Med. , 2009. **82**(3): p. 101–103.

50.   Chiao, E., et al., *Derivation of human embryonic stem cells in standard and chemically defined conditions.* Methods Cell Biol., 2008. **86**: p. 1-14.

51.   Huangfu, D., et al., *Induction of pluripotent stem cells from primary human fibroblasts with only Oct4 and Sox2.* Nat Biotechnol., 2008. **26**(11): p. 1269-75.

Chapter 3 : Non-Adhesive Alginate Hydrogels Support Growth of Pluripotent Stem Cell-Derived Intestinal Organoids

3.1 Introduction

A pivotal development in the fields of developmental biology and regenerative medicine was the use of human pluripotent stem cells (hPSCs) to generate human cell types, tissues, and organoid model systems *in vitro* [1-3]. hPSC-derived organoids are 3-dimensional (3D) organ-like tissues that partially recapitulate structural and functional aspects of the organs after which they are modeled [4-11]. In particular, human intestinal organoids (HIOs) are a useful tool to study intestinal development [12-19], evaluate gut-microbe interactions [20], and model chronic health conditions such as inflammatory bowel disease [21].

HIOs are generated from hPSCs through a step-wise differentiation process resulting in the formation of multi-cellular spheroids which are embedded in a 3D extracellular matrix (ECM) to support growth and development. Spheroids grow into HIOs

over the course of approximately 30 days in culture [5]. Currently, basement membrane-like ECM derived from mouse sarcoma cells, sold under brand names such as Matrigel or Cultrex, are standard for organoid culture as they mimic the basement membrane and help to support epithelial growth. There are many issues with these cell-derived ECMs, including batch-to-batch variability, inability to control biophysical and biochemical properties, and a potential for pathogen transfer [22]. Perhaps most importantly, cell-derived ECMs typically have an uncharacterized protein composition and introduce a largely uncontrollable biological variability into experimental design. Lastly, cell-derived ECMs have a high cost, hindering scale-up. Collectively, these factors limit biological control during experiments and hamper downstream clinical applications. These limitations have prompted investigation into fully defined synthetic matrices to support organoid culture *in vitro*. Thus far only polyethylene glycol (PEG) has been utilized for HIO culture, motivating research into other hydrogel systems. Recent work has shown that modified PEG hydrogels can be engineered to support HIO growth [23], or to support epithelium-only organoids (enteroids) generated from isolated murine or human intestinal stem cells [24]. These studies focused on engineering hydrogels to mimic the stiffness, adhesivity, and degradation dynamics required to support cellular viability and attachment [23, 24]. However, given that hPSC-derived HIOs are comprised of both epithelium and an outer mesenchyme with a supportive basement membrane, we hypothesized that HIOs may create their own niche and thus may be amenable to growth in substrates lacking inherent cell recognition.

In this work, we present evidence that native (unmodified) alginate can be used as a simple hydrogel system that supports HIO growth and development *in vitro* and

transplantation *in vivo* into immunocompromised mice. Alginate is an FDA approved polysaccharide derived from algae that is favorable due to its biocompatibility and ease of manipulation. Use of alginate does not require specialized bioengineering skills, and gelation is controlled by crosslinking with calcium; thus, alginate can be implemented using commercially available reagents without a need for further modification. Since unmodified alginate does not possess cell adhesive properties and its hydrophilic nature inhibits protein adsorption, it is a minimally supportive matrix that provides mechanical support for HIOs in a 3D environment. Here, we report that alginate hydrogels supported HIO viability and development *in vitro.* HIOs cultured in alginate grew optimally at a stiffness that was comparable to previously described PEG hydrogels optimized for HIOs [23], and the resulting alginate-grown HIOs were highly similar to Matrigel-grown HIOs *in vitro*. Alginate and Matrigel-grown HIOs underwent similar engraftment and maturation when transplanted *in vivo*, and both closely resembled human fetal intestine after transplantation*.* Collectively, these results demonstrate the effectiveness of alginate as a support matrix for HIOs and as an alternative for cell-derived ECM. Alginate overcomes many limitations of Matrigel and is significantly more cost effective than either Matrigel or PEG, making it a promising solution to improve experimental control and increase the clinical potential of organoids.

3.2 Results

Alginate Hydrogels Support HIO Viability

We identified alginate as a potential HIO growth matrix based on its cost-effectiveness, biocompatibility, mild gelation conditions [25], ability to control physical and

86

biochemical properties [26, 27], and viscoelastic behavior [28]. Many extracellular matrices and soft tissues exhibit viscoelastic behavior *in vivo* [29], including embryonic tissue [30]. Previous work demonstrated that modified PEG hydrogels engineered to mimic the adhesive and biomechanical properties of Matrigel could support HIO development [23, 24]; however, we hypothesized that due to the combined mesenchymal and epithelial composition of HIOs that establishes a laminin-rich basement membrane [5, 31], a simple non-adhesive hydrogel with a similar stiffness to Matrigel may also support HIO growth. Thus, we explored the potential of unmodified alginate to support HIO expansion.

After inducing hPSCs toward an intestinal lineage as previously described [5, 14, 16, 18, 32], 3D hindgut spheroids self-assemble and detach from the 2D monolayer. These spheroids develop into HIOs over the course of approximately 30 days in 3D culture. Spheroids were collected and embedded in Matrigel or in alginate hydrogels spanning a range of polymer densities (0.5%-4% wt/vol). Alginate solutions containing spheroids were ionically crosslinked with a calcium chloride solution to form 3D hydrogel networks. Since matrix mechanical properties have been shown to impact HIO viability [23] as well as epithelial cell behavior [33], we varied the properties of alginate hydrogels by varying polymer density in order to identify an optimal matrix to support cell viability (Figure 3-1). Using rheometry, we measured the mechanical properties of alginate gels with an *in situ* gelation test. Rheological data confirm that both the storage and loss moduli of alginate hydrogels increase with increasing polymer density. The storage and loss moduli of 0.5% alginate were most similar to Matrigel, while those of 1% alginate were

higher than Matrigel but similar to PEG hydrogels optimized for HIO formation as reported by others [23] (Figure 3-1A).

To optimize alginate growth conditions throughout the course of HIO development, we established metrics of success at both early and late time points. We examined spheroid viability at days 3 and 7 after encapsulation to assess the initial response of spheroids to alginate (Fig 3-1B, C), as well as quantified overall HIO yield after 28 days, calculated as the percentage of embedded spheroids which matured into HIOs (Figure 3-1D). Using live-dead staining, HIO viability was quantified as the percentage of spheroid area live-stained at days 3 and 7 post-encapsulation. Results presented in Figure 3-1C represent combined data from 3 independent experiments where n ≥ 6 spheroids were analyzed at each condition. At 3 days post-encapsulation, none of the Matrigel spheroids (0%) displayed signs of death while spheroids in all concentrations of alginate displayed some cell death. After 3 days, spheroids in both 0.5% alginate and 4% alginate displayed significant decreases in viability, while spheroids in 1%, 2%, and 3% alginate displayed similar viability compared to spheroids in Matrigel (Figure 3-1C). We noted a highly variable degree of viability in 4% alginate with some spheroids exhibiting high viability and others exhibiting complete death. By 7 days post-encapsulation, spheroids embedded in both 1% and 2% alginate retained the highest viability and spheroids grown in 0.5%, 3%, and 4% alginate exhibited decreased average viability from day 3 to day 7 with multiple spheroids showing 0% viability in each of these conditions (Figure 3-1C). On the other hand, spheroids grown in 1% and 2% alginate remained nearly 100% viable with only a few spheroids displaying cell death. Thus, by day 7 it is apparent that spheroid survival depends on alginate density, with 1% and 2% alginate best supporting viability.

HIO yield was calculated as the percentage of spheroids at day 1 of encapsulation that gave rise to HIOs after 28 days (Figure 3-1D). All of the alginate concentrations tested produced significantly lower HIO yields than Matrigel, although we note that our yield in Matrigel is 3.7 fold higher than those reported by others [31]. The low HIO yields at day 28 as compared with high viability in alginate at day 7 suggests that additional death may occur later in HIO development, or that certain spheroids do not expand in alginate. HIO yield was highest in 1% alginate as compared with all other alginate formulations tested, although there was no significant difference in yield between 0.5%, 1%, and 2% alginate. We selected 1% or 2% alginate as the optimal concentrations for future experiments since these concentrations resulted in the highest spheroid viability at early time points as well as highest overall HIO yield. We further encapsulated spheroids from 3 additional hPSC lines in Matrigel or 1% alginate and observed very similar growth between lines, resulting in HIOs with expected morphology (Figure 3-2A, B) and comparable yields between 1% alginate and Matrigel across all 4 lines (Figure 3-2C).

The Epithelium of Alginate-Grown HIOs and Matrigel-Grown HIOs is Indistinguishable

After 28 days of culture, we used histological techniques to compare HIOs cultured in alginate and Matrigel. Histological analysis with hematoxylin and eosin (H&E) staining revealed that HIOs cultured in both alginate and Matrigel form an inner epithelium surrounded by an outer mesenchyme (Figure 3-3A). While the epithelium of alginate and Matrigel-grown HIOs appears quite similar histologically, the mesenchyme of Matrigel-grown HIOs invades the surrounding matrix whereas alginate-grown HIOs do not appear to invade the hydrogel.

HIOs cultured in both alginate and Matrigel were examined for the presence of markers of intestinal epithelial patterning, mesenchyme formation, and polarization (Figure 3-3B) as well as markers of fully differentiated intestinal cell types including enterocytes, goblet cells, and enteroendocrine cells (Figure 3-3C). The epithelium of both alginate and Matrigel-grown HIOs expressed the intestinal epithelial marker CDX2, confirming that alginate-grown HIOs differentiate along an intestinal lineage as observed in Matrigel-grown HIOs. Additionally, both alginate and Matrigel-grown HIOs expressed the duodenum marker PDX1 throughout the epithelium, indicating that HIOs cultured in both matrices became patterned into proximal small intestine [14]. Alginate and Matrigel-grown HIOs expressed the tight junction marker ZO-1 at apical surfaces suggesting proper epithelial polarization. Additionally, both alginate and Matrigel-grown HIOs supported the development of an outer mesenchyme as evidenced by the presence of VIM expression surrounding the epithelium.

SOX9 is expressed in progenitor cells in HIOs [20], and we observed that the majority of epithelial cells in both alginate and Matrigel-grown HIO expressed SOX9 after 28 days of culture *in vitro.* Co-staining with the proliferation marker KI67 indicated that both alginate and Matrigel-grown HIOs are proliferative (Figure 3-3C). Additionally, both alginate and Matrigel-grown HIOs gave rise to differentiated epithelial cell types *in vitro* as HIOs cultured in the two matrices displayed epithelial cells expressing markers for small intestinal enterocytes (DPP4), goblet cells (MUC2), and enteroendocrine cells (CHGA). This suggests that differentiation within alginate-grown HIOs develops along a similar timeline when compared to Matrigel-grown HIOs.

Although we observed differentiated cell markers within HIOs, the abundance of differentiation was generally low. To report the frequency of differentiation, stemness, and proliferation across multiple HIOs and across different batches of HIOs, we quantified the percentage of HIOs expressing the markers DPP4, MUC2, CHGA, LYZ, DEFA5, VIL1, ZO-1, CDX2, OLFM4, and KI67 across 3 independent experiments (Figure 3-3D). Our results demonstrated that alginate and Matrigel-grown HIOs expressed all markers with a similar frequency; however, we noted variability across batches of HIOs. Our data suggests that batch-to-batch variability is the most likely explanation for expression differences between experiments, and this batch effect is seen in alginate and Matrigel-grown HIOs. We also carried out qRT-PCR analysis to compare HIOs from multiple cell lines and further confirmed that alginate or Matrigel-grown HIOs express key epithelial markers at similar levels between growth matrices and across hESC or hiPSC lines (Figure 3-2D). Taken together, these results demonstrate that alginate-grown HIOs resemble Matrigel-grown HIOs and suggest that alginate is an effective alternative to Matrigel for supporting HIO development *in vitro*.

Transplanted Alginate HIOs Mature in vivo

We next explored the engraftment and maturation potential of alginate-grown HIOs *in vivo*. Matrigel-grown HIOs and HIOs cultured in synthetic matrices have been shown to develop into more mature intestinal tissue after transplantation into immunocompromised (NSG) mice [18, 19, 23, 34], so a key success criterion of alginate HIOs is the ability to undergo similar maturation following transplantation into NSG mice. HIOs grown in both 2% alginate (n=12 mice) and Matrigel (n=11 mice) were dissociated

from their growth matrices and implanted beneath the kidney capsules of NSG mice (Figure 3-4A). After 10 weeks *in vivo*, transplanted HIOs (tHIOs) previously cultured in alginate developed crypt-villus structures with associated submucosa, lamina propria, and muscularis mucosae resulting in a comparable architecture to tHIOs previously cultured in Matrigel (H&E staining). Both alginate and Matrigel tHIOs displayed goblet cells throughout the villi (Alcian blue/PAS staining) as well as organized collagen fibers in the submucosa (Trichrome staining) (Figure 3-4B). The structure and features of alginate and Matrigel tHIOs both closely resembled human fetal intestinal tissue (Figure 3-4B). The epithelium of alginate tHIOs demonstrated evidence that they retained intestinal lineage identity (CDX2+) and remained patterned into duodenum (PDX1+) following transplantation (Figure 3-4C). Alginate and Matrigel tHIOs both formed ZO-1+ tight junctions at the apical surface of the epithelium, similar to fetal intestinal tissue. Additionally, both alginate and Matrigel tHIOs demonstrated the expected localization of mesenchyme inside and below villi as demonstrated by VIM staining.

After growth *in vivo*, alginate tHIOs increased in maturity as evidenced by lack of expression of SOX9 throughout the villi and increased expression of markers for differentiated cell types (Figure 3-4D). Both SOX9 and KI67 became localized to the crypt-like domains of alginate and Matrigel tHIOs as expected, suggesting the development of a mature crypt-villus axis with proliferative progenitor cells residing in the crypts. The proper localization of intestinal stem cells to the crypts in both alginate and Matrigel tHIOs was confirmed by OLFM4 expression [35]. Alginate and Matrigel tHIOs similarly expressed DPP4*,* MUC2, and CHGA throughout the epithelium. Additionally, both alginate and Matrigel tHIOs supported the differentiation of Paneth cells localized to

crypts as evidenced by co-expression of LYZ and DEFA5, consistent with previous reports [19, 34]. Staining patterns in alginate and Matrigel tHIOs for all markers closely resembled staining patterns in human fetal intestine. Taken together, these results demonstrate that HIOs grown in alginate differentiate and mature *in vivo* to a similar degree as Matrigel-grown HIOs and highlights alginate as a viable alternative to Matrigel for HIO culture.

The Epithelium of Alginate and Matrigel-Grown HIOs Share a High Degree of Molecular Similarity in vitro and in vivo

We utilized RNA sequencing analysis to determine the degree of similarity or difference between alginate and Matrigel-grown HIO epithelia in an unbiased manner. In order to reduce variance across samples and specifically assess epithelial gene expression, we isolated the epithelium from alginate and Matrigel-grown HIOs and tHIOs, further expanded this epithelium in identical culture conditions, and then performed bulk RNA-sequencing (Figure 3-5A). The epithelium from *in vitro* grown HIOs was isolated to create alginate and Matrigel HIO-derived epithelium-only (HdE) cultures. After 10 weeks *in vivo*, the epithelium from alginate and Matrigel tHIOs was similarly isolated and cultured *in vitro* to create alginate and Matrigel transplanted HIO-derived epithelium (tHdE) (Figure 3-5A). Following RNA-sequencing, the transcriptomic data for individual replicates from all 4 groups were analyzed for their similarity using Pearson's correlation coefficient. Alginate and Matrigel HdEs clustered together with high correlation, and similarly alginate and Matrigel tHdEs formed a cluster with high correlation. These clusters suggest that differences between culture conditions (*in vitro* vs. transplantation) are the main drivers

of variability between samples as enteroids from *in vitro* grown alginate and Matrigel HIOs are more similar to each other than they are to their transplant-derived counterparts even when grown in uniform culture conditions. This is consistent with previous data showing that HIOs grown *in vitro* are immature/fetal in nature, and transplanted HIOs become more mature/adult-like [20].

Additionally, we utilized differential expression analysis to compare alginate and Matrigel HdEs and tHdEs (Figure 3-5C). There was a high degree of similarity between alginate HdEs (aHdEs) and Matrigel HdEs (mHdEs) with only 32 genes (2.3%) showing significant differences in expression. Similarly, there was high similarity between alginate transplant-derived HdEs (atHdEs) and Matrigel transplant-derived HdEs (mtHdEs) with only 42 genes (3%) displaying significant differences in expression. In contrast, comparison of aHdEs to atHdEs and mHdEs to mtHdEs revealed 730 (51.7%) and 908 (64.4%) genes, respectively, with significant differences in expression. This analysis confirms that the epithelium of alginate HIOs is nearly identical to Matrigel HIOs both *in vitro* and *in vivo*. Genes that are significantly changed in all comparison groups is presented in Table 3-1.

Alginate Does Not Support Expansion of Epithelium-Only Enteroids

To further test the hypothesis that mesenchyme is critical in forming a niche to support epithelial growth in alginate, and to assess whether alginate can be applied to culture primary human epithelial-only organoids (enteroids), we established primary human fetal enteroid cultures in Matrigel and tested if we could transfer enteroids into alginate. For our experiments, intact small enteroid cysts were manually removed from

Matrigel and re-embedded in 1% alginate or Matrigel (Figure 3-6). Epithelial cysts were viable when transferred into alginate; however, alginate did not support the growth of enteroids while enteroids expanded robustly in Matrigel (Figure 3-6A). Staining for the basement membrane protein Laminin revealed that the epithelium of enteroids grown in unmodified alginate laid down a basement membrane in an inside-out formation compared with enteroids in Matrigel. That is, Laminin was deposited on the inside of the cyst lumen whereas Laminin surrounded the outside of the epithelial cysts in Matrigel (Figure 3-6B). This suggests that intestinal epithelial cells are able to lay down a basement membrane in the absence of mesenchymal cells and in the absence of an exogenous ECM (i.e. Matrigel), but that epithelial polarization is altered in this context. There were almost no proliferative epithelial cells observed in enteroids grown in alginate. In contrast, enteroids grown in Matrigel were highly proliferative as assessed by staining for KI67 (Figure 3-6C). Thus, unmodified alginate does not provide a sufficient niche to support intestinal epithelial proliferation. To investigate whether mesenchymal cells are necessary to promote a niche in a bioinert environment, we cultured intestinal enteroids in the presence of mesenchymal cells isolated from the human fetal intestine. Utilizing a hanging drop co-culture system to generate enteroid-mesenchyme aggregates, we co-cultured enteroids plus intestinal mesenchyme in Matrigel or alginate. In contrast to epithelium-only enteroids grown in alginate, epithelium-mesenchyme aggregates exhibited increased growth and proliferation in alginate (Figure 3-6A, C). Notably, however, epithelium-mesenchyme aggregates grown in alginate still remained inside-out with the mesenchyme restricted to the lumen of the cysts. This suggests that the presence of mesenchyme is sufficient to at least partially establish an epithelial niche that promotes

epithelial proliferation in alginate and provides evidence that primary epithelium-only enteroid cultures are not suitable for growth in unmodified alginate.

3.3 Discussion

In this work we identified alginate as a minimally supportive growth matrix which supports HIO development both *in vitro* and *in vivo*. We showed that HIO survival is dependent upon alginate polymer density, with concentrations of 1%-2% alginate (wt/vol) selected to best support viability at early time points as well as maximize overall HIO yield. The mechanical properties of alginate and PEG hydrogels optimized for HIO formation were similar, confirming the reliance of HIO viability on matrix stiffness [23]. While alginate supported HIO survival *in vitro*, the resulting yields after 28 days were significantly lower than yields in Matrigel. However, the yields we observed in 1% and 2% alginate are comparable with yields previously reported for HIOs cultured in Matrigel, and could likely be optimized by sorting spheroids for size or characteristic to improve yield [31]. Further, alginate-grown HIOs can be passaged and maintained for at least 90 days *in vitro* without significant decreases in expression of key markers (Figure 3-7A), further demonstrating the utility of alginate as a replacement to Matrigel.

It is unclear whether alginate results in lower overall yield of HIOs as compared with previously described synthetic polymers since viability was only reported at early time points in previous work [23]. Lower HIO yields in alginate as compared to Matrigel may be due to the inability of cells to remodel the hydrogel, lack of interactions with serum proteins, or the lack of growth factors present in Matrigel. A comparison of HIO yield in four-arm polyethylene glycol with maleimide groups at each terminus (PEG-4MAL)

modified with the adhesive peptide RGD and crosslinked with the protease degradable peptide GPQ-W as previously described [23, 36] did not provide conclusive evidence on whether decreased yields in alginate may be due to lack of adhesive or degradable cues (Figure 3-7B). To further resolve ways in which matrix properties affect HIO characteristics, future work should investigate longer-term studies with a larger sample size and include alginates modified with adhesive/degradable peptides to compare results within a single hydrogel system rather than introducing variability across hydrogels by utilizing PEG-4MAL.

HIOs cultured in alginate resulted in tissue indistinguishable from Matrigel HIOs at the epithelial level. Importantly, both matrices supported further differentiation and maturation *in vivo*, illustrating that HIOs cultured in alginate retain the potential to develop into mature intestinal tissue that resembles human fetal intestine. While the epithelia from alginate and Matrigel-grown HIOs were highly similar, it remains unclear whether or not there are differences at the mesenchymal level. It is interesting to note that the mesenchyme of alginate-grown HIOs did not invade the surrounding matrix as in Matrigel-grown HIOs. Further research is necessary to elucidate potential mesenchymal differences between alginate and Matrigel-grown HIOs.

Given the similarities between alginate and Matrigel-grown HIOs, alginate is an effective alternative to Matrigel-based culture systems which eliminates reliance on animal-derived materials and reduces cost, thereby increasing translational potential. The alginate utilized in our experiments costs approximately 320 times less than PEG and 700-900 times less than Matrigel (~$0.44 alginate vs. ~$140 PEG vs. ~$300-$400 Matrigel per 10 mL, depending on type), presenting a critical cost advantage for both

basic and translational studies. Of note, PEG-4MAL-grown HIOs need to be passaged and embed in fresh gels approximately once per week due to degradation of the hydrogel whereas alginate-grown HIOs can be cultured for up to 30 days without passaging due to the non-degradable nature of alginate, presenting an additional advantage for cost and ease of use.

From a biological standpoint, perhaps the most interesting observation of HIO culture in alginate is that HIOs do not require external cues from the extracellular matrix. The alginate we utilized in this work was not modified with adhesive peptides to support HIO growth and was thus biologically inert, providing purely mechanical support to developing HIOs. The lack of adhesive or biochemical cues from the hydrogel suggests that HIOs are able to create their own niche, likely through the basement membrane and trophic support that is established between the epithelium and mesenchyme. This hypothesis is strengthened by the inability of intestinal epithelium-only enteroids to proliferate in unmodified alginate unless they are co-cultured with mesenchymal cells. The lack of chemical modifications makes alginate a simple system which lends nicely toward large scale production, but the polymer can easily be modified for further research [37, 38]. Future experiments testing alginates modified with adhesive/degradable cues may enable primary enteroid culture in alginate in the absence of mesenchymal cells. However, as a natural matrix, alginate does come with the limitation of batch-to-batch variability as with Matrigel [39], but our experiments found that alginate was able to optimally support growth over a range of conditions, so small variations between batches should not cause a large change in matrix efficacy. The system described here can likely

be implemented to support additional 3D culture systems in a simple, cost-effective manner to advance regenerative medicine.

3.4 Methods

hESC/hIPSC Lines and Generation of hPSC-Derived Intestinal Organoids

Human ES line H9 (NIH registry #0062) was obtained from the WiCell Research Institute. Human ES Line H1 (NIH registry #0042) was obtained from Dr. James Wells. Rockefeller University Embryonic Stem Cell Line 2 (NIH registry # 0013) Germ Layer Reporter (RUES2-GLR) was obtained as a kind gift from Dr. Ali Brivanlou [40]. Human iPSC Line 72.3 was obtained from Cincinnati Children's Hospital Medical Center [41]. All experiments using human ES cells were approved by the University of Michigan Human Pluripotent Stem Cell Research Oversight Committee. hPSC lines are routinely karyotyped to ensure normal karyotype and monthly mycoplasma monitoring is conducted on all cell lines using the MycoAlert Mycoplasma Detection Kit (Lonza). H9 cells were authenticated using Short Tandem Repeat (STR) DNA profiling [42] at the University of Michigan DNA Sequencing Core and exhibited an STR profile identical to the STR characteristics published by Josephson et al. [43].

Stem cell maintenance and generation of hindgut spheroids was performed as described previously [5, 14, 20]. Briefly, hPSC lines were induced to differentiate into endoderm using Activin A (100ng/mL, R & D Systems) for 3 days in RPMI1640 media supplemented with 0%, 0.2%, 2% HyClone dFBS on subsequent days. Endoderm was induced to differentiate into the intestinal lineage by treating cells for 5-6 days with FGF4 (500ng/mL, generated as previously described [44]) and CHIR99021 (2µM). After

differentiation, free-floating hindgut spheroids were collected from differentiated stem cell cultures after days 5 and 6 of hindgut specification and plated in either Matrigel or alginate droplets on a 24-well tissue culture grade plate and maintained in organoid growth medium. Matrigel was diluted with Advanced DMEM/F12 to a final protein concentration of 8 mg/mL. Organoid growth media consisted of Advanced DMEM/F12 supplemented with 1X B27 (Thermo Fisher, Waltham, MA), GlutaMAX (Gibco, 1X), penicillin-streptomycin (Gibco, 100 U ml^{-1} penicillin; 100 µg ml^{-1} streptomycin), HEPES buffer (Gibco, 15 mM), epidermal growth factor (EGF) (R&D Systems; 100 ng/mL), Noggin-Fc (100ng/mL) (purified from conditioned media [45]), and R-Spondin2 (5% conditioned medium [46]). Media was changed every 5-7 days.

Maintenance of HIOs

For studies of up to 30 days, alginate and Matrigel-grown HIOs were not passaged. For the 90 day study of alginate-grown HIOs, organoids were passaged in a similar manner to previously described methods for hydrogel or Matrigel-grown HIOs [5, 23]. Briefly, HIOs were dislodged from the alginate hydrogel by pipetting up and down and transferred to a sterile Petri dish. Excess alginate was removed by cutting it away with a scalpel, and HIOs were manually cut in half with a scalpel. HIO halves were transferred to fresh alginate solutions and re-embed in a clean 24-well tissue culture grade plate upon gelation with calcium chloride.

Epithelial Isolation

Generation of HdEs and tHdEs from HIOs and tHIOs was performed using previously described methods to isolate the epithelium [47]. HIOs and tHIOs were incubated in dispase (07923; STEMCELL Technologies) for 30 minutes on ice. Following

incubation, dispase was removed and replaced with 100% fetal bovine serum for 15 minutes on ice. To mechanically separate the epithelium from mesenchyme, a volume of advanced Dulbecco's modified Eagle medium/F12 (12634010; Gibco) equal to the initial volume of fetal bovine serum was added to the tissue before vigorously pipetting the mixture several times. Epithelial fragments then settled to the bottom where they were collected manually on a stereoscope by pipet. The epithelium was washed with ice-cold advanced Dulbecco's modified Eagle medium/F12 and allowed to settle to the bottom of a 1.5-mL Eppendorf tube. The media was then withdrawn from the loose tissue pellet and replaced with Matrigel on ice. The Matrigel containing the isolated epithelium was gently mixed to evenly suspend the cells before being pipetted into individual 50 μL droplets in a 24-well plate. The plate containing the droplets was incubated at 37°C for 15 minutes to allow the Matrigel to solidify before adding LWRN growth media containing Thiazovivin (2.5 μmol/L), SB431542 (100 nmol/L), CHIR99021 (4 μmol/L), and Y27632 (10 μmol/L). LWRN growth media was produced as previously described [47]. In summary, conditioned media from L-WRN cells containing Wnt3a, Rspondin3, and Noggin was mixed at a ratio of 1:1 with 2✕ basal media comprised of 214 mL advanced Dulbecco's modified Eagle medium/F12, 5 mL GlutaMAX (Gibco, Japan) (100✕, 200 mmol/L), 5 mL HEPES (100✕, 1 mol/L), 5 mL N2 supplement (100✕), 10 mL B27 supplement (50✕), 5 mL penicillin/streptomycin (100✕), 1 mL N-acetylcystine (500 mmol/L), and 5 mL nicotinamide (1 mol/L). After 24 hours, the media was replaced with LWRN growth media containing TZV (2.5 μmol/L), SB431542 (100 nmol/L), and CHIR99021 (4 μmol/L). After 3 days, cultures were maintained with LWRN growth media replaced every other day.

Culture of Intestinal Epithelium and Intestinal Mesenchyme

Human fetal intestinal enteroids were generated by isolating the crypts from human fetal intestinal tissue and expanding them in Matrigel droplets as previously described [47]. After expansion in Matrigel, enteroids were passaged either as single cells or as small epithelial chunks and re-embed in 1% alginate and Matrigel. Enteroids were enzymatically dissociated into single cells with TrypLE Express (ThermoFisher) and dissociated into small chunks via syringe. Enteroids were cultured in LWRN medium in all conditions.

Intestinal mesenchyme was isolated from human fetal duodenum that was separated from the epithelium and expanded in culture. For co-culture experiments, small enteroids were mechanically removed from Matrigel 3 days after passaging. Mesenchyme was passaged into single cells and counted using a hemocytometer. Enteroids were suspended in 10 µL droplets of LWRN medium on the bottom of a tissue culture dish with 1 enteroid per droplet. 2,000 mesenchymal cells were added to each droplet for a total droplet volume of no more than 20 µL. After placing the lid onto the plate, the plate was flipped upside down to establish hanging drop co-cultures. The plate containing hanging drops was floated in a larger tissue culture plate containing sterile PBS and left in a tissue culture incubator overnight for 16 hours to allow for aggregation of epithelium with mesenchyme. The plate containing the hanging drops was then quickly flipped to an upright position. Co-culture aggregates were carefully removed by pipetting and suspended in 1% alginate and Matrigel solutions. Cultures were maintained for up to 10 days. LWRN medium was changed approximately every 3 days.

Human Tissue

Normal, de-identified human fetal intestinal tissue was obtained from the University of Washington Laboratory of Developmental Biology. Tissue sections were obtained from formalin fixed, paraffin embedded 14-15 week fetal intestinal specimens. All research utilizing human tissue was approved by the University of Michigan institutional review board.

Mouse Kidney Capsule Transplantation

The University of Michigan and Cincinnati Children's Hospital Institutional Animal Care and Use Committees approved all animal research. Prior to transplantation, HIOs were mechanically dissociated from either alginate or Matrigel by pipetting up and down and scraping away alginate/Matrigel with a scalpel. HIOs were implanted under the kidney capsules of immunocompromised NOD-scid IL2Rg-null (NSG) mice (Jackson Laboratory strain no. 0005557) as previously described [19]. In summary, mice were anaesthetized using 2% isoflurane. A left-flank incision was used to expose the kidney after shaving and sterilization with isopropyl alcohol. HIOs cultured in alginate and Matrigel were surgically implanted beneath mouse kidney capsules using forceps. Prior to closure, an intraperitoneal flush of Zosyn (100 mg kg^{-1}; Pfizer) was administered. Mice were euthanized for retrieval of tHIOs after 10 weeks. Results shown are representative of two experiments performed with a total of n=11 mice (Matrigel tHIOs) and n=12 mice (alginate tHIOs), with at least one organoid implanted per kidney capsule, depending on HIO size.

Alginate Gel Formation

Low viscosity sodium alginate powder (Alfa Aesar, B25266) was dissolved in 1 mL of 1 x PBS or H_2O to dilutions of 0.5%-4% (wt/vol). The alginate solution was then heated

to 98°C for 30 minutes on a heating block to improve sterility and ensure that the alginate fully dissolved. Excess alginate solutions were stored at room temperature and used within 1 week of initial preparation. Spheroids were suspended in the alginate solutions at a density of approximately 50 spheroids per 45 µL. 5 µL droplets of 2% (wt/vol) calcium chloride (Sigma-Aldrich, 449709) were deposited on the bottom of 24-well tissue culture plates (Nunclon). 45 µL of alginate containing spheroids was then pipetted directly onto the calcium chloride solution to initiate ionic crosslinking, which began instantaneously upon pipetting. Gels were formed one plate at a time to avoid calcium chloride evaporation. The gels polymerized at room temperature for 5-10 minutes and were then placed into a tissue culture incubator and allowed to fully set for 20 minutes at 37°C before media was added, replicating the protocol for Matrigel. HIOs cultured in 1% and 2% alginate were used to obtain all data in Figures 3-2 : 3-7.

Mechanical Characterization of Alginate Hydrogels

The storage and loss moduli of the alginate gels were determined by performing *in situ* gelation tests on an AR-G2 rheometer equipped with a peltier stage and 20 mm measurement head. In brief, 90µL of alginate was deposited onto the bottom of the rheometer while 10µL of 2% $CaCl_2$ was deposited onto the measurement head. The head was lowered to a gap height of 300µm initiating gelation upon contact, and then the edges of the gel were sealed with mineral oil. The mechanical response of the gels was recorded by performing time sweep measurements at a constant strain of 6% and a frequency of 1 rad/s. The time sweep was continued until storage and loss moduli reached steady state indicating completion of gelation. Rheological testing of alginate was carried out at room temperature, representing the initial gelation conditions of

alginate which polymerizes at room temperature within 5 minutes prior to storage at 37°C. Matrigel rheology was carried out in the same manner but measurements were obtained at 37°C as Matrigel takes over 20 minutes to polymerize and gelation occurs at 37°C.

Viability Assay and Quantification

Alginate gels and Matrigel droplets were incubated in 1 μM Calcein-AM (live; ThermoFisher), and 0.5 μM Ethidium-homodimer (dead; ThermoFisher) in PBS for 30 minutes. Samples were imaged using an Olympus IX73 Inverted microscope or Nikon A-1 confocal microscope. Quantification of viability was performed by calculating the percentage of the total projected area of a spheroid/organoid that stained positive for the live or dead stain using ImageJ (National Institute of Health, USA). The results are representative of three independent experiments performed with n ≥ 6 gel samples per experimental group.

RNA-Sequencing and Bioinformatics Analysis

RNA isolation and analysis was carried out as previously described [47]. RNA from each sample was isolated using MagMAX-96 Total RNA (AM1830; Applied Biosystems) RNA isolation kits and used as input for library generation with Takara SMARTer Stranded Total RNA Sample Prep Kit (634876; Takara Bio USA). Samples were sequenced for 50-bp single-end reads across 10 lanes on an Illumina HiSeq 2500 by the University of Michigan DNA Sequencing Core. All reads were quantified using Kallisto pseudo alignment to an index of transcripts from all human genes within the Ensembl GRCh38 database [48]. Gene level data generated from Kallisto was used to create normalized data matrix of pseudoaligned sequences (Transcripts Per Million, TPM) and

differential expression was calculated using the Bioconductor package DEseq2. Estimated counts per transcript using the Bioconductor package tximport. Differential expression analysis was performed using the Bioconductor package DESeq2 using gene count data [49]. A gene was considered to be differentially expressed if it had a 2-fold or larger difference between groups and an adjusted *P* value of .01 or less. Principal component analysis and sample clustering were performed in R with log2 transformed and centered gene counts of gene level data on all genes that had a sum of at least 10 counts across all samples. Replicates for all samples were clustered by Euclidian distance, and pairwise Pearson correlation coefficients were plotted in R. All reads are deposited at the EMBL-EBI ArrayExpress archive under accession E-MTAB-7000.

RNA Extraction and quantitative RT-PCR Analysis

qRT-PCR experiments were carried out as previously described (Miller et al., 2018). RNA was extracted using the MagMAX-96 Total RNA Isolation System (Life Technologies). RNA quality and concentration was assessed using a Nanodrop 2000 spectrophotometer (Thermo Scientific). Isolated RNA was used to generate a cDNA library using the SuperScript VILO cDNA master mix kit (Invitrogen) according to manufacturer's instructions. qRT-PCR analysis was conducted using Quantitect SYBR Green Master Mix (Qiagen) on a Step One Plus Real-Time PCR system (Life Technologies). Expression was calculated as a change relative to ECAD expression using arbitrary units, which were calculated by the following equation: [2^(ECAD Ct - Gene Ct)] x 10,000. Expression was normalized to ECAD as we analyzed epithelial-specific genes and there were variable levels of epithelium between samples. A Ct value

106

of 40 or greater was considered not detectable. A list of primer sequences used can be found in Table 3-2.

Tissue Preparation, Immunohistochemistry, Electron Microscopy and imaging

Paraffin Sectioning and Staining

HIO and tHIO tissues were fixed in 4% Paraformaldehyde (Sigma) overnight and then dehydrated in an alcohol series: 30 minutes each in 25%, 50%, 75% Methanol:PBS/0.05% Tween-20, followed by 100% Methanol, and then 100% Ethanol. Tissue was processed into paraffin using an automated tissue processor (Leica ASP300). Paraffin blocks were sectioned 7 uM thick, and immunohistochemical staining was performed as previously described (Spence et al., 2009). A list of antibody information and concentrations used can be found in the Supplemental Experimental Procedures. H&E staining was performed using Harris Modified Hematoxylin (FisherScientific) and Shandon Eosin Y (ThermoScientific) according to manufacturer's instructions. Alcian blue/PAS staining was performed using the Newcomer supply Alcian Blue/PAS Stain kit (Newcomer Supply, Inc.) according to manufacturer's instructions. Trichrome staining was performed by the University of Michigan *in vivo* Animal Core.

Imaging and Image Processing

Fluorescently stained slides were imaged on a Nikon A-1 confocal microscope. Brightness and contrast adjustments were carried out using ImageJ (National Institute of Health, USA) and adjustments were made uniformly across images.

Quantification and Statistical Analysis

107

Statistical analyses and plots were generated in Prism 6 software (GraphPad). If more than two groups were being compared within a single experiment, an unpaired one-way ANOVA was performed followed by Tukey's multiple comparisons test to compare the mean of each group with the mean of every other group within the experiment unless otherwise specified. For all statistical tests, a significance value of 0.05 was used. For every analysis, the strength of p values is reported in the figures according the following: $p > 0.05$, $*p \leq 0.05$, $**p \leq 0.01$, $***p \leq 0.001$, $****p \leq 0.0001$. Details of statistical tests can be found in the figure legends.

Accession Numbers

RNA-seq data have been deposited in the ArrayExpress database at EMBL-EBI under accession number ArrayExpress: E-MTAB-7000.

Author Contributions

Project conceptualization: M.M.C., S.H., S.T., and J.R.S. Experimental design: M.M.C., J.R.S., M.C., S.H., Y.S., E.A., M.H., A.J.G., and A.J.P. Experiments and data collection: M.M.C., M.C., S.H., Y.S., Y.-H.T., A.W., B.J., N.S., M.H., and A.J.G. Data analysis and interpretation: M.M.C., M.C., S.H., Y.-H.T., A.W., M.S.N., B.J., N.S., S.T., M.H., A.J.P, and J.R.S. Critical materials: A.J.G. (modified PEG hydrogels). Writing manuscript: M.M.C. and J.R.S. Editing manuscript: all authors.

Acknowledgments

3.5 Figures

Figure 3-1. Alginate supports HIO survival *in vitro*.

(a): Rheological characterization of alginate hydrogels. Data shown are the mean ± standard deviation from n≥3 gels per condition. **(b)**: Representative images of live (Calcein AM, green) and dead (Ethidium homodimer-1, red) staining of spheroids in alginate and Matrigel after 7 days in culture. Scale bar = 100μm. **(c)**: Quantification of spheroid viability after 3 and 7 days encapsulated in alginate or Matrigel. Percentage of live area denotes area of spheroid expressing live marker over total spheroid area. Data are combined from 3 independent experiments with n>6 spheroids per condition per experiment. Each point depicts viability of an individual spheroid, while bars depict mean and standard error. Significance was calculated with a one-way ANOVA and Tukey's multiple comparisons test. **(d)**: Quantification of HIO yield after 28 days in culture. HIO yield was calculated as the percentage of spheroids which gave rise to HIOs. Data shown are the average yields from 3 independent experiments with n>100 spheroids per condition. Each point depicts overall yield from one experiment, while bars depict mean and standard error. Significance was calculated with a one-way ANOVA and Tukey's multiple comparisons test.
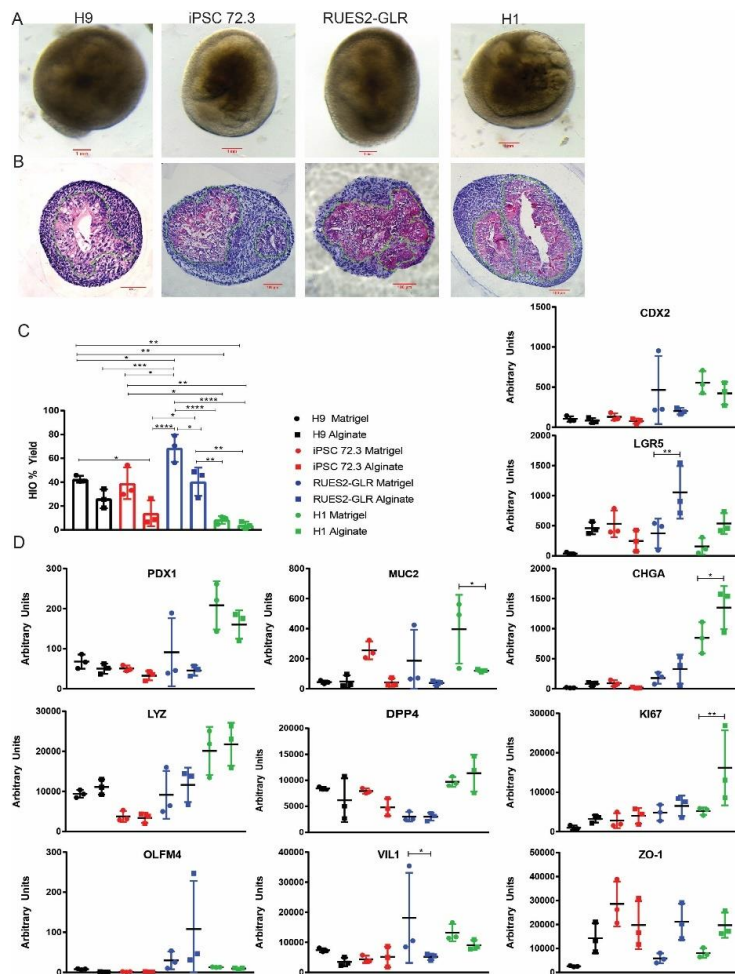
Figure 3-2. Alginate supports HIO culture across multiple hPSC lines.

(a): Brightfield images of HIOs derived from 4 independent hPSC lines cultured in 1% alginate for 28 days in vitro. Scale bar = 1 mm. **(b):** Hematoxylin and eosin (H&E) staining of HIOs derived from 4 independent hPSC lines cultured in 1% alginate for 28 days. Dashed lines outline the epithelium. **(c)**: Quantification of HIO yield after 28 days in culture for HIOs derived from 4 independent hPSC lines. HIO yield was calculated as the percentage of spheroids which gave rise to HIOs. Data shown are the average yields from 3 independent experiments with n>100 spheroids per condition. Each point depicts overall yield from one experiment, while bars depict mean and standard error. Significance was calculated with a one-way ANOVA and Tukey's multiple comparisons test. **(d)**: QRT-PCR analysis of CDX2, LGR5, PDX1, MUC2, CHGA, LYZ, DPP4, KI67, OLFM4, VIL1, ZO-1 expression in HIOs derived from 4 independent hPSC lines cultured in 1% alginate and Matrigel for 28 days in vitro. Expression levels are normalized to ECAD expression to account for varying amounts of epithelium in HIOs. Each point is representative of 6-10 HIOs pooled from the same batch. Data represent the mean ± standard error of the mean. Significance was calculated with a one-way ANOVA and Tukey's multiple comparisons test where expression was compared between alginate and Matrigel-grown HIOs for each line.
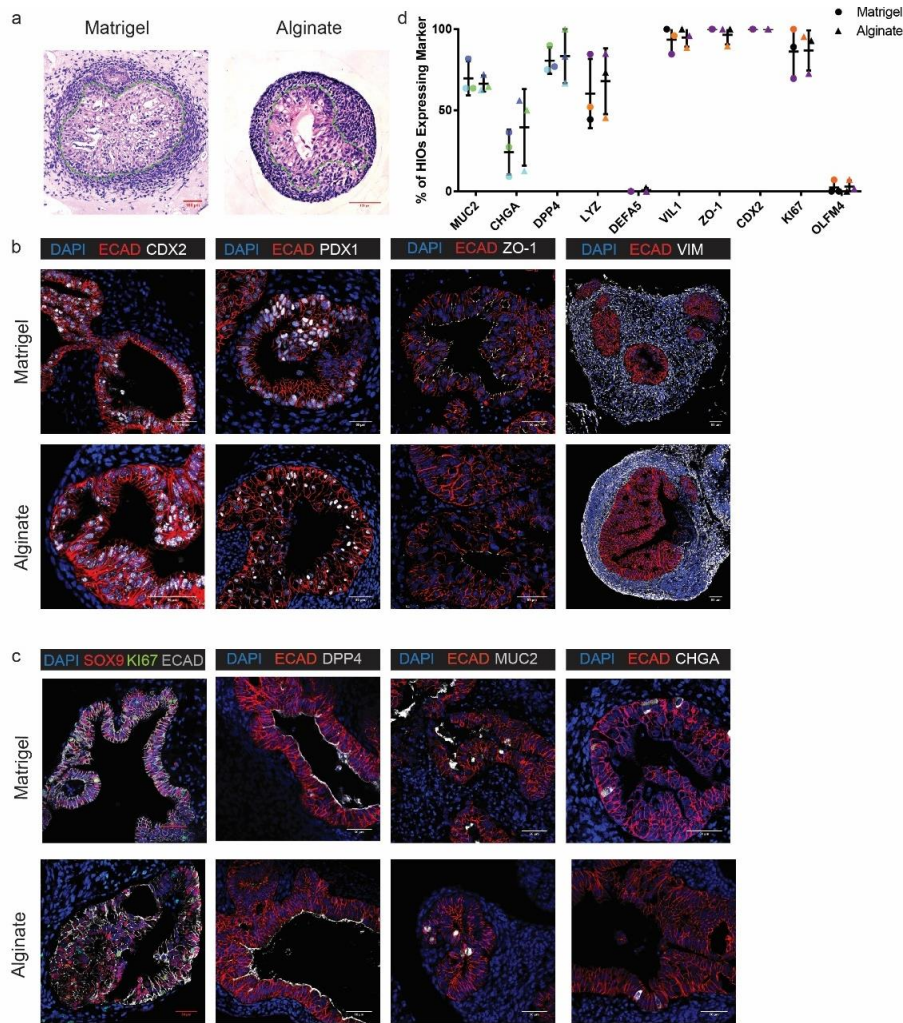
Figure 3-3. Epithelium of alginate-grown HIOs resembles epithelium of Matrigel-grown HIOs *in vitro*.

(a): Hematoxylin and eosin staining of HIOs cultured in 1% alginate and Matrigel for 28 days. Dashed lines outline the epithelium. **(b)**: Representative images of general epithelial marker staining in HIOs cultured in 1% alginate and Matrigel for 28 days. Markers shown are ECAD (epithelial marker), CDX2 (intestinal epithelium marker), PDX1 (duodenum marker), ZO-1 (tight junction marker), and VIM (mesenchymal marker). Scale bar = 50µm. **(c)**: Representative images of specific epithelial cell marker staining in HIOs cultured in 1% alginate and Matrigel for 28 days. Markers shown are SOX9 (progenitor cell marker), KI67 (proliferative cell marker), DPP4 (small intestinal brush border enzyme marker), MUC2 (goblet cell marker), and CHGA (enteroendocrine marker). Scale bar = 50µm. **(d)**: Frequency of mature cell type differentiation in 1% alginate and Matrigel. Points depict the percentage of HIOs expressing each marker as assessed by protein staining for 3 independent experiments with n≥6 HIOs per experiment. Each color represents one matched experiment. Significance was calculated with a one-way ANOVA and Tukey's multiple comparisons test.
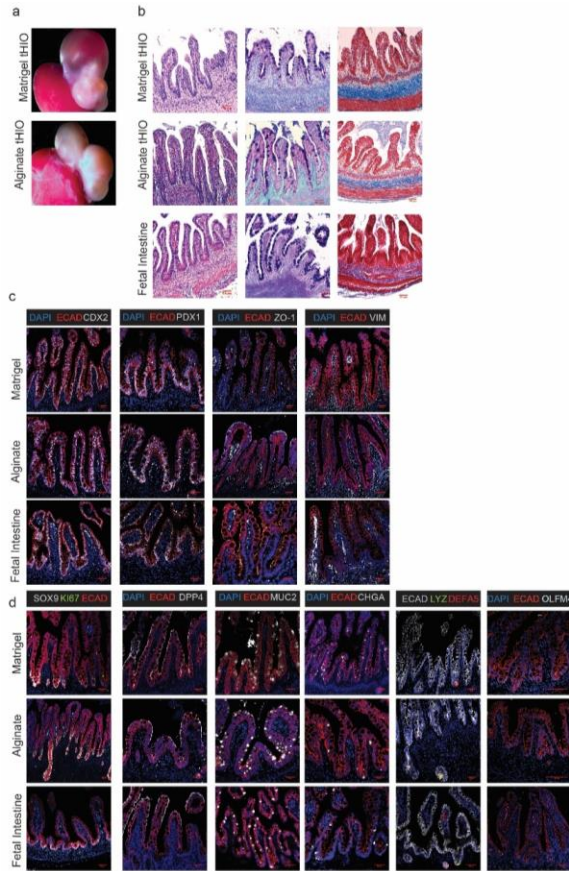
Figure 3-4. Alginate-grown HIOs mature in a similar manner as Matrigel-grown HIOs *in vivo*.

a): Dissected kidneys containing tHIOs cultured in alginate or Matrigel. HIOs were cultured in either Matrigel or 2% alginate dissolved in H_2O and transplanted after 28 days of culture in vitro. tHIOs were removed after 10 weeks *in vivo*. **(b)**: Hematoxylin and eosin, Alcian blue/PAS, and Trichrome staining reveal the presence of mature crypt-villus structures in alginate and Matrigel tHIOs. Scale bar = 50µm (H&E and Alcian blue/PAS), Scale bar = 100 µm Trichrome. **(c)**: Representative images of general epithelial marker staining in tHIOs from alginate and Matrigel. Markers shown are ECAD (epithelial marker), CDX2 (intestinal epithelium marker), PDX1 (duodenum marker), and VIM (mesenchymal marker). Scale bar = 50µm**. (d)**: Representative images of specific epithelial cell marker staining in tHIOs from alginate and Matrigel. Markers shown are SOX9 (progenitor cell marker), KI67 (proliferative cell marker), DPP4 (small intestinal brush border enzyme marker), MUC2 (goblet cell marker), CHGA (enteroendocrine cell marker), LYZ and DEFA5 (Paneth cell markers), and OLFM4 (intestinal stem cell marker). Two transplant experiments were conducted with a total of n=11 Matrigel transplanted and n=12 alginate transplanted mice. Scale bar = 50µm for all markers except OLFM4 scale bar = 100µm.
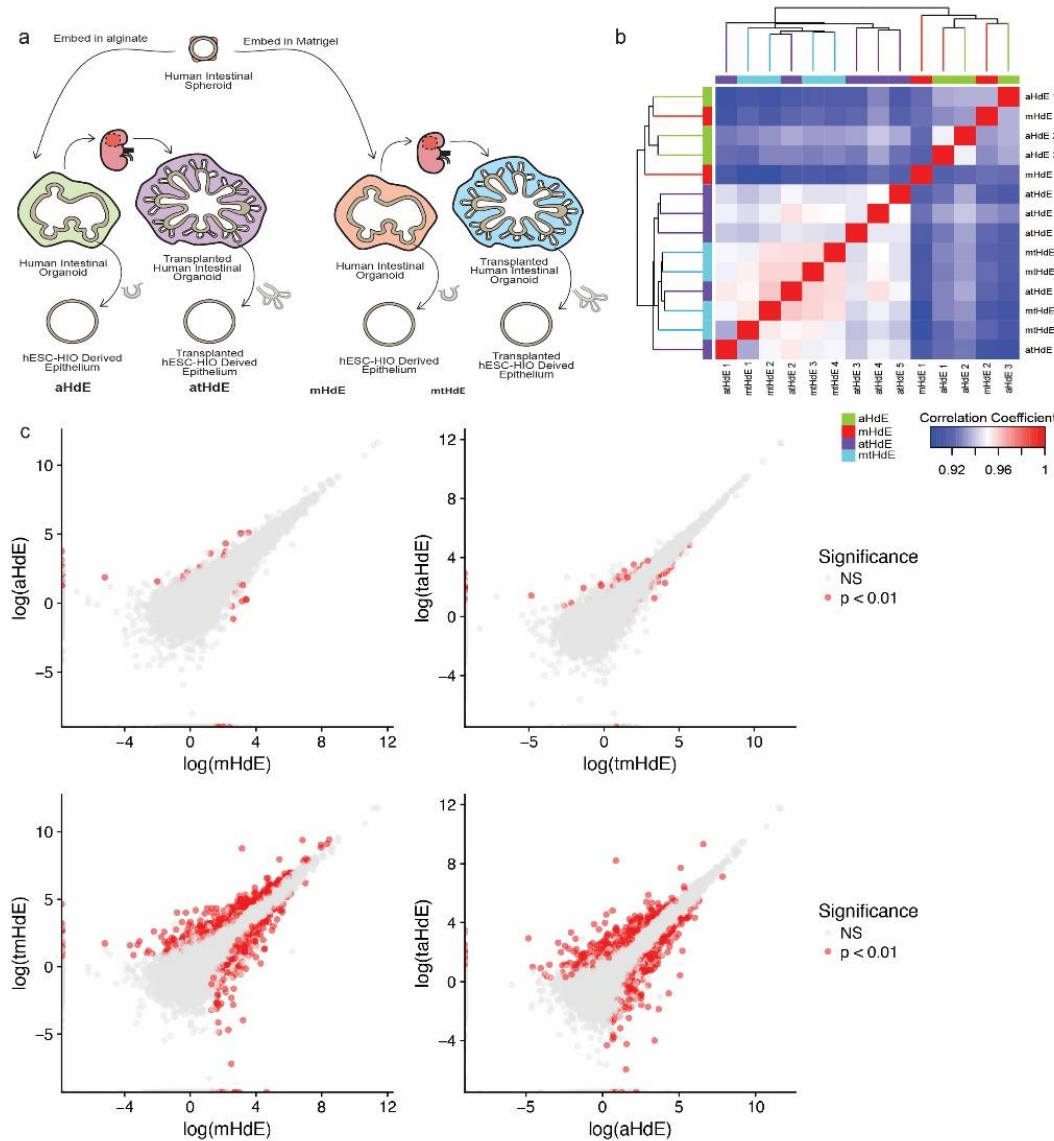
Figure 3-5. RNA-seq comparison of alginate and Matrigel-grown HIO epithelia.

(a): Schematic overview of sample groups included in RNA-seq analysis. Epithelia were extracted from alginate and Matrigel-grown HIOs both after culture *in vitro* and after transplantation into mice. **(b)**: Clustering HdEs and tHdEs by sample similarity using Pearson's correlation coefficient (n=3 aHdE, n=2 mHdE, n=5atHdE, n=4mtHdE). Clusters formed between aHdEs and mHdEs as well as between atHdEs and mtHdEs. **(c)**: Differential expression analysis comparing aHdEs to mHdEs, atHdEs to mtHdEs, mHdEs to mtHdEs, and aHdEs to atHdEs. Red dots represent genes with significant differences in expression (p < 0.01). In these plots, the alginate and Matrigel samples are nearly identical. RNA-seq data have been deposited in the ArrayExpress database at EMBL-EBI (www.ebi.ac.uk/arrayexpress) under accession number E-MTAB-7000. See also Table 3-1.

114
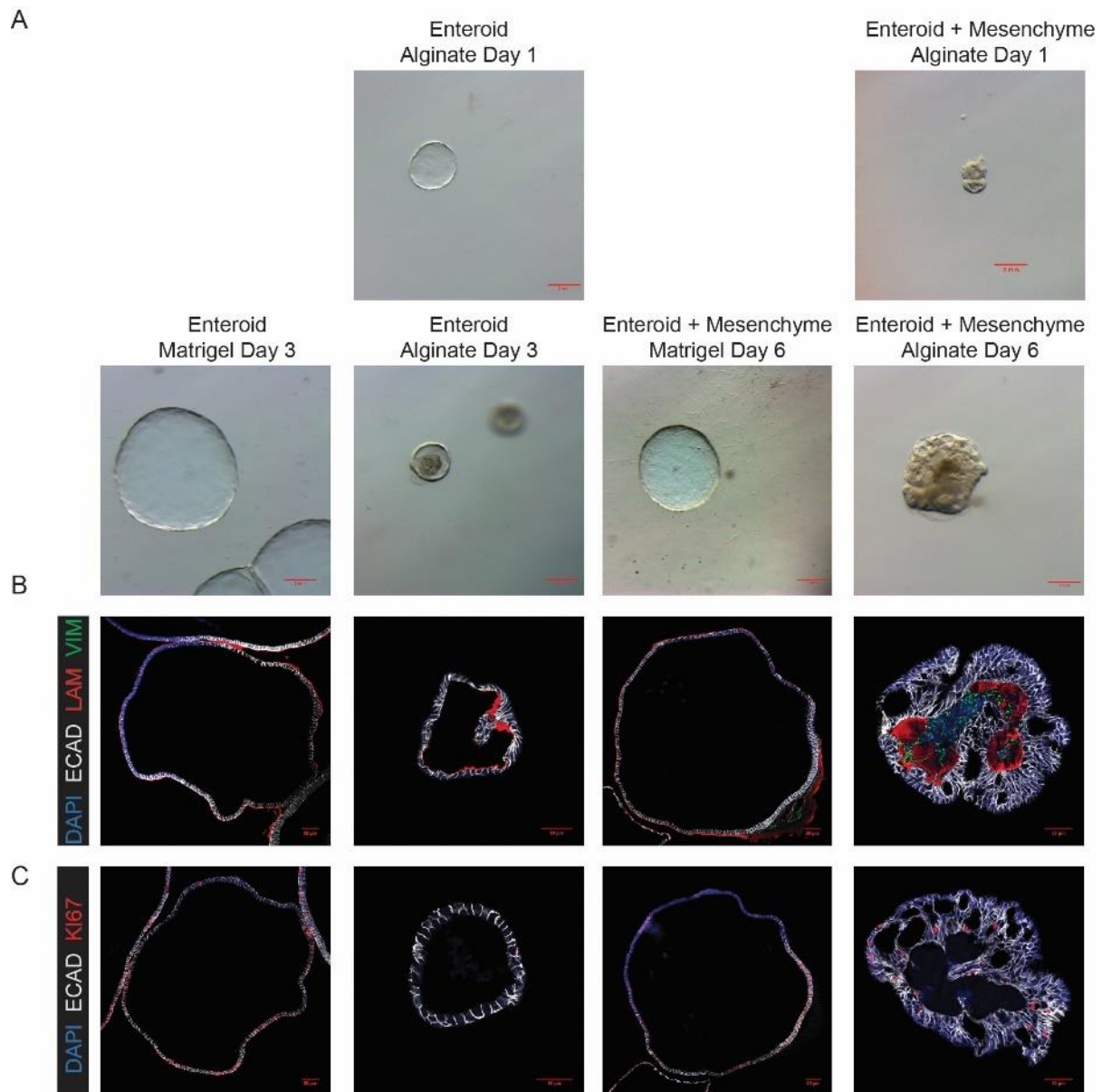
Figure 3-6. Alginate does not recapitulate intestinal epithelial niche in the absence of mesenchymal support.
(a): Brightfield images of fetal intestinal enteroids cultured in Matrigel and re-embed in 1% alginate and Matrigel either alone or co-cultured with fetal intestinal mesenchymal cells. Scale bar = 1 mm. **(b)**: Representative images of intestinal enteroids embed in alginate and Matrigel with and without mesenchyme after 7 days stained for ECAD, LAM, and VIM. Scale bar = 50 µm. **(c)**: Representative images of intestinal enteroids embed in alginate and Matrigel with and without mesenchyme after 7 days stained for ECAD and KI67. Scale bar = 50 µm.
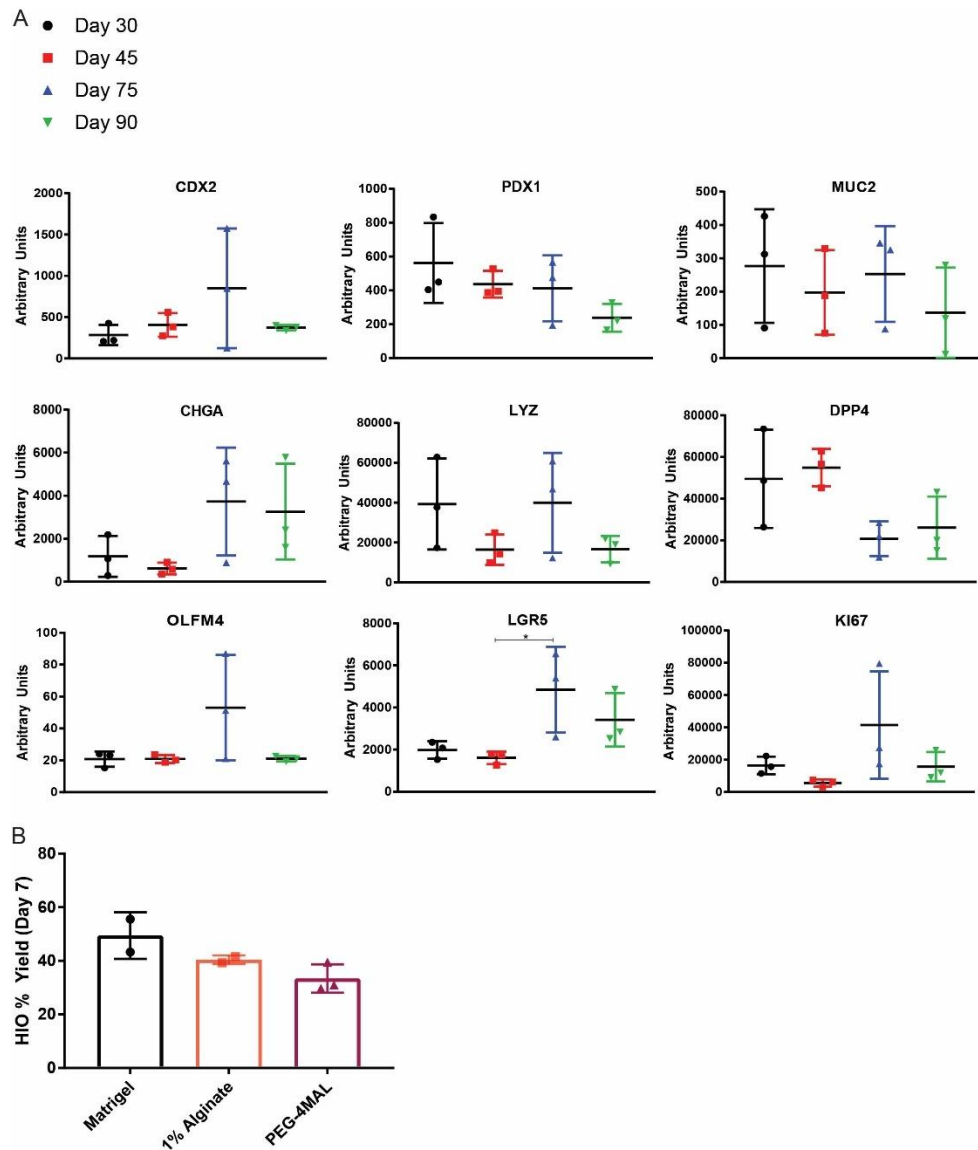
Figure 3-7. Further characterization of alginate-grown HIOs.

(a): QRT-PCR analysis of CDX2, LGR5, PDX1, MUC2, CHGA, LYZ, DPP4, KI67, OLFM4, VIL1, and ZO-1 expression in HIOs cultured in 1% alginate over time for 90 days. Expression levels are normalized to ECAD to account for varying amounts of epithelium in HIOs. Each point is representative of 6-10 HIOs pooled from the same batch. Data represent the mean ± standard error of the mean. Significance was calculated with a one-way ANOVA and Tukey's multiple comparisons test. **(b):** Quantification of the percentage of spheroids which gave rise to organoids after 7 days of culture in Matrigel, 1% alginate, and 4% PEG-4MAL. Data shown are the average yields from 2 (alginate and Matrigel) or 3 (PEG-4MAL) independent experiments with n>100 spheroids per condition. Each point depicts overall yield from one experiment, while bars depict mean and standard error. Significance was calculated with a one-way ANOVA and Tukey's multiple comparisons test.

3.6 Tables

total mtHdE vs atHdE	total aHdE vs atHdE	total mHdE vs mtHdE
A2M; ADM; ANKRD12; ANKRD37; AQP5; BACE1; BBOX1; BHLHE40; CDH12; CREB5; DIXDC1; DUSP6; EFNA1; EGR1; GRASP; GSTM1; HDAC4; HILPDA; HIVEP1; IRF1; KATNAL2; KCNE3; KDM3A; KLF9; LINC00511; LINC01473; LINC01515; MB21D2; MIR222HG; NFATC2; NFIL3; NR1D1; PELI2; PFKFB3; PIM3; PITX1; SERTAD2; SLC9B2; SLIT3; UMAD1; ZNF512; ZNF692	A4GNT; AADAC; ABHD2; ABTB2; ACE2; ACKR4; ACSL1; ACSL5; ACSS1; ACSS3; ACTR3B; ACVR2B; ADAM15; ADAMTS10; ADARB1; ADCK1; ADGRG7; ADH1C; ADRA2A; AGFG2; AGTR1; AHCYL2; AKAP2; AKR1B10; AKR1C3; ALDH1A3; ALDH1B1; ALDOB; ALPK3; AMDHD2; AMOTL1; ANGPTL3; ANKRD1; ANKRD12; ANKRD36B; ANO1; ANPEP; ANXA4; AP1S2; APBB1; APBB2; APOA2; APOA4; APOC3; APOL1; APOL6; AQP5; ARHGAP42; ARHGAP44; ARHGEF17; ARID3A; ARID3B; ARL5B; ARRB2; ASCL2; ATP13A1; ATP5D; AXL; B3GALT5; B4GALNT4; BAIAP2L2; BCL11B; BCL2L14; BCL2L15; BCORL1; BCR; BICC1; BIK; BMP5; BNIP3; BNIP3L; BPIFB1; BTBD8; BTNL3; C11orf95; C14orf39; C15orf48; C17orf78; C1orf116; C1orf220; C21orf91; C3orf52; C4orf47; C6orf223; C9orf152; C9orf16; CA2; CACNA1D; CACNA1H; CADPS2; CAPG; CAPN6; CARD6; CASP1; CASP4; CASP7; CBX2; CCDC33; CCDC68; CCDC8; CCL2; CCL20; CCNE1; CCNJL; CD37; CD44; CD47; CD82; CDH17; CDH2; CDHR2; CDKL3; CDKN1C; CDKN2C; CEACAM5; CEACAM6; CECR2; CELSR1; CEMIP; CES2; CFAP221; CFAP74; CFI; CFTR; CH17-340M24.3; CHMP4C; CHRM3; CISD3; CKAP4; CKB; CLDN2; CLU; CLUH; CNGA1; CNTN4; COBLL1; COCH; COL16A1; COL2A1; COL4A6; COL5A1; COL6A1; COL6A2; COX5A; CPNE2; CPT1A; CRIM1; CRIP2; CRNDE; CROT; CSGALNACT1; CTNNA3; CTSA; CTSC; CTSD; CTSS; CXCL1; CXCL3; CXCL6; CXCL8; CXCR4; CXXC4; CYP2B6; CYP2C18; CYP2C19; CYP2C9; CYP4F12; CYP4F3; CYP4V2; CYTIP; DAPP1; DDAH2; DDX49; DDX60; DENND2D; DGKZ; DHX58; DKK3; DLGAP1; DLGAP4; DMBT1; DPF3; DSC2; DSC3; DZIP1; DZIP1L; E2F5; EEF1A2; EFEMP2; EFNB2; EGFL7; EHD2; EHF; EGLU7; ELOVL7; EML1; ENO2; ENTPD3; EPDR1; EPHB2; EPM2A; EPOR; ERICH5; ESPN; ESRRA; EVL; EXOSC4; F2R; F3; FABP2; FABP3; FABP5; FAM102A; FAM189A2; FAM46A; FAM69B; FAS; FBLN1; FBLN2; FBP1; FER1L6; FERMT2; FGFBP1; FIRRE; FKBP10; FLCN; FLRT2; FMOD; FN1; FNBP1; FOXC1; FOXO1; FOXP2; FRMD4B; FRMD6; FSCN1; FSTL1; FUT2; FUT3; FUT4; FZD7; GABRB2; GALNT4; GAS6; GATA4; GATA5; GBA; GCDH; GDNF; GIPC2; GJA1; GJB2; GJC1; GLIS3; GMDS; GMPR; GNPDA1; GPD1; GPD1L; GPR160; GPR176; GPRC5B; GPS1; GPX2; GRHL3; GSDMB; GSTM4; GTF2A2; GUCY1A2; GULP1; GYPC; HABP2; HAS2; HAVCR1; HEATR5A; HECTD3; HERC6; HFM1; HHEX; HIC2; HID1; HIP1R; HIST1H2AI; HIST3H2A; HLA-B; HOMER2; HPGD; HPN; HR; HSD17B2; ID4; IFI44; IFI6; IFIH1; IFIT3; IFRD1; IGF2; IGF2BP1; IGF2BP2; IGFBP4; IGFBP5; IHH; IL18; IL1RN; INO80E; INPP4B; INPP5F; IQCE; IRF8; IRS1; IRS2; ISX; ISYNA1; ITPR1; JAK2; JMJD7; KCNE3; KCNF1; KCNN4; KCNQ1; KDM6A; KIAA1211L; KIAA1324; KIF13A; KIFC3; KIRREL3; KLF12; KLF4; KRT17; KRT6B; L1CAM; L3MBTL1; LACTB2; LAMA1; LAMA3; LAMP1; LCN2; LDB2; LEMD1; LGALS1; LGALS4; LGALS9; LGALS9B; LGALS9C; LGR5; LIN28B; LINC01559; LIPA; LIPG; LRIG1; LRP2BP; LRP4; LRP8; LSAMP; LY75-CD302; LYN; LYSMD2; LYZ; MAGED2; MAGED4; MAGED4B; MALL; MAML3; MAOB; MAP1LC3A; MAPK15; MARCKS; MBOAT2; MDFI; MDK; METTL7A; MEX3A; MFAP2; MFGE8; MFSD1; MGAM2; MGAT5; MID1; MIER3; MIR22HG; MIR3142HG; MIR7515HG; MLF1; MLLT3; MMP1; MMP10; MMP19; MMP7; MPC1; MPDZ; MPP1; MRPS12; MRPS6; MS4A8; MSN; MT1G; MTG2; MTSS1L; MUC1; MUC13; MUC17; MUC3A; MUC4; MVP; MXRA7; MYB; MYH14; MYRFL; N4BP2; NAV2; NBL1; NCOA4; NCR3LG1; NDRG1; NDUFB3; NECTIN3; NES; NFATC1; NFIA; NFIB; NGEF; NID1; NME4; NME7; NMI; NMU; NMUR2; NPC1L1; NQO1; NR3C2; NR4A2; NRCAM; NSF; NT5E; NTRK2; NUAK1; NUDT22; NXN; NYNRIN; OAS3; OAT; OBSCN; OBSL1; OLFM4; ONECUT2; ONECUT3; OSR2; OTC; OTUB2; OTUD1; OXCT1; P3H3; P4HA1; PACSIN3; PALM; PANCR; PARM1; PARP9; PCDH19; PCLO; PDE3B; PDZD8; PELI2; PGAP2; PGC; PHACTR3; PI3; PIGR; PIGZ; PIK3AP1; PIP5K1B; PITX1; PLA2G2A; PLA2G4F; PLAC4; PLCB1; PLCB3; PLCL2; PLEKHF2; PLEKHG5; PLEKHS1; PLOD2; PLXND1; PMEPA1; PMM1; PNPO; POLR3K; POU2F1; PPIC; PPP1R14A; PPP1R1B; PRDM1; PRDM16; PRDM2; PRKCB;	A2M; ABCC4; ABCF1; ABLIM2; ACSL1; ACSS1; ADAM15; ADCY6; ADH1C; ADRA2A; AFG3L2; AFP; AGAP4; AGTR1; AHCYL2; AK1; AKAP8; AKR1B10; AKR1C3; ALDH1A2; ALDH1A3; ALDH1B1; ALDOB; ALG1; ALG13; ALG14; ALPK3; AMN1; ANKRD34C-AS1; ANKRD36C; ANKRD45; ANO1; ANPEP; ANXA1; AOAH; AP1B1; AP1M2; AP2B1; AP2M1; APOA2; APOA4; APOL6; APP; ARF3; ARHGAP11A; ARHGAP24; ARHGEF2; ARHGEF38; ARID3A; ARIH2OS; ARL6IP4; ARL6IP6; ASNSD1; ASPH; ASS1; ATG3; ATP1B1; ATP2C2; ATP5B; ATP5C1; ATP5D; ATP5G1; ATP5G3; ATP5J2; ATP5L; ATP6V1E1; ATP6V1F; ATPIF1; AURKAIP1; B2M; BAAT; BACE1; BACE2; BAIAP2L2; BANK1; BARX2; BBOX1; BBS7; BCL2L12; BCL2L15; BCL7B; BET1L; BHLHE40; BHLHE41; BICC1; BID; BIN1; BLNK; BNIP1; BOP1; BRIP1; BRMS1; C14orf2; C1orf54; C1QBP; C6orf132; C6orf141; C6orf201; C9orf152; C9orf16; C9orf78; CA9; CABIN1; CACNA2D1; CADM2; CADPS2; CALM2; CARD6; CASD1; CASP1; CASP4; CASP7; CBR1; CCDC112; CCDC124; CCDC170; CCDC6; CCDC65; CCDC69; CCDC94; CCL2; CCL25; CCNJ; CCSER1; CCT8; CD2BP2; CD44; CD82; CDC25B; CDC42EP1; CDC42EP5; CDH12; CEACAM5; CEACAM6; CECR2; CENPB; CENPE; CEP41; CES2; CFAP221; CFAP44; CFAP74; CFB; CFTR; CHMP4C; CHN2; CHURC1; CINP; CISD1; CISD3; CIZ1; CKB; CKMT1A; CLCN7; CLDN18; CLDN2; CLIP4; CLTA; CLTB; CLU; CLUH; CMPK1; CNGA1; CNNM3; CNTN4; COL16A1; COL28A1; COL2A1; COMMD1; COMMD3-BMI1; COPE; COQ3; CORO1B; COTL1; COX4I1; COX5B; COX6B1; COX7B; CPE; CPT1A; CPVL; CREB3L1; CREB5; CREBBP; CREBZF; CRTAP; CRYGS; CSK; CSRNP1; CSRNP2; CTSE; CTSS; CXCL1; CYB5R2; CYBA; CYP1A1; CYP2C18; CYP2C19; CYP4F12; CYP4F3; CYSLTR1; CYSTM1; DCXR; DDIT3; DDRGK1; DDX27; DDX41; DDX60; DEPDC7; DHX37; DHX38; DLG3; DLGAP1; DLGAP4; DMBT1; DMTF1; DMXL2; DNAJC1; DNAJC22; DNM1; DOCK9; DPH5; DPP4; DSTN; DTNA; DTX3L; DUS1L; DUSP6; DYRK4; DZIP1L; EBNA1BP2; ECI1; EDF1; EFHD2; EFNA1; EFNA5; EHF; EI24; EIF1AX; EIF2S1; EIF3K; EIF5A; ELF3; EMD; EPHA7; EPHB2; EPN1; EPSTI1; ERCC1; EREG; ERICH1; ERVMER61-1; EVL; EXOC3; F2R; F3; FAM102A; FAM126A; FAM129B; FAM149B1; FAM160A1; FAM189A2; FAM217A; FAM76A; FAM83G; FANCA; FASN; FBLN1; FBXO21; FBXW4; FECH; FERMT2; FIBP; FIRRE; FIS1; FKBP2; FKRP; FLRT3; FMO5; FMOD; FN1; FN3K; FOXP2; FOXQ1; FPGS; FRG1; FRY; FSCN1; FSIP2; FTX; GALNT12; GALNT13; GALNT4; GAPLINC; GATA4; GATA5; GBP1; GCLC; GFER; GJA1; GJB2; GJC1; GMDS; GMPR; GOLGA5; GOLIM4; GPATCH11; GPD1; GPR160; GPRC5B; GPRIN3; GPT2; GPX1; GPX2; GRHL3; GSDMD; GSR; GSTM1; GSTM3; GSTM4; GTF2B; GTF3C6; GTPBP4; HABP2; HAVCR1; HECTD3; HERC3; HERC4; HID1; HINT3; HIP1R; HIST1H2AJ; HIST1H2BN; HIST4H4; HIVEP3; HLA-B; HLA-DQB1; HMGA2; HMGN1; HMGN5; HNF1B; HNRNPA2B1; HNRNPDL; HNRNPUL2-BSCL2; HOXB3; HOXB4; HOXB5; HOXB7; HOXB8; HOXB9; HR; HSD17B4; HSPA5; HSPE1; HYOU1; HYPK; IDH1; IFI44; IFI6; IFIH1; IFIT3; IFIT5; IFITM2; IFITM3; IGF2; IGF2BP1; IGFBP4; IGFBP5; IL15RA; IL18; IL1RN; IL32; INPP4B; INPP5A; IQCE; IQGAP2; IRAK1; IRF1; IRF8; ISX; ISY1; JAK2; KCNK1; KCNQ1; KDM1B; KDM6A; KIAA1143; KIAA1324; KIF1C; KIZ; KLF9; KLK10; KLK7; KNTC1; KRT1; KRT8; KRT80; L3MBTL1; LAMB1; LANCL2; LASP1; LCN2; LDLRAP1; LETM1; LGALS9; LGALS9B; LGMN; LIN28B; LINC00843; LINC00863; LINC00976; LINC01146; LINC01355; LINC01473; LINC01515; LINC01612; LIPG; LRIG1; LRP8; LRRC59; LRRFIP1; LSM12; LSM14A; LSM5; LUC7L; LURAP1L; LYN; LYPLAL1; LYRM1; LYZ; MAGED2; MAGED4B; MALRD1; MAP2K3; MAPKAPK3; MAST4; MB21D2; MBD3; MBOAT2; MCUR1; MEAF6; MEIS2; MEST; METTL7A; MEX3A; MFAP3; MFGE8; MFHAS1; MGAM2; MGAT2; MIR10A; MIR7515HG; MLPH; MLX; MMP1; MMP7; MON2; MPDZ; MRGBP; MRPL1; MRPL12; MRPL20; MRPL4; MRPL40; MRPL9; MRPS11; MRPS18A; MRPS23; MRPS25; MRPS26; MRPS6; MS4A8; MSANTD2; MSN; MSRB1; MT1G; MT-ATP6; MT-CO2; MT-CO3; MTDH; MTHFD1; MTIF2; MTM1;

117

	PRKD1; PRLR; PROM1; PRR26; PRR3; PRR5L; PRRG4; PRRT2; PRSS12; PSMB10; PSMB8; PSMB9; PSME2; PTPRG; PTPRS; PTPRU; PWAR6; PXDN; PYCARD; PYGB; QKI; RAB20; RAB27A; RAB30; RAB37; RAB3B; RAB6B; RABEP2; RAMP1; RAP1GAP; RASA4; RASAL1; RASGRF2; RASL11B; RASSF5; RB1CC1; RBM45; RBP2; RBP4; RDX; REG4; REPS2; RERG; RGL1; RGL3; RGS10; RGS5; RIMS2; RIPK3; RLBP1; RNASE4; RND1; RND3; RNF144A; RNF144B; RNF152; RNF223; ROR1; RPS6KL1; RUBCNL; S100A14; S100A4; SALL2; SAMD9; SBK1; SCAMP5; SCIN; SCNN1A; SCPEP1; SDC1; SDC2; SEC11C; SELENBP1; SEMA3A; SEMA5A; SERPINA5; SERPINB9; SERPINE1; SERPINE2; SERPINH1; SETBP1; SFN; SFXN4; SGPP2; SH3BP4; SH3PXD2A; SHH; SHISA2; SHKBP1; SI; SIM2; SIPA1L2; SLC12A2; SLC20A1; SLC25A39; SLC26A3; SLC26A9; SLC28A3; SLC29A4; SLC2A1; SLC2A10; SLC2A3; SLC38A11; SLC39A10; SLC40A1; SLC46A3; SLC4A4; SLC5A1; SLC5A3; SLC6A20; SLC8B1; SLC9A2; SLC9A3; SLFN5; SMAD7; SMARCA1; SMIM14; SMIM24; SMO; SNX25; SORL1; SOX11; SOX2; SPARC; SPDEF; SPNS2; SPOCD1; SPRY2; SPRYD3; SPSB1; SPTLC2; SQSTM1; SRD5A3; SRM; SRPRB; ST3GAL4; ST6GALNAC3; STARD13; STC1; STEAP1; STEAP2; STEAP3; STK17B; STMN3; STON2; STXBP1; SYBU; SYCP2L; SYNE1; SYNJ1; SYNPR; SYT13; SYT7; SYTL5; TAP1; TCF4; TCN1; TCP10L; TDRP; TENM3; TES; TET1; TEX261; TFPI; TGFA; TGFBR3; TIAM2; TIMP3; TINAG; TLR4; TM4SF20; TMC5; TMEM139; TMEM154; TMEM171; TMEM37; TMEM47; TMEM51; TMEM63C; TMPRSS2; TMSB4X; TMTC4; TNFAIP2; TNFRSF14; TNFRSF25; TNFSF10; TNFSF13; TNS4; TP53I3; TPM2; TPMT; TPP1; TPST1; TRAK2; TRANK1; TRIM14; TRIM71; TRO; TRPM5; TSTA3; TTYH1; TUBD1; TYRO3; UBA7; UBD; UBE2E2; UBXN10; UGT1A1; UQCRQ; UTP14A; VAT1; VCAN; VDR; VEGFB; VIM; VNN1; VSIG1; WASF3; WDR54; WDR81; WNK4; WSB1; YPEL1; ZBTB10; ZBTB18; ZDHHC11B; ZMAT1; ZMYND8; ZNF165; ZNF253; ZNF423; ZNF525; ZNF713; ZNF91; ZNRF3	MUC1; MUC17; MUC3A; MUM1; MVP; MX1; MYBBP1A; MYBL2; MYH14; MYH9; MYO15B; MZT2B; NAA20; NAALAD2; NACA; NAPA; NAPEPLD; NARS; NBL1; NCOA7; NDUFA13; NDUFB10; NDUFB3; NDUFB7; NDUFB9; NDUFS5; NDUFS7; NEDD4; NEDD8-MDP1; NELL1; NFATC2; NFIB; NFIL3; NFIX; NFKBIZ; NGEF; NHSL1; NID1; NKIRAS2; NLRP2; NME1-NME2; NME2; NMI; NMU; NOB1; NOC2L; NOMO3; NOP10; NOTCH3; NPM1; NQO1; NR1D1; NSA2; NT5C3A; NT5E; NUBP1; OAT; OBSCN; OBSL1; OCLN; ODF2L; OLFM4; ONECUT2; OPRK1; OSGIN1; OTC; P4HA1; PABPC4; PAQR5; PARM1; PARP10; PARP14; PARP9; PCDH20; PCMTD1; PCNX4; PCSK5; PCYT2; PDAP1; PDCL3; PDE3B; PDGFRL; PDHB; PDHX; PDZD8; PES1; PET100; PFKFB2; PGC; PHB2; PHLPP1; PI3; PIGF; PIGR; PILRB; PIM3; PIR; PITX2; PKIA; PKP3; PLA2G3; PLAC4; PLAU; PLCG2; PLEKHB1; PLEKHG2; PLEKHS1; PLIN2; PLS3; PLXNA2; PMS1; PMVK; PNPLA2; POC1B-GALNT4; POLD2; POLR3K; PPARG; PPARGC1A; PPFIBP1; PPFIBP2; PPIG; PPP1R14B; PPP1R1B; PPP2R3B; PPP6R1; PRDX2; PRH1; PRKACB; PRKAG2; PRKAR2A; PROM1; PRPS2; PRR4; PRRG4; PRSS2; PSMB8; PSMB9; PSMC3; PSMC5; PSME1; PSME2; PTCSC3; PTGES2; PTMA; PTPRS; PWAR6; PXDC1; PXDN; PYCARD; PYGB; QDPR; QKI; RAB11B; RAB11FIP4; RAB20; RAB27B; RAB37; RAB3B; RAB40B; RABGAP1L; RAMP1; RAPH1; RASSF3; RASSF5; RASSF8; RBM14; RBP2; RBPMS; RCAN3; RCC1; RDX; RELA; RELL1; REPIN1; REPS2; RETSAT; RFX3-AS1; RFX5; RGL3; RGN; RGS5; RHOB; RHOBTB1; RIC8A; RNASE1; RNASEK; RNASET2; RNF125; RNF130; RNF144B; RNPS1; ROBO2; ROR1; RPL11; RPL12; RPL23A; RPL27; RPL36; RPL36A-HNRNPH2; RPL36AL; RPL37A; RPL38; RPL7; RPN1; RPS10-NUDT3; RPS11; RPS18; RPS27A; RPS6KA2; RPS6KB2; RRBP1; RRP12; RSPH1; S100A14; S100A16; S100A4; SAMD9; SAP30; SARS; SBDS; SBF2; SCAMP5; SDC1; SDF2L1; SDF4; SEC11C; SEC14L2; SEMA3A; SERBP1; SERF2; SERPINA5; SERPINB1; SERPINE2; SETD7; SFT2D1; SFTA2; SGPP2; SH3BP4; SH3KBP1; SH3PXD2A; SHB; SIN3B; SLC26A3; SLC2A3; SLC34A2; SLC38A11; SLC38A4; SLC39A10; SLC39A14; SLC40A1; SLC46A3; SLC4A4; SLC5A1; SLC5A3; SLC9A3; SLC9A3R1; SLC9B2; SLFN11; SLK; SLPI; SMAGP; SMARCA1; SMIM14; SMIM24; SNRPD2; SNRPG; SNX18; SNX4; SOX11; SP110; SPAG7; SPDEF; SPTAN1; SPTBN2; SPTLC2; SQSTM1; SRA1; SRRM1; SRSF1; SRSF5; SSR1; SSRP1; ST6GALNAC4; STAP2; STEAP1; STEAP3; STRN4; STX10; STXBP4; SULT1A2; SUMO3; SYAP1; SYBU; SYT13; SYTL5; TACSTD2; TAGLN2; TAP2; TAS2R10; TAS2R30; TAS2R4; TAX1BP1; TBC1D30; TBCA; TBCK; TCEAL1; TCEAL9; TCERG1; TCF19; TCIRG1; TDRP; TFIP11; TGFA; TGFBI; THG1L; THOP1; TIMM13; TIMM44; TIMP3; TIPARP; TK2; TKT; TLE3; TLR4; TM4SF20; TMA16; TMA7; TMC5; TMCO3; TMEM154; TMEM171; TMEM18; TMEM220; TMEM232; TMEM47; TMEM8A; TMPRSS2; TMPRSS5; TMSB10; TMX4; TNFAIP2; TNFAIP3; TNFRSF11A; TNFRSF14; TNFSF10; TNFSF13; TNIP1; TOMM34; TPM3; TPMT; TRAF3IP2; TRIB2; TRIM16; TRIM24; TRIM25; TRIM36; TRIM71; TRMT6; TRO; TSPAN6; TSR3; TSTA3; TTC7A; TTR; TUBB2B; TUBB6; TUBGCP5; TUFM; TXN2; TXNDC12; TXNIP; TXNRD1; TYRO3; U2AF1L4; UBN1; UBTF; UGGT1; UHRF2; UQCC2; UQCRB; UQCRQ; URGCP-MRPS24; UROS; USP19; USP37; USP44; VCAN; VDAC1; VDR; VEPH1; VIL1; VPS37B; VPS72; WARS; WASF3; WBP11; WDR27; WDR54; WHRN; XBP1; XRCC6; YBX1; YBX3; YIPF3; ZBTB11; ZBTB46; ZBTB7B; ZFHX2; ZFP91-CNTF; ZMYM1; ZNF141; ZNF320; ZNF334; ZNF43; ZNF44; ZNF493; ZNF512; ZNF598; ZNF606; ZNF678; ZNF692; ZNF84; ZPR1; ZSCAN30; ZWILCH
aHdE vs atHdE::mHdE vs aHdE::mHdE vs mtHdE	**aHdE vs atHdE::mHdE vs aHdE**	**mHdE vs aHdE::mHdE vs mtHdE**
ALDOB; ANPEP; IGF2; MGAM2	ACE2; CYP2C9; EEF1A2; FSTL1; MDFI; PLCB1	AFP; ANXA1; C6orf201; CCDC112; GAPLINC; NEDD8-MDP1; PPFIBP1; PRSS2; RPS6KA2; URGCP-MRPS24
aHdE vs atHdE::mtHdE vs atHdE	**mHdE vs mtHdE::mtHdE vs atHdE**	**aHdE vs atHdE::mHdE vs mtHdE**
ANKRD12; AQP5; KCNE3; PELI2; PITX1	A2M; BACE1; BBOX1; BHLHE40; CDH12; CREB5; DUSP6; EFNA1; GSTM1; IRF1; KLF9; LINC01473; LINC01515; MB21D2; NFATC2; NFIL3; NR1D1; PIM3; SLC9B2; ZNF512; ZNF692	ACSL1; ACSS1; ADAM15; ADH1C; ADRA2A; AGTR1; AHCYL2; AKR1B10; AKR1C3; ALDH1A3; ALDH1B1; ALPK3; ANO1; APOA2; APOA4; APOL6; ARID3A; ATP5D; BAIAP2L2; BCL2L15; BICC1; C9orf152; C9orf16; CADPS2; CARD6; CASP1; CASP4; CASP7; CCL2; CD44; CD82; CEACAM5; CEACAM6; CECR2; CES2; CFAP221; CFAP74; CFTR; CHMP4C; CISD3; CKB; CLDN2; CLU; CLUH; CNGA1; CNTN4; COL16A1; COL2A1; CPT1A; CTSS;

		CXCL1; CYP2C18; CYP2C19; CYP4F12; CYP4F3; DDX60; DLGAP1; DLGAP4; DMBT1; DZIP1L; EHF; EPHB2; EVL; F2R; F3; FAM102A; FAM189A2; FBLN1; FERMT2; FIRRE; FMOD; FN1; FOXP2; FSCN1; GALNT4; GATA4; GATA5; GJA1; GJB2; GJC1; GMDS; GMPR; GPD1; GPR160; GPRC5B; GPX2; GRHL3; GSTM4; HABP2; HAVCR1; HECTD3; HID1; HIP1R; HLA-B; HR; IFI44; IFI6; IFIH1; IFIT3; IGF2BP1; IGFBP4; IGFBP5; IL18; IL1RN; INPP4B; IQCE; IRF8; ISX; JAK2; KCNQ1; KDM6A; KIAA1324; KRT17; L3MBTL1; LCN2; LGALS9; LGALS9B; LIN28B; LIPG; LRIG1; LRP8; LYN; LYZ; MAGED2; MAGED4B; MBOAT2; METTL7A; MEX3A; MFGE8; MIR7515HG; MMP1; MMP7; MPDZ; MRPS6; MS4A8; MSN; MT1G; MUC1; MUC17; MUC3A; MVP; MYH14; NBL1; NCOA7; NDUFB3; NFIB; NGEF; NID1; NMI; NMU; NQO1; NT5E; OAT; OBSCN; OBSL1; OLFM4; ONECUT2; OTC; P4HA1; PARM1; PARP9; PDE3B; PDZD8; PGC; PI3; PIGR; PLAC4; PLEKHS1; POLR3K; PPP1R1B; PROM1; PRRG4; PSMB8; PSMB9; PSME2; PTPRS; PWAR6; PXDN; PYCARD; PYGB; QKI; RAB20; RAB37; RAB3B; RAMP1; RASSF5; RBP2; RDX; REPS2; RGL3; RGS5; RNF144B; ROR1; S100A14; S100A4; SAMD9; SCAMP5; SDC1; SEC11C; SEMA3A; SERPINA5; SERPINE2; SGPP2; SH3BP4; SH3PXD2A; SLC26A3; SLC2A3; SLC38A11; SLC39A10; SLC40A1; SLC46A3; SLC4A4; SLC5A1; SLC5A3; SLC9A3; SMARCA1; SMIM14; SMIM24; SOX11; SPDEF; SPTLC2; SQSTM1; STEAP1; STEAP3; SYBU; SYT13; SYTL5; TDRP; TGFA; TIMP3; TLR4; TM4SF20; TMC5; TMEM154; TMEM171; TMEM47; TMPRSS2; TNFAIP2; TNFRSF14; TNFSF10; TNFSF13; TPMT; TRIM71; TRO; TSTA3; TYRO3; UQCRQ; VCAN; VDR; WASF3; WDR54
unique mtHdE vs atHdE	**unique aHdE vs atHdE**	**unique mHdE vs mtHdE**
ADM; ANKRD37; DIXDC1; EGR1; GRASP; HDAC4; HILPDA; HIVEP1; KATNAL2; KDM3A; LINC00511; MIR222HG; PFKFB3; SERTAD2; SLIT3; UMAD1	A4GNT; AADAC; ABHD2; ABTB2; ACKR4; ACSL5; ACSS3; ACTR3B; ACVR2B; ADAMTS10; ADARB1; ADCK1; ADGRG7; AGFG2; AKAP2; AMDHD2; AMOTL1; ANGPTL3; ANKRD1; ANKRD36B; ANXA4; AP1S2; APBB1; APBB2; APOC3; APOL1; ARHGAP42; ARHGAP44; ARHGEF17; ARID3B; ARL5B; ARRB2; ASCL2; ATP13A1; AXL; B3GALT5; B4GALNT4; BCL11B; BCL2L14; BCORL1; BCR; BIK; BMP5; BNIP3; BNIP3L; BPIFB1; BTBD8; BTNL3; C11orf95; C14orf39; C15orf48; C17orf78; C1orf116; C1orf220; C21orf91; C3orf52; C4orf47; C6orf223; CA2; CACNA1D; CACNA1H; CAPG; CAPN6; CBX2; CCDC33; CCDC68; CCDC8; CCL20; CCNE1; CCNJL; CD37; CD47; CDH17; CDH2; CDHR2; CDKL3; CDKN1C; CDKN2C; CELSR1; CEMIP; CFI; CH17-340M24.3; CHRM3; CKAP4; COBLL1; COCH; COL4A6; COL5A1; COL6A1; COL6A2; COX5A; CPNE2; CRIM1; CRIP2; CRNDE; CROT; CSGALNACT1; CTNNA3; CTSA; CTSC; CTSD; CXCL3; CXCL6; CXCR4; CXXC4; CYP2B6; CYP4V2; CYTIP; DAPP1; DDAH2; DDX49; DENND2D; DGKZ; DHX58; DKK3; DPF3; DSC2; DSC3; DZIP1; E2F5; EFEMP2; EFNB2; EGFL7; EHD2; ELOVL7; EML1; ENO2; ENTPD3; EPDR1; EPM2A; EPOR; ERICH5; ESPN; ESRRA; EXOSC4; FABP2; FABP3; FABP5; FAM46A; FAM69B; FAS; FBLN2; FBP1; FER1L6; FGFBP1; FKBP10; FLCN; FLRT2; FNBP1; FOXC1; FOXO1; FRMD4B; FRMD6; FUT2; FUT3; FUT4; FZD7; GABRB2; GAS6; GBA; GCDH; GDNF; GIPC2; GLIS3; GNPDA1; GPD1L; GPR176; GPS1; GSDMB; GTF2A2; GUCY1A2; GULP1; GYPC; HAS2; HEATR5A; HERC6; HFM1; HHEX; HIC2; HIST1H2AI; HIST3H2A; HOMER2; HPGD; HPN; HSD17B2; ID4; IFRD1; IGF2BP2; IHH; INO80E; INPP5F; IRS1; IRS2; ISYNA1; ITPR1; JMJD7; KCNF1; KCNN4; KIAA1211L; KIF13A; KIFC3; KIRREL3; KLF12; KLF4; KRT6B; L1CAM; LACTB2; LAMA1; LAMA3; LAMP1; LDB2; LEMD1; LGALS1; LGALS4; LGALS9C; LGR5; LINC01559; LIPA; LRP2BP; LRP4; LSAMP; LY75-CD302; LYSMD2; MAGED4; MALL; MAML3; MAOB; MAP1LC3A; MAPK15; MARCKS; MDK; MFAP2; MFSD1; MGAT5; MID1; MIER3; MIR22HG; MIR3142HG; MLF1; MLLT3; MMP10; MMP19; MPC1; MPP1; MRPS12; MTG2; MTSS1L; MUC13; MUC4; MXRA7; MYB; MYRFL; N4BP2; NAV2; NCR3LG1; NDRG1; NECTIN3; NES; NFATC1; NFIA; NME4; NME7; NMUR2; NPC1L1; NR3C2; NR4A2; NRCAM; NSF; NTRK2; NUAK1; NUDT22; NXN; NYNRIN; OAS3; ONECUT1; OSR2; OTUB2; OTUD1; OXCT1; P3H3; PACSIN3; PALM; PANCR; PCDH19; PCLO; PGAP2; PHACTR3; PIGZ; PIK3AP1; PIP5K1B; PLA2G2A; PLA2G4F; PLCB3; PLCL2; PLEKHF2; PLEKHG5; PLEKHH2; PLOD2; PLXND1; PMEPA1; PMM1; PNPO; POU2F1; PPIC; PPP1R14A; PRDM1; PRDM16; PRDM2; PRKCB; PRKD1; PRLR; PRR26; PRR3; PRR5L; PRRT2;	ABCC4; ABCF1; ABLIM2; ADCY6; AFG3L2; AGAP4; AK1; AKAP8; ALDH1A2; ALG1; ALG13; ALG14; AMN1; ANKRD34C-AS1; ANKRD36C; ANKRD45; AOAH; AP1B1; AP1M2; AP2B1; AP2M1; APP; ARF3; ARHGAP11A; ARHGAP24; ARHGEF2; ARHGEF38; ARIH2OS; ARL6IP4; ARL6IP6; ASNSD1; ASPH; ASS1; ATG3; ATP1B1; ATP2C2; ATP5B; ATP5C1; ATP5G1; ATP5G3; ATP5J2; ATP5L; ATP6V1E1; ATP6V1F; ATPIF1; AURKAIP1; B2M; BAAT; BACE2; BANK1; BARX2; BBS7; BCL2L12; BCL7B; BET1L; BHLHE41; BID; BIN1; BLNK; BNIP1; BOP1; BRIP1; BRMS1; C14orf2; C1orf54; C1QBP; C6orf132; C6orf141; C9orf78; CA9; CABIN1; CACNA2D1; CADM2; CALM2; CASD1; CBR1; CCDC124; CCDC170; CCDC6; CCDC65; CCDC69; CCDC94; CCL25; CCNJ; CCSER1; CCT8; CD2BP2; CDC25B; CDC42EP1; CDC42EP5; CENPB; CENPE; CEP41; CFAP44; CFB; CHN2; CHURC1; CINP; CISD1; CIZ1; CKMT1A; CLCN7; CLDN18; CLIP4; CLTA; CLTB; CMPK1; CNNM3; COL28A1; COMMD1; COMMD3-BMI1; COPE; COQ3; CORO1B; COTL1; COX4I1; COX5B; COX6B1; COX7B; CPE; CPVL; CREB3L1; CREBBP; CREBZF; CRTAP; CRYGS; CSK; CSRNP1; CSRNP2; CTSE; CYB5R2; CYBA; CYP1A1; CYSLTR1; CYSTM1; DCXR; DDIT3; DDRGK1; DDX27; DDX41; DEPDC7; DHX37; DHX38; DLG3; DMTF1; DMXL2; DNAJC1; DNAJC22; DNM1; DOCK9; DPH5; DPP4; DSTN; DTNA; DTX3L; DUS1L; DYRK4; EBNA1BP2; ECI1; EDF1; EFHD2; EFNA5; EI24; EIF1AX; EIF2S1; EIF3K; EIF5A; ELF3; EMD; EPHA7; EPN1; EPSTI1; ERCC1; EREG; ERICH1; ERVMER61-1; EXOC3; FAM126A; FAM129B; FAM149B1; FAM160A1; FAM217A; FAM76A; FAM83G; FANCA; FASN; FBXO21; FBXW4; FECH; FIBP; FIS1; FKBP2; FKRP; FLRT3; FMO5; FN3K; FOXQ1; FPGS; FRG1; FRY; FSIP2; FTX; GALNT12; GALNT13; GBP1; GCLC; GFER; GOLGA5; GOLIM4; GPATCH11; GPRIN3; GPT2; GPX1; GSDMD; GSR; GSTM3; GTF2B; GTF3C6; GTPBP4; HERC3; HERC4; HINT3; HIST1H2AJ; HIST1H2BN; HIST4H4; HIVEP3; HLA-DQB1; HMGA2; HMGN1; HMGN5; HNF1B; HNRNPA2B1; HNRNPDL; HNRNPUL2-BSCL2; HOXB3; HOXB4; HOXB5; HOXB7; HOXB8; HOXB9; HSD17B4; HSPA5; HSPE1; HYOU1; HYPK; IDH1; IFIT5; IFITM2; IFITM3; IL15RA; IL32; INPP5A; IQGAP2; IRAK1; ISY1; KCNK1; KDM1B; KIAA1143; KIF1C; KIZ; KLK10; KLK7; KNTC1; KRT8; KRT80; LAMB1; LANCL2; LASP1; LDLRAP1; LETM1; LGMN; LINC00843; LINC00863; LINC00976; LINC01146; LINC01355; LINC01612; LRRC59; LRRFIP1; LSM12; LSM14A; LSM5; LUC7L; LURAP1L; LYPLAL1; LYRM1; MALRD1; MAP2K3; MAPKAPK3; MAST4; MBD3; MCUR1; MEAF6; MEIS2; MEST; MFAP3; MFHAS1; MGAT2; MIR10A; MLPH; MLX; MON2; MRGBP; MRPL1; MRPL12; MRPL20; MRPL4; MRPL40; MRPL9; MRPS11; MRPS18A; MRPS23;

	PRSS12; PSMB10; PTPRG; PTPRU; RAB27A; RAB30; RAB6B; RABEP2; RAP1GAP; RASA4; RASAL1; RASGRF2; RASL11B; RB1CC1; RBM45; RBP4; REG4; RERG; RGL1; RGS10; RIMS2; RIPK3; RLBP1; RNASE4; RND1; RND3; RNF144A; RNF152; RNF223; RPS6KL1; RUBCNL; SALL2; SBK1; SCIN; SCNN1A; SCPEP1; SDC2; SELENBP1; SEMA5A; SERPINB9; SERPINE1; SERPINH1; SETBP1; SFN; SFXN4; SHH; SHISA2; SHKBP1; SI; SIM2; SIPA1L2; SLC12A2; SLC20A1; SLC25A39; SLC26A9; SLC28A3; SLC29A4; SLC2A1; SLC2A10; SLC6A20; SLC8B1; SLC9A2; SLFN5; SMAD7; SMO; SNX25; SORL1; SOX2; SPARC; SPNS2; SPOCD1; SPRY2; SPRYD3; SPSB1; SRD5A3; SRM; SRPRB; ST3GAL4; ST6GALNAC3; STARD13; STC1; STEAP2; STK17B; STMN3; STON2; STXBP1; SYCP2L; SYNE1; SYNJ1; SYNPR; SYT7; TAP1; TCF4; TCN1; TCP10L; TENM3; TES; TET1; TEX261; TFPI; TGFBR3; TIAM2; TINAG; TMEM139; TMEM37; TMEM51; TMEM63C; TMSB4X; TMTC4; TNFRSF25; TNS4; TP53I3; TPM2; TPP1; TPST1; TRAK2; TRANK1; TRIM14; TRPM5; TTYH1; TUBD1; UBA7; UBD; UBE2E2; UBXN10; UGT1A1; UTP14A; VAT1; VEGFB; VIM; VNN1; VSIG1; WDR81; WNK4; WSB1; YPEL1; ZBTB10; ZBTB18; ZDHHC11B; ZMAT1; ZMYND8; ZNF165; ZNF253; ZNF423; ZNF525; ZNF713; ZNF91; ZNRF3	MRPS25; MRPS26; MSANTD2; MSRB1; MT-ATP6; MT-CO2; MT-CO3; MTDH; MTHFD1; MTIF2; MTM1; MUM1; MX1; MYBBP1A; MYBL2; MYH9; MYO15B; MZT2B; NAA20; NAALAD2; NACA; NAPA; NAPEPLD; NARS; NDUFA13; NDUFB10; NDUFB7; NDUFB9; NDUFS5; NDUFS7; NEDD4; NELL1; NFIX; NFKBIZ; NHSL1; NKIRAS2; NLRP2; NME1-NME2; NME2; NOB1; NOC2L; NOMO3; NOP10; NOTCH3; NPM1; NSA2; NT5C3A; NUBP1; OCLN; ODF2L; OPRK1; OSGIN1; PABPC4; PAQR5; PARP10; PARP14; PCDH20; PCMTD1; PCNX4; PCSK5; PCYT2; PDAP1; PDCL3; PDGFRL; PDHB; PDHX; PES1; PET100; PFKFB2; PHB2; PHLPP1; PIGF; PILRB; PIR; PITX2; PKIA; PKP3; PLA2G3; PLAU; PLCG2; PLEKHB1; PLEKHG2; PLIN2; PLS3; PLXNA2; PMS1; PMVK; PNPLA2; POC1B-GALNT4; POLD2; PPARG; PPARGC1A; PPFIBP2; PPIG; PPP1R14B; PPP2R3B; PPP6R1; PRDX2; PRH1; PRKACB; PRKAG2; PRKAR2A; PRPS2; PRR4; PSMC3; PSMC5; PSME1; PTCSC3; PTGES2; PTMA; PXDC1; QDPR; RAB11B; RAB11FIP4; RAB27B; RAB40B; RABGAP1L; RAPH1; RASSF3; RASSF8; RBM14; RBPMS; RCAN3; RCC1; RELA; RELL1; REPIN1; RETSAT; RFX3-AS1; RFX5; RGN; RHOB; RHOBTB1; RIC8A; RNASE1; RNASEK; RNASET2; RNF125; RNF130; RNPS1; ROBO2; RPL11; RPL12; RPL23A; RPL27; RPL36; RPL36A-HNRNPH2; RPL36AL; RPL37A; RPL38; RPL7; RPN1; RPS10-NUDT3; RPS11; RPS18; RPS27A; RPS6KB2; RRBP1; RRP12; RSPH1; S100A16; SAP30; SARS; SBDS; SBF2; SDF2L1; SDF4; SEC14L2; SERBP1; SERF2; SERPINB1; SETD7; SFT2D1; SFTA2; SH3KBP1; SHB; SIN3B; SLC34A2; SLC38A4; SLC39A14; SLC9A3R1; SLFN11; SLK; SLPI; SMAGP; SNRPD2; SNRPG; SNX18; SNX4; SP110; SPAG7; SPTAN1; SPTBN2; SRA1; SRRM1; SRSF1; SRSF5; SSR1; SSRP1; ST6GALNAC4; STAP2; STRN4; STX10; STXBP4; SULT1A2; SUMO3; SYAP1; TACSTD2; TAGLN2; TAP2; TAS2R10; TAS2R30; TAS2R4; TAX1BP1; TBC1D30; TBCA; TBCK; TCEAL1; TCEAL9; TCERG1; TCF19; TCIRG1; TFIP11; TGFBI; THG1L; THOP1; TIMM13; TIMM44; TIPARP; TK2; TKT; TLE3; TMA16; TMA7; TMCO3; TMEM18; TMEM220; TMEM232; TMEM8A; TMPRSS5; TMSB10; TMX4; TNFAIP3; TNFRSF11A; TNIP1; TOMM34; TPM3; TRAF3IP2; TRIB2; TRIM16; TRIM24; TRIM25; TRIM36; TRMT6; TSPAN6; TSR3; TTC7A; TTR; TUBB2B; TUBB6; TUBGCP5; TUFM; TXN2; TXNDC12; TXNIP; TXNRD1; U2AF1L4; UBN1; UBTF; UGGT1; UHRF2; UQCC2; UQCRB; UROS; USP19; USP37; USP44; VDAC1; VEPH1; VIL1; VPS37B; VPS72; WARS; WBP11; WDR27; WHRN; XBP1; XRCC6; YBX1; YBX3; YIPF3; ZBTB11; ZBTB46; ZBTB7B; ZFHX2; ZFP91-CNTF; ZMYM1; ZNF141; ZNF320; ZNF334; ZNF43; ZNF44; ZNF493; ZNF598; ZNF606; ZNF678; ZNF84; ZPR1; ZSCAN30; ZWILCH
unique mHdE vs aHdE		
C3; CCDC175; CETN3; CXCR5; IGFBP1; JDP2; MTERF4; MYT1; NRP1; OMA1; SULT1A3; UBXN7		

Table 3-1. Overlap of differentially expressed genes

Gene Target	Forward Primer Sequence	Reverse Primer Sequence
GAPDH	CTCTGCTCCTCCTGTTCGAC	TTAAAAGCAGCCCTGGTGAC
ECAD	TTGACGCCGAGAGCTACAC	GACCGGTGCAATCTTCAAA
CDX2	GGGCTCTCTGAGAGGCAGGT	GGTGACGGTGGGGGTTTAGCA
LGR5	CAGCGTCTTCACCTCCTACC	TGGGAATGTATGTCAGAGCG
PDX1	CGTCCGCTTGTTCTCCTC	CCTTTCCCATGGATGAAGTC
MUC2	TGTAGGCATCGCTCTTCTCA	GACACCATCTACCTCACCCG
CHGA	CTGTCCTGGCTCTTCTGCTC	TGACCTCAACGATGCATTTC
LYZ	ACAAGCTACAGCATCAGCGA	GTAATGATGGCAAAACCCCA
DPP4	TCCCGGTGGGAGTACTATGA	CAGGGCTTTGGAGATCTGAG
KI67	CAGGGCTTTGGAGATCTGAG	TGACTTCCTTCCATTCTGAAGAC
OLFM4	ACCTTTCCCGTGGACAGAGT	TGGACATATTCCCTCACTTTGGA
VIL1	CCAAAGGCCTGAGTGAAATC	CCTGGAGCAGCTAGTGAACA
ZO-1	GGGAACAACATACAGTGACGC	CCCCACTCTGAAAATGAGGA

Table 3-2. Primer Information.

Note: All primer sequences were obtained from http://primerdepot.nci.nih.gov. All annealing temperatures are near 60°C.

Primary Antibody	Source	Catalog #	Dilution
Goat anti-E-cadherin	R&D Systems	af748	1:500
Mouse anti-E-cadherin	BD Transduction Laboratories	610181	1:500
Goat anti-Vimentin	R&D Systems	mab2105	1:500
Mouse anti-CDX2	BioGenex	MU392A-UC	1:300
Rabbit anti-PDX1	Epitomics, Inc	3470-1	1:300
Rabbit anti-ZO-1	Cell Signaling	13663	1:300
Rabbit anti-MUC2	Santa Cruz Biotechnology	sc-15334	1:300
Goat-anti CHGA	Santa Cruz Biotechnology	sc-1488	1:300
Goat-anti SOX9	R&D Systems	af3075	1:300
rabbit-anti KI67	Thermo Scientific	RM-9106-S1	1:300
Goat-anti DPP4	R&D Systems	af954	1:300
Goat-anti LYZ	Santa Cruz Biotechnology	sc-27958	1:300
Rabbit-anti DEFA5	Abcam	ab180515	1:300
Rabbit-anti OLFM4	Abcam	ab85046	1:300
Rabbit-anti LGR5	Abcam	ab75850	1:300
Goat-anti Villin	Santa Cruz	sc-7672	1:300

Table 3-3. Antibody Information.

3.7 References

1. Huch, M., et al., *The hope and hype of organoid research.* Development, 2017. **144**: p. 938-941.

2. Johnston, D.S., *The Renaissance of Developmental Biology.* PLoS Biology, 2015.

3. Little, M.H., *Organoids: a Special Issue.* Development, 2017. **144**: p. 935-937.

4. Takebe, T., et al., *Vascularized and functional human liver from an iPSC-derived organ bud transplant.* Nature, 2013. **499**: p. 481-484.

5. Spence, J.R., et al., *Directed differentiation of human pluripotent stem cells into intestinal tissue in vitro.* Nature, 2011. **470**(7332): p. 105-109.

6. Eiraku, M., et al., *Self-organizing optic-cup morphogenesis in three-dimensional culture.* Nature, 2011. **472**(7341): p. 51-6.

7. Lancaster, M., et al., *Cerebral organoids model human brain development and microcephaly.* Nature, 2013. **501**(7467): p. 373-9.

8. Takasato, M., et al., *Directing human embryonic stem cell differentiation towards a renal-lineage generates a self-organizing kidney.* Nature Cell Biology, 2014. **16**: p. 118-126.

9. Miller, A.J., et al., *In Vitro Induction and In Vivo Engraftment of Lung Bud Tip Progenitor Cells Derived from Human Pluripotent Stem Cells.* Stem Cell Reports, 2018. **10**(1): p. 101-119.

10. Dye, B., et al., *A bioengineered niche promotes in vivo engraftment and maturation of pluripotent stem cell derived human lung organoids.* eLife, 2016.

11. Dye, B., et al., *In vitro generation of human pluripotent stem cell derived lung organoids.* eLife, 2015.

12. Singagoga, K.L. and J.M. Wells, *Generating human intestinal tissues from pluripotent stem cells to study development and disease.* The EMBO Journal, 2015. **34**(9): p. 1149-1163.

13. Munera, J., et al., *Differentiation of Human Pluripotent Stem Cells into Colonic Organoids via Transient Activation of BMP Signaling.* Cell Stem Cell, 2017. **21**(1): p. 51-64.

14. Tsai, Y.-H., et al., *In vitro patterning of pluripotent stem cell-derived intestine recapitulates in vivo human development.* Development, 2017. **144**(6): p. 1045-1055.

15. Aurora, M. and J.R. Spence, *hPSC-derived lung and intestinal organoids as models of human fetal tissue.* Dev Biol., 2016. **420**(2): p. 230-238.

16. Tsai, Y.-H., et al., *LGR4 and LGR5 Function Redundantly During Human Endoderm Differentiation.* Cel Mol Gastroenterol Hepatol., 2016. **2**(5): p. 648-662.

17. Dedhia, P.H., et al., *Organoid Models of Human Gastrointestinal Development and Disease.* Gastroenterology, 2016. **150**(5): p. 1098-1112.

18. Finkbeiner, S.R., et al., *Generation of tissue-engineered small intestine using embryonic stem cell-derived human intestinal organoids.* Biology Open, 2015. **4**(11): p. 1462-1472.

19. Finkbeiner, S.R., et al., *Transcriptome-wide Analysis Reveals Hallmarks of Human Intestine Development and Maturation In Vitro and In Vivo.* Stem Cell Reports, 2015. **4**: p. 1140-1155.

20. Hill, D.R., et al., *Bacterial colonization stimulates a complex physiological response in the immature human intestinal epithelium.* eLife, 2017. **6**.

21. Wells, J.M. and J.R. Spence, *How to make an intestine.* Development, 2014. **141**: p. 752-760.

22. Czerwinski, M. and J.R. Spence, *Hacking the Matrix.* Cell Stem Cell, 2017. **20**(1): p. 9-10.

23. Cruz-Acuna, R., et al., *Synthetic hydrogels for human intestinal organoid generation and colonic wound repair.* Nature Cell Biology, 2017. **19**(11): p. 1326-1335.

24. Gjorevski, N., et al., *Designer matrices for intestinal stem cell and organoid culture.* Nature, 2016. **539**: p. 560-564.

25. Lee, K.Y. and D.J. Mooney, *Alginate: properties and biomedical applications.* Prog Polym Sci., 2012. **37**(1): p. 106-126.

26. Jeon, O., et al., *Biochemical and Physical Signal Gradients in Hydrogels to Control Stem Cell Behavior.* Advanced Materials, 2013. **25**(44): p. 6366-6372.

27. Samorezov, J.E., C.M. Morlock, and E. Alsberg, *Dual Ionic and Photo-Crosslinked Alginate Hydrogels for Micropatterned Spatial Control of Material Properties and Cell Behavior.* Bioconjugate Chemistry, 2015. **26**(7): p. 1339-1347.

28. Webber, R.E. and K.R. Shull, *Strain dependence of the viscoelastic properties of alginate hydrogels.* Macromolecules, 2004. **37**(16): p. 6153-6160.

29. Chaudhuri, O., *Viscoelastic hydrogels for 3D cell culture.* Biomaterials Science, 2017. **5**: p. 1480-2490.

30. Forgacs, G., et al., *Viscoelastic Properties of Living Embryonic Tissue: a Quantitative Study.* Biophysical Journal, 1998. **74**: p. 2227-2234.

31. Arora, N., et al., *A process engineering approach to increase organoid yield.* Development, 2017. **144**: p. 1128-1136.

32. McCracken, K., et al., *Generating human intestinal tissue from pluripotent stem cells in vitro.* Nature Protocols, 2011. **6**(12): p. 1920-1928.

33. Enemchukwu, N.O., et al., *Synthetic matrices reveal contributions of ECM biophysical and biochemical properties to epithelial morphogenesis.* The Journal of Cell Biology, 2016. **212**(1): p. 113-124.

34. Watson, C., et al., *An in vivo model of human small intestine using pluripotent stem cells.* 2014, 2014. **20**(11): p. 1310-1314.

35. Dame, M., et al., *Identificaion, isolation and characterization of human LGR5-positive colon adenoma cells.* Development, 2018. **145**(6).

36. Cruz-Acuna, R., et al., *PEG-4MAL hydrogels for human organoid generation, culture, and in vivo delivery.* Nature Protocols, 2018. **13**: p. 2102-2119.

37. Rowley, J.A., G. Madlambayan, and D.J. Mooney, *Alginate hydrogels as synthetic extracellular matrix materials.* Biomaterials, 1999. **20**: p. 45-53.

38. Augst, A.D., H.J. Kong, and D.J. Mooney, *Alginate Hydrogels as Biomaterials.* Macromolecular Bioscience, 2006. **6**: p. 623-633.

39. Fu, S., et al., *Rheological Evaluation of Inter-grade and Inter-batch Variability of Sodium Alginate.* AAPS PharmSciTech, 2010. **11**(4): p. 1662-1674.

40. Martyn, I., et al., *Self-organization of a human organizer by combined Wnt and Nodal signalling.* Nature, 2018. **558**: p. 132-135.

41. McCracken, K., et al., *Modeling human development and disease in pluripotent stem cell-derived gastric organoids.* Nature, 2015. **516**(7531): p. 400-404.

42. Matsuo, Y., C. Nishizaki, and H. Drexler, *Efficient DNA fingerprinting method for the identification of cross-culture contamination of cell lines.* Human Cell, 1999. **12**(3): p. 149-154.

43. Josephson, R., et al., *A molecular scheme for improved characterization of human embryonic stem cell lines.* BMC Bioloy, 2006. **4**(28).

44.   Leslie, J., et al., *Persistence and toxin production by Clostridium difficile within human intestinal organoids result in disruption of epithelial paracellular barrier function.* Infection and Immunity, 2015. **83**(1): p. 138-145.

45.   Heijmans, J., et al., *ER stress causes rapid loss of intestinal epithelial stemness through activation of the unfolded protein response.* Cell Rep, 2013. **3**(4): p. 1128-1139.

46.   Bell, S., et al., *R-spondin 2 is required for normal laryngeal-tracheal, lung and limb morphogenesis.* Development, 2008. **135**(6): p. 1049-1058.

47.   Tsai, Y.-H., et al., *A Method for Cryogenic Preservation of Human Biopsies and Subsequent Organoid Culture.* Cellular and Molecular Gastroenterology and Hepatology, 2018.

48.   Bray, N.L., et al., *Near-optimal probabilistic RNA-seq quantification.* Nature Biotechnology, 2016. **34**: p. 525-527.

49.   Love, M.I., W. Huber, and S. Anders, *Moderated estimation of fold change and dispersion for RNA-seq with DESeq2.* Genome Biology, 2014. **15:550**.

Chapter 4 : Suspension Culture Promotes Serosal Mesothelial Development in Human Intestinal Organoids

4.1 Introduction

Human intestinal organoids (HIOs) are 3D tissues derived from human pluripotent stem cells (hPSCs) that mimic the structure and function of the human intestine [1, 2]. However, HIOs lack some key cell types found in the native intestine including vasculature and neurons [3-7]. HIOs offer advantages over 2D cell-based model systems that do not recapitulate the 3D architecture of human organs, or animal models that do not always mimic human physiology [8]. While HIOs are a promising tool to study intestinal development and disease, they have been hindered by reliance on basement membrane extracellular matrix (ECM) products (i.e. Matrigel). These ECMs support growth but introduce biological variability and are not amenable to clinical applications due to high cost and xenogeneic origin [9]. We have recently demonstrated that HIOs,

which possess both epithelium and mesenchyme, create their own basement membrane and can thus be cultured in biologically inert alginate hydrogels [10]. The observation that HIOs can grow in the absence of a biochemically supportive ECM led us to hypothesize that HIOs may not require extrinsic support. Here, we demonstrate that a 3D substrate is dispensable for HIO culture and that HIOs can be cultured in suspension. This technique increases the simplicity of HIO culture, streamlines maintenance while enhancing the ability to scale-up, and reduces experimental cost and variability. Notably, while HIOs cultured in suspension possessed expected epithelial cell types, they exhibited enhanced mesenchymal organization including a serosal mesothelial-like layer.

The serosal mesothelium is the outermost layer of the intestine comprised of a single layer of squamous mesothelial cells [11]. It provides a protective boundary for the intestine and creates a lubricating, frictionless surface [12] that is involved in homeostasis and disease [13-19]. The serosa also plays a critical role in development via contributions to mesenchyme, especially vascular smooth muscle, in multiple organs [20-23]. Despite the need to better understand this tissue, a serosal mesothelium has never been described in complex 3D models of the human intestine.

We compared suspension HIOs to the developing human intestine and show that the serosal mesothelial layer within suspension HIOs is similar to that of the human intestine at the cellular, molecular, and functional level. Using suspension HIOs, we interrogated signaling pathways that control mesothelial differentiation. By carrying out a targeted inhibitor screen, our results implicate Hedgehog (HH) and WNT signaling as key regulators of serosal mesothelial formation in the human intestine. Overall, these studies

introduce added complexity to the HIO model system in order to study development of the intestinal mesenchyme and serosa.

4.2 Results

HIOs Grow and Mature in Suspension Culture

Based on our observation that HIOs can be cultured in unmodified alginate, a bioinert hydrogel that provides purely mechanical support [10], we hypothesized that the 3D support provided by ECM may be dispensable for HIO development. We tested this hypothesis using suspension culture as an alternative method to grow HIOs (Appendix A). Suspension culture has been utilized in other organoid systems [24-26] and is a simple, cost-effective method that is amenable to scale-up. Intestinal hindgut spheroids were generated using a previously described method [1-3, 27]. Instead of transferring spheroids to a 3D droplet of alginate or Matrigel, we transferred spheroids to a low attachment plate containing HIO growth media (Figure 4-1A). By 4 weeks of culture, suspension HIOs resembled alginate and Matrigel HIOs as assessed by bright field microcopy and hematoxylin and eosin (H&E) staining, with a defined inner epithelium and outer mesenchyme (Figure 4-1A, B).

We used histological techniques to examine the effects of suspension culture. HIOs cultured in suspension developed an inner ECAD+ epithelium surrounded by VIM+ mesenchyme. The epithelium of suspension HIOs expressed the intestinal transcription factor CDX2 as well as the duodenum marker PDX1. Additionally, suspension HIOs had a properly polarized epithelium as the tight junction marker ZO-1 was expressed across the apical surface (Figure 4-1C). Suspension HIOs expressed the proliferation marker

KI67 throughout the epithelium and mesenchyme, demonstrating that HIOs are able to proliferate in suspension. Similar to alginate and Matrigel HIOs cultured *in vitro*, the epithelium of suspension HIOs was largely immature as evidenced by broad expression of the progenitor marker SOX9 [28]. However, suspension HIOs gave rise to differentiated intestinal epithelial cell types including DPP4+ enterocytes, MUC2+ goblet cells, and CHGA+ enteroendocrine cells (Figure 4-1D) [10]. To directly compare suspension HIOs to alginate and Matrigel HIOs, we performed qRT-PCR and found that expression levels of most markers tested displayed no significant differences between conditions (Figure 4-2B). While HIOs are relatively immature *in vitro* [3, 29], we found that suspension HIOs undergo maturation when transplanted into mice, as has been described for alginate and Matrigel HIOs [5, 10] (Figure 4-2B-E). Together, these results demonstrate that suspension culture supports the development of HIOs and gives rise to an epithelium that resembles alginate and Matrigel HIOs *in vitro* and *in vivo.*

HIOs Cultured in Non-Adherent Conditions Form Putative Serosal Mesothelium

While suspension HIO epithelium was similar to alginate and Matrigel HIOs, we observed differences in mesenchymal organization. In alginate and suspension HIOs, the mesenchyme became radially oriented in a manner that more closely resembled the fetal intestinal mesenchyme. This may be due to the non-adherent nature of alginate and suspension culture, since mesenchymal cells were unable to interact with a surrounding matrix and spread away from the epithelium as in Matrigel. In order to characterize mesenchymal differences across culture conditions, we performed H&E staining. Notably, we observed an outer cell layer in alginate and suspension HIOs that resembled the

serosal mesothelium of the developing human intestine [11, 30], while a defined outer layer was not observed in Matrigel HIOs (Figure 4-1D).

In order to confirm serosal identity in alginate and suspension HIOs, we performed immunostaining for mesothelial markers. Wilms' tumor protein (WT1) and Cytokeratin proteins are well characterized markers of mesothelial cells [13, 23, 31-34]. Additionally, previous studies have indicated that the serosal mesothelium sits on a laminin-rich basement membrane [13, 30]. In Matrigel HIOs, a serosal mesothelium was never observed as WT1 was disperse throughout the mesenchyme, and Matrigel HIOs did not form an outer basement membrane (Figure 4-1E). In both alginate and suspension HIOs, we observed a putative serosal mesothelium marked by co-expression of WT1 and pCK, and lined by a LAM+ basement membrane (Figure 4-1E). Mesothelial staining patterns in alginate and suspension HIOs resembled the serosal mesothelium of the human fetal intestine. Additionally, suspension HIOs formed a microvillus-lined surface typical of mesothelial cells based on TEM and immunostaining for the microvillus marker VIL1 (Figure 4-3A) [12]. We assessed levels of the secreted fibrinolytic agent, t-PA, which mediates fibrinolytic activity of the serosa, and found that suspension HIOs had higher levels of t-PA secreted into the media than Matrigel HIOs (Figure 4-3B). This suggests that HIO-serosa exhibits some expected functions of human serosal mesothelium, including fibrinolytic activity and microvillus formation [12, 35].

HIO-Serosa Resembles Human Serosa at the Molecular Level

To characterize the developing human serosa and more closely compare HIO-serosa to human fetal serosa, we analyzed published single cell RNA-sequencing

(scRNA-seq) human fetal intestine data and generated scRNA-seq data for suspension HIOs [4, 36] (Figure 4-3C, D). From the human fetal data, we identified a small subset of cells within mesenchymal cluster 8 that expressed mesothelial markers *WT1* [37], *UPK3B [38]*, *MSLN* [39], and *KRT19* [40] (Figure 4-3E). In order to better define the subset of human fetal serosal cells, we computationally extracted and re-clustered 761 cells from cluster 8 to identify a subset of cells (sub-cluster 2) as human serosal mesothelium based on expression of *WT1*, *UPK3B*, *MSLN*, and *KRT19* (Figure 4-4A). We similarly performed scRNA-seq on suspension HIOs, which displayed expected epithelial (cluster 4) and mesenchymal (clusters 0, 1, 2, 3) cell lineages (Figure 4-4B). We identified cells within cluster 2 that expressed mesothelial markers (Figure 4-4B, 4-3F). We computationally extracted cluster 2 and performed sub-clustering on 989 cells to identify sub-cluster 0 as a serosa-like population expressing the highest levels of *WT1*, *UPK3B*, *MSLN*, and *KRT19* (Figure 4-4C).

From the extracted serosa sub-clusters within human intestine and suspension HIOs, we obtained lists of the most differentially expressed genes defined as a $\log_2$ fold >1.5 in expression of a gene in the serosa cluster relative to all other clusters (Table S1). The human fetal and HIO-serosa shared 45 genes in common: 18.6% of all genes or 31.0% and 31.6% of genes in each list, respectively - a statistically significant overlap (Figure 4-4D). When comparing any cluster to all other clusters (fetal intestine, suspension HIO, fetal serosa, HIO-serosa), the average overlap between gene sets is 2.4%. This suggests that comparing *in vivo* to *in vitro* serosa has a 7.8-fold increase in gene expression overlap than would be expected by chance. The list of genes upregulated in both human and HIO-serosa revealed well-documented mesothelial genes

and markers that are not well defined in the literature including *CAV1, CAV2,* and *EZR* (Figure 4-4D). Histological analysis confirms that these markers are expressed in human fetal and HIO-serosa (Figure 4-3G). This analysis provides further confirmation that HIO-serosa resembles human intestinal serosa and identifies previously under-studied genes that mark this population.

HIO-Serosa Retains Functional Capability to Differentiate into Smooth Muscle-Like Cells

Mesothelial cells have a well-described function of giving rise to mesenchymal cells including vascular smooth muscle [20, 22, 23]. Additionally, previous studies have demonstrated that isolated mesothelial cells undergo differentiation into smooth muscle-like cells *in vitro* [41, 42]. In order to test if HIO-serosa exhibits the expected functionality of differentiating into smooth muscle-like cells, we devised a FACS strategy to enrich serosal cells. We observed that human and HIO-serosa express PDPN and ECAD but not EPCAM (Figure 4-4E, 4-5A). This allowed us to separate serosa (PDPN+/ECAD+/EPCAM-) from epithelium (PDPN-/ECAD+/EPCAM+) and non-serosal mesenchyme (PDPN-/ECAD-/EPCAM-) (Figure 4-5B). We performed qRT-PCR on the sorted cell populations and verified that serosal mesothelial genes including *WT1* and *UPK3B* were significantly enriched in the sorted PDPN+/ECAD+/EPCAM- population (Figure 4-4F, 4-5C).

Sorted HIO-serosa cells were cultured *in vitro* for 24 hours as an initial time point (Isolated HIO-Serosa) and compared to sorted cells cultured for 7 days. We observed a significant increase in the percentage of cells that were αSMA+ after 7 days compared to the 24-hour time point, as 30.8 ± 6% of cells expressed αSMA after 7 days (Figure 4-4G,

H). We additionally performed qRT-PCR to compare freshly sorted HIO-serosa to HIO-serosa cells cultured *in vitro* for 7 days (Figure 4-4H) and observed increased expression of smooth muscle markers *ACTA2* and *TAGLN* (Figure 4-4I). These results demonstrate that HIO-serosa behaves in a manner typical of mesothelial cells differentiating into smooth-muscle like cells.

HIO-Serosa Formation is Enhanced in Suspension Culture

Our data has suggested that suspension and alginate HIOs possess an organized serosa-like layer whereas Matrigel HIOs sometimes possess few disorganized WT1+ cells. In order to further interrogate similarities and differences, we combined scRNA-seq analyses of 28-day HIOs cultured in Matrigel, alginate, and suspension. We observed that cells from all 3 conditions were represented in every cluster (Figure 4-6A). The proportion of cells that were epithelial was similar between culture conditions, while mesenchymal populations contributed different proportions (Figure 4-6A, 4-7B-D). From this combined analysis, we identified a population within cluster 3 that expressed mesothelial markers (Figure 4-6A). We computationally extracted and re-clustered this population, revealing that sub-cluster 1 was enriched for *WT1, UPK3B, MSLN,* and *KRT19* (Figure 4-6B). Within sub-cluster 1, 82.8% of cells originated from suspension HIOs, with 11.0% and 6.2% from alginate and Matrigel HIOs, respectively (Figure 4-6C). We additionally compared the distribution of cells within each sub-cluster across conditions and found that 61.5% of suspension HIO cells in cluster 3 fell into the mesothelial sub-cluster 1, compared with 31.6% and 6.7% in alginate and Matrigel,

respectively (Figure 4-6D). This analysis suggests that serosa formation is enhanced in suspension culture.

To further quantitate HIO-serosa formation across conditions, we calculated the percentage of HIOs cultured in suspension, alginate, and Matrigel that formed a serosa. We observed the highest frequency of serosa formation in suspension culture, and observed that serosa formation decreased as alginate density increased (Figure 4-6E). Similarly, we observed high expression of the mesothelial markers *WT1* and *UPK3B* by qRT-PCR in suspension culture with decreased expression in alginate HIOs and little to no expression in Matrigel HIOs (Figure 4-6F). If serosa formation was driven solely by lack of adhesion, we would expect to see no differences based on alginate gels of any concentration, given that alginate gels of increasing polymer concentration exhibit a higher storage modulus [10]. These data suggest that compressive or attractive forces from the ECM may hinder mesothelial development, while the absence of compressive forces in suspension culture promotes organization of a serosal mesothelium.

Hedgehog and WNT Signaling are Implicated in Serosal Mesothelial Development

Based on similarities between human and HIO-serosa, we utilized suspension HIOs to investigate signaling pathways involved in serosa formation, since little is known about mesothelial cell differentiation in the human intestine [43, 44]. Prior to interrogating signaling pathways involved in serosa formation, we determined when serosa first differentiates by analyzing an scRNA-seq time-course on HIOs [4] as well as immunofluorescent staining (Figure 4-8A,B, 4-5F). We found that HIO-serosa formation begins after day 7 of culture and is complete between day 14-28. Using this

135

developmental timeline, we applied activators/inhibitors of major signaling pathways known to be involved in mesothelial differentiation or intestinal mesoderm development [45-53] using suspension HIOs, and assessed their effects on the serosa.

Suspension HIOs were grown for 7 days before applying signaling activators/inhibitors to the culture medium so as not to interfere with early developmental patterning. Starting on day 8, we treated suspension HIOs with inhibitors of the FGF (SU5402), BMP (Noggin), Notch (DAPT), WNT (IWR1), and HH (Cyclopamine) signaling pathways. To assess serosa differentiation, we devised a qualitative grading scheme to score HIOs based on staining for WT1 and pCK. Scoring ranged from 0 to 3, where 0 indicated no serosa, 1 indicated a partial WT1+pCK+ outer serosa, 2 indicated a complete or 'perfect' serosa with WT1+pCK+ staining surrounding the HIO, and 3 indicated a full or partial outer serosa with additional ectopic WT1 staining in the mesenchyme (Figure 4-8C).

45.5 ± 6% of HIOs in basal media were scored '2', a complete serosa (Figure 4-8D). We compared the percentage of HIOs with score 2 in basal media to inhibitor-treated HIOs to determine if blocking key signaling pathways led to a change in the frequency of HIO-serosa formation. Inhibiting FGF, BMP, or Notch signaling did not significantly alter the percentage of HIOs that formed a complete serosa (Figure 4-8E, 4-9A). On the other hand, inhibition of WNT or HH signaling with IWR1 or Cyclopamine, respectively, led to a significant decrease in the percentage of HIOs with score 2 (Figure 5E).

To follow up on these findings, we pursued HH and WNT modulation experiments. Inhibition of HH signaling with Cyclopamine in suspension HIOs led to a majority of HIOs with score 3, indicating that HH inhibition led to excess WT1 expression throughout the

mesenchyme, while activation of HH signaling with SAG resulted in a majority of HIOs scoring 2 (Figure 4F, 4-9B). Cyclopamine treatment led to a significant decrease in the percentage of HIOs with score 2 compared to control or SAG treatment, while SAG-treated HIOs had a significantly higher proportion of score 2 compared to controls (Figure 4F). Thus, HH signaling may be necessary to restrict WT1 localization to the outer cell layer in the developing intestine.

In order to determine if HH modulation directly affects the intestinal serosa, we FACS isolated serosal mesothelial cells from suspension HIOs and treated these cells with SAG and Cyclopamine. After 7 days, we used immunofluorescence to stain for WT1 and αSMA, and calculated the percentage of cells in each condition that expressed each marker. We found that the percentage of αSMA+ cells in the Cyclopamine group was significantly lower than the percentage of αSMA+ cells in both the basal media and SAG groups (Figure 4-9C), suggesting that HH inhibition may block the ability of mesothelial cells to differentiate into αSMA+ mesenchymal cells. This is consistent with observations in the mesothelium of the developing mouse lung (Dixit et al., 2013).

Inhibition of WNT signaling with IWR1 resulted in a majority of HIOs with a score of 1 (Figure 4G, 4-9B), suggesting that endogenous WNT signaling may be required for proper serosal mesothelial formation. Stimulation of WNT signaling with CHIR-99021 caused aberrant serosa formation and resulted in HIOs with score 0 or 3 (Figure 4G, 4-9B), suggesting that altered WNT signaling disrupts serosa formation. IWR1 treatment did not significantly alter HIO length, suggesting that WNT inhibition stunts mesothelial development without limiting the overall growth of suspension HIOs. Together, these

137

results suggest that HH and WNT signaling are necessary for proper differentiation and patterning of the human intestinal serosal mesothelium.

4.3 Discussion

In this work we described suspension culture as an alternative to hydrogel or Matrigel culture for human intestinal organoids. Suspension culture provides an advantage over Matrigel by removing biological variability and reducing cost. Strikingly, HIOs cultured in non-adherent alginate or suspension formed a serosal mesothelium that resembled that of the human fetal intestine. scRNA-seq analysis of HIOs revealed a serosa population that was significantly similar to the human serosa cluster. We hypothesize that non-adherent culture conditions (alginate, suspension) promote mesothelial development compared to Matrigel as HIO mesenchymal cells are able to self-organize rather than migrating away from the epithelium. There were some differences in gene expression between human and HIO serosal mesothelium, which can be attributed to differences between the *in vivo* environment and *in vitro* culture [54]. Suspension culture enhances HIO-serosa formation compared to alginate-grown HIOs which suggests that lack of a compressive environment may enable mesothelial differentiation and organization. The emergence of a serosal mesothelium in suspension may be due to the fact that suspension culture mimics early developmental events *in vivo* in which the gut tube is essentially suspended in fluid [55].

In order to evaluate the functionality of HIO-serosa, we devised a method to FACS-purify mesothelial cells from suspension HIOs and confirmed that they undergo expected differentiation into smooth muscle-like cells *in vitro.* Thus, HIOs are a promising model

system to study mesothelial development and differentiation within a human model system *in vitro*. The ability to culture and sort mesothelial cells from HIOs may prompt further studies into factors driving mesothelial to mesenchymal differentiation. Additionally, isolated HIO-serosa may be a promising source of mesothelial cells for therapeutic approaches [45, 56, 57].

HIO-serosa serves as an *in vitro* model system to study how the serosa originates from mesodermal progenitors in the developing human intestine. Contrary to reports on the mesothelium of the heart [49], we did not find mesothelial differentiation to be dependent upon BMP or FGF. This may highlight organ or species-specific differences in mesothelial development. We demonstrated that inhibition of WNT or HH signaling disrupted serosa formation in suspension HIOs. However, the precise mechanism by which WNT and HH play a role in serosal development, including whether these pathways have a direct vs. indirect effect, is still unclear. FACS isolated HIO-serosal cells treated with Cyclopamine do not have significantly increased WT1 expression, but rather exhibit lower levels of αSMA expression compared to controls (Figure 4-9C), while whole HIOs treated with Cyclopamine exhibit excess ectopic WT1 expression in the mesenchyme (Figure 4F, 4-9C). This data suggests that HH is not directly inducing or blocking serosa differentiation, but may function to limit the ability of serosa to differentiate into other cell types such as αSMA+ mesenchyme. Based on these results, we propose a model where blocking HH inhibits the ability of WT1+ serosal cells to differentiate into non-serosal cell types such as smooth muscle-like cells.

Limitations of the Study

139

The yield of HIOs in suspension is reduced compared with Matrigel HIOs (Figure 4-2A), which could be due to heterogeneity in spheroids [58]. While we have shown that HIO-serosa is similar to human serosa, some mesothelial functions may be lost *in vitro*. Nonetheless, suspension HIOs present an improved method to study this poorly understood cell type. In addition, it is currently unclear how HH and WNT control serosa differentiation. HH and WNT inhibitors/activators/ligands were added to the culture media of complete HIOs and thus likely impacted other cell types in the HIO in addition to the serosa. Moreover, combinatorial studies have yet to be carried out. To more precisely understand how these pathways work individually and in combination, and how they influence a complex multi-tissue system like an HIO, activator/inhibitor experiments coupled with single cell approaches may be needed. This work highlights the usefulness of suspension HIOs as a model to study human mesothelial development, but further work is necessary to determine specific mechanisms that control the development of this cell type.

Author contributions:

Project conceptualization: M.M.C., S.H., J.R.S.

Experimental design: M.M.C., J.R.S., S.H., Y.-H.T.

Experiments and data collection: M.M.C., S.H., Y.-H.T., A.W., N.G., E.M.H., N.S., C.B.

Data analysis and interpretation: M.M.C., C.C., J.W., S.H., Y.-H.T., A.W., N.G.

Writing manuscript: M.M.C., J.R.S.

Editing manuscript: all authors

Declaration of Interests: The authors declare no competing interests.

4.4 Methods

Data and Code Availability: Sequencing data used in this study is deposited at EMBL-EBI ArrayExpress. Single-cell RNA sequencing of human tissue: human fetal intestine (ArrayExpress: E-MTAB-9489) [36]; human fetal intestine (ArrayExpress: E-MTAB-9363) [4]; human fetal intestine (ArrayExpress: E-MTAB-11335) – this study; HIO (ArrayExpress: E-MTAB-9228) [4]; HIO (ArrayExpress: E-MTAB-10187) [29]; HIO (ArrayExpress: E-MTAB-10268) [29]; HIO (ArrayExpress: E-MTAB-11338) – this study; HIO (ArrayExpress: E-MTAB-11347) – this study. Accession numbers for deposited data are also provided in the Key Resources Table. Code used for single cell analysis and data visualization can be found at: https://github.com/jason-spence-lab/Capeling_2022.

Experimental Model and Subject Details

hESC/hIPSC Lines and Generation of hPSC-Derived Intestinal Organoids

This study includes data from HIOs generated across 4 hPSC lines: Human ES lines H9 (NIH registry #0062, RRID: CVCL_9773, female) and UM63-1 (NIH registry #0277, RRID: CVCL_R782), as well as human iPSC lines WTC11 (RRID: CVCL_Y803, male) and 72.3 [59]. All experiments using hPSCs were approved by the University of Michigan Human Pluripotent Stem Cell Research Oversight Committee. hPSC lines and HIOs are routinely monitored for mycoplasma using the MycoAlert Mycoplasma Detection Kit (Lonza). hPSC lines are routinely karyotyped and H9 cells were authenticated using Short Tandem Repeat (STR) DNA profiling [60] at the University of Michigan DNA Sequencing Core and were found to exhibit an STR profile identical to previously described characteristics [61].

Stem cell maintenance and differentiation into HIOs was carried out as recently described in detail [1, 10, 27, 28, 62]. For an in-depth protocol on HIO suspension culture, see Appendix A. Cell culture was carried out in a 37°C tissue culture incubator. hPSCS were maintained in mTeSR 1 or mTeSR Plus cultured media (Stemcell Tecnologies) and enzymatically passaged with dispase (Gibco). hPSCs underwent directed differentiation into definitive endoderm over a 3-day treatment with Activin A (100ng/mL, R & D Systems) added into RPMI media supplemented with 0%, 0.2%, 2% HyClone dFBS on subsequent days. Endoderm was differentiated into hindgut by treatment with FGF4 (500ng/mL [63]) and CHIR99021 (2µM, APExBIO).

Mid/Hindgut spheroids that budded off from the monolayer during differentiation were collected after days 5 and 6 of hindgut induction. Spheroids were embedded in alginate or Matrigel as previously described [10], or transferred to low attachment plates for

suspension culture to enable growth into HIOs. Organoids were maintained in basal growth media consisting of Advanced DMEM/F12 with 1X B27 (Thermo Fisher), GlutaMAX (Gibco, 1X), penicillin-streptomycin (Gibco, 100 U ml^{-1} penicillin; 100 µg ml^{-1} streptomycin), and HEPES buffer (Gibco, 15 mM). Organoid basal growth media was supplemented with epidermal growth factor (EGF) (R&D Systems; 100 ng/mL), Noggin-Fc (100ng/mL) (purified from conditioned media [64]), and R-Spondin1 (5% conditioned medium [65]) for the first three days of culture to promote patterning into proximal small intestine. On the third day after embedding, media was changed to basal growth media supplemented with EGF alone. HIOs were maintained in EGF-supplemented media for the duration of culture. Media was changed every 5-7 days. Organoids were not passaged to avoid disrupting the serosal mesothelium. Catalog information for all cell culture reagents described here can be found in the Key Resources Table.

Experiments involving pooled sets of HIOs involved n≥10 organoids per experiment. See Figure legends for more information on sample size for each experiment. For experimental treatment groups including the HIO inhibitor screen, equal numbers of HIOs were randomly allocated to each experimental group.

Human Tissue

Normal, de-identified human fetal intestinal tissue was obtained from the University of Washington Laboratory of Developmental Biology and shipped overnight in Belzer-UW Cold Storage Solution (ThermoFisher, NC0952695) with cold packs as previously

described [54]. All research utilizing human tissue was approved by the University of Michigan institutional review board. For experiments involving human fetal small intestinal tissue, the following 8 samples were included: male, 47 days post-conception; female, 59 days post-conception; female, 72 days post-conception; male, 80 days post-conception; male, 85 days post-conception; male, 101 days post-conception; female, 127 days post-conception; female, 132 days post-conception.

Method Details

Generation of Low-Attachment Plates and Suspension Culture

Low attachment plates were generated using previously published methods [66]. In summary, poly (2-hydroxyethyl methacrylate) (pHEMA) coating solution was prepared by dissolving 4g of pHEMA (Thermo Fisher, see Key Resources Table) into 40 mL of 95% ethanol with 10 mM NaOH. The solution was shaken immediately upon addition of pHEMA to avoid precipitation and rotated continuously overnight until fully dissolved. 1 mL of pHEMA coating solution was applied to each well of a 6 well plate inside a biosafety cabinet to generate a low attachment culture plate. The plate was rocked side to side to ensure distribution of pHEMA, and then pHEMA was collected for re-use. The low attachment plate was left in the biosafety cabinet overnight with the plate lid open to allow evaporation of excess coating solution, and UV was turned on for 15 minutes to sterilize the plate. Low attachment plates were rinsed twice with 1XPBS prior to addition of spheroids to remove excess pHEMA. Approximately 200 spheroids were transferred to 1 well of a 6-well low-attachment plate containing 5mL of media for suspension HIO culture. To change media without aspirating organoids in suspension, media was collected under

a stereomicroscope using a P1000 after allowing organoids to settle to the bottom of the plate.

Embedding HIOs in Alginate

Low-viscosity sodium alginate powder (Alfa Aesar) was dissolved in 1 mL of 1 × PBS to a final concentration of 0.5%–2% (w/v) and heated to 98°C for 30 min on a heating block. Spheroids were suspended in alginate at a density of approximately 50 spheroids per 45 µL. 5 µL droplets of 2% (w/v) calcium chloride (Sigma-Aldrich) were deposited on the bottom of 24-well tissue culture plates, and 45 µL of alginate containing spheroids was pipetted directly onto the calcium chloride solution to initiate ionic crosslinking. The gels polymerized at room temperature for 5–10 min and were then placed into a tissue culture incubator and allowed to fully set for 20 min at 37°C before media was added.

Mouse Kidney Capsule Transplantation

The University of Michigan and Cincinnati Children's Hospital Institutional Animal Care and Use Committees approved all animal research. HIOs were cultured for 4 weeks in suspension and then collected for transplantation, at which point HIOs were implanted under the kidney capsules of immunocompromised NOD-scid IL2Rg-null (NSG) mice (Jackson Laboratory strain no. 0005557) as previously described [3, 5]. In summary, mice were anaesthetized using 2% isoflurane. A left-flank incision was used to expose the kidney after shaving and sterilization with isopropyl alcohol. HIOs cultured in suspension were surgically implanted beneath mouse kidney capsules using forceps. Prior to closure, an intraperitoneal flush of Zosyn (100 mg kg^{-1}; Pfizer) was

administered. Mice were euthanized for retrieval of tHIOs after 8 weeks. Results shown are representative of one experiment performed with a total of n=6 mice, with at least one organoid implanted per kidney capsule depending on HIO size.

Flow Cytometric Analysis of HIOs

Suspension HIOs were transferred to a Petri dish containing TrypLE Express (Thermo Fisher) and mechanically cut into small pieces using a scalpel. TrypLE and dissociated HIOs were then transferred to a 15 mL conical tube and placed into a tissue culture incubator at 37°C. HIOs were digested in TrypLE at 37°C until the tissue was fully dissociated (~1.5 - 2 hours), and tissue was agitated roughly every 15 minutes during digestion by vortexing and pipetting up and down with a P1000. Once digestion was complete, reactions were quenched by adding a 2X volume of DMEM: F12 media. HIO suspensions were passed through a 70 µm filter and then centrifuged at 300g for 5 min at 4°C. Cells were then rinsed in staining buffer (1XPBS, 2% BSA, 1X PenStrep, 10 mM Y-27632 (Reagents Direct)), centrifuged, and re-suspended in an appropriate volume of staining buffer for antibody staining (100-200 µl). Cell suspensions were stained with conjugated FACS antibodies (Key Resources Table) and DAPI (0.2 µg/ml) at 4 °C for 30 minutes. Cells were then rinsed with 3 mL of staining buffer, centrifuged, and re-suspended in 500 µL staining buffer. Flow cytometric analysis was performed using a Sony SY3200 cell sorter and accompanying software.

Cells were first gated on PDPN, and then passed through a secondary gate on ECAD and EPCAM. From the PDPN+ population, a PDPN+/ECAD+/EPCAM- population was

146

collected as HIO serosal mesothelium. From the PDPN- population, a PDPN-/ECAD+/EPCAM+ population was collected as HIO epithelium, and a PDPN-/ECAD-/EPCAM- population was collected as HIO mesenchyme.

Culture of Isolated HIO-Serosa

Following FACS isolation, PDPN+/ECAD+/EPCAM- serosa was plated on Matrigel-coated 24-well plates in basal organoid growth media supplemented with 10 mM Y-27632 (Reagents Direct) and 0.4 ug/mL Hydrocortisone (Sigma-Aldrich) [67]. Y-27632 was removed after 24 hours for 7-day cultures. For HH modulation experiments, Cyclopamine (5 µM) or SAG (2 µM) was added to basal organoid growth media with 0.4 ug/mL Hydrocortisone for 6 days following the 24-hour culture in basal media. See Key Resources Table.

HIO-Serosa Signaling Screen

Hindgut spheroids were collected and cultured in suspension with basal organoid growth medium supplemented with (EGF) (100 ng/mL), Noggin-Fc (100ng/mL), and R-Spondin2 (5% conditioned medium) for 3 days. On the third day after collection, media was changed to basal organoid growth medium supplemented with only EGF (100 ng/mL). After 7 days, signaling activators or inhibitors were applied by changing cultured medium to organoid growth medium supplemented with EGF (100 ng/mL – basal medium control condition) and signaling compounds, including DAPT (10 µM ng/mL), IWR1 (10 µM), CHIR99021 (2 µM), Cyclopamine (5 µM), SAG (2 µM), SU5402 (10 µM), Noggin-Fc (100 ng/mL), BMP4 (100 ng/mL), SHH (33.3 ng/mL), and WNT3A (250 ng/mL). See Key Resources Table for

catalog information. HIOs were then cultured in medium containing signaling compounds for 3 weeks (28 days total in culture). After 28 days, HIOs were collected and fixed for immunofluorescence staining or flash-frozen for qRT-PCR analysis.

To score HIOs and determine effects of signaling compounds on serosal mesothelium, an entire batch of matched HIOs was fixed and stained for WT1 and pCK. Each HIO in one plane of section was given a score between 0 and 3 based on WT1 and pCK immunofluorescent staining. Scoring was as follows – 0: no WT1+/pCK+ serosal mesothelium present or aberrant WT1 expression in the mesenchyme but not outer layer. 1: partial WT1+/pCK+ serosal mesothelium on the outside of the HIO but not covering the entire organoid. 2: WT1+/pCK+ serosal mesothelium covering the entire HIO. 3: complete or partial WT1+/pCK+ serosal mesothelium on the outside of the HIO combined with ectopic WT1 expression throughout the mesenchyme.

Single Cell Preparation of Tissue for Single Cell RNA Sequencing

Previously published methods were utilized to carry out cell dissociations [54]. Tubes and pipette tips were washed with HBSS containing 1% BSA prior to dissociation protocol to prevent adhesion of cell suspensions to the plastic. Centrifugation steps were carried out at 10⁰C unless otherwise stated. The Neural Tissue Dissociation Kit (Miltenyi, cat. no. 130-092-628) was used for all RNA-seq dissociations.

Human fetal intestinal tissue or human intestinal organoids was dissociated into single cells by first mechanically cutting tissue into small pieces using a scalpel in a Petri dish

containing cold 1X HBSS with Mg^{2+}, Ca^2. Tissue fragments were then transferred to a 15

mL conical tube and treated with Mix 1 for 15 minutes $10^{o}C$. Mix 2 was added to the tube

and the remainder of the digestion was carried out at $10^{o}C$ until tissue was fully digested.

Every 10 minutes, the cell solution was pipetted up and down with a P1000 and assessed

under a stereo microscope to determine whether the digestion was complete. Once tissue

was digested into a single-cell suspension, cells were passed through a 70 µm filter

coated with 1% BSA in 1X HBSS. The filtered cell suspension was centrifuged for 5

minutes at 500g, and the cell pellet was resuspended in 500µL 1X HBSS with Mg^{2+}, Ca^{2+}.

1 mL Red Blood Cell Lysis buffer (Roche cat. No 11814389001) was added to the cell

suspension and the tube containing cells was placed on a rocker at $4^{o}C$ for 15 minutes.

The cell suspension was centrifuged for 5 minutes at 500g, and the pellet was washed

by resuspending in 2 mL HBSS with 1% BSA. Centrifugation and re-suspension were

repeated such that cells were washed twice and then counted with a hemocytometer.

Cells were then centrifuged and resuspended to reach a final concentration of 1000

cells/µL and kept on ice while transferred to the University of Michigan Advanced

Genomics Core where single cell droplets were immediately prepared on the 10x

Chromium according to manufacturer instructions. A target of 5,000-10,000 cells captured

was utilized. The Chromium Next GEM Single Cell 3' Library Construction Kit v3.1 (10x

Genomics) was used to prepare single cell libraries according to manufacturer

instructions.

RNA Extraction and quantitative RT-PCR Analysis

qRT-PCR experiments were carried out as previously described (Miller et al., 2018). RNA was extracted using the MagMAX-96 Total RNA Isolation System (Life Technologies) or Qiagen RNeasy Mini kit for FACS samples. A Nanodrop 2000 spectrophotometer (Thermo Scientific) was used to assess RNA quality and concentration, and then a cDNA library was generated from isolated RNA using the SuperScript VILO cDNA master mix kit (Invitrogen. qRT-PCR analysis was conducted using the QuantiTect SYBR Green PCR Kit (Qiagen) on a Step One Plus Real-Time PCR system (Life Technologies). Gene expression levels were calculated as a change relative to GAPDH or ECAD expression using arbitrary units, which were calculated by the following equation: [2^ (GAPDH/ECAD Ct - Gene Ct)] x 10,000. Expression was normalized to ECAD for epithelial genes as there were variable levels of epithelium between samples. A Ct value of 40 or greater was considered not detectable. A list of primer sequences used can be found in the Key Resources Table and Table S2.

Tissue Preparation, Immunohistochemistry, and Imaging

Paraffin Sectioning and Staining

HIO and tHIO tissues were fixed in 4% Paraformaldehyde (Sigma) overnight, washed with PBS, and then dehydrated in an alcohol series: 30 minutes each in 25%, 50%, 75% Methanol:PBS/0.05% Tween-20, followed by 100% Methanol, 100% Ethanol and 70% Ethanol. Tissue was processed into paraffin using an automated tissue processor (Leica ASP300). Paraffin blocks were sectioned 7 uM thick, and immunohistochemical staining was performed as previously described [68]. Briefly, slides were rehydrated in a series of HistoClear, 100% Ethanol, 95% Ethanol, 70% Ethanol, 30% Ethanol, DI H_2O with 2

changes of 3 minutes each. Antigen retrieval as performed in 1X sodium citrate buffer in a vegetable steamer for 40 minutes. Following antigen retrieval, slides were washed in PBS and permeabilized for 10 minutes in 0.1% TritonX-100 in 1xPBS, blocked for 45 minutes in 0.1% Tween-20, 5% normal donkey serum in 1XPBS. Antibodies used in this study can be found in the Key Resources Table. Primary antibodies were diluted in block and applied overnight at 4ºC. Slides were then washed 3 times in 1X PBS. Secondary antibodies and DAPI were diluted in block and applied for 40 minutes at room temperature. Slides were then washed 3 times in 1X PBS and cover slipped with ProLong Gold.

H&E staining was performed using Harris Modified Hematoxylin (FisherScientific) and Shandon Eosin Y (ThermoScientific) according to manufacturer's instructions. Alcian blue/PAS staining was performed using the Newcomer supply Alcian Blue/PAS Stain kit (Newcomer Supply, Inc.) according to manufacturer's instructions. Trichrome staining was performed by the University of Michigan *in vivo* Animal Core.

Imaging and Image Processing

Fluorescently stained slides were imaged on a Nikon A-1 confocal microscope. Brightness and contrast adjustments were carried out using ImageJ (National Institute of Health, USA) [69] and adjustments were made uniformly across images.

Transmission Electron Microscopy

Suspension HIOs cultured for 28 days were collected for TEM and prepared using conventional TEM sample preparation methods described by the University of Michigan BRCF Microscopy and Image Analysis Laboratory. HIOs were fixed in 3% glutaraldehyde + 3% paraformaldehyde in 0.1M cacodylate buffer (CB), pH 7.2 until ready for sample prep. Samples were then washed 3 times for 15 minutes in 0.1M CB. After washing, samples were processed for 1 hour on ice in a post-fixation solution of 1.5% $K_4Fe(CN)_6$ + 2% OsO_4 in 0.1M CB. Samples were then washed 3 times in 0.1M CB, and 3 times in 0.1M Na_2 + Acetate Buffer, pH 5.2, followed by en bloc staining for 1 hour in 2% Uranyl Acetate + 0,1M Na_2 + Acetate Buffer, pH 5.2. Samples were then processed overnight in an automated tissue processor, including dehydration from H_2O through 30%, 50%, 70%, 80%, 90%, 95%, 100% ethanol, followed by 100% acetone. Samples were infiltrated with Spurr's resin at a ratio of acetone: Spurr's resin of 2:1 for 1 hour, 1:1 for 2 hours, 1:2 for 16 hours, and absolute Spurr's resin for 24 hours. After embedding and polymerization, samples were sectioned on an ultramicrotome. TEM sample grids were imaged on a JEOL JEM 1400 PLUS TEM.

ELISA for t-PA Expression

HIOs were cultured in Matrigel or suspension for 28 days *in vitro*. Conditioned media was collected from n>3 wells of HIOs after 28 days and stored at -80°C until testing. Expression of human t-PA in the conditioned media was detected using a human t-PA ELISA kit (ThermoFisher) according to manufacturer's instructions. The absorbance of each microwell was read on a Molecular Devices SpectraMax M5e microplate reader, using 450 nm as the primary wave length.

Quantification and Statistical Analysis

Statistical analyses and plots were generated in Prism 8 software (GraphPad). If more than two groups were being compared within a single experiment, an unpaired one-way ANOVA was performed followed by Tukey's multiple comparisons test to compare the mean of each group with the mean of every other group within the experiment unless otherwise specified. For all statistical tests, a significance value of 0.05 was used. For every analysis, the strength of p values is reported in the figures according the following: $p > 0.05$, $*p \leq 0.05$, $**p \leq 0.01$, $***p \leq 0.001$, $****p \leq 0.0001$. Details of statistical tests can be found in the figure legends. With the exception of scRNA-seq, three hPSC lines were used across experiments with at least 3 independent experiments and at least 3 technical replicates per experiment.

Computational Analysis of Single-Cell RNA Sequencing Data

Overview

To visualize distinct cell populations within the single-cell RNA sequencing dataset, we employed the general workflow outlined by the Scanpy Python package [70]. This pipeline includes the following steps: filtering cells for quality control, log normalization of counts per cell, extraction of highly variable genes, regressing out specified variables, scaling, reducing dimensionality with principal component analysis (PCA) and uniform manifold approximation and projection (UMAP) [71, 72], and clustering by the Louvain algorithm [73].

Sequencing Data and Processing FASTQ Reads into Gene Expression Matrices

All single-cell RNA sequencing was performed at the University of Michigan Advanced Genomics Core with an Illumina Novaseq 6000. The 10x Genomics Cell Ranger pipeline was used to process raw Illumina base calls (BCLs) into gene expression matrices. BCL files were demultiplexed to trim adaptor sequences and unique molecular identifiers (UMIs) from reads. Each sample was then aligned to the human reference genome (hg19) to create a filtered feature bar code matrix that contains only the detectable genes for each sample.

Quality Control

To ensure quality of the data, all samples were filtered to remove cells expressing too few or too many genes (Figure 4-3C-E/Figure 4-4A - <500, >10000; Figure 4-4B-C/Figure 4-3F - <500, >8000; Figure 4-6/Figure 4-5 - <500, >8000; Figure 4-5F,G/Figure 4A -<500, >10000), with high UMI counts (Figure 4-3C-E/Figure 4-4A – 60000; Figure 4-4B-C/Figure 4-3F – 50000; Figure 4-6/Figure 4-5 – 50000; Figure 4-5F,G/Figure 4A - 60000), or a fraction of mitochondrial genes greater than 0.1.

Normalization and Scaling

Data matrix read counts per cell were log normalized, and highly variable genes were extracted. Using Scanpy's simple linear regression functionality, the effects of total reads per cell and mitochondrial transcript fraction were removed. The output was then scaled by a z-transformation. Following these steps, a total of (Figure 4-3C-E/Figure 4-4A - 51790 cells, 1710 genes; Figure 4-4B-C/Figure 4-3F – 4619 cells, 4167 genes;

Figure 4-6/Figure 4-5 – 13055 cells, 2117 genes; Figure 4-5F,G/Figure 4A – 52689 cells, 2615 genes) were kept for clustering and visualization.

Variable Gene Selection

Highly variable genes were selected by splitting genes into 20 equal-width bins based on log normalized mean expression. Normalized variance-to-mean dispersion values were calculated for each bin. Genes with log normalized mean expression levels between 0.125 and 3 and normalized dispersion values above 0.5 were considered highly variable and extracted for downstream analysis.

Batch Correction

We have noticed batch effects when clustering data due to technical artifacts such as timing of data acquisition or differences in dissociation protocol. To mitigate these effects, we used the Python package BBKNN (batch balanced k nearest neighbors) [74]. BBKNN was selected over other batch correction algorithms due to its compatibility with Scanpy and optimal scaling with large datasets. This tool was used in place of Scanpy's nearest neighbor embedding functionality. BBKNN uses a modified procedure to the *k* nearest neighbors' algorithm by first splitting the dataset into batches defined by technical artifacts. For each cell, the nearest neighbors are then computed independently per batch rather than finding the nearest neighbors for each cell in the entire dataset. This helps to form connections between similar cells in different batches without altering the PCA space. After completion of batch correction, cell clustering should no longer be driven by technical artifacts.

Dimension Reduction and Clustering

Principal component analysis (PCA) was conducted on the filtered expression matrix followed. Using the top principal components, a neighborhood graph was calculated for the nearest neighbors (Figure 4-3C-E/Figure 4-4A – 16 principal components, 30 neighbors; Figure 4-4B-C/Figure 4-3F – 12 principal components, 15 neighbors; Figure 4-6/Figure 4-5 – 12 principal components, 15 neighbors; Figure 4-5F,G/Figure 4A – 16 principal components, 30 neighbors). BBKNN was implemented when necessary and calculated using the top 50 principal components with 3 neighbors per batch. The UMAP algorithm was then applied for visualization on 2 dimensions. Using the Louvain algorithm, clusters were identified with a resolution of (Figure 4-3C-E/Figure 4-4A – 0.8; Figure 4-4B-C/Figure 4-3F – 0.35; Figure 4-6/Figure 4-5 – 0.65, Figure 4-5F,G/Figure 4A - 1).

Cluster Annotation

Using canonically expressed gene markers, each cluster's general cell identity was annotated. Markers utilized include epithelium (*CDH1, EPCAM, CDX2, PDX1, VIL1, CLDN4*), mesenchyme (*VIM, COL1A2, PDGFRA, DCN, TCF21, COL3A1, FOXF1*), neuronal (*POSTN, S100B, STMN2, ELAV4*), endothelial (*ESAM, CDH5, CD34, KDR*), immune (*CD53, VAMP8, CD48, ITGB2*), and serosal mesothelium (*MSLN, WT1, UPK3B, PDPN*).

Sub-Clustering

After annotating clusters within the UMAP embedding, specific clusters of interest were identified for further sub-clustering and analysis. The corresponding cells were extracted from the original filtered but unnormalized data matrix to include (Figure 4-4A – 1040 cells, Figure 4-4C – 962 cells, Figure 4-6B/C – 1903 cells, Figure 4-5G, Figure 4A - 8179). The extracted cell matrix then underwent log normalization, variable gene extraction, linear regression, z transformation, and dimension reduction to obtain a 2-dimensional UMAP embedding for visualization.

4.5 Figures
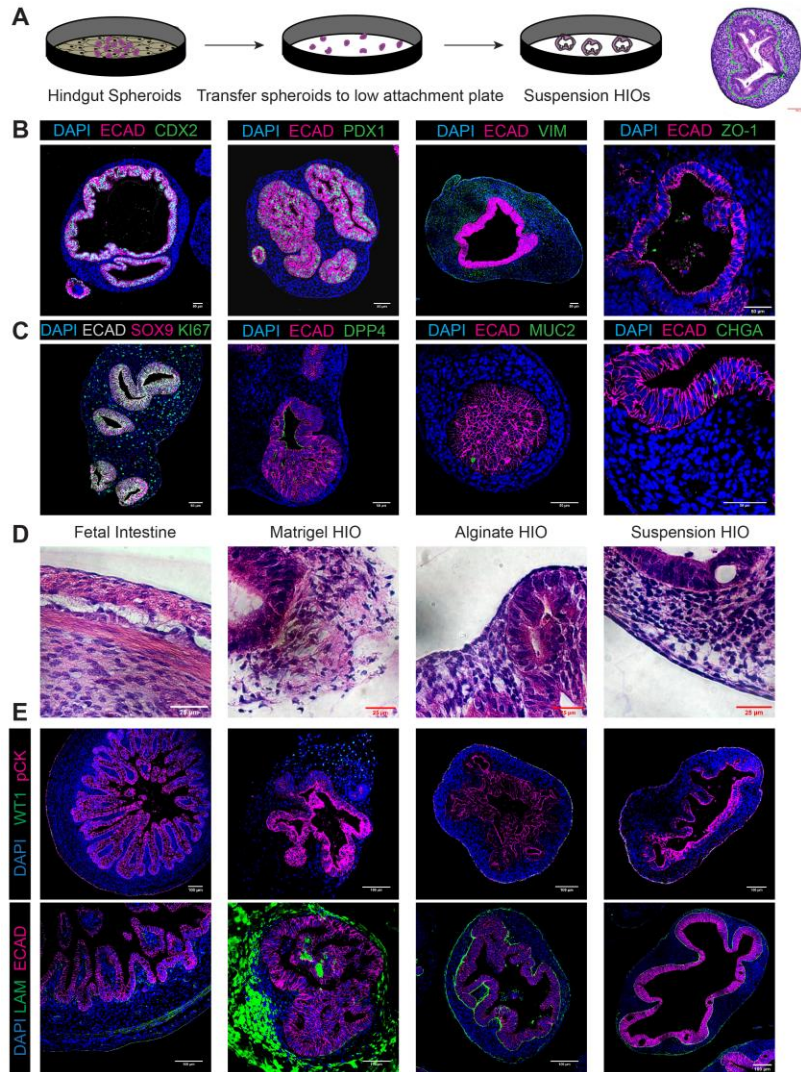
Figure 4-1. Suspension Culture Supports HIO Growth and Serosa Formation

(a): Schematic depicting HIO suspension culture. Right: Hematoxylin and eosin (H&E) stain of a 28-day suspension HIO. The epithelium is outlined in green. **(b):** Representative images of HIOs cultured in suspension for 28 days. Markers shown are ECAD, CDX2, PDX1, VIM, and ZO-1. Scale bar = 50µm. **(c):** Representative images of epithelial cell marker staining in HIOs cultured in suspension for 28 days. Markers shown are SOX9, KI67, DPP4, MUC2, and CHGA. Scale bar = 50µm. **(d):** H&E staining of the outer mesenchymal layer in human fetal intestine compared to HIOs cultured in Matrigel, 1% alginate, and suspension for 28 days. Scale bar = 25µm. **(e):** Representative images of mesothelial markers in human fetal intestine compared to HIOs cultured in Matrigel, 1% alginate, and suspension for 28 days. Markers shown are WT1, pan-Cytokeratin (pCK), LAM, and ECAD. Scale bar = 100µm.

158
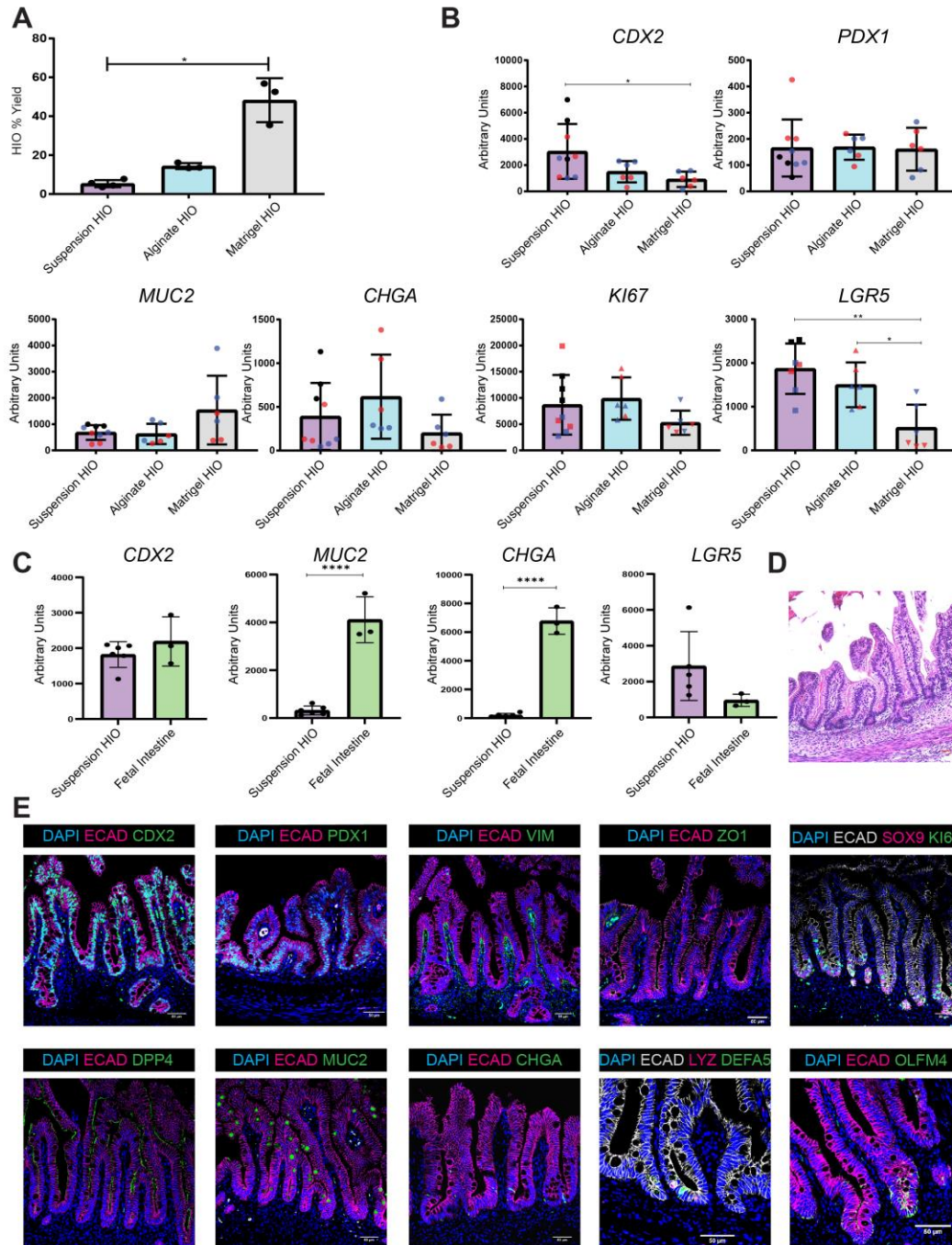
Figure 4-2. Suspension HIOs Resemble Alginate and Matrigel-Grown HIOs in vitro and in vivo.

(a): Quantification of HIO yield after 28 days. HIO yield was calculated as the percentage of spheroids which gave rise to HIOs. Data shown are average yields from 4 independent experiments (in suspension, biological replicates) with n>200 spheroids per condition, compared to previously published data for alginate and Matrigel (Capeling et al., 2019). Each point depicts mean yield from one experiment, while bars depict

159

mean and standard error. Significance was calculated with a one-way ANOVA and multiple comparisons test. **(b):** qRT-PCR analysis of CDX2, PDX1, MUC2, CHGA, KI67, and LGR5 expression in HIOs derived from 3 independent hPSC lines cultured in 1% alginate, Matrigel, and suspension for 28 days *in vitro* (biological replicates. Expression levels are normalized to ECAD expression to account for varying amounts of epithelium in HIOs. Each point is representative of 6-10 HIOs pooled from the same batch. Data represent the mean ± standard error of the mean. Significance was calculated with a one-way ANOVA and multiple comparisons test. **(c)**: qRT-PCR analysis of CDX2, MUC2, CHGA, and LGR5 expression in HIOs derived from 2 independent hPSC lines cultured in suspension for 28 days *in vitro* (biological replicates) compared to 11-week human fetal intestine (technical replicates). Expression levels are normalized to ECAD expression to account for varying amounts of epithelium. Data represent the mean ± standard error of the mean. Significance was calculated with a one-way ANOVA and multiple comparisons test. **(d)**: Hematoxylin and eosin staining in suspension HIOs cultured for 28 days *in vitro* and then transplanted beneath the kidney capsule of immunocompromised mice for 8 weeks *in vivo*. Scale bar = 100μm. **(e)**: Representative images of epithelial cell marker staining in suspension tHIOs. Markers shown are ECAD, CDX2, PDX1, VIM, ZO1, SOX9, KI67, DPP4, MUC2, CHGA, LYZ (Paneth cell marker), DEFA5 (Paneth cell marker), and OLFM4 (intestinal stem cell marker). Scale bar = 50μm.
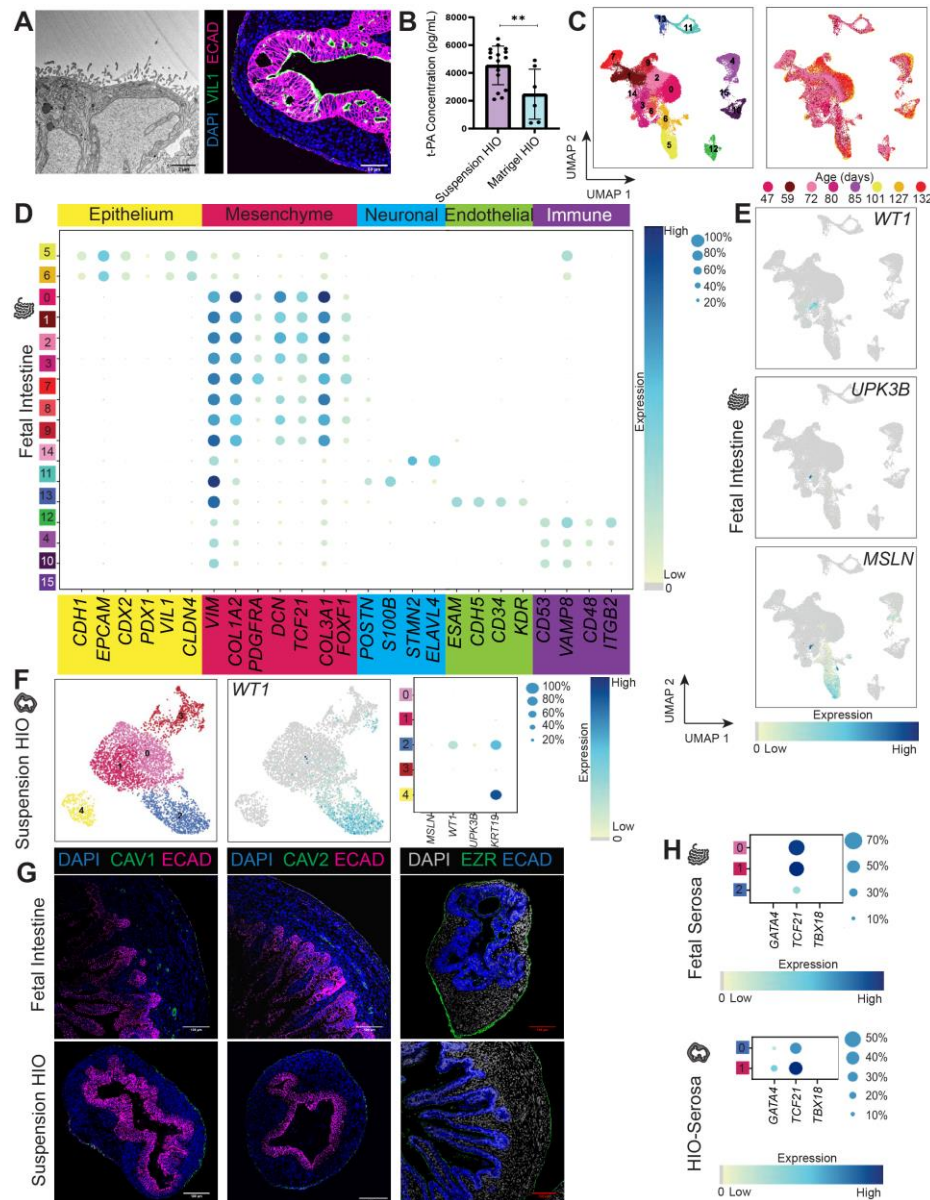
Figure 4-3. Characterization and scRNA-seq Analysis of Human Fetal Small Intestine and Suspension HIOs.

(a): Left: Transmission electron micrograph depicting microvilli lining on the surface of a 28-day suspension HIO. Right: Immunofluorescent image of VIL1 marker staining in the ECAD+ mesothelium of a 28-day suspension HIO. **(b):** Results from an ELISA for t-PA concentration in conditioned media collected from 28-day HIOs cultured in Matrigel and suspension. **(c):** Left: UMAP plot of 51,790 cells extracted from 8 human fetal small intestinal samples (duodenum, jejunum, and ileum) ranging from day 47 to day 132 profiled with scRNA-seq predicted 15 cell clusters. Data were visualized using Uniform Manifold Approximation and Projection (UMAP) dimensional reduction. The batch correction algorithm BBKNN was utilized to account for batch differences between samples. Right: UMAP plot of human fetal intestinal samples indicating sample age of

individual cells. **(d):** Dotplot of genes in human fetal intestinal samples associated with major cell classes: epithelial, mesenchymal, neuronal, endothelial, immune, and mesothelial. Dot size denotes the proportion of cells in a given cluster expressing each marker. Dot color indicates expression level within the cluster based on normalized z-score. Clusters are colored by class assignment: epithelium = yellow, mesenchyme = red/pink, neuronal = light blue, endothelial = green, immune = purple, serosa/mesothelial = dark blue. **(e):** Feature plots for mesothelial-specific markers WT1, MSLN, and UPK3B, highlighting the mesothelial population within a subset of cluster 8. **(f):** Feature plot for mesothelial-specific markers WT1 and dot plot for MSLN, WT1, UPK3B, and KRT19 in an analysis of 4,619 cells from 28-day suspension HIOs (Figure 4-4B), highlighting mesothelial gene expression within a subset of cluster 2. **(g):** Representative images of non-canonical mesothelial marker staining in human fetal intestine and suspension HIOs. Markers shown are ECAD, EZR, CAV1, and CAV2. Scale bar = 50µm. **(h):** Feature plots and dotplots for mesothelial markers GATA4, TCF21, and TBX18 depicting expression in extracted clusters of human fetal intestinal serosa as well as HIO-serosa. We observed expression of the mesothelial marker TCF21 in both human and HIO-serosa but did not observe high expression of the mesothelial markers GATA4 or TBX18 in either population, which may highlight organ and/or species-specific differences in mesothelial gene expression as these markers have been more commonly described in mesothelial cells of the mouse lung and heart.
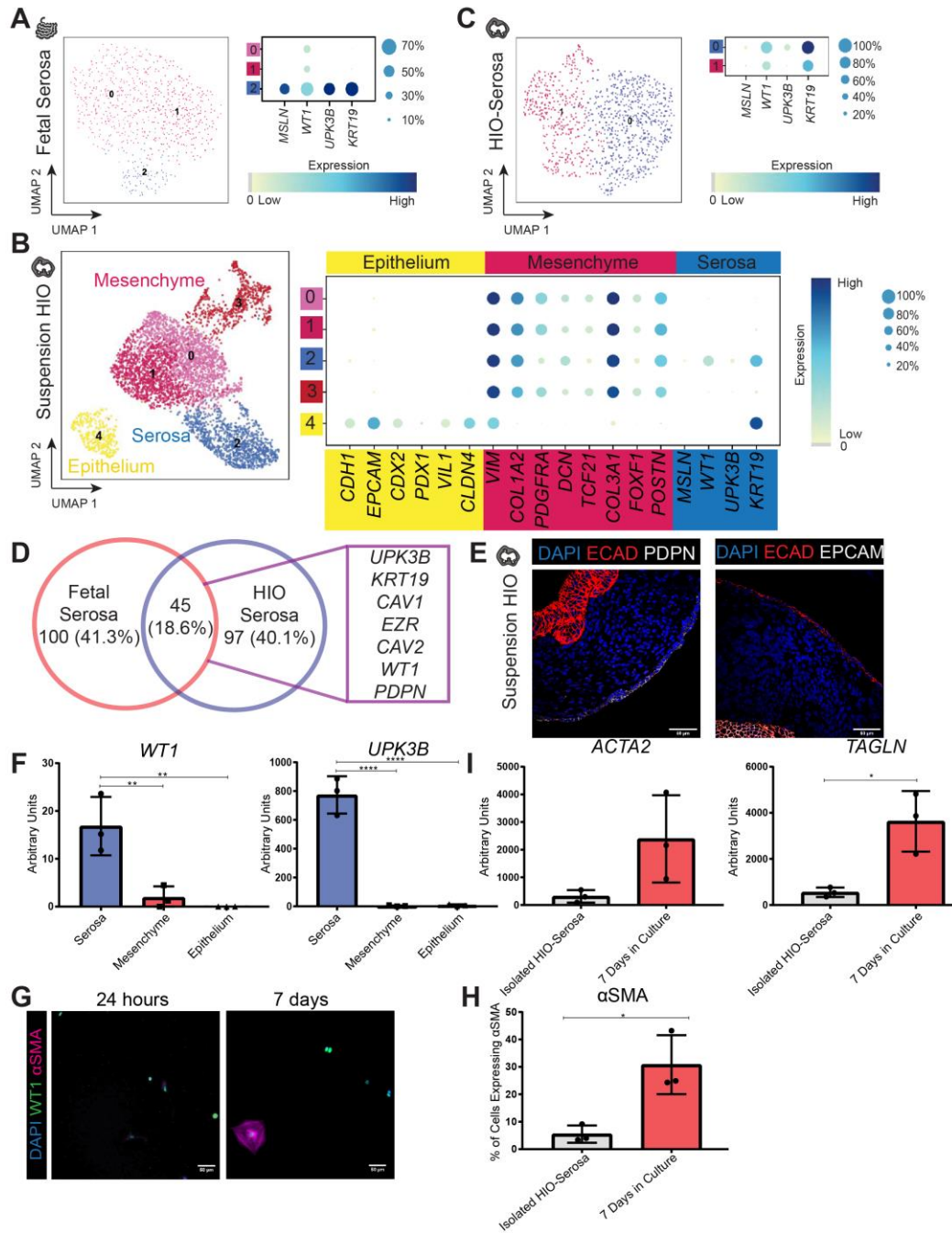
Figure 4-4. HIO-Serosa is Molecularly and Functionally Similar to Human Serosa.

(a): Left: UMAP plot of 761 cells computationally extracted from a sub-cluster within cluster 8 of the analysis on human fetal small intestine (Figure 4-3). Right: Dotplot of mesothelial genes highlighting the mesothelial population within cluster 2 (human fetal serosa). For all dotplots in Figure 4-4, dot size denotes the proportion of cells in a cluster expressing each marker, and dot color indicates expression level within the cluster based on normalized z-score. **(b):** Left: UMAP plot of 4,619 cells from 28-day suspension HIOs. Right: Dotplot of genes in suspension HIOs associated with major cell classes. **(c):** Left:

UMAP plot of 989 cells computationally extracted from cluster 2 of the analysis on suspension HIOs (Figure 4-4B). Right: Dotplot of mesothelial genes highlighting the mesothelial population within cluster 0 (HIO-serosa). **(d):** Venn diagram depicting genes that are significantly enriched (log$_2$ fold >1.5 in expression of a gene in the serosa cluster relative to all other clusters) in human fetal serosa (cluster 2, Figure 4-4A) and suspension HIO-serosa (cluster 0, Figure 4-4C). **(e):** Representative images of mesothelial markers used for FACS sorting in 28-day suspension HIOs (ECAD, EPCAM, and PDPN). Scale bar = 50µm. **(f):** qRT-PCR analysis of *WT1* and *UPK3B* expression in FACS-isolated serosa, mesenchyme, and epithelium from suspension HIOs. **(g):** Representative images of FACS-sorted HIO-serosa stained for WT1 and αSMA after 24 hours or 7 days cultured *in vitro*. Scale bar = 50µm. **(h):** Quantification of the percentage of DAPI+ FACS-sorted HIO-serosa cells that express αSMA. Each point represents 1 independent experiment with cells isolated from suspension HIOs from 3 different hPSC lines. **(i):** qRT-PCR analysis of ACTA2 and TAGLN expression in FACS-sorted HIO-serosa cells immediately after sorting or after 7 days in culture. For all graphs in Figure 4-4, data represent the mean ± standard error of the mean. Significance was calculated with a one-way ANOVA and multiple comparisons test. For all qRT-PCR data, expression levels are normalized to GAPDH. Each point is representative of sorting results from one pooled batch of HIOs, across n=3 independent experiments (biological replicates).
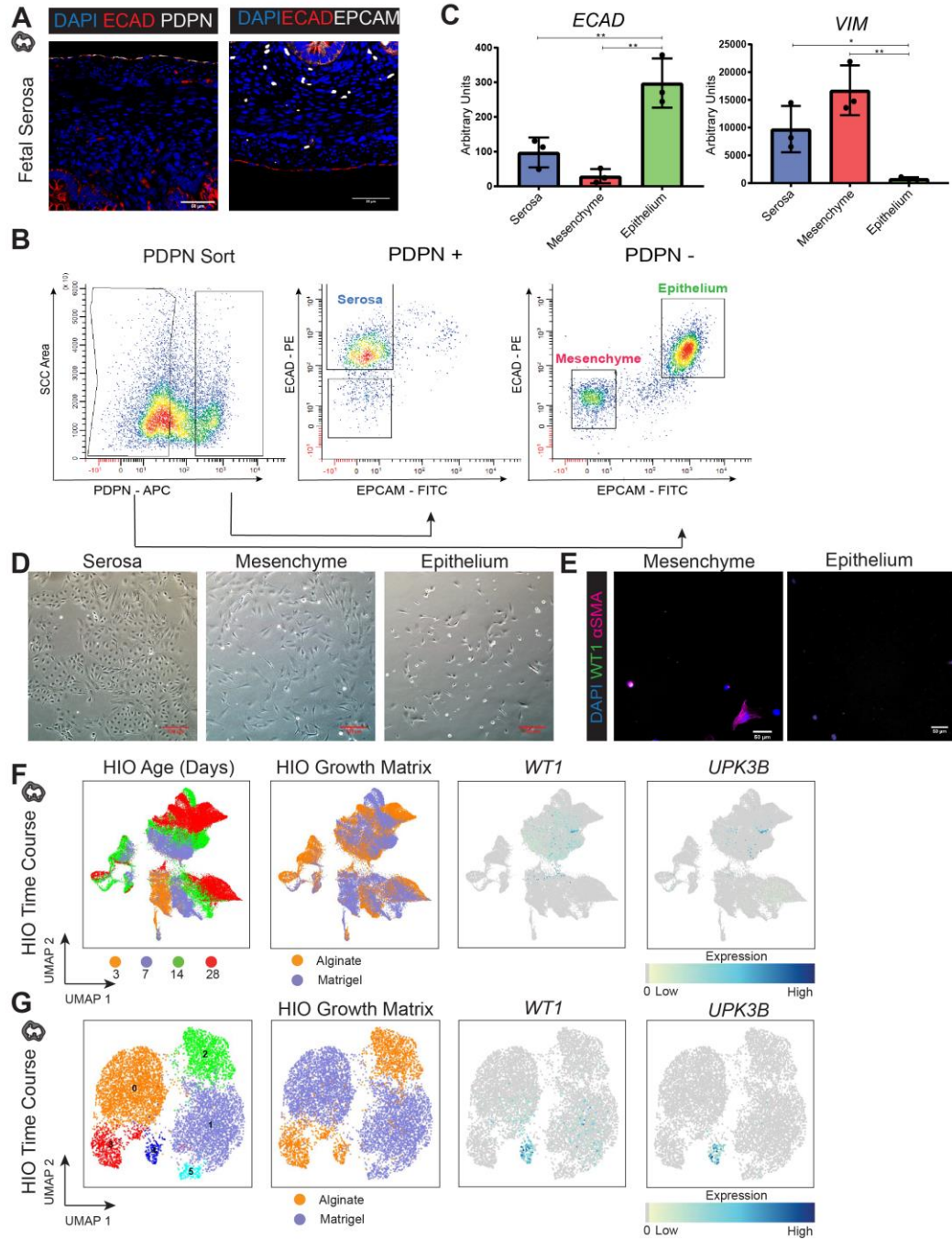
Figure 4-5. Validation of HIO-Serosa FACS Isolation and Extraction of Serosa Cluster from HIO Time Course.

(a): Representative images of mesothelial markers used for FACS sorting in human fetal intestine. Markers shown are ECAD, EPCAM, and PDPN. Scale bar = 50μm. **(b):** FACS plots demonstrating sorting strategy to isolate serosa, mesenchyme, and epithelium from suspension HIOs. Cells were first gated on PDPN. PDPN+/- cells were then sorted based on ECAD and EPCAM, and PDPN+/ECAD+/EPCAM- cells were collected as serosa, while PDPN-/ECAD-/EPCAM- cells were collected as

165

mesenchyme, and PDPN-/ECAD+/EPCAM+ cells were collected as epithelium. **(c):** qRT-PCR analysis of *ECAD* and *VIM* expression in FACS-isolated serosa, mesenchymal, and epithelial populations from 3 independent batches of suspension HIOs. Expression levels are normalized to GAPDH. Each point is representative of sorting results from one pooled batch of HIOs. Data represent the mean ± standard error of the mean. Significance was calculated with a one-way ANOVA and multiple comparisons test. **(d):** Bright field images of FACS-sorted serosa, mesenchymal, and epithelial populations from suspension HIOs cultured in basal media. Scale bar = 100μm. **(e):** Representative images of FACS-sorted mesenchyme and epithelium from suspension HIOs stained for WT1 and pCK after 24 hours in culture in basal media. Scale bar = 50μm. **(f):** Left: UMAP plot of 52,689 cells HIOs cultured in alginate and Matrigel collected at day 3, 7, 14, and 28 profiled with scRNAseq predicted 19 cell clusters. Right: Feature plots for mesothelial markers *WT1* and *UPK3B* in the alginate/Matrigel HIO time course dataset depicting a serosal mesothelial population at the boundary between cluster 3 and cluster 4. **(g):** Left: UMAP plot of 8,179 cells extracted from clusters 3 and 4 of the analysis in Figure 4-5A. Right: Feature plots for mesothelial markers *WT1* and *UPK3B* in the analysis on extracted clusters 3 and 4 depicting a serosal mesothelial population in sub-cluster 4.
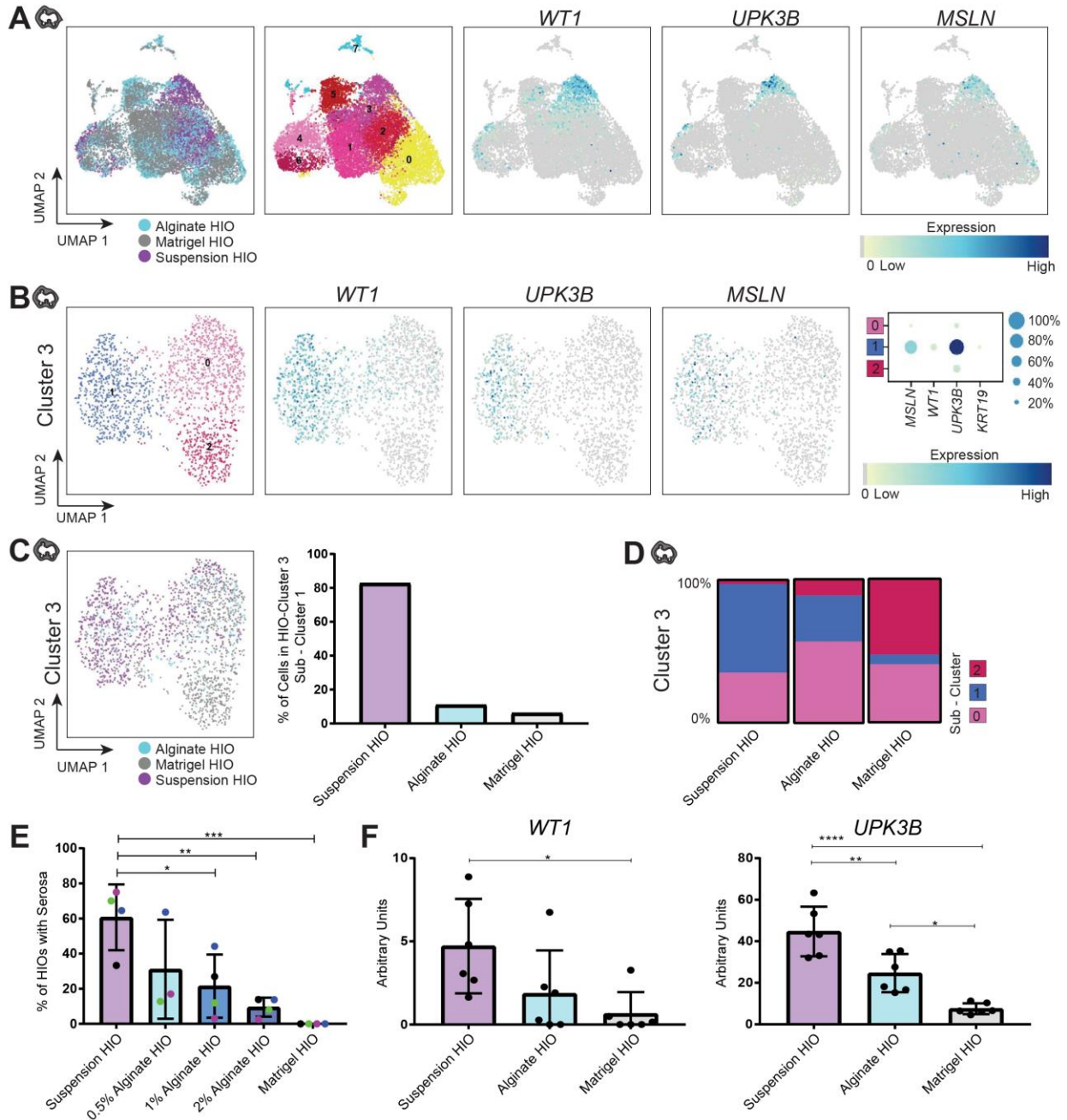
Figure 4-6. Comparing HIO-Serosa Between Matrigel, Alginate, and Suspension Culture.

(a): UMAP plot of 13,055 cells from 28-day alginate, Matrigel, and suspension HIOs. The batch correction algorithm BBKNN was utilized. Feature plots for mesothelial markers *WT1*, *MSLN,* and *UPK3B,* highlighting the mesothelial population within cluster 3. **(b):** Left: UMAP plot of 1,903 cells computationally extracted from cluster 3 of the analysis on alginate, Matrigel, and suspension HIOs (Figure 4-6A). Middle: Feature plots for mesothelial markers *WT1*, *MSLN,* and *UPK3B,* highlighting the mesothelial population within cluster 1. Right: Dotplot of mesothelial genes. **(c):** Left: UMAP plot of

167

computationally extracted HIO-serosa (cluster 3, sub-cluster 1) separated by culture condition. Right: Quantification of the percentage of cells within cluster 3, sub-Cluster 1 that are derived from each condition. **(d):** Distribution of the cells from alginate, Matrigel, and suspension HIOs in cluster 3 that were extracted into sub-clusters 0, 1, or 2. **(e):** Quantification of the percentage of HIOs in 4 independent batches that form a full or partial WT1+ pCK+ outer serosa. Each dot represents data from one batch, each color dot depicts an independent batch of HIOs (biological replicates), and bars depict mean and standard error. Significance was calculated with a one-way ANOVA and multiple comparisons test. **(f):** qRT-PCR analysis of *WT1* and *UPK3B* expression in HIOs derived from 2 independent hPSC lines cultured in suspension for 28 days *in vitro*. Expression levels are normalized to GAPDH. Each point is representative of 6-10 HIOs pooled from the same batch (biological replicates). Data represent the mean ± standard error of the mean. Significance was calculated with a one-way ANOVA and multiple comparisons test.
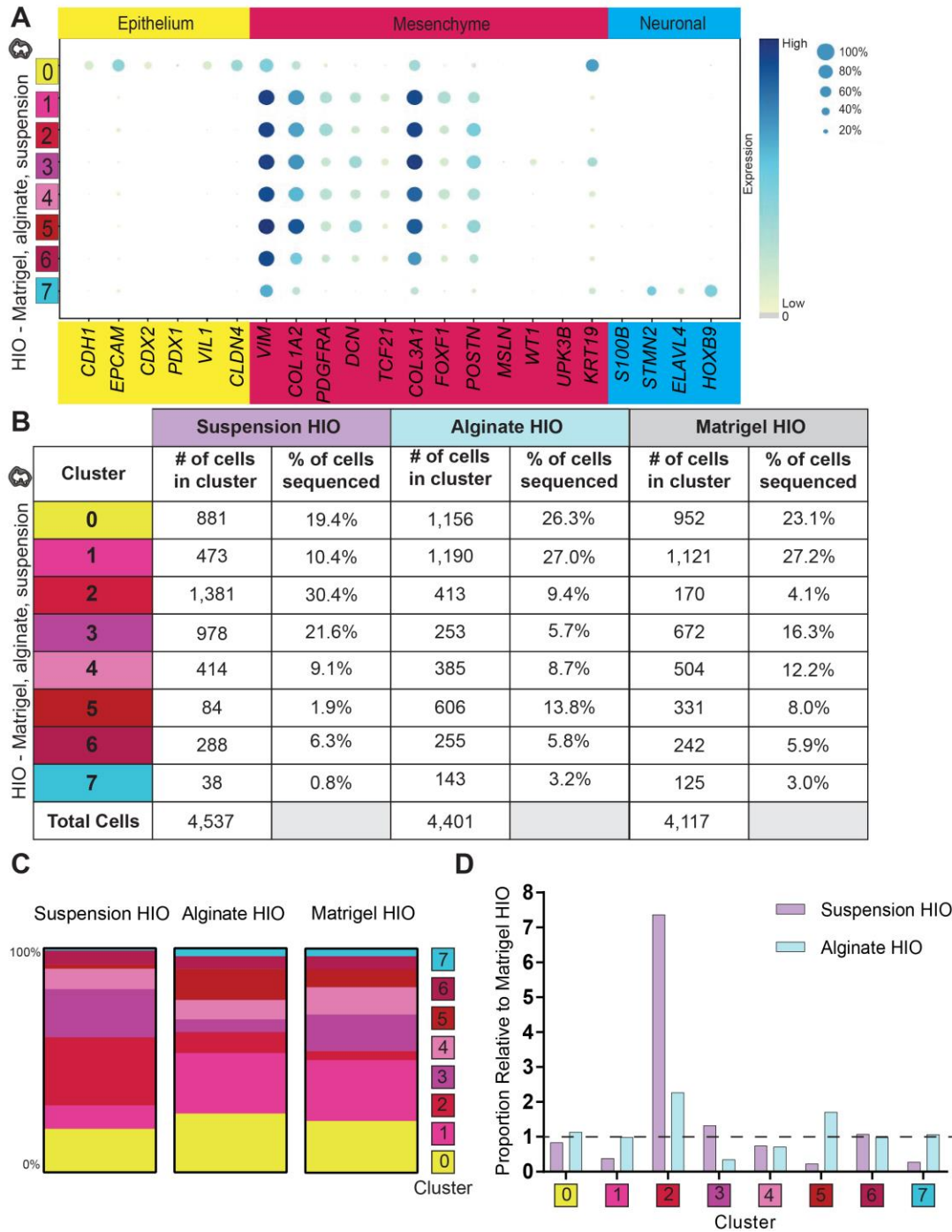
Figure 4-7. Analysis of Cell Types Within HIOs by Culture Condition.

(a): Dotplot of genes in human fetal intestinal samples associated with major cell classes: epithelial, mesenchymal, and a small neuronal population in cluster 7. Dot size denotes the proportion of cells in a given cluster expressing each marker. Dot color indicates expression level within the cluster based on normalized z-score. Clusters are colored by class assignment: epithelium = yellow, mesenchyme = red/pink, neuronal =

light blue. **(b):** Analysis of the contribution to each cluster based on HIO culture condition. Data shown are the number of cells in each cluster that came from HIOs cultured in suspension vs. alginate vs. Matrigel as well as the percentage of cells in each culture condition that were sorted into individual clusters. **(c):** Visual representation of the percentage of cells in each HIO culture condition that were sorted into clusters 0-7 using data from the table in Figure 4-7B. **(d):** Comparison of the proportion of cells from alginate and suspension HIOs in each cluster, normalized to Matrigel HIOs. Notably, the proportion of cells in epithelial cluster 0 was comparable between HIO culture conditions while there were differences in the contribution to mesenchymal clusters.
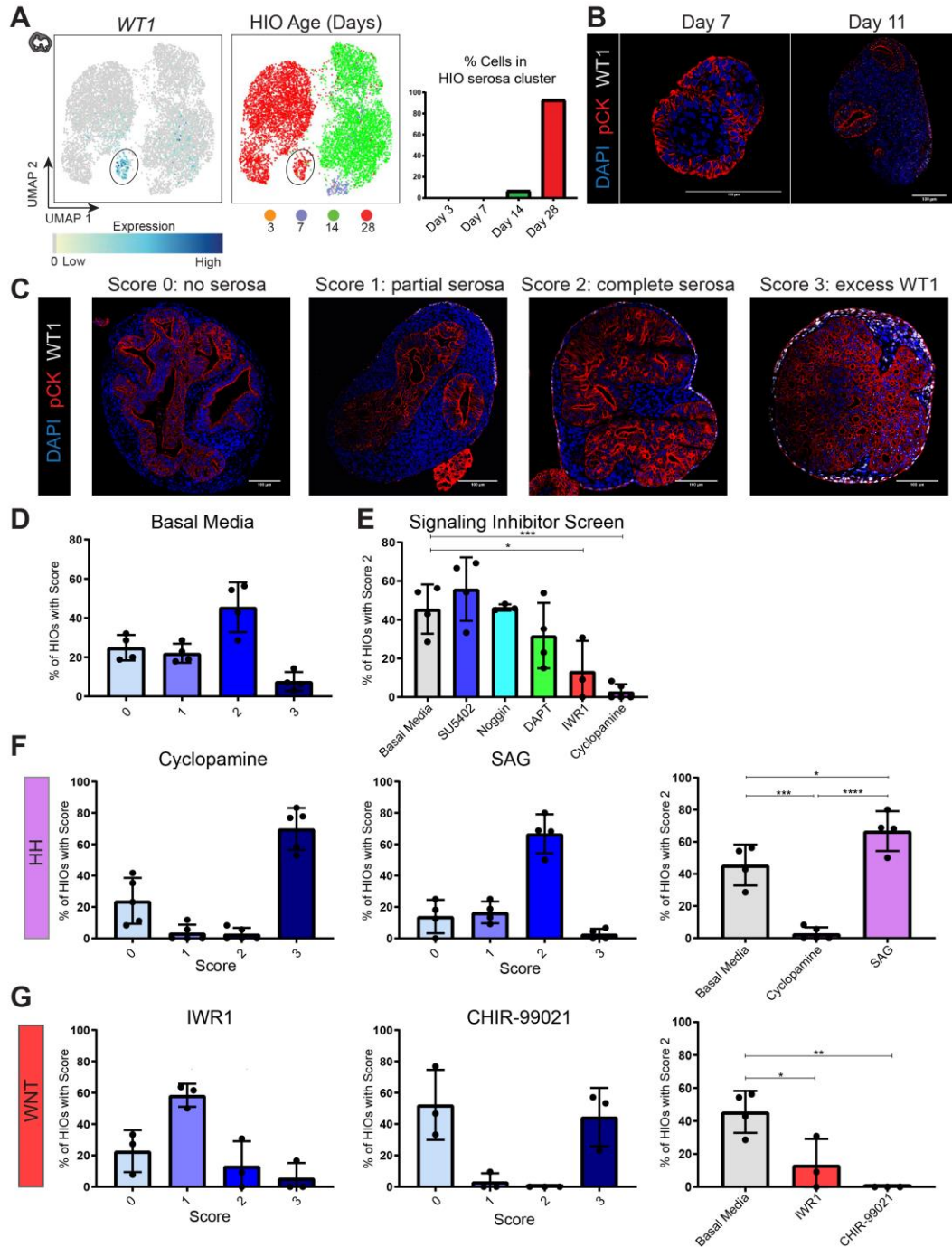
Figure 4-8. Signaling Pathways Implicated in Serosa Formation.

(a): UMAP plot of 8,179 cells extracted from clusters 3 and 4 (alginate and Matrigel HIO time-course, Figure 4-5). Right: Quantification of the percentage of cells within the serosal sub-cluster 4 that originate from HIOs collected at day 3, 7, 14, and 28. **(b):** Representative image of suspension HIOs collected at day 7 and 11 stained for WT1 and pCK. Scale bar = 100µm. **(c):** Qualitative scoring system to rank HIOs based on WT1 and pCK expression. 0 = no serosa, 1 = partial serosa, 2 = complete serosa, 3 = full or partial

serosa plus ectopic WT1 expression in mesenchyme. Scale bar = 100µm. **(d):** Graph depicting the percentage of HIOs in control basal media that received each score (0-3) across 4 independent experiments (biological replicates). **(e):** Comparison of the percentage of HIOs that formed a complete serosa (score 2) in basal media to HIOs treated with inhibitors SU5402 (FGF), Noggin (BMP), DAPT (Notch), IWR1 (WNT), and Cyclopamine (HH). Significance was calculated in relation to the control basal media condition. **(f):** Quantification of the percentage of HIOs from 4 independent experiments that scored 0-3 in basal media or media supplemented with SAG or Cyclopamine. Right: Comparison of the percentage of HIOs that received score 2 in basal media compared to SAG and Cyclopamine treatment. **(g):** Quantification of the percentage of HIOs from 3 independent experiments that scored 0-3 in basal media or media supplemented with IWR1 or CHIR-99021. Right: Comparison of the percentage of HIOs that received score 2 in basal media compared to IWR1 and CHIR-99021 treatment. For all graphs in Figure 4-8, data represent the mean ± standard error of the mean. Significance was calculated with a one-way ANOVA and multiple comparisons test.
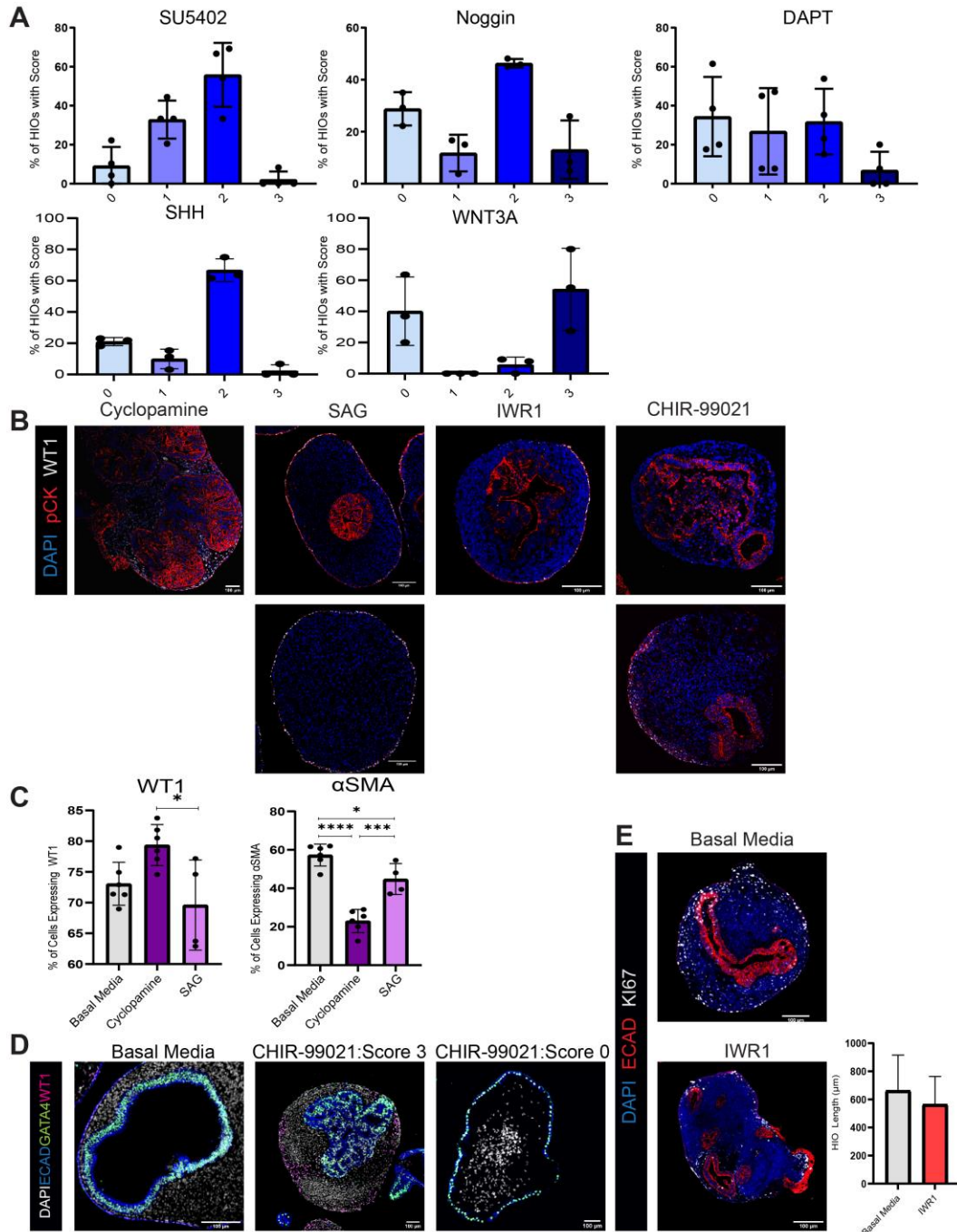
Figure 4-9. Analysis of Hedgehog and Other Signaling Pathways in HIO-Serosa.

(a): Distribution depicting the percentage of HIOs treated with SU5402, Noggin, DAPT, WNT3A, and SHH that received each score (0-3). **(b):** Representative images of suspension HIOs treated with Cyclopamine, SAG, IWR1, and CHIR-99021 stained for pCK and WT1. Images depict the most common score(s) for each condition – Cyclopamine: 3, SAG: 2, IWR1: 1, and CHIR-99021: 0 (top) and 3 (bottom). Many SAG-treated HIOs formed an inner epithelium with outer serosal mesothelium (top), while others formed a complete serosal mesothelium but did not form an inner epithelium

(bottom). **(c):** Percentage of FACS-isolated HIO-serosa cells that expressed WT1 or αSMA after treatment with SAG or Cyclopamine. HIO-serosa cells were isolated and cultured on Matrigel coated plates in basal media for 24 hours, followed by SAG or Cyclopamine treatment for 6 days before fixation and staining. **(d):** Representative images of CHIR-99021 treated suspension HIOs stained for ECAD and GATA4, depicting proximal intestinal patterning in HIOs with both score 0 and score 3. **(e):** Left: Representative images or IWR1 treated suspension HIOs stained for ECAD and KI67. Right: Chart depicting HIO length in IWR1-treated HIOs compared to basal media controls.

4.6 Tables

Human Fetal Serosal Mesothelium					Suspension HIO Serosal Mesothelium				
Gene Name	scores	logfoldchanges	pvals	pvals_adj	Gene Name	scores	logfoldchanges	pvals	pvals_adj
KLK11	19.664995	30.550547	1.14E-30	1.57E-28	CTGF	29.652313	4.6661983	1.90E-135	1.55E-132
CST6	9.594012	29.423937	1.65E-14	7.33E-13	ITIH5	21.892258	4.109821	9.30E-84	2.03E-81
CRB2	9.698785	29.204231	1.06E-14	4.84E-13	EPS8L1	24.094704	4.0449743	1.41E-97	4.72E-95
RSPO1	9.653414	28.591484	1.28E-14	5.77E-13	PODXL	30.471014	3.9790587	2.04E-142	2.02E-139
WNT10A	8.603934	28.531483	1.14E-12	4.24E-11	KRT19	49.442513	3.9566572	8.597e-321	2.8831754e-316
TMEM151A	7.843884	28.074549	3.00E-11	9.37E-10	TMEM151A	34.7348	3.9310405	7.67E-174	1.72E-170
UPK3B	12.711713	11.941951	4.45E-20	3.14E-18	LGALS2	29.447855	3.8006415	3.30E-135	2.63E-132
CA9	9.130588	10.634462	1.19E-13	4.85E-12	UPK3B	17.93687	3.7465878	6.01E-61	7.04E-59
SLPI	25.052698	10.597825	2.62E-37	4.62E-35	CYR61	35.44144	3.6893878	1.51E-192	5.63E-189
MSLN	45.745586	9.374531	3.05E-55	1.05E-52	ITGA3	22.04573	3.6500702	1.73E-85	4.03E-83
TM4SF1	29.491514	9.362832	5.17E-42	1.12E-39	AMOTL2	29.808138	3.639367	9.45E-139	8.57E-136
KRT19	25.717596	9.132164	4.51E-38	8.32E-36	BICDL1	17.80822	3.5898354	3.08E-60	3.57E-58
TGM1	7.478653	9.065398	1.43E-10	4.14E-09	KLK11	16.288404	3.5858052	6.71E-52	5.86E-50
PDZK1IP1	10.715831	8.819979	1.45E-16	7.86E-15	CDH1	15.885403	3.5634243	8.56E-50	6.93E-48
MYRF	8.910528	8.704715	3.05E-13	1.20E-11	CARNS1	22.563797	3.5152314	5.48E-89	1.44E-86
CLIC3	15.153727	8.427419	4.10E-24	3.83E-22	PLA2G2A	17.332542	3.456353	7.58E-58	8.07E-56
SPOCK2	14.973323	7.8228726	7.73E-24	7.10E-22	SPRR2F	26.879618	3.265038	1.21E-124	7.96E-122
OLR1	8.002896	7.724854	1.50E-11	4.75E-10	TMEM235	20.944164	3.1413176	4.83E-80	9.43E-78
CXADR	13.95312	7.5088563	3.37E-22	2.83E-20	TRNP1	32.134262	3.1022995	7.06E-163	1.08E-159
EPS8L1	8.785839	7.2321334	5.13E-13	1.97E-11	PYGM	18.926628	3.0977752	3.77E-68	5.29E-66
RASSF7	10.770085	7.0214767	1.13E-16	6.19E-15	CLDN15	17.174757	3.0619593	3.21E-57	3.34E-55

CARNS1	7.3642163	6.961567	2.31E-10	6.49E-09	DNAJC22	20.877228	3.0571384	7.30E-80	1.41E-77
CAV1	25.575178	6.9154572	3.78E-38	7.11E-36	ASPHD1	26.782635	3.0372868	8.62E-121	4.98E-118
BDKRB1	7.9614797	6.7218084	1.78E-11	5.64E-10	EZR	41.696095	2.9720962	5.88E-254	9.86E-250
BCAM	24.13325	6.7114925	1.75E-36	2.98E-34	BCAM	31.24827	2.9696383	1.25E-158	1.67E-155
GPM6A	7.429596	6.681921	1.73E-10	4.93E-09	CAVIN1	21.87794	2.9570003	1.65E-86	3.96E-84
TSPAN7	7.306412	6.637787	2.94E-10	8.18E-09	PARM1	25.48324	2.9017363	7.59E-113	3.74E-110
IL18	7.7846494	6.545817	3.78E-11	1.16E-09	TMEM37	22.410254	2.898663	1.86E-90	5.16E-88
S100A10	47.505714	6.482778	3.56E-59	1.44E-56	CXADR	30.88109	2.8940032	1.99E-156	2.56E-153
ALDH1A2	15.396485	6.419163	1.47E-24	1.44E-22	ATP7B	17.58802	2.8671439	8.13E-60	9.34E-58
TFPI2	11.047748	6.3749166	3.54E-17	2.01E-15	CRB2	32.98928	2.86699	2.41E-174	5.78E-171
TSPO	17.325068	6.301117	1.67E-27	1.93E-25	SCG5	32.00509	2.8376203	4.89E-166	8.63E-163
C19orf33	17.685617	6.238655	4.68E-28	5.49E-26	WT1	33.445026	2.8043668	4.26E-180	1.19E-176
PTGS1	8.749288	6.217185	5.84E-13	2.23E-11	FGF9	24.621897	2.8004248	3.29E-107	1.36E-104
KRT18	26.56285	6.166995	2.12E-39	4.10E-37	TAGLN	15.931556	2.7804031	8.88E-51	7.44E-49
SMTNL2	8.380885	6.0815067	2.86E-12	9.83E-11	CDH3	22.505394	2.7516084	5.27E-92	1.59E-89
PLLP	9.693387	6.081416	1.00E-14	4.60E-13	DAB2	16.871735	2.7391682	7.06E-56	7.05E-54
CFH	10.260186	6.071401	9.25E-16	4.64E-14	PPP2R2C	17.44443	2.7113705	1.43E-59	1.62E-57
TMEM88	8.582712	5.876366	1.21E-12	4.43E-11	PLLP	17.863708	2.674498	4.32E-62	5.23E-60
CLDN15	18.84365	5.8402796	8.50E-30	1.10E-27	SORBS2	19.767233	2.67388	1.02E-73	1.66E-71
KRT8	33.232033	5.8381567	1.10E-46	2.82E-44	MYRF	40.58723	2.6372972	1.55E-247	1.73E-243
C3	8.647403	5.8191833	9.10E-13	3.41E-11	ALDH1A2	20.610994	2.6026037	5.10E-80	9.88E-78
ADIRF	8.905544	5.679411	3.00E-13	1.18E-11	TNFSF13B	21.647243	2.5641952	1.07E-87	2.73E-85
DPP4	10.725273	5.5276	1.27E-16	6.94E-15	C16orf74	18.160421	2.555691	7.88E-64	1.01E-61
FGF9	9.515102	5.477374	2.11E-14	9.22E-13	SERTAD4-AS1	24.720125	2.541244	4.22E-108	1.79E-105

SPINT2	16.20246	5.265341	6.21E-26	6.61E-24	PRKG1	21.741016	2.534079	5.06E-87	1.23E-84
CRIP1	28.342306	5.2230706	1.28E-42	2.84E-40	HSBP1L1	17.951948	2.5288846	1.76E-62	2.16E-60
HHIP	8.445379	5.198665	2.11E-12	7.49E-11	SOX6	16.632137	2.5110953	5.63E-55	5.41E-53
MT1E	8.542446	5.171245	1.42E-12	5.16E-11	TNFRSF12A	18.97484	2.5081692	2.14E-69	3.09E-67
PROCR	11.8116045	5.094393	1.35E-18	8.42E-17	OGFRL1	16.083937	2.4773867	1.14E-51	9.87E-50
CFI	8.22162	4.9950004	5.48E-12	1.84E-10	CFI	27.508175	2.469598	7.38E-134	5.75E-131
DSG2	7.5123115	4.981233	1.18E-10	3.47E-09	B3GNT2	17.967222	2.4502418	8.46E-63	1.05E-60
EZR	18.119734	4.9394145	6.55E-29	8.16E-27	RAB33A	25.861473	2.4223754	4.03E-119	2.15E-116
REC8	13.641634	4.9343038	8.55E-22	7.00E-20	BMP4	23.771921	2.4190335	1.12E-103	4.21E-101
ANXA1	18.183903	4.89498	4.11E-29	5.19E-27	PLP2	32.204727	2.402363	2.07E-175	5.33E-172
MGP	28.417784	4.846702	2.99E-45	7.15E-43	KRT18	28.474783	2.338542	6.78E-141	6.50E-138
CAV2	12.892484	4.841079	1.52E-20	1.14E-18	FRMD4B	19.16767	2.3272696	3.34E-71	5.12E-69
MAL2	7.2712994	4.8338084	3.26E-10	9.01E-09	KRT8	34.412167	2.3136778	6.88E-194	3.30E-190
GJA1	9.821889	4.7447124	5.38E-15	2.53E-13	CAV1	16.467972	2.3087647	1.33E-54	1.25E-52
GAS6	18.055523	4.7352777	6.61E-29	8.18E-27	LINC01638	17.657572	2.289096	1.32E-61	1.59E-59
PLP2	12.929016	4.6902575	1.29E-20	9.78E-19	PTGDS	16.61088	2.2768176	1.55E-55	1.54E-53
WT1	13.296576	4.6501155	2.79E-21	2.20E-19	PRCD	20.346176	2.2767444	3.75E-79	6.98E-77
ID4	11.628869	4.6436534	2.60E-18	1.59E-16	CAV2	20.427399	2.2758431	8.15E-80	1.55E-77
LGALS2	13.608031	4.6354685	8.35E-22	6.89E-20	TRIB1	16.40807	2.2756188	6.21E-54	5.73E-52
LINC01133	9.957647	4.595946	2.93E-15	1.41E-13	ANXA2	25.006044	2.2740917	1.43E-114	7.28E-112
NSG1	8.369534	4.5455437	2.76E-12	9.58E-11	PDE4DIP	15.733566	2.2739146	4.92E-50	4.04E-48
SORBS2	7.600344	4.436809	7.71E-11	2.28E-09	EEF1A2	28.638258	2.248765	8.70E-145	9.12E-142
MISP	7.7193756	4.4264994	4.64E-11	1.41E-09	GADD45A	21.37564	2.2399306	4.82E-87	1.18E-84
REEP1	9.763473	4.4144926	6.57E-15	3.07E-13	PARD6B	22.712637	2.2325766	3.41E-96	1.11E-93
PTPRF	10.589773	4.362564	1.96E-16	1.05E-14	ID4	33.370552	2.2106543	4.24E-185	1.42E-181

SLC16A1	9.617613	4.2972064	1.27E-14	5.73E-13	ATF3	20.819292	2.1894233	2.22E-84	4.99E-82
RPRD1B	11.098447	4.29021	2.27E-17	1.30E-15	PDPN	24.298193	2.1752632	3.95E-108	1.70E-105
MEGF6	8.120822	4.2822895	8.11E-12	2.66E-10	CITED2	18.618992	2.1650906	2.92E-67	3.98E-65
SLC9A3R1	11.522043	4.182529	3.59E-18	2.19E-16	STK26	17.77527	2.1589396	1.79E-62	2.20E-60
ID1	9.006329	4.157145	1.82E-13	7.30E-12	CEBPB	24.58667	2.1504865	1.32E-112	6.31E-110
WNT2B	10.616186	4.1458673	1.62E-16	8.73E-15	GOLIM4	29.061167	2.1487384	3.77E-147	4.36E-144
CRYAB	9.574289	4.1084294	1.45E-14	6.48E-13	BNC1	17.162077	2.1294332	8.03E-59	8.88E-57
MST1	8.790711	4.095047	4.00E-13	1.54E-11	CAPN6	19.172302	2.1220722	1.50E-71	2.32E-69
SLIT3	10.610973	4.045951	1.63E-16	8.76E-15	CYSTM1	18.81552	2.1123297	1.90E-69	2.76E-67
UCHL1	8.02048	3.9998739	1.23E-11	3.94E-10	MGP	16.891672	2.110843	1.85E-58	2.03E-56
VAMP8	11.280205	3.9280026	7.69E-18	4.58E-16	MYL9	24.799177	2.1033418	1.39E-112	6.58E-110
PCSK1N	7.903269	3.8768418	2.02E-11	6.37E-10	DMKN	21.105728	2.0944946	3.45E-85	7.92E-83
SEMA3C	12.4176035	3.8533275	7.41E-20	5.15E-18	SH3BP5	23.07641	2.093354	7.52E-99	2.60E-96
NPW	8.356848	3.8373833	2.80E-12	9.69E-11	GCA	28.75153	2.068465	1.23E-146	1.38E-143
TNNT1	17.859331	3.82894	2.93E-29	3.71E-27	ASS1	16.539553	2.061432	1.65E-55	1.62E-53
SELENBP1	12.555413	3.6644707	4.03E-20	2.86E-18	SERPINB9	21.558308	2.0565937	4.78E-89	1.26E-86
ANXA3	12.274075	3.5538557	1.19E-19	8.11E-18	CDC42EP1	17.98066	2.0342824	5.11E-64	6.64E-62
ANXA2	22.527155	3.5164304	8.16E-37	1.42E-34	ARID5B	25.740942	2.0314648	2.31E-120	1.31E-117
COL18A1	11.60789	3.4605935	1.94E-18	1.20E-16	CSDC2	15.750288	2.0243843	7.15E-51	6.06E-49
EPHB6	7.4375954	3.451758	1.46E-10	4.23E-09	MIR22HG	17.09603	2.0131173	6.23E-59	6.96E-57
ARL4D	7.6641235	3.4172733	5.63E-11	1.68E-09	RASSF7	16.164284	1.9871433	5.36E-53	4.82E-51
ITGA3	7.320899	3.4084787	2.42E-10	6.81E-09	PCSK1N	26.273094	1.9827012	1.55E-126	1.08E-123
LGALS3	15.767444	3.3544075	6.21E-26	6.61E-24	MSANTD1	16.953896	1.9814748	5.52E-58	5.91E-56
POSTN	9.413927	3.3449082	1.72E-14	7.61E-13	NECTIN2	28.61379	1.9736559	9.65E-145	9.81E-142
S100A6	25.528814	3.3421955	1.34E-43	3.09E-41	NEK7	16.391794	1.9601825	2.27E-54	2.11E-52

ID2	11.2393675	3.2475412	8.77E-18	5.18E-16	CA11	21.050644	1.9394045	6.95E-85	1.59E-82
CD200	7.4070716	3.1937335	1.63E-10	4.66E-09	FRZB	25.596804	1.9307498	3.90E-121	2.30E-118
PDPN	9.194116	3.1913683	5.75E-14	2.41E-12	RHOB	22.905746	1.9232506	2.34E-100	8.34E-98
MT2A	7.4293814	3.1743736	1.54E-10	4.43E-09	RSRP1	23.18207	1.9229103	5.40E-100	1.91E-97
CRIM1	9.284487	2.9809833	3.73E-14	1.58E-12	FLRT3	22.098896	1.9051293	1.46E-92	4.54E-90
CYSTM1	8.049508	2.9370356	8.60E-12	2.81E-10	DSC3	17.657915	1.9011427	1.08E-62	1.34E-60
COL9A3	8.399463	2.9317589	1.94E-12	6.93E-11	CAMK2N1	25.551504	1.8746679	4.06E-120	2.27E-117
IGFBP6	12.359706	2.929181	4.72E-20	3.32E-18	SPINT2	30.973948	1.8726807	2.65E-163	4.23E-160
CTSH	8.343143	2.8167834	2.22E-12	7.89E-11	FLNC	21.778198	1.8575133	1.46E-90	4.07E-88
FLRT2	9.768184	2.7928545	3.84E-15	1.84E-13	DSC2	20.478954	1.8483567	3.32E-82	6.96E-80
RARRES2	20.545769	2.778426	2.66E-35	4.32E-33	HOOK1	16.83786	1.847017	8.84E-58	9.38E-56
TPM1	27.606827	2.7718675	4.10E-48	1.14E-45	SPARC	35.793564	1.8458652	3.41E-200	2.29E-196
RERG	8.378854	2.7463913	2.00E-12	7.12E-11	PTPRF	25.791365	1.8396081	5.25E-122	3.20E-119
GAS1	9.936069	2.614497	2.04E-15	9.98E-14	C4orf48	27.008488	1.8339932	2.70E-132	2.01E-129
NDFIP2	8.459141	2.580289	1.29E-12	4.72E-11	ZNF330	19.919819	1.82287	4.96E-77	8.71E-75
C2orf40	10.677714	2.568246	5.86E-17	3.28E-15	BNC2	19.949902	1.8178393	2.05E-77	3.65E-75
FLRT3	7.9395685	2.5607953	1.34E-11	4.26E-10	KLF6	20.24129	1.8147045	1.36E-80	2.70E-78
NPDC1	10.023558	2.5396209	1.09E-15	5.44E-14	GABARAPL1	22.45191	1.800921	1.05E-95	3.37E-93
TMEM176B	8.288541	2.5348005	2.69E-12	9.38E-11	LDOC1	20.592035	1.7945617	4.62E-82	9.62E-80
CD151	14.449869	2.532161	5.91E-24	5.45E-22	APLP1	24.613707	1.7817756	8.79E-113	4.27E-110
PTGIS	7.7456427	2.509498	3.30E-11	1.02E-09	TM7SF2	19.65012	1.7714367	1.93E-76	3.30E-74
HCFC1R1	13.920169	2.462848	2.83E-23	2.50E-21	RAMP1	16.297686	1.7627745	1.47E-54	1.37E-52
S100A16	7.693217	2.4558153	3.79E-11	1.16E-09	GIT1	17.847328	1.7611405	6.38E-64	8.20E-62
HTRA1	13.053741	2.4323368	1.41E-21	1.13E-19	CELF2	21.79805	1.7519848	2.30E-91	6.72E-89

SAT1	7.9037137	2.4121642	1.79E-11	5.67E-10	GATA6	16.010057	1.7471462	1.22E-52	1.08E-50
TSTD1	8.74947	2.3686533	2.91E-13	1.15E-11	COL18A1	23.64265	1.737791	1.78E-105	7.18E-103
SERPING1	12.404848	2.3203907	1.72E-20	1.27E-18	MAF	16.219788	1.7261444	8.09E-54	7.39E-52
EFEMP1	11.844262	2.2363813	2.08E-19	1.39E-17	SEZ6L2	20.27496	1.7066746	6.68E-81	1.35E-78
ISYNA1	8.256313	2.2332265	2.81E-12	9.69E-11	ANXA11	20.038061	1.7059959	1.16E-78	2.11E-76
AEBP1	8.180541	2.1660364	4.06E-12	1.37E-10	TSPAN2	16.952139	1.6985948	7.87E-59	8.74E-57
ODC1	7.836664	2.1630673	1.91E-11	6.03E-10	LAMC1	16.970982	1.6599748	2.07E-58	2.26E-56
CPE	10.406319	2.1622946	9.92E-17	5.46E-15	DSG2	23.538736	1.6592985	5.62E-105	2.17E-102
CD9	11.039719	2.1291463	5.45E-18	3.28E-16	ODC1	20.461359	1.6572069	5.40E-82	1.12E-79
C4orf48	8.993375	2.0940616	8.96E-14	3.69E-12	SLC9A3R1	16.785448	1.6364042	1.86E-57	1.97E-55
CEBPB	8.469726	2.02867	1.15E-12	4.26E-11	DAPK3	17.856636	1.6258665	5.63E-64	7.29E-62
FKBP11	8.163277	2.0141764	3.68E-12	1.25E-10	NPW	21.28257	1.6118813	1.70E-88	4.42E-86
CAPN2	8.685167	2.0080528	3.73E-13	1.44E-11	CXXC5	16.313887	1.593404	6.53E-55	6.22E-53
BCHE	8.555516	1.9661294	6.68E-13	2.53E-11	BCO2	16.324886	1.5781735	7.16E-55	6.80E-53
ANXA11	8.960493	1.8651102	8.91E-14	3.67E-12	DSP	16.487532	1.5667361	1.14E-55	1.14E-53
RNH1	11.824815	1.8493822	9.61E-20	6.62E-18	LMNA	20.177223	1.5600585	1.23E-80	2.45E-78
LY6E	12.312826	1.8258693	1.82E-20	1.34E-18	HS2ST1	16.076992	1.5492014	2.85E-53	2.57E-51
BSG	14.129413	1.7767302	2.01E-24	1.93E-22	NEO1	19.05618	1.5473539	4.34E-72	6.81E-70
ATP2B1	7.9557743	1.7379681	8.20E-12	2.69E-10	AFDN	18.361393	1.5421276	9.85E-68	1.38E-65
TMEM98	11.594876	1.7284669	2.36E-19	1.57E-17	LAMA5	16.40631	1.537077	2.85E-55	2.77E-53
TPT1	24.686962	1.7124761	1.88E-44	4.43E-42	COL9A3	21.691547	1.5304537	4.73E-91	1.36E-88
RHOB	7.8319454	1.6688163	1.67E-11	5.28E-10	GLS	16.17713	1.5186846	7.35E-54	6.76E-52
CSRP1	7.280944	1.6137663	1.77E-10	5.02E-09	TRAPPC2L	25.902441	1.5096533	1.30E-123	8.41E-121
TIMP1	12.231586	1.6107887	1.31E-20	9.91E-19	EFHC1	15.897664	1.4737438	2.29E-52	2.02E-50
CRIP2	8.964269	1.5827278	6.59E-14	2.75E-12	CDCA7L	16.074488	1.4704396	2.04E-53	1.84E-51

Gene					Gene				
CD59	8.758981	1.5166066	1.44E-13	5.82E-12	DST	16.565966	1.4617443	1.70E-56	1.72E-54
HINT1	11.374324	1.3612689	4.93E-19	3.18E-17	ALCAM	17.058413	1.443637	1.15E-59	1.31E-57
TSPAN3	7.88451	1.2724386	8.56E-12	2.80E-10	CDH2	16.300434	1.4267693	2.84E-55	2.77E-53
ZFAS1	9.815558	1.2667357	6.49E-16	3.29E-14	TNNT1	21.732254	1.3878348	8.14E-92	2.44E-89
EIF3M	8.112807	1.2169648	2.37E-12	8.35E-11	CYTL1	16.29137	1.3850138	6.41E-55	6.13E-53
C1R	7.2851753	1.2110935	1.23E-10	3.60E-09	DUSP1	17.284178	1.3839333	1.90E-61	2.28E-59
MIF	9.463215	1.2101496	3.50E-15	1.68E-13	NAXE	16.284245	1.364576	1.19E-54	1.12E-52
TMSB4X	18.67882	1.1628479	2.89E-35	4.66E-33	TMEM98	24.457075	1.3545002	2.40E-112	1.12E-109
HSPB1	9.507479	1.1532584	2.18E-15	1.06E-13	EFNB2	16.107069	1.3113575	7.54E-54	6.91E-52
PRDX5	8.169181	1.0474216	2.06E-12	7.33E-11	MAB21L2	17.282001	1.2728063	2.63E-61	3.14E-59
NPC2	7.4434342	1.0145999	4.74E-11	1.44E-09	TMEM219	19.96285	1.2692114	4.11E-79	7.61E-77
RPL12	15.583651	0.97864795	2.33E-28	2.77E-26	SARAF	23.76058	1.2218196	5.44E-107	2.22E-104
MT-CO1	9.481712	0.97632384	6.87E-15	3.20E-13	MYADM	19.146439	1.2205272	1.22E-73	1.96E-71
RPS3	16.341051	0.96637225	6.72E-29	8.27E-27	FIS1	21.145374	1.2118468	1.46E-87	3.71E-85
FIS1	7.304459	0.9661645	8.67E-11	2.56E-09	SNHG8	19.440634	1.2003042	3.24E-75	5.45E-73
RPL39	15.950983	0.9071807	4.93E-30	6.41E-28	EIF3M	23.217947	1.1057825	2.28E-102	8.39E-100
RPL7	13.85354	0.8799331	2.72E-25	2.80E-23	MYL12B	21.84417	1.0982901	2.33E-92	7.12E-90
SPARC	10.056919	0.85613483	7.97E-17	4.42E-15	LGALS3BP	17.57239	1.0827522	2.70E-63	3.39E-61
EEF2	8.993253	0.81859463	3.91E-14	1.66E-12	CD151	16.70924	1.0601918	7.38E-58	7.89E-56
RPL36A	7.4507747	0.8139774	4.80E-11	1.45E-09	EEF2	24.602694	0.95266616	3.15E-111	1.45E-108
RPS24	16.75809	0.8097491	2.93E-33	4.51E-31	TPT1	35.21792	0.8766073	6.54E-198	3.66E-194
COX6C	8.132345	0.792467	1.15E-12	4.26E-11	GNAS	17.020622	0.566955	8.46E-60	9.69E-58
RPL10A	11.873495	0.7850023	3.15E-20	2.28E-18	EEF1B2	16.570189	0.5404701	1.04E-56	1.07E-54
RPL31	14.114801	0.77407616	8.88E-29	1.08E-26	RPL7	16.743744	0.5270401	4.76E-58	5.12E-56
COX7C	10.975495	0.7687625	1.60E-19	1.08E-17	RPS12	26.180206	0.49044684	3.32E-125	2.23E-122

RPL26	13.550904	0.74091583	1.76E-24	1.71E-22	RPS24	23.031618	0.48783457	3.03E-101	1.09E-98
MT-ND4	7.285493	0.72578585	1.68E-10	4.80E-09	RPL12	19.202497	0.47207987	1.35E-73	2.17E-71
RPS2	11.298914	0.7067236	7.79E-19	4.97E-17	RPL19	24.709808	0.44598812	4.88E-114	2.44E-111
PPDPF	9.021133	0.6913904	6.73E-15	3.14E-13	RPS14	25.481197	0.43808565	2.25E-119	1.24E-116
RPL37A	13.991946	0.69063425	1.70E-25	1.76E-23	RPS27	22.67315	0.43651918	4.33E-98	1.47E-95
RPS14	12.9779415	0.6821061	1.70E-22	1.44E-20	RPL18A	20.025578	0.43272093	9.63E-79	1.76E-76
RPL29	14.736781	0.6657843	1.56E-29	1.99E-27	RPL41	20.499212	0.42976433	6.47E-82	1.33E-79
BTF3	7.4194264	0.6550929	4.42E-11	1.35E-09	RPL26	18.864815	0.42137456	3.36E-71	5.12E-69
RPL38	10.4453335	0.6501819	7.27E-18	4.36E-16	RPS27A	20.852373	0.4192702	3.15E-84	6.99E-82
RPS18	12.326211	0.65006053	4.04E-21	3.14E-19	RPS6	21.418552	0.417301	3.08E-89	8.26E-87
RPL37	11.863722	0.61741364	4.36E-21	3.37E-19	RPS4X	19.227232	0.40704226	9.29E-74	1.51E-71
RPL3	10.802194	0.6164877	8.43E-18	4.99E-16	RPL3	17.732658	0.40432763	1.61E-63	2.03E-61
RPS6	10.77247	0.6155498	7.32E-18	4.37E-16	RPL10A	16.149517	0.40407977	6.73E-54	6.20E-52
RPL41	13.370074	0.6022525	1.32E-23	1.20E-21	RPS23	21.059357	0.40225768	3.93E-86	9.28E-84
RPLP0	8.880967	0.60209596	4.21E-14	1.78E-12	RPS3A	19.688955	0.39299816	6.93E-77	1.21E-74
RPL7A	11.136233	0.5956117	2.07E-19	1.39E-17	RPL37	19.343914	0.39147145	2.37E-74	3.90E-72
RPL34	11.065496	0.5627758	8.47E-19	5.36E-17	RACK1	16.8667	0.39141443	2.29E-58	2.49E-56
RPL13	13.374207	0.54843074	5.39E-24	5.00E-22	RPL5	19.713013	0.38471672	2.93E-77	5.18E-75
EEF1A1	10.561801	0.54582375	2.84E-17	1.62E-15	RPLP1	22.81288	0.38246402	2.65E-99	9.27E-97
RPS25	11.11419	0.5385042	5.89E-20	4.11E-18	RPL13	21.478048	0.37735593	6.75E-90	1.86E-87
RPS12	8.43741	0.4968905	7.51E-13	2.84E-11	RPL35A	19.636995	0.37317857	1.17E-76	2.01E-74
RPL28	11.870907	0.4784694	8.53E-22	7.00E-20	RPS9	20.318933	0.3614434	2.70E-81	5.52E-79
RPS28	7.49803	0.44708386	4.52E-11	1.37E-09	RPL29	18.338976	0.3572364	3.09E-68	4.35E-66
RPL8	8.049397	0.44356135	2.34E-12	8.26E-11	RPL18	16.282232	0.35198566	9.36E-55	8.87E-53

RPL13A	9.103745	0.42266285	4.67E-16	2.40E-14	EEF1A1	18.223122	0.3425877	1.65E-67	2.29E-65
RPL32	8.513439	0.4033654	2.12E-13	8.45E-12	RPS2	17.74559	0.3423105	3.01E-64	3.93E-62
RPLP1	9.667592	0.40303963	8.54E-16	4.30E-14	RPL28	16.34452	0.3389938	3.07E-55	2.98E-53
RPL14	7.364098	0.40264153	4.31E-11	1.32E-09	RPL11	19.220886	0.3373152	3.65E-74	5.98E-72
RPS19	8.218872	0.3972511	7.95E-13	3.00E-11	RPS3	19.675323	0.33659413	2.89E-77	5.12E-75
RPS23	8.642302	0.3796199	9.30E-14	3.82E-12	RPL34	17.66958	0.33544558	8.49E-64	1.08E-61
RPS15	7.789232	0.3638472	6.24E-12	2.08E-10	RPL37A	16.999937	0.30786672	1.14E-59	1.30E-57

Table 4-1. Gene Expression in Human Fetal Serosal Mesothelium and Suspension HIO-Serosa.

Related to Figure 4-4. Table contains all genes enriched in the human fetal serosa and HIO-serosa sub-clusters extracted from scRNA-seq analyses (Figure 4-4). Genes highlighted in yellow have a $\log_2$ fold >1.5 in expression in the serosa cluster relative to all other clusters and were thus included in the analysis shown in Figure 4-4D.

Fetal Serosa - Unique		Overlap	HIO Serosa - Unique	
CST6	VAMP8	KLK11	CTGF	DMKN
RSPO1	SEMA3C	CRB2	ITIH5	SH3BP5
WNT10A	TNNT1	TMEM151A	PODXL	GCA
CA9	SELENBP1	UPK3B	CYR61	ASS1
SLPI	ANXA3	KRT19	AMOTL2	SERPINB9
MSLN	EPHB6	MYRF	BICDL1	CDC42EP1
TM4SF1	ARL4D	CXADR	CDH1	ARID5B
TGM1	LGALS3	EPS8L1	PLA2G2A	CSDC2
PDZK1IP1	POSTN	RASSF7	SPRR2F	MIR22HG
CLIC3	S100A6	CARNS1	TMEM235	MSANTD1
SPOCK2	ID2	CAV1	TRNP1	NECTIN2
OLR1	CD200	BCAM	PYGM	NEK7
BDKRB1	MT2A	ALDH1A2	DNAJC22	CA11
GPM6A	CRIM1	KRT18	ASPHD1	FRZB
TSPAN7	IGFBP6	PLLP	CAVIN1	RSRP1
IL18	CTSH	CLDN15	PARM1	DSC3
S100A10	FLRT2	KRT8	TMEM37	CAMK2N1
TFPI2	RARRES2	FGF9	ATP7B	FLNC
TSPO	TPM1	SPINT2	SCG5	DSC2
C19orf33	RERG	CFI	TAGLN	HOOK1
PTGS1	GAS1	DSG2	CDH3	SPARC
SMTNL2	NDFIP2	EZR	DAB2	ZNF330
CFH	C2orf40	MGP	PPP2R2C	BNC2
TMEM88	NPDC1	CAV2	TNFSF13B	KLF6
C3	TMEM176B	PLP2	C16orf74	GABARAPL1
ADIRF	CD151	WT1	SERTAD4-AS1	LDOC1
DPP4	PTGIS	ID4	PRKG1	APLP1
CRIP1	HCFC1R1	LGALS2	HSBP1L1	TM7SF2
HHIP	S100A16	SORBS2	SOX6	RAMP1
MT1E	HTRA1	PTPRF	TNFRSF12A	GIT1
PROCR	SAT1	SLC9A3R1	OGFRL1	CELF2
REC8	TSTD1	PCSK1N	B3GNT2	GATA6
ANXA1	SERPING1	NPW	RAB33A	MAF
MAL2	EFEMP1	ANXA2	BMP4	SEZ6L2
GJA1	ISYNA1	COL18A1	FRMD4B	TSPAN2
GAS6	AEBP1	ITGA3	LINC01638	LAMC1
LINC01133	CPE	PDPN	PTGDS	DAPK3
NSG1	CD9	CYSTM1	PRCD	CXXC5
MISP	FKBP11	COL9A3	TRIB1	BCO2
REEP1	CAPN2	FLRT3	PDE4DIP	DSP
SLC16A1	BCHE	ODC1	EEF1A2	LMNA
RPRD1B	RNH1	C4orf48	GADD45A	HS2ST1

MEGF6	LY6E	CEBPB	PARD6B	NEO1
ID1	BSG	ANXA11	ATF3	AFDN
WNT2B	ATP2B1	RHOB	CITED2	LAMA5
CRYAB	TMEM98		STK26	GLS
MST1	TPT1		GOLIM4	TRAPPC2L
SLIT3	CSRP1		BNC1	
UCHL1	TIMP1		CAPN6	
CD59	CRIP2		MYL9	

Table 4-2. Overlapping Genes Expressed in Human Fetal Serosal Mesothelium and Suspension HIO-Serosa.

List of genes that are uniquely expressed or found in both human fetal serosal mesothelium and suspension HIO-serosa, as defined by the top differentially expressed genes in each population (logfoldchange>1.5, Table 4-1).

REAGENT or RESOURCE	SOURCE	IDENTIFIER
Antibodies		
Goat polyclonal anti-E-cadherin	R&D Systems	Cat#AF748; RRID: AB_355568
Mouse monoclonal anti-E-cadherin	BD Transduction Laboratories	Cat#610181; RRID: AB_397580
Goat monoclonal anti-Vimentin	R&D Systems	Cat#MAB2105; RRID: AB_2241653
Mouse monoclonal anti-CDX2	BioGenex	Cat#MU392A-UC; RRID: AB_2650531
Rabbit monoclonal anti-PDX1	Cell Signaling Technology	Cat#5679; RRID: AB_10706174
Rabbit monoclonal anti-ZO-1	Cell Signaling Technology	Cat# 13663; RRID: AB_2798287
Rabbit polyclonal anti-MUC2	Santa Cruz Biotechnology	Cat# sc-15334; RRID: AB_2146667
Goat polyclonal anti-CHGA	Santa Cruz Biotechnology	Cat# sc-1488; RRID: AB_2276319
Goat polyclonal anti-SOX9	R&D Systems	Cat# AF3075; RRID: AB_2194160
Rabbit monoclonal anti-KI67	Thermo Scientific	Cat# RM-9106-S1; RRID: AB_149792
Goat polyclonal anti-DPPIV	R&D Systems	Cat# AF954; RRID: AB_355739
Goat polyclonal anti-LYZ	Santa Cruz Biotechnology	Cat# sc-27958; RRID: AB_2138790
Rabbit monoclonal anti-DEFA5	Abcam	Cat# ab180515
Rabbit polyclonal anti-OLFM4	Abcam	Cat# ab85046; RRID: AB_10670544
Mouse monoclonal anti-αSMA-Cy3	Sigma-Aldrich	Cat# C6198; RRID: AB_476856
Rabbit monoclonal anti-WT1	Abcam	Cat# ab89901; RRID: AB_2043201
Mouse monoclonal anti-pan Cytokeratin	Abcam	Cat# ab86734; RRID: AB_10674321
Rabbit polyclonal-anti Laminin	Abcam	Cat# ab11575; RRID: AB_298179
Rabbit polyclonal anti-EpCAM	Sigma-Aldrich	Cat# HPA026761; RRID: AB_1848198
Rabbit polyclonal anti-PDPN	Santa Cruz Biotechnology	Cat# sc-134482; RRID: AB_2162079
Rabbit polyclonal anti-CAV1	Atlas Antibodies	Cat# HPA049326; RRID: AB_2680714
Rabbit polyclonal anti-CAV2	Atlas Antibodies	Cat# HPA044810; RRID: AB_2679098
Mouse monoclonal anti-Ezrin	Sigma-Aldrich	Cat# E8897; RRID: AB_476955
Goat polyclonal anti-GATA4	Sana Cruz Biotechnology	Cat# sc-1237; RRID: AB 2108747
Monoclonal anti-ECAD-PE	Miltenyi Biotec	Cat# 130-111-992; RRID: AB_2657482
Monoclonal anti-EpCAM-FITC	Miltenyi Biotec	Cat# 130-111-115; RRID: AB_2657492
Monoclonal anti-PDPN-APC	Miltenyi Biotec	Cat# 130-107-016; RRID: AB_2653263
Donkey anti-mouse 488	Jackson ImmunoResearch	Cat#715-545-150; RRID: AB_2340846
Donkey anti-mouse Cy3	Jackson ImmunoResearch	Cat#715-165-150; RRID: AB_2340813
Donkey anti-mouse 647	Jackson ImmunoResearch	Cat#715-605-150; RRID: AB_2340862
Donkey anti-rabbit 488	Jackson ImmunoResearch	Cat#711-545-152; RRID: AB_2313584
Donkey anti-rabbit Cy3	Jackson ImmunoResearch	Cat#711-165-152; RRID: AB_2307443

Donkey anti-rabbit 647	Jackson ImmunoResearch	Cat#711-605-152 RRID: AB_2492288
Donkey anti-goat 488	Jackson ImmunoResearch	Cat#705-545-147; RRID: AB_2336933
Donkey anti-goat Cy3	Jackson ImmunoResearch	Cat#705-165-147; RRID: AB_2307351
Donkey anti-goat 647	Jackson ImmunoResearch	Cat#705-605-147; RRID: AB_2340437
Biological Samples		
Human Fetal Small Intestine	University of Washington Laboratory of Developmental Biology	N/A
Chemicals, Peptides, and Recombinant Proteins		
Activin A	R&D	Cat#338-AC
FGF4	Purified in house	[63]
CHIR99021	APExBIO	Cat# A3011
Epidermal Growth Factor (EGF)	R&D Systems	Cat# 236-EG
Recombinant Human Noggin-FC, purified from HEK293 cells expressing FC-tagged Noggin	Purified in house	[75]
Human R-Spondin1 Conditioned Medium from Cultrex HA-R-Spondin1-Fc 293 T Cells	R&D Systems	Cat# 3710-001-01
B27 supplement	Thermo Fisher	Cat#17504044
HEPES	Thermo Fisher	Cat#15630080
GlutaMAX	Gibco	Cat#35050061
Penicillin-Streptomycin	Gibco	Cat# 15070063
Dispase	Life Technologies	Cat#17105-041
Poly (2-hydroxyethyl methacrylate) (pHEMA)	Sigma-Aldrich	Cat#P3932
Calcium Chloride	Sigma-Aldrich	Cat# 449709
TrypLE Express Enzyme	Gibco	Cat# 12604013
Hydrocortisone	STEMCELL Technologies	Cat#07904
Y27632	Stemgent	Cat#04-0012
SAG	STEMCELL Technologies	Cat#73414
Cyclopamine	Selleckchem	Cat#S1146
IWR1	R&D Systems	Cat#3532
SU5402	Santa Cruz Biotechnology	Cat#215543-92-3
DAPT	Calbiochem	Cat#565784
SHH	R&D Systems	Cat#1845-SH
WNT3A	R&D Systems	Cat# 5036-WN
Red Blood Cell Lysis Buffer	Roche	Cat#11814389001
Critical Commercial Assays		
Neural Tissue Dissociation Kit (P)	Miltenyi	Cat#130-092-628
SuperScript VILO cDNA Synthesis Kit	ThermoFisher	Cat#11754250
MagMAX-96 Total RNA Isolation Kit	Ambion	Cat#AM1830
QuantiTect SYBR Green PCR Kit	Qiagen	Cat#204145
Chromium Next GEM Single Cell 3' Library Construction Kit v3	10x Genomics	Cat#PN-1000075
Chromium Next GEM Single Cell 3' Library Construction Kit v2	10x Genomics	Cat#PN-120237
Human t-PA ELISA Kit	ThermoFisher	Cat#BMS258-2
Deposited Data		
Raw scRNA-seq data (human fetal duodenum)	Holloway et al., 2021	ArrayExpress: E-MTAB-9489
Raw scRNA-seq data (human fetal small intestine)	Holloway et al., 2020	ArrayExpress: E-MTAB-9363

Raw scRNA-seq data (human fetal small intestine)	This study	ArrayExpress: E-MTAB-11335
Raw scRNA-seq data (HIO)	Holloway et al., 2020	ArrayExpress: E-MTAB-9228
Raw scRNA-seq data (HIO)	Yu et al., 2021	ArrayExpress: E-MTAB-10187
Raw scRNA-seq data (HIO)	Yu et al., 2021	ArrayExpress: E-MTAB-10268
Raw scRNA-seq data (HIO)	This study	ArrayExpress: E-MTAB-11338
Raw scRNA-seq data (HIO)	This study	ArrayExpress: E-MTAB-11347
Experimental Models: Cell Lines		
H9 ESC	WiCell	NIH registry #0062, RRID: CVCL_9773
UM 63-1 ESC	MStem Cell Laboratories	NIH registry #0277, RRID: CVCL_R782
iPSC 72.3	Cincinnati Children's Hospital	N/A
iPSC WTC11	Coriell Institute	RRID: CVCL_Y803
Oligonucleotides		
Primer: GAPDH Forward: CTCTGCTCCTCCTGTTCGAC	IDT	N/A
Primer: GAPDH Reverse: TTAAAAGCAGCCCTGGTGAC	IDT	N/A
Primer: ECAD Forward: TTGACGCCGAGAGCTACAC	IDT	N/A
Primer: ECAD Reverse: GACCGGTGCAATCTTCAAA	IDT	N/A
Primer: CDX2 Forward: GGGCTCTCTGAGAGGCAGGT	IDT	N/A
Primer: CDX2 Reverse: GGTGACGGTGGGGTTTAGCA	IDT	N/A
Primer: PDX1 Forward: CGTCCGCTTGTTCTCCTC	IDT	N/A
Primer: PDX1 Reverse: CCTTTCCCATGGATGAAGTC	IDT	N/A
Primer: MUC2 Forward: TGTAGGCATCGCTCTTCTCA	IDT	N/A
Primer: MUC2 Reverse: GACACCATCTACCTCACCCG	IDT	N/A
See Table S2 for all other primer sequences	IDT	N/A
Primer: CHGA Forward: CTGTCCTGGCTCTTCTGCTC	IDT	N/A
Primer: CHGA Reverse: TGACCTCAACGATGCATTTC	IDT	N/A
Primer: LYZ Forward: ACAAGCTACAGCATCAGCGA	IDT	N/A
Primer: LYZ Reverse: GTAATGATGGCAAAACCCCA	IDT	N/A
Primer: DPP4 Forward: TCCCGGTGGGAGTACTATGA	IDT	N/A
Primer: DPP4 Reverse: CAGGGCTTTGGAGATCTGAG	IDT	N/A
Primer: KI67 Forward: CAGGGCTTTGGAGATCTGAG	IDT	N/A
Primer: KI67 Reverse: TGACTTCCTTCCATTCTGAAGAC	IDT	N/A
Primer: LGR5 Forward: CAGCGTCTTCACCTCCTACC	IDT	N/A
Primer: LGR5 Reverse: TGGGAATGTATGTCAGAGCG	IDT	N/A
Primer: MSLN Forward: CCTGAGGACATTCGCAAGTGGA	IDT	N/A
Primer: MSLN Reverse: CTTCCCTTCACAAAGCGGTCGA	IDT	N/A
Primer: ACTA2 Forward: CAGCCAAGCACTGTCAGG	IDT	N/A
Primer: ACTA2 Reverse: CCAGAGCCATTGTCACACAC	IDT	N/A
Primer: TAGLN Forward: ACCCTCCATGGTCTTCAAGCAGAT	IDT	N/A
Primer: TAGLN Reverse: ATCTCCACGGTAGTGCCCATCATT	IDT	N/A
Primer: EPCAM Forward: CTGCCAAATGTTTGGTGATG	IDT	N/A
Primer: EPCAM Reverse: CTTCTGACCCCAGCAGTGTT	IDT	N/A
Primer: VIM Forward: CTTCAGAGAGAGGAAGCCGA	IDT	N/A
Primer: VIM Reverse: ATTCCACTTTGCGTTCAAGG	IDT	N/A
Primer: PDGFRA Forward: ATTGCGGAATAACATCGGAG	IDT	N/A

Primer: PDGFRA Reverse: GCTCAGCCCTGTGAGAAGAC	IDT	N/A
Software and Algorithms		
ImageJ	Schneider et al., 2012	https://imagej.nih.gov/ij/
Prism 8.3.0	GraphPad	https://www.graphpad.com/scientific-software/prism/
Scanpy, Ingest	[70]	https://github.com/theislab/scanpy
BBKNN	(Polański et al., 2020)	https://github.com/Teichlab/bbknn
UMAP	[71]	https://github.com/lmcinnes/umap
Python 3.7.3	Python	Python.org
Detailed methods and code for scRNAseq analysis	GitHub	https://github.com/jason-spence-lab/Capeling_2022
Other		
Matrigel	Corning	Cat#354234
Alginate	Alfa Aesar	Cat# B25266
Histoclear II	National Diagnostics	Cat#HS-202

Table 4-3. Key Resources Table: Chapter 4.

List of key reagents described in the Methods of Chapter 4.

4.7 References

1. McCracken, K., et al., *Generating human intestinal tissue from pluripotent stem cells in vitro.* Nature Protocols, 2011. **6**(12): p. 1920-1928.

2. Spence, J.R., et al., *Directed differentiation of human pluripotent stem cells into intestinal tissue in vitro.* Nature, 2011. **470**(7332): p. 105-109.

3. Finkbeiner, S.R., et al., *Transcriptome-wide Analysis Reveals Hallmarks of Human Intestine Development and Maturation In Vitro and In Vivo.* Stem Cell Reports, 2015. **4**(6): p. 1140-1155.

4. Holloway, E.M., et al., *Differentiation of Human Intestinal Organoids with Endogenous Vascular Endothelial Cells.* Developmental Cell, 2020. **54**(4): p. 516-528.e7.

5. Watson, C., et al., *An in vivo model of human small intestine using pluripotent stem cells.* Nature Medicine, 2014. **20**: p. 1310-1314.

6. Schlieve, C.R., et al., *Neural Crest Cell Implantation Restores Enteric Nervous System Function and Alters the Gastrointestinal Transcriptome in Human Tissue-Engineered Small Intestine.* Stem Cell Reports, 2017. **9**(3): p. 883-896.

7. Workman, M.J., et al., *Engineered human pluripotent-stem-cell-derived intestinal tissues with a functional enteric nervous system.* Nature Medicine, 2016. **23**: p. 49-59.

8. Dedhia, P.H., et al., *Organoid Models of Human Gastrointestinal Development and Disease.* Gastroenterology, 2016. **150**(5): p. 1098-1112.

9. Czerwinski, M. and J.R. Spence, *Hacking the Matrix.* Cell Stem Cell, 2017. **20**(1): p. 9-10.

10. Capeling, M., et al., *Nonadhesive Alginate Hydrogels Support Growth of Pluripotent Stem Cell-Derived Intestinal Organoids.* Stem Cell Reports, 2019. **12**(2): p. 381–394.

11. Bloom, W. and D.W. Fawcett, *A textbook of histology, 10th edition.* 1975, Saunders: Phildadelphia, PA, USA. p. 1033.

12. Mutsaers, S.E., *The mesothelial cell.* The International Journal of Biochemistry & Cell Biology, 2004. **36**(1): p. 9-16.

13. Winters, N.I. and D.M. Bader, *Development of the Serosal Mesothelium.* Journal of Developmental Biology, 2013. **1**: p. 64-81.

14. Federici, S., et al., *Multiple intestinal atresia with apple peel syndrome: successful treatment by five end-to-end anastomoses, jejunostomy, and*

transanastomotic silicone stent. Journal of Pediatric Surgery, 2003. **38**: p. 1250-1252.

15.   Pumberger, W., et al., *Duodeno-jejunal atresia with volvulus, absent dorsal mesentery, and absent superior mesenteric artery: a hereditary compound structure in duodenal atresia?* American journal of Medical Genetics, 2002. **109**: p. 52-55.

16.   Waldhausen, J.H. and R.S. Sawin, *Improved long-term outcome for patients with jejunoileal apple peel atresia.* Journal of Pediatric Surgery, 1997. **32**: p. 1307-1309.

17.   Sulaiman, H., et al., *Presence and distribution of sensory nerve fibers in human peritoneal adhesions.* Annals of Surgery, 2001. **234**: p. 256-261.

18.   Dobbie, J., *Pathogenesis of peritoneal fibrosing syndromes (sclerosing peritonitis) in peritoneal dialysis.* Peritoneal Dialysis International, 1992. **12**(1): p. 14-27.

19.   Bridda, A., et al., *Peritoneal Mesothelioma: A Review.* Medscape General Medicine, 2007. **9**(2): p. 32.

20.   Carmona, R., et al., *Cells Derived from the Coelomic Epithelium Contribute to Multiple Gastrointestinal Tissues in Mouse Embryos.* PLOS One, 2013. **8**(2): p. e55890.

21.   Dettman, R.W., et al., *Common epicardial origin of coronary vascular smooth muscle, perivascular fibroblasts, and intermyocardial fibroblasts in the avian heart.* Developmental Biology, 1998. **193**(2): p. 169-181.

22.   Que, J., et al., *Mesothelium contributes to vascular smooth muscle and mesenchyme during lung development.* PNAS, 2008. **105**(43): p. 16626-16630.

23.   Wilm, B., et al., *The serosal mesothelium is a major source of smooth muscle cells of the gut vasculature.* Development, 2005. **132**: p. 5317-5328.

24.   Hohwieler, M., et al., *Human pluripotent stem cell-derived acinar/ductal organoids generate human pancreas upon orthotopic transplantation and allow disease modelling.* Gut, 2017. **66**(3): p. 473-486.

25.   Kumar, S.V., et al., *Kidney micro-organoids in suspension culture as a scalable source of human pluripotent stem cell-derived kidney cells.* Development, 2019. **146**(5): p. dev172361.

26.   Takahashi, Y., et al., *A Refined Culture System for Human Induced Pluripotent Stem Cell-Derived Intestinal Epithelial Organoids.* Stem Cell Reports, 2018. **10**(1): p. 314-328.

27.   Capeling, M., et al., *Generation of small intestinal organoids for experimental intestinal physiology.* Methods Cell Biol., 2020. **159**: p. 143-174.

28.   Hill, D.R., et al., *Bacterial colonization stimulates a complex physiological response in the immature human intestinal epithelium.* eLife, 2017. **6**.

29.   Yu, Q., et al., *Charting human development using a multi-endodermal organ atlas and organoid models.* Cell, 2021. **184**(12): p. 3281-3298.e22.

30.   Mutsaers, S.E., *Mesothelial cells: Their structure, function and role in serosal repair.* Respirology, 2002. **7**: p. 171-191.

31.   Chan, R., et al., *Characterization of two monoclonal antibodies in an immunohistochemical study of keratin 8 and 18 expression.* Am J Clin Pathol, 1988. **89**: p. 472-480.

32.   Foley-Comer, A.J., et al., *Evidence for incorporation of free-floating mesothelial cells as a mechanism of serosal healing.* Journal of Cell Science, 2002. **115**: p. 1383-1389.

33.   Watt, A.J., et al., *GATA4 is essential for formation of the proepicardium and regulates cardiogenesis.* PNAS, 2004. **101**: p. 12573-12578.

34.   Kumar-Singh, S., et al., *WT1 mutation in malignant mesothelioma and WT1 immunoreactivity in relation to p53 and growth factor receptor expression, cell-type transition, and prognosis.* J Pathol 1997. **181**: p. 67-74.

35.   Ziprin, P., et al., *Laparoscopic-type environment enhances mesothelial cell fibrinolytic activity in vitro via a down-regulation of plasminogen activator inhibitor-1 activity.* Surgery, 2003. **134**(5): p. 758-765.

36.   Holloway, E.M., et al., *Mapping Development of the Human Intestinal Niche at Single-Cell Resolution.* Cell Stem Cell, 2021. **28**(3): p. 568-580.e4.

37.   Rudat, C., et al., *Upk3b Is Dispensable for Development and Integrity of Urothelium and Mesothelium.* PLOS One, 2014. **9**.

38.   Kanamori-Katayama, M., et al., *LRRN4 and UPK3B are markers of primary mesothelial cells.* PLOS One, 2011. **6**.

39.   Rinkevich, Y., et al., *Identification and prospective isolation of a mesothelial precursor lineage giving rise to smooth muscle cells and fibroblasts for mammalian internal organs, and their vasculature.* Nature Cell Biology, 2012. **14**: p. 1251-1260.

40.   Lua, I., et al., *Myofibroblastic Conversion and Regeneration of Mesothelial Cells in Peritoneal and Liver Fibrosis.* Am J Pathool, 2015. **185**: p. 3258–3273.

41.   Kawaguchi, M., D.M. Bader, and B. Wilm, *Sesrosal Mesothelium Retains Vasculogenic Potential.* Developmental Dynamics, 2007. **236**(11): p. 2973-2979.

42.   Wada, A.M., et al., *Epicardial/Mesothelial Cell Line Retains Vasculogenic Potential of Embryonic Epicardium.* Circulation Research, 2003. **92**(5): p. 525-531.

43.   Thomason, R.T., D.M. Bader, and N.I. Winters, *A Comprehensive Timeline of Mesodermal Development in the Quail Small Intestine.* Developmental Dynamics, 2012. **241**(11): p. 1678-1694.

44.   Winters, N.I., R.T. Thomason, and D.M. Bader, *Identification of a novel developmental mechanism in the generation of mesothelia.* Development, 2012. **139**(16): p. 2926-2934.

45.   Colunga, T., et al., *Human Pluripotent Stem Cell-Derived Multipotent Vascular Progenitors of the Mesothelium Lineage Have Utility in Tissue Engineering and Repair.* Cell Reports, 2019. **26**: p. 2566–2579.

46.   VanDussen, K., et al., *Notch signaling modulates proliferation and differentiation of intestinal crypt base columnar stem cells.* Development, 2012. **139**(3).

47.   Verzi, M.P. and R.A. Shivdasani, *Wnt signaling in gut organogenesis.* Organogenesis, 2008. **4**(2): p. 87-91.

48.   Tian, H., et al., *Opposing activities of Notch and Wnt signaling regulate intestinal stem cells and gut homeostasis.* Cell Reports, 2015. **11**(1): p. 33-42.

49.   Kruithof, B.P.T., et al., *BMP and FGF regulate the differentiation of multipotential pericardial mesoderm into the myocardial or epicardial lineage.* Developmental Biology, 2006. **295**(2): p. 507-522.

50.   Schlueter, J., J. Manner, and T. Brand, *BMP is an important regulator of proepicardial identity in the chick embryo.* Developmental Biology, 2006. **295**(2): p. 546-558.

51.   Inagaki, N.F., et al., *Generation of mesothelial progenitor-like cells from mouse-induced pluripotent stem cells.* FEBS Letters, 2019. **593**: p. 386–394.

52.   Dixit, R., X. Ai, and A. Fine, *Derivation of lung mesenchymal lineages from the fetal mesothelium requires hedgehog signaling for mesothelial cell entry* Development, 2013. **140**(21): p. 4398-4406.

53.   Kolterud, A., et al., *Paracrine Hedgehog signaling in stomach and intestine: new roles for hedgehog in gastrointestinal patterning.* Gastroenterology, 2009. **137**(2): p. 618-628.

54.   Miller, A.J., et al., *In Vitro and In Vivo Development of the Human Airway at Single-Cell Resolution.* Developmental Cell, 2020. **53**(1): p. 117-128.e6.

55.   Pansky, B., *Review of Medical Embryology.* 1982.

56.   Herrick, S.E. and S.E. Mutsaers, *The Potential of Mesothelial Cells in Tissue Engineering and Regenerative Medicine Applications.* Int J Artif Organs, 2007. **30**: p. 527-540.

57.   Lachaud, C.C., et al., *Use of mesothelial cells and biological matrices for tissue engineering of simple epithelium surrogates.* Frontiers in Bioengineering and Biotechnology, 2015. **3**.

58.   Arora, N., et al., *A process engineering approach to increase organoid yield.* Development, 2017. **144**: p. 1128-1136.

59.   McCracken, K.W., et al., *Modelling human development and disease in pluripotent stem-cell-derived gastric organoids.* Nature, 2014. **516**(7531): p. 400-404.

60.   Matsuo, Y., C. Nishizaki, and H. Drexler, *Efficient DNA fingerprinting method for the identification of cross-culture contamination of cell lines.* Human Cell, 1999. **12**(3): p. 149-154.

61.   Josephson, R., et al., *A molecular scheme for improved characterization of human embryonic stem cell lines.* BMC Biology, 2006. **4**(28).

62.   Tsai, Y.-H., et al., *In vitro patterning of pluripotent stem cell-derived intestine recapitulates in vivo human development.* Development, 2017. **144**(6): p. 1045-1055.

63.   Sugawara, S., et al., *Production of an aminoterminally truncated, stable type of bioactive mouse fibroblast growth factor 4 in Escherichia coli.* Journal of Bioscience and Bioengineering, 2014. **117**(5): p. 525-530.

64.   Heijmans, J., et al., *ER stress causes rapid loss of intestinal epithelial stemness through activation of the unfolded protein response.* Cell Reports, 2013. **3**: p. 1128-1139.

65.   Ootani, A., et al., *Sustained in vitro intestinal epithelial culture within a Wnt-dependent stem cell niche.* Nature Medicine, 2009. **15**(6): p. 701-706.

66.   Choi, K., M. Vodyanik, and I. Slukvin, *Hematopoietic differentiation and production of mature myeloid cells from human pluripotent stem cells.* Nature Protocols, 2011. **6**: p. 296–313.

67.   Yung, S., F.K. Li, and T.M. Chan, *Peritoneal Mesothelial Cell Culture and Biology.* Peritoneal Dialysis International, 2006. **26**: p. 162-173.

68.   Spence, J.R., et al., *Sox17 regulates organ lineage segregation of ventral foregut progenitor cells.* Developmental Cell, 2009. **17**: p. 62-74.

69.   Schneider, C.A., W.S. Rasband, and K.W. Eliceiri, *NIH Image to ImageJ: 25 years of image analysis.* Nature Methods, 2012. **9**: p. 671–675

70.   Wolf, F.A., P. Angerer, and F.J. Theis, *SCANPY: large-scale single-cell gene expression data analysis.* Genome Biology, 2018. **19**(15).

71.   McInnes, L., J. Healy, and J. Melville, *UMAP: Uniform Manifold Approximation and Projection for Dimension Reduction.* arXiv e-prints, 2018. **1802.03426**.

72.   Becht, E., et al., *Dimensionality reduction for visualizing single-cell data using UMAP.* Nature Biotechnology, 2019. **37**: p. 38-44.

73.   Blondel, V.D., et al., *Fast unfolding of communities in large networks.* J. Stat. Mech., 2008.

74.   Polański, K., et al., *BBKNN: fast batch alignment of single cell transcriptomes.* Bioinformatics, 2020. **36**(3): p. 964-965.

75.   Heijmans, J., et al., *ER stress causes rapid loss of intestinal epithelial stemness through activation of the unfolded protein response.* Cell Rep, 2013. **3**(4): p. 1128-1139.

Chapter 5 : Discussion and Future Directions

5.1 Introduction

In this chapter, I outline the current limitations and unanswered questions in the field of intestinal developmental biology, review my contributions to the field described within this dissertation, and identify intriguing new directions and propose future experiments based on this work that will help fill some of the most pressing current gaps in the field.

5.2 Overview of Gaps of Knowledge in the Field of Intestinal Biology

While our understanding of human intestinal biology has greatly advanced in recent years, some gaps in understanding still remain. In particular, many details surrounding early human intestinal developmental events remain unknown. Three main gaps in the field include difficulties in predicting human biology from *in vivo* animal models, an inadequate ability to accurately mimic human physiology using current *in vitro* models, and limited access to human fetal tissue which makes it difficult to study human development or benchmark the success of human *in vitro* models.

First, it has been established that differences between human and mouse biology make it difficult to draw conclusions about human development and disease from

mouse models. More than 80% of new therapeutics that have been rigorously tested and shown to be efficacious in mice fail when they reach clinical trials and are tested on humans [1]. For Crohn's disease specifically, the overall success rate for drug development is only 19%, which again highlights discrepancies between human and mouse biology [2]. The failure of mouse models may be due to known differences between the mouse and human intestine, including taller villi with no mucosal folds in the mouse small intestine compared to human, and different regional locations of goblet and Paneth cells.

While there are many documented differences between mouse and human intestinal biology, numerous unanswered questions remain. For example, EGF has been commonly used as an *in vitro* media supplement to support human intestinal epithelial cultures since it was initially shown to support growth of mouse intestinal epithelial cultures [3]. As an example of how mouse physiology does not accurately represent human biology, it has recently been shown that EGF is not abundantly expressed in the developing human intestinal stem cell niche, but is rather expressed throughout the villi which contain differentiated intestinal epithelial cell types [4]. Culture of human enteroids with factors that are more robustly expressed in the human stem cell niche such as NRG1 led to enhanced cellular diversity compared with EGF [4]. Such differences highlight the need for improved human *in vitro* intestinal models, especially as tools for preclinical testing that may increase the success rate of drug development.

This highlights another gap in the field as *in vitro* intestinal models fail to recapitulate the complex architecture of the human intestine. In particular, many

intestinal *in vitro* models solely focus on the epithelium in either 2D or 3D and fail to consider the impacts of the mesenchyme, serosal mesothelium, and other cell types found within the submucosa and muscularis propria. While the intestinal mesenchyme plays key roles in development and disease and is frequently involved in crosstalk with the epithelium, intestinal mesenchymal cells are highly understudied compared to the intestinal epithelium. At the time of writing, a Pubmed search for "intestinal epithelium" resulted in roughly 125,000 results whereas a search for "intestinal mesenchyme" or "intestinal mesenchymal cell" resulted in less than 3,000 results. An increased understanding of the intestinal mesenchyme and other non-epithelial cell types is imperative for understanding developmental progression as well as for developing better treatments for disease. While HIOs provide a model of both epithelium and mesenchyme, they still lack key cell types including neurons and immune cells and are relatively immature *in vitro*. My work in Chapter 4 provided a means to study perhaps the most understudied layer of the human intestine, the serosal mesothelium (less than 1,500 Pubmed hits), but there are still many unknowns surrounding how non-epithelial intestinal cell types play a role in development and disease progression.

Given the limited availability of human fetal tissue and few published studies using human fetal tissue, there are many gaps in our understanding of human intestinal development. While cellular-based model systems such as organoids enable us to study early human development, it is difficult to benchmark the success of these systems compared to early-stage human fetal tissue and thus conclusions drawn from organoids about development do not necessarily predict human development *in vivo*. Increased experiments on human fetal tissue will help to fill in knowledge gaps and

provide a basis for developing improved *in vitro* human model systems. Additionally,

studies which provide a means to benchmark similarities between organoids and human

tissue will greatly advance the field [5].

5.3 Contributions of this Dissertation Work to the Field

The overarching goal of this work was to create improved *in vitro* models of the

human intestine that better represent the native tissue in order to more accurately study

human development and disease. More specifically, this work aimed to eliminate

reliance on naturally-derived ECM basement membrane products like Matrigel that limit

both basic and translational studies using organoids. A secondary aim of this work was

to derive human intestinal organoids with increased organization that closely mimic

human tissue, particularly with regard to organization of the intestinal mesenchymal

layers. In this dissertation, I have described an updated, in-depth method to generate

human intestinal organoids (HIOs) (Chapter 2), engineered two defined culture methods

for HIOs that eliminate reliance on Matrigel (Chapters 3 and 4, Appendix A), and

defined a serosal mesothelial population within HIOs that has not previously been

described (Chapter 4).

The updated protocol for generating HIOs (Chapter 2) describes modifications to

the original protocol [6] as well as new applications for HIOs, including isolation of HIO

epithelium and mesenchyme for experiments on individual tissue layers and co-culture

with microbes for studies on the microbiome. This protocol fills a previous gap in the

organoid field of generating reproducible intestinal organoids, as I provide step-by-step

instructions and clear images depicting each step. The HIO directed differentiation

protocol is heavily dependent on the starting state of pluripotent stem cells, especially in

regard to density and colony size prior to endoderm specification. Confusion over starting cell state has caused many researchers from other institutions to train in the Spence lab and observe HIO differentiation first-hand, as it can be challenging to generate HIOs by following older protocols. My goal with the updated protocol was to increase transparency over each step of the differentiation process by clearly describing key steps, defining all materials including reagents that have been updated since the original protocol was published (for example, WNT3A has since been replaced with CHIR-99021), and showing images depicting how cells/spheroids/organoids should look over time. Additionally, I describe key applications of HIO technology that increase utility of the HIO model system. This protocol will serve as a major resource in the field to aid researchers across multiple institutions in generating reproducible HIOs.

In addition to updating the HIO generation protocol, I created novel culture methods for HIOs. Matrigel has been a limiting factor for organoid research due to its xenogeneic origin, poorly defined composition, and non-tunable properties, which has prompted multiple studies into defined alternatives that increase reproducibility and relevance to human tissue [7]. To address this issue, I developed defined alginate hydrogels (Chapter 3) and suspension culture (Chapter 4) as Matrigel-free culture systems that support HIO growth. Both of these systems provide increased control over experiments, are significantly cheaper than Matrigel, and are less susceptible to supply chain issues such as the Matrigel shortage during the Covid-19 pandemic. Additionally, both alginate and suspension culture are bioinert as these systems do not provide biochemical cues to HIOs, and HIOs cannot adhere to, degrade, or remodel their environment.

The alginate and suspension culture systems I developed in this work present improved alternatives to traditionally used Matrigel and offer advantages to the organoid field. In addition to eliminating the variability and experimental control issues associated with Matrigel, alginate or suspension culture are significantly cheaper and easier to work with than Matrigel culture. Suspension culture in particular is highly amenable to scale-up experiments as HIOs could be cultured in larger suspension bioreactors, which increases the translational potential of HIOs as replacement tissue or as drug-screening tools. The finding that HIOs can grow in a bioinert environment sheds light on the ability of these organoids to create their own niche through interactions between the intestinal epithelium and mesenchyme, although further work is necessary to better understand the role of the mesenchyme in the intestinal stem cell niche.

To further enhance the utility of suspension culture for HIOs or other organoid systems, I have additionally provided a step-by-step protocol describing methods to generate HIOs and culture them in suspension (Appendix A). In particular, I highlight methods to characterize suspension HIOs and ensure reproducibility, as well as methods to isolate the serosa from suspension HIOs via FACS for studies on mesothelial cells. This protocol will make it easier for other labs to adopt suspension culture in a reproducible manner.

Perhaps the most notable finding from this work is the formation of a serosal mesothelium in HIOs cultured in bioinert conditions (both alginate and suspension culture). While the serosa is one of the four main layers of the gut and plays a large role in both disease and homeostasis [8, 9], almost nothing is known about the developmental origin of this cell type, particularly in the human intestine. My work has

201

created a model system to study the human serosal mesothelium *in vitro* as I have shown that the serosa found within suspension HIOs is highly similar to that of the human intestine. Additionally, I have demonstrated that suspension HIOs can be used as a model to interrogate mesothelial development and found a preliminary role for HH and WNT signaling in serosa formation and patterning. Further work is necessary to better understand how the human serosal mesothelium is formed. Suspension HIOs are a useful model system to continue answering questions about serosal development, including how the serosa interacts with and contributes to developing intestinal mesenchyme, and will facilitate further studies to answer unknown questions in the field.

Taken together, this body of work has led to advanced understanding of human intestinal development and provided improved model systems to better study the human intestine *in vitro*. The protocols described herein will serve as guides for researchers looking to adapt organoid technologies into their labs. In particular, alginate and suspension culture methods serve as tools to better model intestinal development, particularly development of the serosal mesothelium, in a reproducible manner and such systems increase the clinical potential of organoids.

5.4 Future Directions

5.4.1 The Role of Hedgehog and WNT Signaling in Serosal Mesothelial Development and Patterning

In Chapter 4, I began to uncover mechanistic insights into signaling pathways involved in development and differentiation of the human intestinal serosal mesothelium. In particular, I described a role for the HH and WNT pathways in serosal development. However, it remains unknown whether these pathways are directly acting

on serosal mesothelial cells or have an indirect effect on other cells within the epithelium or mesenchyme. Further, it is unclear which components of the HH and WNT pathways are most involved in serosa formation, or how these pathways interact with each other.

To begin answering these questions, I performed FISH to assess the spatial expression of HH pathway components in the intestine, as I identified a clear mesothelial phenotype upon both stimulation and inhibition of HH signaling within HIOs. In particular, I assessed the expression of three well described HH target genes that also play a role in HH signaling – *SMO*, *PTCH1*, *and HHIP.* I observed that both the human fetal serosa and HIO-serosa express *SMO*, *PTCH1*, *and HHIP*, which is consistent with our scRNA-seq data (Figure 5-1). *SMO* and *PTCH1* are expressed broadly throughout the mesenchyme in both human fetal intestine and suspension HIOs. *HHIP* appears to be expressed broadly in HIOs, with enrichment in the smooth muscle layers in the fetal intestine. *PTCH1 and HHIP* are enriched in mesenchyme adjacent to the epithelium in the fetal intestine and HIO, as is expected given that the epithelium is a known source of SHH and IHH. Additionally, *HHIP* appears to be enriched in the serosa compared to the underlying mesenchyme, suggesting that regulation of HH signaling may be important for serosal mesothelial cells as *HHIP* acts to regulate and inhibit HH expression levels [10]. Together, I take this expression to mean that both serosa and different compartments of the mesenchyme (i.e. epithelium-adjacent, smooth muscle) are responsive to HH signaling and therefore different compartments of the intestine (or HIOs) may respond differently to activation or inhibition in HH signaling (Figure 5-1).

To directly address how HH activation/inhibition may affect the different intestinal compartments (serosa vs. mesenchyme), I FACS isolated serosal mesothelial cells (PDPN+/ECAD+/EPCAM-) and mesenchymal cells (PDPN-/ECAD-/EPCAM-) from suspension HIOs. I then placed these populations in 2D culture overnight to allow cells to attach to the tissue culture dish. After 24 hours, I added SAG or Cyclopamine to the media of experimental wells for 6 days and compared these to control cells cultured in basal media. I stained all conditions (mesenchyme + SAG, mesenchyme + Cyclopamine, mesenchyme controls, serosa + SAG, serosa + Cyclopamine, serosa controls) for WT1 and αSMA to calculate the percentage of cells in each condition that expressed WT1 or αSMA.

When analyzing the serosal cells, I found that there was no statistically significant difference in the percentage of cells expressing WT1 when comparing basal media, SAG, and Cyclopamine. However, as was mentioned in Chapter 4, the percentage of αSMA+ cells in the Cyclopamine group was significantly lower than the percentage of αSMA+ cells in both the basal media and SAG groups (Figure 5-1B), suggesting that HH inhibition may block the ability of mesothelial cells to differentiate into other mesenchymal cell types. This is consistent with observations in the mesothelium of the developing mouse lung (Dixit et al., 2013), in which it has been shown that HH inhibition blocks mesothelial cell entry/differentiation into the underlying mesenchymal space. HIO-serosal cells treated with Cyclopamine have slightly increased WT1 expression compared to controls, though not statistically significant. This suggests that HH is not acting directly on the serosa or mesenchyme, but must work in concert with other signals to induce WT1 expression.

Further supporting the idea that HH is indirectly acting on mesenchyme and serosa, in the new experiment where I isolated mesenchyme and treated with SAG or Cyclopamine, I did not observe any WT1+ cells in any of the mesenchymal cell groups, indicating that altered HH signaling is not directly causing HIO-mesenchyme to differentiate into WT1+ cells (Figure 5-1C).

Based on these results, I propose a model where HH signaling acts indirectly on the serosa and mesenchyme. Blocking HH inhibits the ability of these cells to differentiate into non-serosal cell types (i.e. smooth muscle), therefore leading to ectopic WT1 expression. My data suggests that activating HH signaling is required for differentiation into non-WT1 lineages, but does not necessarily disrupt serosa formation, or directly influence the differentiation into serosal lineages. Thus, HH signaling may have an effect on the patterning and differentiation potential of serosal mesothelial cells, but not necessarily impact the initial formation of the serosal mesothelium.

As my work in Chapter 4 also indicated a role for WNT signaling in serosa formation, I FACS-isolated serosa and mesenchyme from suspension HIOs and treated these cells with both IWR1 and CHIR-99021 to determine how WNT signaling impacts the serosa vs. mesenchyme. I observed similar percentages of cells that expressed αSMA in basal media conditions compared to IWR1 and CHIR-99021 groups (Figure 5-1D). However, I found that a significantly higher percentage of cells in the IWR1-treated group expressed WT1 compared to basal media or CHIR-99021 treatment. This is in contrast to the effects noted for IWR1 treatment of whole HIOs, in which WNT inhibition caused stunted mesothelial development (score 1, Chapter 4). This result suggests that WNT inhibition at early time points prior to or during serosa formation may stunt

205

mesothelial development, while inhibiting WNT on fully differentiated mesothelial cells may actually promote WT1 expression. Alternatively, WNT inhibition may work to stunt mesothelial development through an indirect mechanism via contributions to other cell types.

As support for the idea that WNT inhibition at later time points (post serosa formation) may promote WT1 expression, treating HIOs with IWR1 from day 14-28 caused a majority of HIOs to score 3 (Figure 5-1E). I have shown that serosa formation is completed between day 14-28, and that a score of 3 indicates excess WT1 in the mesenchyme. Thus, this experiment suggests that WNT signaling may impact serosa formation in a time-dependent manner. Since WNT inhibition at early time points stunts serosa formation and WNT inhibition at late time points after the serosa has begun to form causes excess WT1 expression, I hypothesize that WNT signaling may be necessary for early serosal differentiation, and that regulation of WNT signaling is important for proper serosal patterning at later timepoints. However, the role of WNT signaling in serosal mesothelial development remains unclear. It will be important to repeat WNT modulation experiments with increased replicates, as well as to test other specific WNT activators/inhibitors in addition to IWR1 and CHIR-99021 as CHIR-99021 may additionally modulate TGF-β, Notch, and MAPK signaling.

Moving forward, it will be necessary to further elucidate how HH and WNT impact formation and differentiation of the human intestinal serosal mesothelium. It remains unclear which pathway components are involved, how these pathways interact with other cell types surrounding the serosa, and the timeline on which they are acting. To begin answering these questions, we could conduct a time-course experiment on HIOs

to analyze the spatial locations of HH and WNT pathway components pre- and post-serosa formation via FISH. It would be especially interesting to observe HIOs between 7 and 14 days in culture, as the serosa begins to form during this period. This would enable us to better understand whether these pathways are acting directly on the serosa at early time points as mesothelial cells are differentiating, and which ligands and receptors are at play. Additionally, we could treat HIOs with HH and WNT inhibitors and activators and send these treated HIOs for scRNA-seq analysis pre- and post-serosa formation. This would provide additional insight into how HH and WNT are impacting specific cell populations over time compared to control HIOs. scRNA-seq on HH and WNT-modulated HIOs would additionally provide a means for assessing receptor-ligand interactions using computational toolsets in order to better understand which specific HH or WNT ligands and receptors play a role during serosa formation [11].

An alternative approach to screening for signaling mechanisms involved in serosa formation would be to utilize a genome-wide CRISPR screen to identify regulators of serosa formation. Genes that are knocked out and do not give rise to HIO-serosa may be implicated in serosa formation. This approach may provide insights into additional signaling pathways that play a role in serosa development, as the initial signaling screen described in Chapter 4 only evaluated 5 signaling pathways and may have excluded key regulators of serosa development. In particular, it may be useful to further examine a potential role for BMP and FGF signaling in intestinal serosal mesothelial development, as these pathways have been implicated in development of the mesothelium of the heart [12]. While my initial signaling screen did not indicate a

decrease in serosa formation when FGF or BMP signaling was inhibited, it may be worth repeating this experiment with different, more specific inhibitors and activators of these pathways. Similarly, we could perform scRNA-seq on pooled genetic perturbation screens via Perturb-seq [13] to gain additional insights into the role of HH and WNT signaling on the serosal mesothelium. While effective, CRISPR-based screening methods may be technically challenging.

Additionally, it may be relevant to examine how the concentration on HH/WNT inhibitor compounds on serosa formation. HH has been shown to play a role in development of the intestinal smooth muscle [14, 15], which is supported by our analysis of *PTCH1* expression in the developing human intestine in which *PTCH1* is highly expressed in the muscularis layers and expressed at lower levels in the serosa. Since the epithelium is the major source of SHH ligand in the intestine, it may provide a gradient of HH ligand that decreases radially outward from the epithelium. Thus, higher levels of SHH may promote smooth muscle development in the mesenchyme, while lower levels of SHH may promote mesothelial patterning in the serosa. Treatment of suspension HIOs and HIO-serosa with varying concentrations of Cyclopamine and SAG may reveal a concentration-dependent effect of HH signaling on serosal patterning and development.

5.4.2 Developmental Origin and Progeny of Serosal Mesothelial Cells

In Chapter 4, I demonstrated that suspension HIOs can be used as a model to study human serosal mesothelial development and identified a role for HH and WNT signaling in intestinal serosa formation. However, there are still many unknown questions surrounding mesothelial development. It is currently unknown how human

serosal mesothelial cells differentiate from mesenchymal progenitors, and what progenitor cell state they derive from. Studies in the chick have indicated that the intestinal serosal mesothelium derives from the splanchnic mesoderm in a mechanism distinct from the developing mesothelium of the heart [16, 17]. However, whether or not this mechanism is conserved in a human context, and the exact cell type from which mesothelial cells derive, remains unknown. Questions surrounding the origin of mesothelial cells are difficult to answer based on analyses of human fetal intestinal tissue, as the serosa forms at an early timepoint such that all tissue samples that we have access to have already formed a serosal mesothelium. Thus, suspension HIOs may offer unique insight to determine the mesenchymal precursor cell type from which the serosa derives.

To answer this question, we could utilize computational-based lineage trajectory analyses. A first set of experiments could focus on existing scRNA-seq datasets and combining samples of human fetal small intestine or HIOs sequenced at various timepoints. Computational tools would enable us to predict progenitor cell populations and infer lineage/differentiation trajectories, thus providing insight on how serosal cells originate and differentiate into other mesenchymal populations. However, this may not be the most effective experimental strategy using human tissue as I have observed a serosal mesothelium in human fetal intestinal tissue as early as 55 days post-conception via immunofluorescent staining. Thus, scRNA-seq on human tissue may not provide insights into a pre-serosal population as the serosa appears to form prior to the timepoint that we have access to human fetal tissue. It may be more effective to infer lineage trajectories by sequencing suspension HIOs collected across multiple

timepoints. While computational lineage trajectory predictions are not always accurate, this approach would enable us to generate hypotheses about mesothelial progenitor cells which could then be systematically tested using HIOs *in vitro*.

An alternative approach to understanding serosal mesothelial differentiation would be to utilize a cell barcoding approach combined with scRNA-seq readouts such as the CellTag system pioneered by the Morris lab [18]. Barcoded lineage tracing systems enable unbiased lineage tracing in cellular systems, and such lineage relationships can be inferred using scRNA-seq [19]. This approach is ideal for studying potential relationships between mesenchymal progenitor cells, serosal mesothelial cells, and more differentiated mesenchymal cell types like smooth muscle cells using HIOs as an *in vitro* model system. Using this approach, we could infect suspension HIOs with a first library of heritable random unique molecular indexes, or CellTags, at an early timepoint prior to serosa formation, likely between day 3 – day 7. We could then infect HIOs with a second CellTag library at day 28, at the point in which the serosa has fully developed, and maintain these HIOs in culture for another 2-3 weeks to enable the tagged serosal cells to differentiate into other mesenchymal cell types. We could then perform scRNA-seq on the tagged HIOs and utilize computational analyses to gain an understanding of lineage trajectories leading up to serosa formation as well as serosal differentiation into vascular smooth muscle or other mesenchymal cell states.

Ideally, one of these computational-based toolsets would enable us to identify a mesenchymal population of progenitor cells that differentiates into the serosal mesothelium. We could then identify specific markers for this pre-serosa population from the scRNA-seq data, and design a knockin iPSC line to label and trace these cell

types within HIOs to verify that this progenitor source gives rise to the serosal mesothelium. We could additionally develop functional experiments to better understand the mechanism behind mesothelial cell differentiation. This line of experiments would provide unprecedented insight into the origin of human intestinal serosal mesothelial cells.

Additionally, to gain insight into how the serosal cells contribute to the intestinal mesenchyme during development, we could design a knockin iPSC line to label and trace serosal cells. I have conducted some preliminary experiments attempting to generate a WT1 Cre-ERT2 EGFP knockin line that would enable visualization of WT1+ cells via a GFP reporter, and place an inducible Cre driver under the control of the WT1 promoter for lineage tracing. This line would enable us to evaluate the role of the serosal mesothelium in shaping the intestinal mesenchyme, including vascular smooth muscle, during development. HIOs generated from this line may be particularly useful following transplantation as transplanted HIOs undergo maturation and become vascularized *in vivo*, enabling us to visualize mesothelial contributions to the developing intestinal vasculature.

5.4.3 Generation of Human Intestinal Organoids with Increased Intestinal Cell Types

While the formation of a serosal mesothelium within HIOs greatly increases the utility of this model system to more closely resemble the native intestine and study development of the mesothelial layer, HIOs are still quite immature *in vitro* and lack many of the cell types found in the human intestine. In the epithelium, HIOs do not develop mature Paneth cells *in vitro*. Further, the epithelium does not organize into

defined crypt-villus structures until HIOs are transplanted *in vivo*. In the mesenchyme, HIOs lack organization despite the formation of an outer serosal mesothelium. In particular, HIOs do not form organized muscle layers *in vitro*. Additionally, HIOs do not develop immune cells, neurons, or endothelial cells using the standard organoid differentiation protocol.

More recent protocols have elucidated means to differentiate both neuronal cells and endothelial cells within HIOs [20, 21]. Thus far, protocols to differentiate advanced HIOs with increased diversity of cell types have been independently developed to include only one additional cell type of interest. Future work may focus on combining existing protocols to develop multiple new cell types within HIOs, as well as developing methods to further mature HIOs *in vitro*. For example, it may be possible to differentiate HIOs with an enteric nervous system, serosal mesothelium, and vascular endothelial cells *in vitro* by using a combination of existing protocols. HIOs that more closely resemble the human intestine will increase the relevance of human *in vitro* studies on development and disease.

Creating HIOs with both a serosal mesothelium and endothelial cells is of particular interest as the serosal mesothelium contributes to the developing vascular smooth muscle of the gut [22]. Additionally, it is hypothesized that vascularization from the mouse host may be a major factor in promoting HIO maturation *in vivo*, as HIOs become innervated with mouse vasculature after transplantation [23]. The development of HIOs with both serosa and endothelial cells may enable formation of mature vasculature *in vitro*, and thus lead to more mature intestinal tissue. It would additionally enable further studies on the mechanisms underlying vascular development.

To begin answering this question, I have conducted preliminary experiments to adapt our lab's published protocol that enriches for endogenous vascular endothelial cells in HIOs to suspension culture. This protocol involves treatment of early spheroids with VEGF, BMP4, and FGF2 for 3 days, followed by maintenance in media containing low levels of VEGF [20]. I hypothesized that adaptation of this protocol into suspension culture would enable differentiation of HIOs with both endothelial cells and an outer serosal mesothelium. While this protocol supported induction of endothelial cells in suspension HIOs and caused increased expression of endothelial cell markers (PECAM, CDH5), the growth factors that support endothelial cell induction seemed to inhibit serosa formation as I observed decreased expression of mesothelial markers (WT1, UPK3B, Figure 5-2A) and failed to observe an organized serosal mesothelium (Figure 5-2B) in suspension HIOs treated with vasculogenic factors.

In order to determine whether a decreased growth factor load would accommodate development of both a serosa and endothelial cells, I treated HIOs with varying combinations of vasculogenic growth factors for 3 days followed by maintenance in VEGF. Interestingly, treatment with VEGF alone or VEGF combined with either BMP4 or FGF2 did not lead to a robust induction of endothelial cell markers compared to controls (Figure 5-2A). However, treatment with VEGF or VEGF in combination with BMP4 supported expression of mesothelial markers. This suggests that while a combination of growth factors is necessary for endothelial cell induction, FGF2 may disrupt serosa formation at early timepoints.

Moving forward, it will be necessary to elucidate a modified vascular HIO protocol in suspension to study interactions between the serosa and the developing vasculature.

In particular, generation of HIOs with endothelial cells combined with creation of a WT1 Cre-ERT2 EGFP knockin line for lineage tracing of WT1+ serosal cells would enable effective studies on mesothelial contributions to vascular smooth muscle. The current vascular HIO protocol requires growth factors to be added at quite early time points, day 3-6 of culture, as it was found that endogenous endothelial cells within hindgut spheroids decrease after 3 days [20]. However, the mesenchyme may still be quite plastic at these early time points, and modifications to culture media at this time may alter the state of pre-mesothelial cells such that serosa formation is prevented. Further lines of experimentation may focus on decreasing growth factor concentrations, or application of growth factors at later time points as the serosa has begun to form, in an attempt to increase populations of endogenous endothelial cells while also maintaining serosa formation.

Another cell layer that has been lacking in traditionally cultured Matrigel HIOs is an organized muscularis mucosa or muscularis propria containing smooth muscle cells. While many Matrigel HIOs form αSMA+ cells, they are not organized into a defined smooth muscle layer. I observed in my early work that HIOs cultured in alginate form an organized band of smooth muscle cells that has not been observed in Matrigel. Interestingly, suspension HIOs give rise to few αSMA+ cells but form a serosal mesothelium at high frequency, while alginate HIOs give rise to an organized smooth muscle layer at high frequency but exhibit a lower frequency of serosa formation (Figure 5-2C). This suggests that matrix properties such as stiffness may be driving smooth muscle formation and that serosa and smooth muscle may preferentially form under different conditions.

More recently, I have observed that when suspension HIOs are cultured in EREG, an EGF-family ligand which our lab has found to be a relevant intestinal stem cell niche factor, instead of EGF, they form both a serosal mesothelium and a robust layer of smooth muscle cells (Figure 5-2D). Preliminary work from our lab has additionally shown that HIOs cultured in EREG may give rise to a population of neuronal cells. Thus, EREG may serve to promote the development of multiple cell types within HIOs to create a suspension HIO model with both a serosal mesothelium and muscularis layer. This highlights the necessity of understanding important niche factors *in vivo*, as we have found that EGF may not be the most relevant niche factor to support human organoid growth *in vitro* [4].

Future directions of this work may focus on developing protocols to derive HIOs with a serosa as well as smooth muscle and neuronal cells. Experiments could include developing a grading scheme to characterize smooth muscle and serosa formation in EREG HIOs, and using this scoring system to optimize a concentration of EREG that best promotes both populations. This grading scheme could build upon the 0-3 mesothelial scale developed in Chapter 4, and include a scoring system to additionally grade the degree of smooth muscle formation. It will also be essential to better characterize the epithelium of EREG HIOs to ensure that they form expected epithelial cell types and resemble Matrigel HIOs. Since I have observed that alginate HIOs form a smooth muscle layer as well, we could alternatively culture HIOs in suspension and then transfer them to alginate for differing periods of time to determine whether matrix stiffness/compression may drive smooth muscle differentiation. This method may enable formation of both a serosa and muscularis layers by combining effects of

alginate and suspension culture. While this method may be more technically challenging than simply altering the culture media, it would enable interesting studies on the impact of microenvironment stiffness on intestinal cell differentiation.

5.4.4 Therapeutic Applications of Serosal Mesothelial Cells to Prevent Serosal Adhesions

In addition to aiding basic studies on mesothelial development, suspension HIOs provide a source of mesothelial cells that can be harnessed for therapeutic applications. Serosal adhesions, fibrous bands that form between the intestine and other organs or the body wall which can lead to pain, bloating, and bowel obstruction [24], occur in more than 90% of patients following abdominal surgery [25]. Mesothelial cells are the source of such surgical adhesions [26], as mesothelial cells undergo an epithelial to mesenchymal transition that contributes to fibrosis [27]. Since suspension HIOs form a serosal mesothelium at high frequency, they may serve as a model to study serosal adhesions or provide a source of healthy mesothelial cells that can be used during surgery to prevent adhesion formation.

To investigate the potential for suspension HIOs to study and treat serosal adhesions, there are a few potential experimental strategies. First, we could conduct additional transplantation experiments on suspension HIOs delivered to the mouse intestinal mesentery to determine if the presence of a serosa decreases the ability of HIOs to engraft and adhere. We could transplant equal numbers of suspension and Matrigel HIOs and calculate the percentage of HIOs that successfully engraft in each condition. If fewer suspension HIOs engraft than Matrigel HIOs, this would suggest that the presence of a serosa in the HIOs exhibits functional capability to prevent adhesions.

We could additionally use suspension HIOs as a model of serosal adhesions *in vitro* or *in vivo* to interrogate potential therapeutic treatments to prevent adhesion formation. We could disrupt the serosa of suspension HIOs in an *in vitro* "injury model" by mechanically scraping away the outer layer, and then plate these HIOs in a tissue culture plate containing intestinal mesenchymal cells to simulate adhesion to other organ systems or the body cavity. The injured HIOs would likely attach to the plate creating an "adhesion". This system would provide a model to treat HIOs with compounds that may decrease adhesion formation, such as hydrogel coatings on the plate or anti-mesothelial antibodies, and evaluate whether treatment decreases the severity of HIOs adhering to the plate. However, the fibrotic response of adhesion formation likely involves other cell types including immune cells that are not present in HIOs. Thus, suspension HIOs could also be utilized in an *in vivo* adhesion model after transplantation.

Finally, since adhesions are caused by disruption or injury to the mesothelial layer, suspension HIOs may provide a source of healthy mesothelial cells that could be used during surgery to decrease adhesion formation. To test this hypothesis, we could create adhesions in the mouse intestine using a previously described adhesion model [26] and deliver mesothelial cells from HIOs to the injury site to determine whether the presence of mesothelial cells decreases the likelihood or severity of adhesion formation. If successful, this line of experimentation could also include investigating methods to expand HIO-serosa cells in culture. While I have been able to successfully isolate and culture extracted HIO-serosa from suspension HIOs, the mesothelial cells exhibited low proliferation *in vitro* and began differentiating into smooth muscle-like cells when

cultured in 2D conditions. Therapeutic applications of HIO-serosa would require a high number of isolated mesothelial cells. Thus, we could investigate methods to expand isolated HIO-serosa in culture. For example, we could examine ECM coatings to seed the HIO-serosa cells on and optimize media components to maintain mesothelial cell identity while promoting proliferation.

5.4.5 High Content Organoid-Based Screening Experiments

A major advantage of suspension culture compared to Matrigel is its increased potential for clinical and pre-clinical applications. Matrigel is not suitable for clinical-based work as it is xenogeneic and derived from mouse tumor cells. Additionally, manually embedding, passaging, and removing organoids from 3D Matrigel droplets is technically challenging and time consuming. This limits studies involving organoids to relatively low-throughput experiments. However, organoids have high potential to serve as a tool for drug screening and may work as an improved model system for pre-clinical testing compared to mouse models or 2D cell culture studies. Such drug screening experiments will be most successful at high throughput, such that many compounds could be evaluated to select the best response for a patient or specific disease implication. Suspension culture has the potential to increase the throughput for organoid screening-based experiments, as organoids could be cultured in a larger scale bioreactor that does not require manual embedding or passaging.

Based on this idea, a future direction of this work would be to generate proof of concept data that suspension organoids can be used for high-throughput compound screens and offer advantages over Matrigel HIOs in terms of efficiency and cost. This line of experimentation could also include optimization of HIO yield in suspension, as

the current suspension protocol described in Chapter 4 and Appendix A results in a significantly lower number of organoids compared to Matrigel culture. One potential workaround for this low yield would be to culture HIOs in Matrigel or a defined hydrogel system for the first week in culture to enhance viability, and then transfer these organoids into suspension. However, this approach remains technically challenging and time consuming and may disrupt mesenchymal/mesothelial organization. Another potential avenue to increase HIO yield in suspension would be to introduce low concentrations of ECM protein ligands or mimics into the suspension culture media, although this may also disrupt the organization of HIOs including the formation of a serosal mesothelium.

It would additionally be interesting to adapt the suspension protocol to tissue-derived enteroids, as many disease-modelling studies or patient drug screens would be more relevant if using patient-derived tissue as it is challenging to accurately model disease states using HIOs. Previous work has shown that enteroids derived from intestinal stem cells will reverse polarity when cultured in suspension, and cannot be maintained for long periods of time in suspension culture as they exhibit slower proliferation compared to Matrigel culture [28, 29]. Future lines of experiments involving patient-derived epithelial-only enteroids in suspension could focus on addition of soluble ECM protein ligands or synthetic mimics to the culture media to control polarity reversal and potentially increase proliferation in a Matrigel-free system.

5.5 Concluding Remarks

Overall, this body of work introduces two Matrigel-free systems for intestinal organoid culture that are simple, cost-effective, and eliminate experimental and

translational hurdles associated with mouse tumor-derived ECM products. Importantly,

this work provides a model system to study the intestinal serosal mesothelium *in vitro*,

which opens doors to understand this understudied cell population and its role in

development and disease.

5.6 Figures
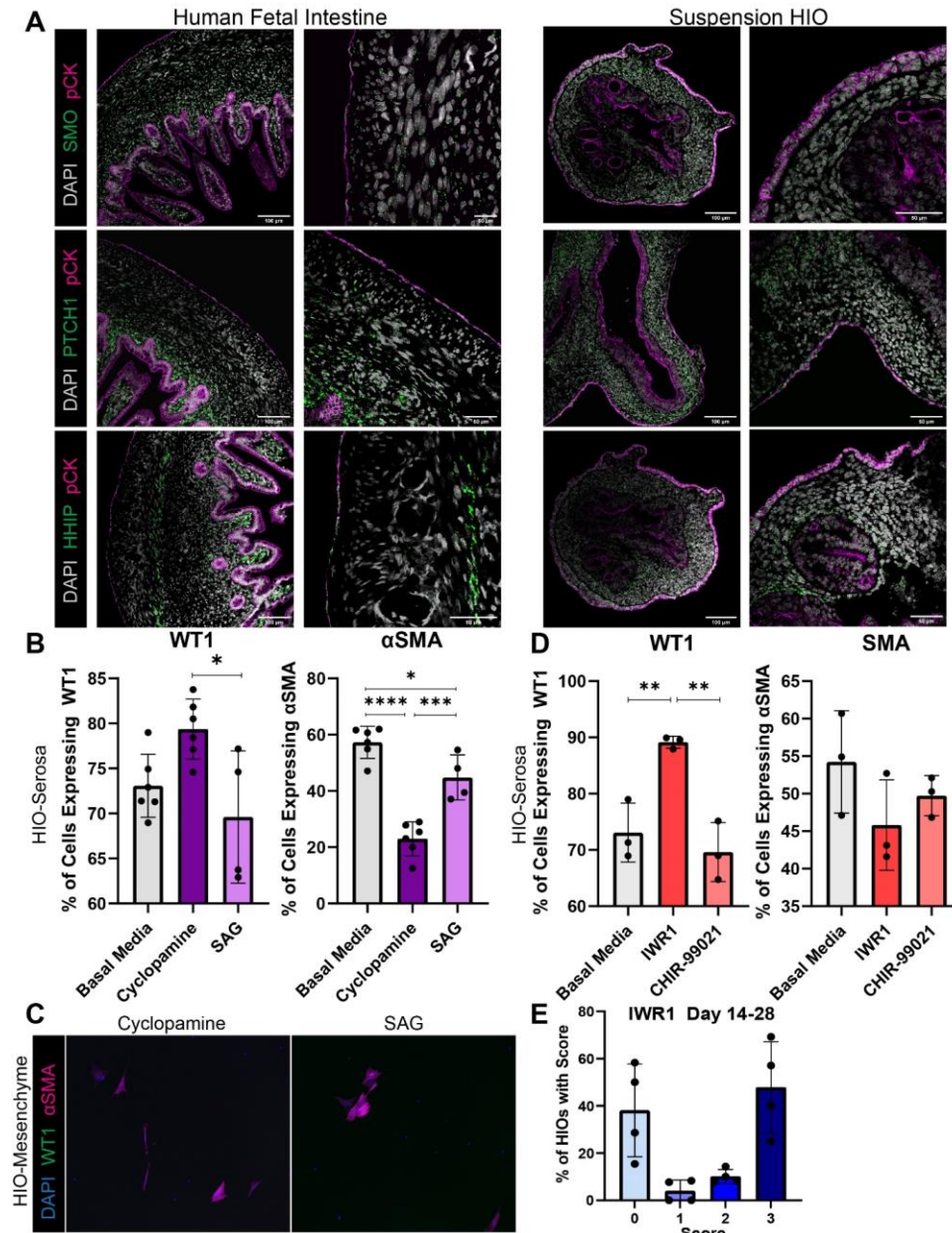
Figure 5-1. HH and WNT Pathway in Differentiation and Patterning of Serosal Mesothelium.

(a): Images depict human fetal small intestine (110 days post-conception) and suspension HIOs (28 days). Fluorescence *in situ* hybridization (FISH) probes shown are *SMO*, *PTCH1*, and *HHIP*. Immunofluorescent markers shown are DAPI and pan-Cytokeratin (pCK). **(b):** Percentage of FACS-isolated HIO-serosa cells that expressed WT1 or αSMA after treatment with SAG or Cyclopamine. HIO-serosa cells were isolated and cultured on Matrigel coated plates in basal media for 24 hours, followed by SAG or

Cyclopamine treatment for 6 days before fixation and staining. **(c):** Images depicting FACS-isolated HIO-mesenchymal cells (PDPN-ECAD-EPCAM-) stained for WT1 and αSMA after treatment with SAG or Cyclopamine. HIO-mesenchymal cells were isolated and cultured on Matrigel coated plates in basal media for 24 hours, followed by treatment for 6 days before fixation and staining. **(d):** Percentage of FACS-isolated HIO-serosa cells that expressed WT1 or αSMA after treatment with IWR1 or CHIR-99021. HIO-serosa cells were isolated and cultured on Matrigel coated plates in basal media for 24 hours, followed by IWR1 or CHIR-99021 treatment for 6 days before fixation and staining. **(e):** Graph depicting the percentage of HIOs treated with IWR1 from day 14-day 28 that received each score (0-3, see Chapter 4) across 4 independent experiments (biological replicates).
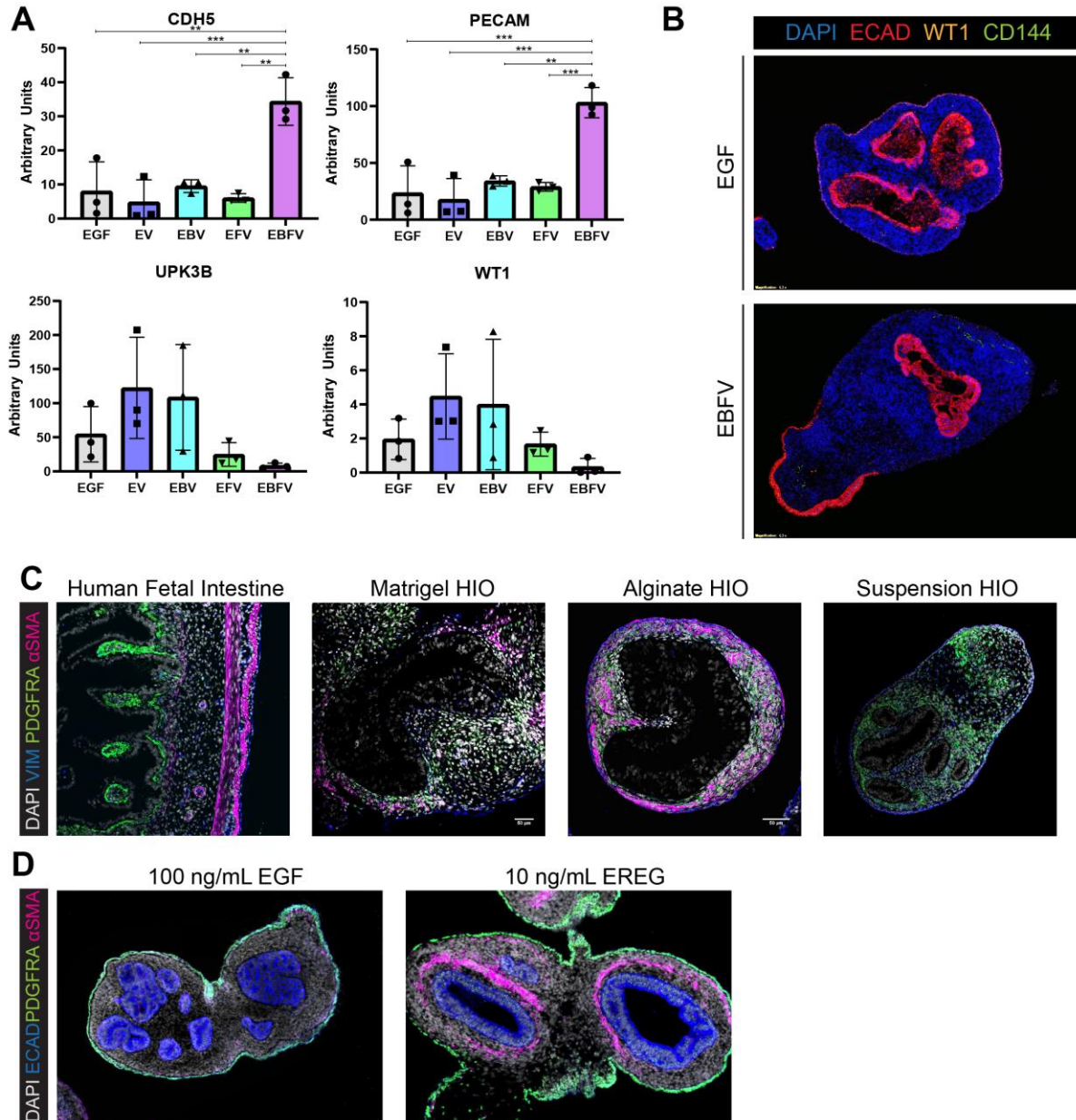
Figure 5-2. Methods to Generate HIOs with Vasculature, Smooth Muscle Bands, and Serosa.

(a): qRT-PCR results from HIOs cultured under standard conditions (EGF) compared to modified vascular induction protocols. HIOs were cultured in ENR medium (containing EGF, Noggin, and R-spondin) for 3 days. On the 3rd day of culture, 50 ng/mL VEGF was added to the ENR for all conditions other than EGF. From Day 3-6, a combination of 50 ng/mL VEGF, 25 ng/mL BMP4, and 25 ng/mL FGF2 was added to media containing EGF, followed by maintenance in 25 ng/mL VEGF up to day 28. Expression levels are normalized to GAPDH. Each point is representative of 6-10 HIOs pooled from the same batch (biological replicates). Data represent the mean ± standard error of the mean. Significance was calculated with a one-way ANOVA and multiple comparisons test. **(b):** Representative images of suspension HIOs cultured in EGF compared to HIOs cultured

223

in EGF, BMP4, FGF2, and VEGF (EBFV) for days 3-6 followed by maintenance in EGF and VEGF. HIOs were stained for DAPI, ECAD, WT1, and CD144. HIOs in EGF form a serosa but do not form many CD144+ endothelial cells, while HIOs cultured in vasculogenic conditions do not form a serosa but give rise to vascular endothelial cells. **(c):** Representative images of 110 day human fetal intestine and 28-day HIOs cultured in Matrigel, 1% alginate, and suspension stained for DAPI, VIM, αSMA, and PDGFRA. **(d):** Representative images of suspension HIOs cultured in 100 ng/mL EGF (standard culture conditions) compared to 10 ng/mL EREG stained for DAPI, ECAD, αSMA, and PDGFRA.

5.7 References

1.   Perrin, S., *Preclinical research: Make mouse studies work.* Nature, 2014. **507**: p. 423–425.

2.   Parker, J.L. and J.C. Kohler, *The success rate of new drug development in clinical trials: Crohn's disease.* J Pharm Pharm Sci, 2010. **13**(2).

3.   Sato, T., et al., *Single Lgr5 stem cells build crypt-villus structures in vitro without a mesenchymal niche.* Nature, 2009. **459**: p. 262-265.

4.   Holloway, E.M., et al., *Mapping Development of the Human Intestinal Niche at Single-Cell Resolution.* Cell Stem Cell, 2021. **28**(3): p. 568-580.e4.

5.   Yu, Q., et al., *Charting human development using a multi-endodermal organ atlas and organoid models.* Cell, 2021. **184**(12): p. 3281-3298.e22.

6.   Spence, J.R., et al., *Directed differentiation of human pluripotent stem cells into intestinal tissue in vitro.* Nature, 2011. **470**(7332): p. 105-109.

7.   Agarwal, T., et al., *Recent advances in chemically defined and tunable hydrogel platforms for organoid culture.* Bio-Design and Manufacturing, 2021. **4**: p. 641– 674.

8.   Winters, N.I. and D.M. Bader, *Development of the Serosal Mesothelium.* Journal of Developmental Biology, 2013. **1**: p. 64-81.

9.   Mutsaers, S.E., *Mesothelial cells: Their structure, function and role in serosal repair.* Respirology, 2002. **7**: p. 171-191.

10.   Chuang, P.T. and A.P. McMahon, *Vertebrate Hedgehog signalling modulated by induction of a Hedgehog-binding protein.* Nature, 1999. **397**(6720): p. 617-21.

11.   Armingol, E., et al., *Deciphering cell–cell interactions and communication from gene expression.* Nature Reviews Genetics, 2021. **22**: p. 71-88.

12.   Kruithof, B.P.T., et al., *BMP and FGF regulate the differentiation of multipotential pericardial mesoderm into the myocardial or epicardial lineage.* Developmental Biology, 2006. **295**(2): p. 507-522.

13.   Dixit, A., et al., *Perturb-seq: Dissecting molecular circuits with scalable single cell RNA profiling of pooled genetic screens.* Cell, 16. **167**(7): p. 1853–1866.e17.

14.   Mao, J., et al., *Hedgehog signaling controls mesenchymal growth in the developing mammalian digestive tract* Development, 2010. **137**(10): p. 1721– 1729.

15. Huycke, T.R., et al., *Genetic and Mechanical Regulation of Intestinal Smooth Muscle Development.* Cell, 2019. **179**(1): p. 90-105.e21.

16. Winters, N.I., R.T. Thomason, and D.M. Bader, *Identification of a novel developmental mechanism in the generation of mesothelia.* Development, 2012. **139**(16): p. 2926-2934.

17. Winters, N.I., A.M. Williams, and D.M. Bader, *Resident progenitors, not exogenous migratory cells, generate the majority of visceral mesothelium in organogenesis.* Developmental Biology, 2014. **391**(2): p. 125-132.

18. Biddy, B.A., et al., *Single-cell mapping of lineage and identity in direct reprogramming.* Nature, 2018. **564**(7735): p. 219–224.

19. Kebschull, J.M. and A.M. Zador, *Cellular barcoding: lineage tracing, screening and beyond.* Nature Methods, 2018. **15**: p. 871–879.

20. Holloway, E.M., et al., *Differentiation of Human Intestinal Organoids with Endogenous Vascular Endothelial Cells.* Developmental Cell, 2020. **54**(4): p. 516-528.e7.

21. Workman, M.J., et al., *Engineered human pluripotent-stem-cell-derived intestinal tissues with a functional enteric nervous system.* Nature Medicine, 2016. **23**: p. 49-59.

22. Wilm, B., et al., *The serosal mesothelium is a major source of smooth muscle cells of the gut vasculature.* Development, 2005. **132**: p. 5317-5328.

23. Watson, C., et al., *An in vivo model of human small intestine using pluripotent stem cells.* Nature Medicine, 2014. **20**: p. 1310-1314.

24. Tabibian, N., et al., *Abdominal adhesions: A practical review of an often overlooked entity.* Ann Med Surg (Lond). , 2017. **15**: p. 9–13.

25. Atta, H.M., *Prevention of peritoneal adhesions: A promising role for gene therapy.* World J Gastroenterol., 2011. **17**(46): p. 5049–5058.

26. Tsai, J.M., et al., *Surgical adhesions in mice are derived from mesothelial cells and can be targeted by antibodies against mesothelial markers.* Sci Transl Med., 2018. **10**(469): p. eaan6735.

27. Koopmans, T. and Y. Rinkevich, *Mesothelial to mesenchyme transition as a major developmental and pathological player in trunk organs and their cavities.* Communications Biology, 2018. **1**(170).

28. Co, J.Y., et al., *Controlling Epithelial Polarity: A Human Enteroid Model for Host-Pathogen Interactions.* Cell Reports, 2019. **26**: p. 2509–2520.

29. Co, J.Y., et al., *Controlling the polarity of human gastrointestinal organoids to investigate epithelial biology and infectious diseases.* Nature Protocols, 2021. **16**: p. 5171–5192.

Appendix A : Culturing hPSC-Derived Human Intestinal Organoids in Suspension for Matrigel-Free Culture and Analysis of the Serosal Mesothelium

A.1 Summary

This protocol describes methods to culture pluripotent stem cell-derived human intestinal organoids (HIOs) in suspension as a defined alternative to Matrigel. HIOs cultured in suspension form an organized mesenchyme and serosal mesothelium that has not been observed in Matrigel HIOs, and thus suspension culture provides a useful model for recapitulating the native intestine and serosal mesothelium. While HIO yield is lower in suspension compared to Matrigel, suspension culture is simple, cost-effective, and amenable to scale-up for high throughput experiments.

For complete details on the use and execution of this protocol, please refer to [1-4].

A.2 Before you begin

This protocol describes suspension culture for pluripotent stem cell-derived human intestinal organoids (HIOs) which contain both epithelium and mesenchyme [2, 4], and is not suitable for long term culture or passaging of tissue-derived epithelial-only enteroids [5]. We have successfully utilized this protocol with multiple human embryonic stem cell (ESC) lines (H9 and UM 63-1) and human induced pluripotent stem cell (iPSC) lines (72.3 and WTC11) and it is likely to work well with other hESC/iPSC lines. Success may vary if utilizing resources from different commercial sources than those described in the Key Resources Table.

Though not explicitly described in the following steps, sterile technique and work in a tissue culture hood is essential throughout this protocol. We recommend a Labconco horizontal clean bench containing a dissecting microscope/stereoscope for ease of working with organoids.

Institutional permissions

All experiments using hPSCs were approved by the University of Michigan Human Pluripotent Stem Cell Research Oversight Committee. Readers may need to obtain institutional permission before conducting experiments using hPSCs.

Aliquoting and storing of cell culture reagents

Timing: 2 weeks (if purifying FGF4, Noggin, and R-spondin in-house), or 3 hours (if aliquoting from commercially available sources).

Note: These steps should be taken before beginning any other section of the protocol.

Note: Matrigel should be stored at -80ºC and needs to be thawed at 4ºC overnight prior to dilution and coating plates for cell culture

CRITICAL: Once thawed, Matrigel must be kept at 4ºC or on ice at all times to prevent it from polymerizing and forming a solid.

1. Prepare concentrated aliquots of growth-factor reduced Matrigel ready to be diluted to 100 µg/mL with cold DMEM/F12 for coating cell culture plates.

- After aliquoting, Matrigel should be stored at -80ºC until use.

2. Prepare 5 mg/mL aliquots of Dispase II powder by dissolving in DMEM/F12.

- Dispase aliquots should be stored at -20ºC until use.

3. Prepare 1 mL and 10 mL aliquots of Hyclone defined FBS.

- Aliquots of dFBS should be stored at -80ºC until use.

4. Reconstitute Activin A using 1xPBS to a concentration of 100 µg/mL.

- Store aliquots of Activin A at -80ºC until use.

5. Purify human recombinant FGF4 utilizing previously described methods [6].

- Prepare 500 µg/mL aliquots in 1xPBS.

- Store aliquots of FGF4 at -80ºC until use.

Optional: Commercially available recombinant human FGF4 can be used in place of purifying FGF4 protein and should be aliquoted and stored in the same manner.

6. Prepare 10 mM aliquots of CHIR-99021 in DMSO.

- For 10 mg of CHIR-99021, add 215 µL DMSO.

- Store aliquots at -20ºC until use.

7. Reconstitute human EGF to 100 µg/mL in 1xPBS.

- Store aliquots at -80ºC until use.

8. Purify recombinant human Noggin from a HEK293 cell line expressing Fc-tagged Noggin [7] using the Protein A Agarose Kit.

- Prepare 100 µg/mL aliquots and store at -80ºC until use.

Optional: Commercially available recombinant human Noggin protein can be utilized as a replacement and should be aliquoted and stored in the same manner.

9. Prepare human R-Spondin1 conditioned medium from Cultrex HA-R-Spondin1-Fc 293 T cells.

- Prepare 10 mL aliquots of conditioned medium and store at -80ºC until use.

Optional: Commercially available recombinant human R-spondin protein can be utilized as a replacement and should be aliquoted at 500 µg/mL and stored at -80ºC.

Preparation of reagents for hPSC culture

Timing: 2 hours

Note: These steps should be taken prior to passaging hPSCs for differentiation.

10. Dilute an aliquot of growth factor-reduced Matrigel using **cold** DMEM/F12 to a final concentration of 100 µg/mL.

- When passaging a 6-well plate of hPSCs to one 6-well maintenance plate and one 24-well differentiation plate, 18 mL of diluted Matrigel are required.

11. Dilute Dispase solution to a final concentration of 0.2 mg/mL in DMEM/F12.

12. Prepare mTeSR or mTeSR Plus media by combining the basal media with its corresponding supplement.

13. Prepare Day 1 Base Media.

- Add 5 mL of Penicillin-Streptomycin to a 500 mL bottle of RPMI.

14. Prepare Day 2 Base Media.

- Add 5 mL of Penicillin-Streptomycin to a 500 mL bottle of RPMI.

- Add 1 mL of Hyclone dFBS.

15. Prepare Day 3 Base Media.

- Add 5 mL of Penicillin-Streptomycin to a 500 mL bottle of RPMI.

- Add 10 mL of Hyclone dFBS.

Note: Base Media solutions can be stored at 4ºC for up to one month.

Preparation of reagents for organoid culture

Timing: 1 hour

Note: These steps should be taken prior to collecting hindgut spheroids for organoid generation.

16. Prepare Mini Gut Base Media.

- Add 5 mL of Penicillin-Streptomycin to a 500 mL bottle of Advanced DMEM/F12.

- Add 5mL of GlutaMax.

- Add 7.8 mL of HEPES Buffer.

- Add 10 mL of B-27 Supplement.

Note: Mini Gut Base Media can be prepared in advanced and stored at 4ºC for up to 1 month.

17. Prepare "ENR" Organoid Growth Media.

- Add 100 µL of EGF (100 ng/mL) to 100 mL Mini Gut Base Media in a sterile tissue culture bottle.

- Add 100 µL Noggin (100 ng/mL).

- Add 5 mL of R-Spondin 1 conditioned media.

Note: ENR Organoid Growth Media should be used within 2 weeks.

Preparation of poly (2-hydroxyethyl methacrylate) (pHEMA) coating solution for generating low attachment plates

Timing: 24 hours

Note: pHEMA coating solution is stable at room temperature for up to one year and can be prepared in advance according to [8].

Optional: While it is more cost-effective to use pHEMA coating to generate low attachment plates, another option is to use commercially available ultra-low attachment tissue culture plates.

18. Prepare 95% ethanol containing 10 mM NaOH.

- To prepare 40 mL of coating solution, add 1.6 mL of tissue culture-grade H_2O and 400 μL 1M NaOH to 38 mL of pure 200 proof ethanol in a 50 mL conical tube.

19. Add 10% (wt/vol) of poly (2-hydroxyethyl methacrylate) (pHEMA) to the ethanol solution.

- For a 40 mL solution, add 4 g of pHEMA.

CRITICAL: Vigorously shake solution immediately upon addition of pHEMA to prevent precipitation. It is difficult to fully dissolve pHEMA crystals once they aggregate.

20. Place solution in a tube rotator overnight and continuously rotate until the pHEMA is fully dissolved.

Generation of pHEMA-coated low attachment plate

Timing: 24 hours

Note: pHEMA-coated low attachment plates can be generated in advance and stored at room temperature prior to use for up to one month.

21. Determine the appropriate plate size for HIO suspension culture.

Note: For routine HIO culture or experiments involving few experimental conditions, a 6-well plate works best. Typically, one batch of spheroids from one 24-well plate can be cultured in one well of a 6-well plate. If multiple experimental conditions are desired, a 24-well plate can be used instead.

22. Using a serological pipette, transfer enough pHEMA coating solution to each well of the tissue culture plate to coat the bottom. For a 6-well plate, add 1 mL of pHEMA coating solution per well.

Note: pHEMA coating solution is quite viscous, so take care when pipetting.

23. Gently shake the plate back and forth, side to side, until the pHEMA coating solution has covered the entire plate surface.

24. Once the plate surface has been fully coated, collect the pHEMA coating solution from the plate and transfer back to its storage tube for future use using a pipette.

Note: pHEMA coating solution can be re-used many times. It is often helpful to first remove the pHEMA from a coated plate with a serological pipette, and then use a P1000 to remove any excess liquid.

25. Place the pHEMA-coated tissue culture plate in a sterile hood with the plate lid open and turn on the UV for at least 15 minutes.

CRITICAL: pHEMA coating solution is not sterilized, so it is essential that the pHEMA-coated plate is UV-sterilized prior to use for HIO culture to avoid contamination.

26. After sterilization, leave the pHEMA-coated plate in the tissue culture hood with the plate lid open overnight to allow excess liquid to evaporate.

Note: The pHEMA-coated plate is ready for use on the day after coating. pHEMA-coated tissue culture plates can be generated in advance and stored at room temperature. After 24 hours, the lid of the plate can be closed and kept in a sterile hood for storage until use.

Thawing and maintenance of hPSCs

Timing: 1.5 hours to thaw hPSCs, 2 weeks to maintain cells prior to differentiation

Note: hPSCs require time to recover from cryopreservation (typically 2 weeks, or 3-4 passages). Freshly thawed hPSCs may not yield spheroids if a differentiation is attempted on the first few passages. hPSC lines that have been frozen for longer periods of time may require longer recovery periods.

27. Prepare a Matrigel-coated plate to seed freshly thawed hPSCs on.

- Use cold Growth Factor Reduced Matrigel at a concentration of 100 μg/mL (prepared in 'Before You Begin' Step 10) for coating. This is referred to as coating Matrigel.

- For a 6-well maintenance plate of hPSCs, pipette 1mL of coating Matrigel per well.

Note: If thawing one vial of hPSCs, cells should be thawed into one well of a 6-well plate.

- Leave Matrigel-coated plates in a tissue culture hood at room temperature for at least 1 hour prior to passaging.

28. Pipette 5-10 mL of warm DMEM/F12 into a conical tube in a sterile biosafety cabinet.

29. Remove cryopreserved hPSCS from liquid nitrogen storage.

CRITICAL: Use appropriate protective equipment when handling liquid nitrogen.

CRITICAL: Once cells have been removed from liquid nitrogen, work as quickly as possible when thawing.

30. Warm cryovial of hPSCS in a 37ºC water bath until the cells are just thawed.

31. Using a P1000 pipette, add the thawed hPSCS to the vial of DMEM/F12 dropwise.

32. Pellet the cells by centrifugation at 300g for 5 minutes.

33. Aspirate the supernatant, and resuspend hPSCs in an appropriate volume of warm mTeSR Plus (1.5 mL per well of a 6 well plate).

34. Remove Matrigel from the coated plate, and pipette hPSCS in mTeSR Plus into the well.

35. Add 10 mM Y-27632 (1:1000 dilution) to the well.

- Gently rock the plate back and forth, side to side.

- Return the plate to the tissue culture incubator.

CRITICAL: Addition of ROCK inhibitor to the media is critical to increase viability after a thaw.

36. Change media on the plate on the day after passaging, and every other day as needed. If using mTeSR1 instead of mTeSR Plus, media should be changed daily.

Note: See "Culture of hPSCS for differentiation" for notes on hPSC passaging.

37. Maintain hPSCs for 3-4 passages prior to differentiation.

A.3 Step-by-step method details

A.3.1 Culture of hPSCs for differentiation

Timing: 2 hours to passage hPSCs, 4-5 days between passages

This step describes methods to culture hPSCs for routine maintenance and differentiation into hindgut spheroids for generation of human intestinal organoids.

CRITICAL: hPSCs should not be maintained in media containing antibiotics, so proper sterile technique is essential throughout stem cell maintenance and passaging to avoid contamination.

38. Passaging of hPSCs for maintenance and differentiation:

- Observe hPSC confluency and colony size/density under a microscope to determine the appropriate time to begin passaging.

- If there are regions that have begun to spontaneously differentiate, use a sterile P-20 tip to scrape away differentiated regions while looking under a stereoscope within a horizontal clean bench. Differentiated regions can be identified as dense, white colored regions typically at the edges of large or dense colonies.

Note: hPSCs typically require passaging on the fourth day after the last passage but the timing can vary depending on the density at which the cells were seeded. Timing of passaging should be based on overall confluence as well as colony density, as dense colonies will begin to spontaneously differentiate and cause loss of pluripotency.

- When hPSCs are ready for passaging, prepare Matrigel-coated plates to seed freshly split hPSCs on.
  - Use cold Growth Factor Reduced Matrigel at a concentration of 100 µg/mL (prepared in 'Before You Begin' Step 10) for coating. This is referred to as coating Matrigel.
  - For a 6-well maintenance plate of hPSCs, pipette 1mL of coating Matrigel per well.
  - For a 24-well differentiation plate of hPSCS, pipette 0.5 mL of coating Matrigel per well.

- Leave Matrigel-coated plates in a tissue culture hood at room temperature for at least 1 hour prior to passaging

Optional: Rather than coating a plate on the day of passaging, Matrigel-coated plates can be prepared in advance and stored at 4ºC for up to 1 week. Be sure to parafilm any pre-coated plates prior to placement in a refrigerator. If using a cold pre-coated plate, the plate should be brought to room temperature by warming in an incubator or brought

into a tissue culture hood and allowed to reach room temperature prior to cell passaging.

- While plates are coating, remove mTeSR Plus, DMEM/F12, and 0.2 mg/mL Dispase solution from the refrigerator and place at room temperature or in a 37°C water bath to warm up.

- After plates have coated for one hour, add 1 µL of warm Dispase (0.2 mg/mL) to each well of the 6 well plate that is to be passaged.

- Place the hPSC plate containing Dispase into a tissue culture incubator for 10 minutes at 37°C.

Note: For all tissue culture in this protocol, the tissue culture incubator should be set to the standard 37°C and 5% CO_2.

- After 10 minutes, pipette 2 mL of DMEM/F12 into each Dispase-containing well of hPSCs.

- Rock plate back and forth, side to side a few times, and then aspirate the DMEM/F12.

- Pipette 1.5 mL of DMEM/F12 into each well. Rock back and forth, side to side a few times, and then aspirate the DMEM/F12.

- Pipette 1 mL of DMEM/F12 into each well. Rock back and forth, side to side a few times, and then aspirate the DMEM/F12.

- Pipette 3.5 mL of mTeSR Plus into each well of hPSCs that is being passaged.

Note: 3.5 mL of mTeSR Plus per well is a typical volume used for stem cell wells that are roughly 80% confluent. The volume of mTeSR Plus and/or passaging ratio should

239

be adjusted depending on the starting density of stem cells. The passaging density may also need to be optimized or adjusted depending on the cell line that is being used.

- Aspirate the Matrigel coating solution from the tissue culture plates.

Optional: Coating Matrigel can be reused up to 2 times after its initial use. Rather than aspirating Matrigel, the coating Matrigel can be collected by pipetting the liquid from the plate and transferring to a sterile conical tube for future use. It can be helpful in this situation to label the tubes and plates depending on whether the Matrigel is 'new' or 'used'.

- Pipette 1 mL of mTeSR Plus into each well of the freshly coated 6 well plate for hPSC maintenance.

- Remove hPSCs from their current plate by scraping the well with a sterile cell scraper.

- Vigorously pipette hPSCs up and down 4-7 times using a 5 mL serological pipette to break the colonies up into small pieces.

- To maintain a 6-well maintenance plate of hPSCs, spread one well of hPSCs to a 6-well plate by pipetting 0.5 mL of suspended, broken up hPSC colonies from one well to each well of the freshly coated 6-well plate.

- To passage a 24-well plate for differentiation, spread one well of hPSCS to one row of a 24-well plate by pipetting 0.5 mL of suspended, broken up hPSC colonies from one well to each well within one row of the freshly coated 24-well plate. Repeat 3 more times to fill the plate.

- Place newly passaged hPSC plates in a tissue culture incubator.

CRITICAL: Shake plates back and forth, side to side multiple times before placing them back in the incubator to ensure that cells are evenly seeded in each well. Once the plates have been placed in the incubator, do not disturb for at least 2 hours to allow cells to attach.

39. On the day after seeding, change media with fresh mTeSR Plus.

- Rock plate back and forth, side to side to loosen up dead cells/debris.

- Gently aspirate used media from each well.

- Add 1.5 mL of mTeSR plus to each well of a 6-well plate, or 0.5 mL per well of a 24-well plate.

40. Once cells have reached an appropriate density, repeat the passaging process beginning at Step 1.

Note: If using mTeSR1 Media, stem cell plates should be fed every day. If using mTeSR Plus media, plates can be fed every other day but media should always be changed on the day after passaging.

A.3.2 Hindgut spheroid generation from hPSCs

Timing: 8-10 days

This step describes a directed differentiation approach to generate hindgut spheroids from the 24-well plate of hPSCs that was generated in Steps 38-39. The hPSCs are first differentiated into definitive endoderm by treatment with Activin A for 3 days, followed by hindgut differentiation by treatment with FGF4 and CHIR-99021 for 4-

6 days, which results in the formation of 3D hindgut spheroids that bud up from the monolayer and float in the culture media. These hindgut spheroids can be collected and cultured in Matrigel or suspension, as described in this protocol, for maturation into human intestinal organoids.

Note: hPSCS are typically ready to begin differentiation 2 days after passaging. However, stem cells should be evaluated under the microscope every day to determine when to begin differentiation as differentiation efficiency is highly dependent upon the starting cell density and morphology.

Note: Day 1 – Day 3 Base Medias should be prepared before starting Step 41. The base medias can be stored at 4ºC for up to 1 month, while growth factors should be added on the day they are to be used or consumed within 1 week.

Note: See Figure A-1 for an overview of the differentiation protocol.

41. When the 24-well plate of hPSCS has reached 70-80% density, it is ready to begin endoderm differentiation. Prepare a 1:1000 dilution of Activin A in Day 1 Base Media (100 ng/mL). For a 24-well plate, this amounts to 12 µL Activin A in 12 mL of Day 1 Base Media (Day 1 Activin A Media).

42. Change the media in the 24-well hPSC plate from mTeSR Plus to Day 1 Activin A Media by aspirating off the mTeSR Plus and pipetting 0.5 mL of Day 1 Activin A Media per well.

- Return the plate to the tissue culture incubator for 24 hours.

CRITICAL: The starting state of hPSCS prior to beginning differentiation, including colony size and density, is the most critical factor in determining differentiation success. See Troubleshooting 1.

Note: It is helpful to label the plate lid with the date and time of each media change to keep track.

43. On the following day, prepare Day 2 Activin A Media by making a 1:1000 dilution of Activin A in Day 2 Base Media. For a 24-well plate, this amounts to 12 µL Activin A in 12 mL of Day 2 Base Media.

44. 24 hours after Day 1 Activin A Media was added, change the media to Day 2 Activin A Media by aspirating off the Day 1 Media and pipetting 0.5 mL of Day 2 Activin A media per well.

- Return the plate to the tissue culture incubator for 24 hours.

Note: It is normal to see cell death during the endoderm differentiation process as the cells are being cultured in low serum conditions.

CRITICAL: It is essential that Day 2 Activin A is added 24 hours after Day 1 Activin A was added. Leaving the cells in Day 1 Activin A Media for too short or too long a time before changing media can result in an inefficient differentiation.

45. On the following day, prepare Day 3 Activin A Media by making a 1:1000 dilution of Activin A in Day 3 Base Media. For a 24-well plate, this amounts to 12 µL Activin A in 12 mL of Day 3 Base Media.

46. 24 hours after Day 2 Activin A Media was added, change the media to Day 3 Activin A Media by aspirating off the Day 2 Media and pipetting 0.5 mL of Day 3 Activin A media per well.

- Return the plate to the tissue culture incubator for 24 hours.

Note: The highest degree of cell death is typically observed on the day after adding Day 2 Activin A media.

CRITICAL: It is essential that Day 3 Activin A is added 24 hours after Day 2 Activin A was added. Leaving the cells in Day 2 Activin A Media for too short or too long a time before changing media can result in an inefficient differentiation.

47. On the following day, prepare F/C Hindgut Differentiation Media by preparing a 1:1000 dilution of FGF4 (500 ng/mL) and 1:5000 dilution of CHIR-99021 (2µM) in Day 3 Base Media.

Note: Since F/C Hindgut differentiation Media will be used for the next 4-6 days of culture, it can be helpful to prepare this media in 50 mL amounts. For a 50 mL volume, 50 µL of FGF4 and 10 µL CHIR-99021 should be added to a 50 mL conical containing Day 3 Base Media.

48. 24 hours after Day 3 Activin A Media was added, change the media to F/C Hindgut Differentiation Media by aspirating off the Day 3 Media and pipetting 0.5 mL of F/C Media per well.

- Return the plate to the tissue culture incubator for 24 hours.

Note: The cells should now have formed a flat, confluent monolayer at this point. Cells are considered 'definitive endoderm' after the 3rd day of Activin A treatment. However, endoderm induction is not 100% efficient, leaving some non-endodermal cells that will give rise to the mesenchymal layer within HIOs.

49. Continue to change the media to fresh F/C media daily. Since the same media is being added every day, it is no longer critical to change the media at the same

time each day. Hindgut spheroids should begin to emerge on the day after the 4th

media change with F/C media (at the time of the 5th F/C media change)

Note: During the hindgut induction process, the cells should begin organizing into 3D

spider web-like structures.

A.3.3 Collection of hindgut spheroids for culture into HIOs

Timing: 1 hour per day, 3 days

After the differentiation plate has undergone hindgut differentiation for 4 days,

hindgut spheroids will begin to emerge and bud up from the monolayer. Spheroids

should begin to float up into the culture media on the day of the 5th media change to F/C

Hindgut Differentiation Media. These spheroids are referred to as "Day 4 spheroids"

since they emerged after the 4th day of F/C media. After collection, spheroids can be

cultured in Matrigel [2], alginate [9], or suspension to support their growth and

maturation into HIOs over about 4 weeks in culture.

Note: For generation of human small intestinal organoids (HIOs), Day 4 – Day 6

spheroids are typically collected (the day after the 4th F/C media change – the day after

the 6th F/C media change) and then the plate is discarded. Spheroids will continue to

emerge after Day 6, but organoids generated from later spheroids will begin to take on a

more distal fate whereas Day 4 – Day 6 spheroids produce HIOs that resemble proximal

small intestine [10].

Note: If no spheroids emerge, see Troubleshooting 1.

50. On the day after the 4th media change to F/C Hindgut Differentiation Media, observe the differentiation plate under a stereoscope. Hindgut spheroids should have budded off from the monolayer to float in the culture media. See Troubleshooting 1.

51. Use a P1000 pipette to collect the spheroids from each well by removing the media which contains floating spheroids.

Note: It is helpful to work under a stereoscope within a horizontal clean bench during this step to visualize that all spheroids have been collected.

Note: Take care not to scratch the bottom of the plate and disturb the monolayer during this process.

CRITICAL: Work quickly while collecting spheroids so that the plate does not dry out.

52. Transfer the spheroids in media into 1.5 mL Eppendorf tubes.

53. Repeat until spheroids have been collected from all wells.

54. Replace the media in the differentiation plate with fresh F/C hindgut differentiation media.

- If collecting Day 4 or Day 5 spheroids, return the plate to the tissue culture incubator overnight. If collecting Day 6 spheroids, skip the media change and discard the plate.

55. Allow the spheroids to settle to the bottom of the 1.5 mL Eppendorf tubes (10-15 minutes).

56. Once spheroids have settled to the bottom of the tubes, collect spheroids from each tube and combine them all into one 1.5 mL Eppendorf tube.

Optional: To ensure that all spheroids have been collected, allow the tubes to settle for another 10-15 minutes and then collect any additional spheroids that may have been missed on the first collection.

A.3.4 Suspension culture of human intestinal organoids

Timing: 30 minutes for spheroids plating, 28 days for HIO maturation.

This step describes how to transfer hindgut spheroids into suspension culture for generation of HIOs in a simple Matrigel-free system that promotes the organization of an outer serosal mesothelial layer.

CRITICAL: Ensure that Mini Gut Base Media and ENR Organoid Growth Media have been prepared prior to collecting spheroids.

CRITICAL: Ensure that a tissue culture plate has been coated with pHEMA coating solution at least 24 hours in advance of spheroid collection.

Note: The same plate can be used to collect spheroids over multiple days if using individual wells, even once it has been kept in an incubator.

57. Using pHEMA-coated low attachment tissue culture plate that has dried overnight with the plate lid open, rinse each well with 1XPBs.

- Pipette 1.5 mL of 1xPBS into each well, rock the plate back and forth, side to side, and then aspirate off the PBS.

- Repeat with a second wash, and then aspirate off the PBS.

58. Add ENR Organoid Growth Media to the pHEMA-coated plate. For one well of a 6-well plate, 4-5 mL of media should be used.

59. Remove as much media as possible from the 1.5 mL Eppendorf tube containing spheroids (Step 56) without disturbing the spheroids.

- Discard media.

Note: It is helpful to work under a stereoscope during this process to ensure that spheroids are not accidentally removed when removing media.

60. Using a P-20 pipette, transfer spheroids from the 1.5 mL Eppendorf tube to the pHEMA-coated plate containing ENR Organoid Growth Media.

- Rinse the tube with ENR Organoid Growth Media by pipetting media into the tube, and collecting any remaining spheroids. Pipette the media containing additional spheroids into the pHEMA-coated plate.

- Gently rock the plate back and forth, side to side to evenly distribute the spheroids.

- Return the plate to the tissue culture incubator.

CRITICAL: Take care not to scratch the bottom of the pHEMA-coated plate at any time as scratching can disturb the coating and create a region where spheroids/organoids can attach. See Troubleshooting 2.

A.3.5 Changing media on suspension HIOs

Timing: 15 minutes

Change media on the suspension HIOs every 3-5 days, or as necessary depending on the volume of spheroids in the well and the color of the culture media.

61. Working under a stereoscope in a horizontal clean bench, remove the suspension HIO plate from the tissue culture incubator and place on the microscope.

- Allow HIOs to settle to the bottom of the plate

62. While looking under the microscope, use a P1000 to remove used media from the well. Tilt the plate to remove as much media as possible without pipetting up any organoids.

Note: It is often difficult to completely remove all media without pipetting up any HIOs.

63. Once media has been removed, pipette 4-5 mL fresh ENR Organoid Growth Media into each well.

- Return the plate to the tissue culture incubator.

Note: It is important that HIOs are cultured in ENR Organoid Growth Media for the first 3 days to ensure proper patterning into proximal small intestine (duodenum). However, after 3 days, the media can be changed to Mini Gut Basal Media supplemented with just 100 ng/mL EGF. The Noggin and R-spondin are not required to support HIO growth/patterning after the first 3 days, but keeping HIOs in ENR for the duration of culture is also acceptable.

A.3.6 Passaging of suspension HIOs

Timing: 1-2 hours

Suspension HIOs need to be passaged less frequently than Matrigel HIOs as the matrix does not need to be replaced and the mesenchyme is unable to spread into the environment. If suspension HIOs are kept in culture for 28 days or less, passaging is often not required unless the HIOs look particularly large and/or begin accumulating dead cells/debris in the lumen which can be observed as dark content in the center of the HIO. If the HIOs begin to look unhealthy and dark in color or if they are being maintained for long periods of time, it may be time to passage.

Note: It is essential to work under a stereoscope inside of a horizontal clean bench during passaging to visualize the HIOs while maintaining sterility.

64. Using a cut P1000 pipette tip, transfer suspension HIOs to a 6cm Petri dish containing warm DMEM/F12.

65. Sterilize a scalpel and 1 mL syringe with attached 30Gx1 needle by spraying with 70% ethanol.

66. While using the syringe/needle to hold HIOs in place, use the scalpel to cut large HIOs or HIOs that have accumulated dark-colored debris in the lumen into smaller pieces.

Note: HIOs are often cut in half lengthwise during passaging, but may need to be cut again into smaller pieces if they are excessively large.

Optional: For small HIOs, the needle can be used to poke a hole in the lumen to release luminal contents rather than cutting the HIO in half.

67. Transfer HIO pieces to a new well of a low attachment plate.

68. Add fresh ENR Organoid Growth Media to the passaged HIOs.

- Return the plate to the tissue culture incubator.

A.3.6 Validation and analysis of resulting suspension HIOs

Timing: 4 days

This step describes a protocol to perform immunostaining on suspension HIOs to validate that they are properly organized and give rise to all expected cell types.

Optional: While it is recommended that at least a few suspension HIOs from each batch are validated by immunofluorescent staining prior to downstream experiments or analyses, this step is optional.

Optional: Rather than validating expected cell types by immunostaining, it is also acceptable to utilize qRT-PCR to evaluate key differentiation markers. However, this method does not allow for visualization of HIO organization.

69. Collect suspension HIOs in a 1.5 mL Eppendorf tube using a cut P200 pipette tip.

70. Fix HIOs overnight in 4% paraformaldehyde (PFA).

- Remove media from tube containing HIOs.

- Carefully pipette 1mL of 4% PFA onto HIOs.

- Leave HIOs on a tube rocker at 4ºC overnight.

71. After 24 hours, wash PFA off of HIOs by washing 3 times with 1xPBS for 15 minutes.

CRITICAL: Collect waste from all wash steps containing PFA and properly dispose of PFA waste.

72. Transfer HIOs into a disposable plastic base mold using a cut P200 pipette tip.

73. Embed HIOs in HistoGel within the base mold.

- Use a P200 pipette to remove PBS from the mold.

- Heat HistoGel in a microwave oven until the gel has liquified.

CRITICAL: Heat HistoGel in short time increments (3-5 seconds at a time) as it can boil over.

- Use a transfer pipette to fill the mold with HistoGel.

- Use a P10 pipette tip to ensure that HIOs are placed at the bottom of the mold.

Note: It is important that HIOs are all settled at the bottom of the mold so that they are in the same plane of section when sectioning and imaging.

- Leave the HIOs in HistoGel on ice for 5-10 minutes until the gel has solidified.

- Remove the HistoGel from the mold.

- Transfer HIOs in HistoGel to a glass jar or 24-well tissue culture plate for subsequent steps.

74. Dehydrate HIOs for 30 minutes in 25%, 50%, 75% Methanol:PBS/0.05% Tween-20, followed by 30 minutes each in 100% Methanol, 100% Ethanol, and 70% Ethanol.

75. Process HIOs into paraffin overnight using an automated tissue processor.

76. Embed processed HIOs into paraffin within a plastic base mold using a paraffin embedding station.

77. Prepare slides with HIOs for immunostaining.

- Section HIO paraffin blocks into 5-7 µm using a microtome.

- Mount sections onto glass slides.

78. Bake slides at 60ºC for 1 hour in a slide oven.

79. Rehydrate slides in a series of HistoClear, 100% Ethanol, 95% Ethanol, 70% Ethanol, 30% Ethanol, DI H_2O with 2 changes of 3 minutes each.

80. Perform antigen retrieval.

- Dilute 10X sodium citrate buffer to 1X using ddH_2O.

- Place slides in a Coplin jar containing 1X sodium citrate buffer.

- Place the Coplin jar in a vegetable steamer for 40 minutes.

81. Wash slides 3 times with 1X PBS for 5 minutes.

CRITICAL: Do not let slides dry out after this point. After washing slides in the Coplin jar, transfer slides to a moisture chamber to prevent drying.

82. Draw a hydrophobic barrier around tissue sections using a Pap pen.

83. Permeabilize slides for 10 minutes in 0.1% TritonX-100 in 1xPBS.

84. Block slides for 45 minutes in 0.1% Tween-20, 5% normal donkey serum in 1XPBS.

85. Dilute primary antibodies in block, and apply primary antibodies to slides overnight at 4ºC.

- To evaluate general HIO morphology, stain with ECAD (epithelial marker) and VIM (mesenchymal marker).

- To evaluate HIO proliferation, stain with KI67.

- To evaluate patterning into proximal small intestine, stain with CDX2 and PDX1.

- To evaluate HIO epithelial differentiation into key intestinal epithelial cell types, stain for MUC2, CHGA, DPP4, and LYZ.

- To evaluate serosal mesothelial formation, stain for WT1 and pan-Cytokeratin.

86. On the next day, wash slides 3 times in 1xPBS.

87. Dilute secondary antibodies in block, then apply secondary antibodies to slides for 40 minutes at room temperature. Keep slides in the dark.

- Add DAPI nuclear stain at a dilution of 1:10,000 in block with secondary antibodies.

88. Wash slides 3 times in 1xPBS.

89. Add a drop of ProLong Gold to each tissue section, then cover with an appropriately sized coverslip.

Note: ProLong Gold should set overnight at room temperature before imaging.

CRITICAL: Store slides at 4ºC in the dark.

90. Image slides on a fluorescent microscope.

- Confirm that staining patterns resemble expected cell types and morphology [9]. See Troubleshooting 6.

A.3.7 FACS-isolation of mesothelial cells from suspension HIOs

Timing: 6 hours

In addition to eliminating limitations of Matrigel and providing a simple, cost-effective culture system that is amenable to scale-up, one of the main advantages of suspension culture is that it promotes the development of an outer serosal mesothelial

layer within HIOs that has not been observed in Matrigel HIOs. Thus, suspension HIOs provide a useful model to study human intestinal serosal mesothelial development. The serosa can be evaluated within the context of intact HIOs to evaluate interactions with underlying cell types, or the HIO-serosa cells can be isolated for studies on mesothelial cells alone. This step describes a protocol to FACS-isolate mesothelial cells from HIOs based on staining for PDPN, ECAD, and EPCAM as we have demonstrated that mesothelial cells are PDPN+/ECAD+/EPCAM-. This sorting strategy additionally allows for isolation of epithelial (PDPN-/ECAD+/EPCAM+) and mesenchymal (PDPN-/ECAD-/EPCAM-) populations.

Note: Suspension HIOs should develop a serosal mesothelium by day 28 in culture.
Note: It is best to dissociate multiple HIOs for FACS isolation of HIO-serosa in order to obtain a high cell number, as the serosa makes up approximately 10% of cells within the HIO.

91. Using a cut P1000 pipette tip, collect suspension HIOs and transfer them to a 6cm Petri dish.

92. Use a P1000 pipette tip to remove any excess ENR Organoid Growth Media from the dish.

93. Add 5-6 mL of TrypLE to the Petri dish with HIOs.

94. Using a scalpel and 1mL syringe with attached 30Gx1 needle, mechanically cut HIOs into small pieces. Typically, one HIO should be cut into halves or quarters, depending on the size.

Note: This step should be completed while working under a stereoscope in a horizontal clean bench.

95. Transfer cut HIOs in TrypLE to a 15 mL conical tube.

- Add 1-2 mL of TrypLE to the dish to wash any remaining HIO pieces, and then transfer to the tube.

96. Place the conical tube into a tissue culture incubator.

97. Every 15 minutes, remove the conical tube from the incubator and pipette up and down using a P1000 pipette tip to help break up tissue pieces.

- Return the tube to the tissue culture incubator.

- Allow the digestion to continue until HIOs are fully dissociated, which typically takes 1.5 – 2 hours.

Note: It is possible for HIOs to become over-digested, resulting in cell lysis and aggregation of intracellular DNA. If large tissue pieces remain after 1.5 hours, the HIOs can be mechanically cut into smaller pieces and more TrypLE can be added. Do not digest HIOs for more than 2.5 hours, even if some small tissue chunks remain.

98. While HIOs are digesting, prepare staining buffer.

- Dissolve bovine serum albumin (BSA) powder in tissue culture 1xPBS.

Note: It is helpful to prepare 50 mL of 10% BSA in PBS for multiple uses. For a 10% BSA solution, dissolve 5g BSA in 50 mL 1xPBS. 10% BSA can be stored at 4ºC for up to 2 months.

- Place the BSA solution in a 37ºC water bath until the BSA is fully dissolved.

- Filter the 10% BSA solution through a Steriflip filter.

- Dilute 10% BSA to 2% with 1xPBS. For a 50 mL solution, add 10 mL of 10% BSA to 40 mL 1xPBS.

- Add a 1:1000 dilution of Y-27632 (10 mM). For a 50 mL solution of staining buffer, add 50µL of Y-27632.

- Add an appropriate volume of Penicillin-Streptomycin to bring the final concentration to 1X. For a 50 mL solution, add 0.5 mL of PenStrep.

99. Once HIOs are fully digested, filter the TrypLE HIO solution through a 70 µm filter. See Troubleshooting 6.

- Wash the conical tube and filter with staining buffer to minimize cell loss.

100. Pellet the cells by centrifuging for 5 minutes at 300 g in a 4ºC centrifuge.

- While cells are spinning down, label FACS tubes for sorting.

- Aspirate supernatant.

CRITICAL: Prepare unstained and single-antibody control tubes which will be used for setting sorting gates. For the sorting strategy utilized here, a tube of unstained cells should be prepared along with a PDPN-APC tube, an ECAD-PE, an EPCAM-FITC tube, a DAPI tube, and a 'sample' tube with all antibodies which will be used for sorting.

- Prepare tubes to collect sorted cells into by adding 1mL of staining buffer to collection tubes.

101. Resuspend the cells in an appropriate volume of staining buffer. For most staining applications, 100-200 µL is sufficient.

Note: While it is important to prepare unstained and single-antibody control tubes, these tubes do not need many cells. It can be helpful to pipette most of the cells into the 'sample' tube for sorting, and use smaller fractions of cells for the control populations.

- Add conjugated antibodies with dilutions and incubation times according to manufacturer's instructions. For the antibodies listed in the Key Resources Table, incubation at 4ºC for 10 minutes is sufficient.

102.   Wash cells with 3 mL of 1xPBS.

- Spin down the cells at 300 g for 5 minutes.

- Aspirate the supernatant, and wash the cells a second time.

- Resuspend cells in 250-500µL staining buffer.

CRITICAL: Keep cells on ice in between washing steps and in between cell sorting steps.

103.   Perform FACS sorting to isolate PDPN+/ECAD+/EPCAM- HIO-serosa cells. See Troubleshooting 7.

- Create a first gate on PDPN+ cells.

- From this PDPN+ population, create a gate around ECAD+/EPCAM- cells.

- To isolate HIO epithelial and mesenchymal populations, create a gate around PDPN- cells.

- To isolate epithelium, create a gate around ECAD+/EPCAM+ cells from the PDPN- population.

- To isolate mesenchyme, create a gate around ECAD-/EPCAM- cells from the PDPN- population.

Note: For downstream analyses, FACS-isolated HIO-serosa can be maintained in culture on Matrigel coated plates and cultured in Mini Gut Basal Media with 0.4 ug/mL Hydrocortisone. However, HIO-serosa cells will differentiate into αSMA+ smooth muscle-like cells when kept in culture on a 2D surface.

A.4 Expected outcomes

The suspension HIOs generated within this protocol provide a useful model to study human intestinal development in a 3D *in vitro* system, including a model to study human intestinal serosal mesothelial development. It is expected that the directed differentiation protocol will produce 3D hindgut spheroids that will detach and float up into the culture media after days 4-6 of hindgut induction, with approximately 50-200 spheroids per well. Typically, the highest number of spheroids will appear at Day 5 (on the day after the 5th media change to F/C hindgut media), with fewer spheroids on Day 4 and Day 6. Cell death is expected during endoderm differentiation, with the highest degree of cell death typically observed after the second day of Activin A induction. Changes in cell morphology are expected throughout hindgut differentiation, leading up to spheroid formation.

Once spheroids have been plated in suspension, it is expected that they will undergo changes in size and morphology to give rise to 'mature' HIOs by day 28 (Figure A-2A). It is expected that approximately 5% of spheroids that are placed into suspension culture will mature into HIOs (Figure A-2B). This low yield is most apparent during the first week in suspension culture, when cell death is common. The resulting suspension HIOs should form an inner epithelium that gives rise to some differentiated intestinal cell types including enterocytes, goblet cells, and enteroendocrine cells, as well as an outer mesenchymal layer. A majority of suspension HIOs (≈60%) should form an outer serosal mesothelial layer that begins forming after day 7 in culture and is complete by day 28 (Figure A-2C). These serosal mesothelial cells can be isolated by FACS for further studies or analysis. If FACS isolating HIO-serosa cells, it is expected

that ≈10% of sorted cells will be mesothelial after sorting for PDPN, ECAD, and EPCAM (Figure A-2D).

A.5 Limitations

Suspension culture creates a defined system with less uncertainty compared with the poorly defined composition and batch-to-batch variability of Matrigel, is significantly cheaper than Matrigel culture, and easily scales up for large experiments. However, the yield of spheroids that develop into HIOs is decreased in suspension compared to Matrigel (48.3% yield in Matrigel compared to 5.3% yield in suspension (Figure 2)). This yield can be increased by culturing HIOs in Matrigel for the first week prior to transitioning to suspension culture. However, this method introduces the high cost and variability associated with Matrigel, and does not seem to promote mesothelial differentiation to the same degree as suspension culture alone. Additionally, changing media in suspension culture is more time consuming and challenging than changing media on Matrigel HIOs, as the media cannot simply be aspirated in suspension to avoid accidental aspiration of the suspension HIOs due to their non-adherent nature.

While suspension HIOs resemble Matrigel and alginate HIOs, HIOs cultured in any matrix *in vitro* remain immature and resemble early-stage human fetal intestine rather than mature intestinal tissue. Thus, they enable studies on early developmental events but are less useful as a model for studies on mature intestine or adult disease. To address this limitation, HIOs can be cultured *in vitro* prior to transplantation *in vivo* into an immunocompromised mouse host. Suspension HIOs have successfully been transplanted into mice, resulting in more mature tissue after 8-10 weeks [3].

Currently, suspension culture is limited to organoids that contain both epithelium and mesenchyme, and does not support long-term culture of epithelial-only enteroids [5]. When transferred into suspension culture, epithelial-only enteroids undergo a polarity reversal such that the apical surface faces out. However, these apical-out enteroids are not suitable for maintenance cultures as they exhibit slower proliferation capacity and increased stem cell differentiation [5, 11].

A.6 Troubleshooting

Problem 1

No spheroids formed during hindgut differentiation.

Potential solution:

The most likely reason for a failed hindgut differentiation, including low yield or failure of spheroids to form, is an inadequate starting density of hPSCs prior to starting endoderm differentiation. Carefully observe hPSCs under a microscope to ensure 70-80% confluence prior to adding Day 1 Activin A media. This may mean checking the cells in the morning and waiting until the afternoon to start differentiation at an appropriate cell density. If attempts are unsuccessful, it may be useful to troubleshoot different passaging ratios from hPSCs within the same 24-well plate to determine the optimal ratio/density for a particular cell line.

The timing between media changes during hindgut differentiation is also a critical factor in determining differentiation success. Day 2 and Day 3 Activin A media, as well as Day 1 of F/C hindgut media, should be added 24 hours after addition of the previous day's media. Be sure to conduct media changes at the same time of day, or at least

within 1-2 hours of the previous day. Once the cells are in F/C hindgut media and are receiving the same media each day, the timing of media changes is no longer critical.

hPSC health and pluripotency are key drivers of differentiation success. If other troubleshooting options have not resulted in success, the protocol should be repeated using a freshly thawed hPSC line at a low passage. The lines H9 and iPSC 72.3 typically work well, and can be used for troubleshooting. Note that it can take a few passages after thawing a new hPSC line before it is able to generate spheroids after recovering from cryopreservation. If new lines are unsuccessful, the hPSC lines should be karyotyped and tested for mycoplasma to ensure normality.

Problem 2

Spheroids/organoids are sticking to the bottom of the low attachment plate.

Potential solution:

The most likely reason that HIOs will stick to the low attachment plate is that the pHEMA surface has been scratched with a pipette tip during passaging, creating an un-coated region where HIOs can adhere. Take care to avoid scratching the plate surface after coating. If the plate is accidentally scratched, HIOs should be transferred to a freshly coated well to avoid sticking and flattening out of the HIOs in 2D. If HIOs are uniformly sticking (not just in one scratched spot), there may be an issue with the pHEMA coating and fresh pHEMA coating solution should be generated.

Problem 3

Spheroids died after transferring into suspension culture.

Potential solution:

It is normal to experience some cell death during the first 3-5 days of suspension culture, which contributes to the low HIO yield in suspension. However, a high degree of cell death or failure of spheroids to grow/survive into the first week is a sign of a problem. A possible cause of spheroid death is inadequately rinsing pHEMA coating solution from the low attachment plates prior to suspension culture, as excess pHEMA can be toxic to the cells. Ensure that plates have been rinsed at least twice with 1xPBS before spheroids are plated. Additionally, ensure that all media has been recently prepared with freshly thawed growth factors.

Problem 4

Spheroids are clumping together.

Potential solution:

Sometimes spheroids may join/clump together in suspension culture. This can be minimized by pipetting up and down to break up spheroid aggregates during the first few days in culture. If clumping continues, try reducing the density of spheroids plated per well.

Problem 5

Suspension HIOs did not resemble typical HIO morphology based on immunofluorescent staining.

Potential solution:

HIOs are inherently somewhat heterogeneous, so expect some variability between organoids and between batches of organoids. It is normal that some HIOs within a batch may look abnormal. However, if a majority of HIOs do not resemble the expected morphology (inner ECAD+ epithelium surrounded by VIM+ mesenchyme is expected for >95% of HIOs, outer WT1+/pCK+ serosal mesothelium is expected for >60% of HIOs, PDX1+/CDX2+ epithelium is expected for >95% of HIOs), this may reflect abnormalities in the initial spheroids or hPSCs.

Problem 6

Dissociated cells from HIOs form a thick, mucous-like aggregate after filtration.

Potential solution:

Cell aggregation during single-cell dissociation can occur when DNA molecules are released from dying cells, causing neighboring cells to clump together. This can be a sign of over-digestion, and the dissociation time in TrypLE should be reduced. Cell clumping can be reduced by including DNAse1 into the digestion solution. If clumping has occurred, cells should be filtered an additional time prior to sorting to avoid clogging the FACS machine (note that this may reduce yield).

Problem 7

FACS isolation did not produce a high number of PDPN+ECAD+EPCAM- HIO-serosa cells.

Potential solution:

As mesothelial cells only make up a fraction of total cells within suspension HIOs, yield can be increased by dissociating a higher volume of HIOs for FACS isolation. Ensure that cells were stained with conjugated antibodies for an appropriate amount of time, and were washed at least twice after staining. Utilize control antibody groups to properly set sorting gates. Additionally, a few HIOs from the batch can be validated using IF (staining for WT1, pCK) prior to sorting to ensure proper mesothelial differentiation.
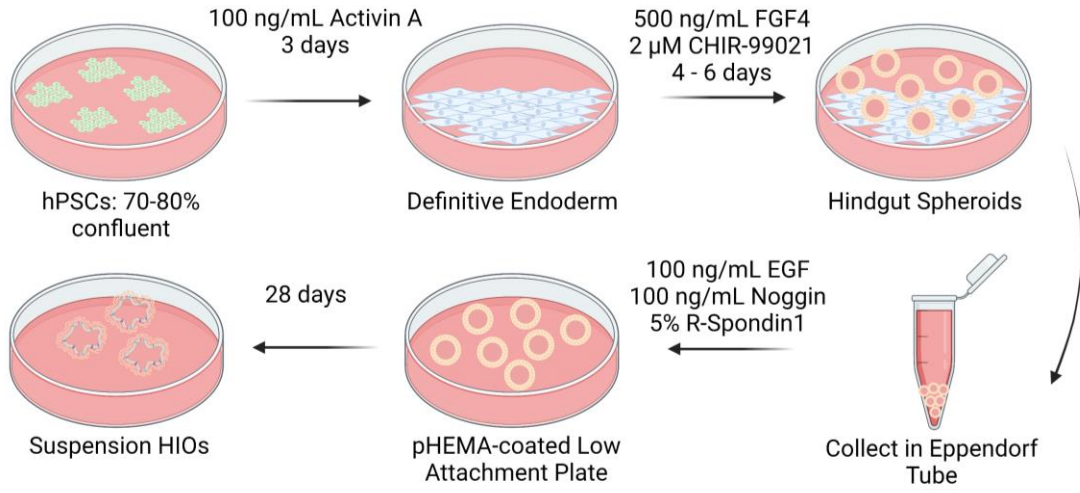
Figure A-1. Directed differentiation of hPSCs into hindgut spheroids for generation of suspension HIOs.

hPSCs are brought through a directed differentiation approach mimicking human intestinal development. First, hPSCs are differentiated into definitive endoderm by a 3-day induction with Activin A. Next, cells are treated with 500 ng/mL FGF4 and 2μM CHIR-99021 for 4-6 days to induce hindgut differentiation. After days 4-6 of hindgut induction, hindgut spheroids will bud off of the monolayer. These spheroids are then collected and transferred into a pHEMA-coated low attachment plate to support their maturation into suspension HIOs over about 4 weeks in culture.
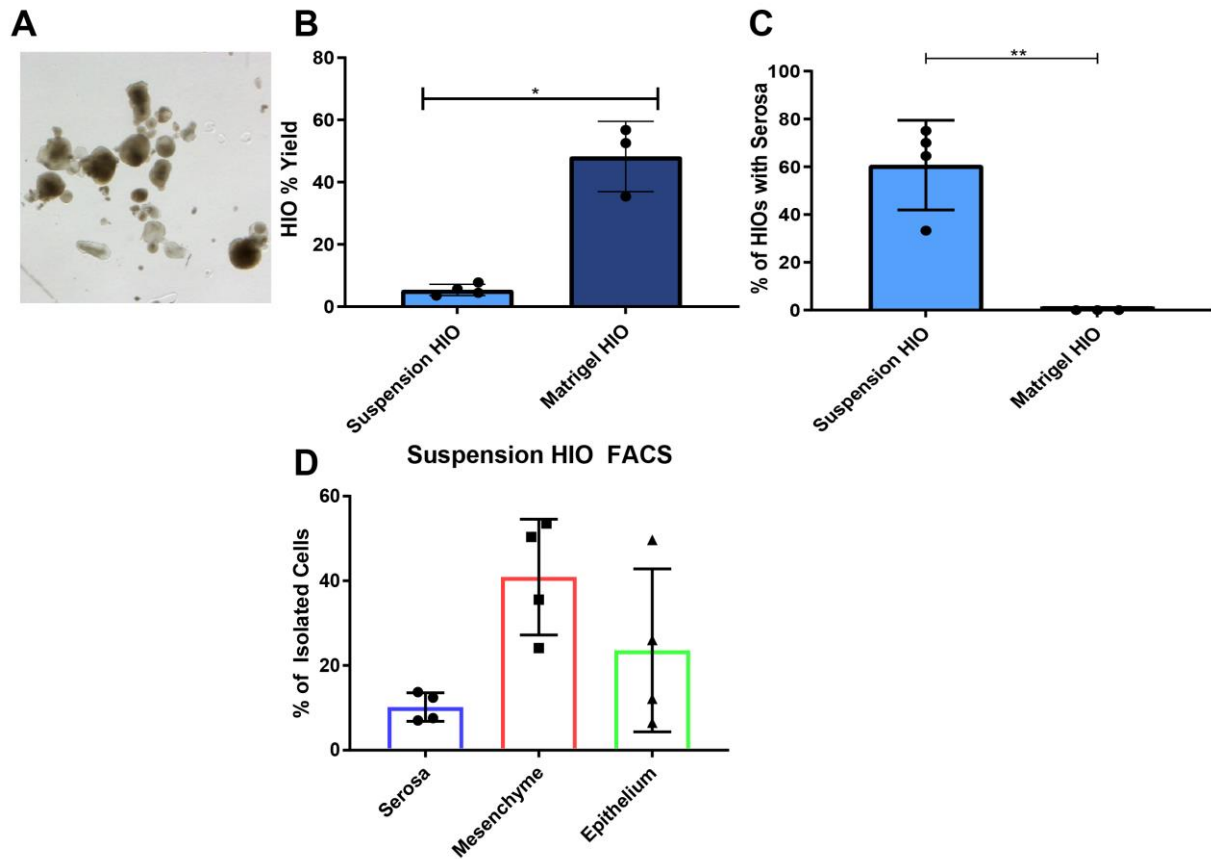
Figure A-2. Anticipated results for suspension HIO culture.

(A): Bright field image depicting suspension HIOs at day 28. (B): Graph depicting the percentage of spheroids that mature into HIOs when cultured in Matrigel or suspension after 28 days. (C): Graph depicting the percentage of HIOs that form a serosal mesothelium in suspension culture or Matrigel after 28 days. Serosa formation was assessed by staining for WT1 and pCK. For all graphs in Figure 2, data represent the mean ± standard error of the mean. Significance was calculated with an unpaired t-test. (D)Calculation of the percentage of FACS-isolated cells from suspension HIOs that were sorted as serosa (PDPN+/ECAD+/EPCAM-), mesenchyme (PDPN-/ECAD-/EPCAM-), or epithelium (PDPN-/ECAD+/EPCAM+)

A.8 Tables

REAGENT or RESOURCE	SOURCE	IDENTIFIER
Antibodies		
Goat polyclonal anti-E-cadherin (1:500)	R&D Systems	Cat#AF748; RRID: AB_355568
Mouse monoclonal anti-E-cadherin (1:500)	BD Transduction Laboratories	Cat#610181; RRID: AB_397580
Goat monoclonal anti-Vimentin (1:500)	R&D Systems	Cat#MAB2105; RRID: AB_2241653
Mouse monoclonal anti-CDX2 (1:300)	BioGenex	Cat#MU392A-UC; RRID: AB_2650531
Rabbit monoclonal anti-PDX1 (1:300)	Cell Signaling Technology	Cat#5679; RRID: AB_10706174
Rabbit polyclonal anti-MUC2 (1:300)	Santa Cruz Biotechnology	Cat# sc-15334; RRID: AB_2146667
Goat polyclonal anti-CHGA (1:300)	Santa Cruz Biotechnology	Cat# sc-1488; RRID: AB_2276319
Rabbit monoclonal anti-KI67 (1:400)	Thermo Scientific	Cat# RM-9106-S1; RRID: AB_149792
Goat polyclonal anti-LYZ (1:300)	Santa Cruz Biotechnology	Cat# sc-27958; RRID: AB_2138790
Rabbit monoclonal anti-WT1 (1:400)	Abcam	Cat# ab89901; RRID: AB_2043201
Mouse monoclonal anti-pan Cytokeratin (1:400)	Abcam	Cat# ab86734; RRID: AB_10674321
Monoclonal anti-ECAD-PE (1:50)	Miltenyi Biotec	Cat# 130-111-992; RRID: AB_2657482
Monoclonal anti-EpCAM-FITC (1:50)	Miltenyi Biotec	Cat# 130-111-115; RRID: AB_2657492
Monoclonal anti-PDPN-APC (1:50)	Miltenyi Biotec	Cat# 130-126-195; RRID: AB_2653263
Chemicals, Peptides, and Recombinant Proteins		
DAPI	ThermoFisher	Cat# D3571
mTeSR Plus Stem Cell Media	STEMCELL Technologies	Cat# 100-0276
DMEM/F12 Cell Culture Media	Thermo Fisher	Cat# 11320033
RPMI 1640 Cell Culture Media	Thermo Fisher	Cat# 11875093
Advanced DMEM/F12 Cell Culture Media	Thermo Fisher	Cat# 12634-010
Growth Factor Reduced Matrigel	Corning	Cat# 354230
Matrigel Basement Membrane	Corning	Cat# 354234
Activin A	R&D	Cat#338-AC
FGF4	Purified in-house	[6]
Commercial FGF4 (Alternative to in-house)	R&D Systems	Cat# 235-F4
CHIR99021	APExBIO	Cat# A3011
Epidermal Growth Factor (EGF)	R&D Systems	Cat# 236-EG
Recombinant Human Noggin-FC, purified from HEK293 cells expressing FC-tagged Noggin	Purified in-house	[12]
Commercial Noggin (Alternative to in-house)	R&D Systems	Cat# 6057-NG
Human R-Spondin1 Conditioned Medium from Cultrex HA-R-Spondin1-Fc 293 T Cells	R&D Systems	Cat# 3710-001-01
Commercial R-Spondin1 (Alternative to in-house)	R&D Systems	Cat# 4645-RS
B27 supplement	Thermo Fisher	Cat#17504044
HEPES	Thermo Fisher	Cat#15630080
GlutaMAX	Gibco	Cat#35050061

Penicillin-Streptomycin	Gibco	Cat# 15070063
Dispase	Life Technologies	Cat#17105-041
Poly (2-hydroxyethyl methacrylate) (pHEMA)	Sigma-Aldrich	Cat#P3932
Ethanol 200-Proof	Fisher Scientific	Cat# 22-032-601
Methanol (Certified ACS)	Fisher Scientific	Cat# A412-4
Histoclear	National Diagnostics	Cat# HS-202
1M NaOH	N/A	N/A
TrypLE Express Enzyme	Gibco	Cat# 12604013
Hydrocortisone	STEMCELL Technologies	Cat#07904
Y27632	Stemgent	Cat#04-0012
Bovine Serum Albumin	Millipore Sigma	Cat# A9647
Tissue Culture-Grade 1xPBS	N/A	N/A
Tween	N/A	N/A
Triton-X	N/A	N/A
Normal Donkey Serum	N/A	N/A
Critical Commercial Assays		
KPL Protein A Agarose Purification Kit	SeraCare	Cat# 553-50-00
Experimental Models: Cell Lines		
H9 ESC	WiCell	NIH registry #0062, RRID: CVCL_9773
UM 63-1 ESC	MStem Cell Laboratories	NIH registry #0277, RRID: CVCL_R782
iPSC 72.3	Cincinnati Children's Hospital	N/A
iPSC WTC11	Coriell Institute	RRID: CVCL_Y803
Other		
Micropipettes and sterile tips	N/A	N/A
Class II Biological Safety Cabinet	N/A	N/A
CO_2 Tissue Culture Incubator	N/A	N/A
Dissecting microscope/stereoscope	N/A	N/A
Labconco horizontal clean bench	N/A	N/A
37ºC Water Bath	N/A	N/A
Conical Tubes (15 mL, 50 mL)	N/A	N/A
1.5 mL Eppendorf tubes	N/A	N/A
6-well tissue culture plate	Corning	Cat# 353046
24-well tissue culture plate	Corning	Cat# 353047
Cell Scraper	N/A	N/A
Scalpel	N/A	N/A
6 cm Petri dish	N/A	N/A
1 mL Syringe	N/A	N/A
30G × 1 Needle	N/A	N/A
FACS Cell Sorter	N/A	N/A
Steriflip Filter Unit	Sigma Aldrich	Cat# SCGP00525
70µm filter	N/A	N/A
5mL FACS tubes	N/A	N/A
Paraformaldehyde	N/A	N/A
Disposable base mold	Thermo Fisher	Cat# 22-363-552
Disposable base mold	Thermo Fisher	Cat# 22-363-553
Histogel	VWR	Cat# 83009-992
Transfer pipette	N/A	N/A

Automated Tissue Processor	Leica	Cat# ASP300
Microtome	N/A	N/A
Glass slides	N/A	N/A
Microtome blades	Thermo Fisher	Cat# 3052835
Embedding Station	N/A	N/A
Slide Oven	N/A	N/A
Coplin Jar	N/A	N/A
Vegetable Steamer	N/A	N/A
Moisture Chamber	N/A	N/A
ImmEdge Hydrophobic Barrier PAP Pen	Thermo Fisher	Cat# H-4000
ProLong Gold	Fisher Scientific	Cat# P36930
Glass Coverslips	N/A	N/A

Table A-1. Key Resources Table: Appendix A.

List of key resources described in the Methods of Appendix A.

Day 1 Base Media: can be stored for 2-4 weeks at 4ºC.

Reagent	Final concentration	Amount
RPMI Medium 1640 (1X)	1X	495 mL
Penicillin-Streptomycin (10,000 U/mL)	100 U/mL penicillin; 100 µg/mL streptomycin	5 mL
Total	**1X**	**500 mL**

Day 2 Base Media: can be stored for 2-4 weeks at 4ºC.

Reagent	Final concentration	Amount
RPMI Medium 1640 (1X)	1X	494 mL
Penicillin-Streptomycin (10,000 U/mL)	100 U/mL penicillin; 100 µg/mL streptomycin	5 mL
Hyclone defined FBS	0.2%	1 mL
Total	**1X**	**500 mL**

Day 3 Base Media: can be stored for 2-4 weeks at 4ºC.

Reagent	Final concentration	Amount
RPMI Medium 1640 (1X)	1X	485 mL
Penicillin-Streptomycin (10,000 U/mL)	100 U/mL penicillin; 100 µg/mL streptomycin	5 mL
Hyclone defined FBS	2%	10 mL
Total	**1X**	**500 mL**

Mini Gut Base Media: can be stored for 2-4 weeks at 4ºC.

Reagent	Final concentration	Amount
Advanced DMEM/F12 medium (1X)	1X	472.2 mL
Penicillin-Streptomycin (10,000 U/mL)	100 U/mL penicillin; 100 µg/mL streptomycin	5 mL
GlutaMax (100x)	1X	5 mL
HEPES Buffer (1M)	15 mM	7.8 mL
B-27 Supplement (50x)	1X	10 mL
Total	**1X**	**500 mL**

ENR Organoid Growth Media: can be at 4ºC and should be used within 2 weeks.

Reagent	Final concentration	Amount
Mini Gut Base Media	1X	95 mL
EGF (100 µg/mL)	100 ng/mL	100 µL
Noggin (100 µg/mL)	100 ng/mL	100 µL
R-Spondin1 Conditioned Media	5%	5 mL
Total	**1X**	**100 mL**

pHEMA Coating Solution: can be stored at room temperature and will last for up to one year.

Reagent	Final concentration	Amount
Ethanol (200 proof)	95%	38 mL
Tissue culture-grade H_2O	4%	1.6 mL
Sodium Hydroxide (NaOH, 1 M)	10 mM	400 µL
poly (2-hydroxyethyl methacrylate) (pHEMA)	10% (wt/vol)	4 g
Total	**1X**	**40 mL**

10X Sodium Citrate Buffer: can be stored at room temperature for 3 months or at 4ºC for longer storage.

Reagent	Final concentration	Amount
Distilled H_2O	10X	995 mL
Tri-sodium citrate (dihydrate)	100 mM	29.49g
1N HCl	pH = 6.0	Varies, adjust based on pH
Tween-20	0.5%	5 mL
Total	10X	1000 mL

Permeabilization Buffer: can be stored at room temperature and will last for up to one month.

Reagent	Final concentration	Amount
1xPBS	1X	10 mL
Triton-X	0.1%	10 µL
Total	**1X**	**10 mL**

Blocking Buffer: can be stored at 4ºC and will last for up to two weeks.

Reagent	Final concentration	Amount
1xPBS	1X	9.5 mL
Normal Donkey Serum	5%	500 µL
Tween-20	0.1%	10 µL
Total	**1X**	**10 mL**

Staining Buffer: can be stored at 4ºC and will last for up to two weeks.

Reagent	Final concentration	Amount
Tissue Culture-Grade 1xPBS	1X	40 mL
10% BSA	2%	10 mL
Y-27632	10 mM	50 µL
Total	**1X**	**10 mL**

Table A-2: Materials and Equipment.

Reagents and amounts utilized for solutions described in Appendix A.

A.9 References

1. McCracken, K., et al., *Generating human intestinal tissue from pluripotent stem cells in vitro.* Nature Protocols, 2011. **6**(12): p. 1920-1928.

2. Spence, J.R., et al., *Directed differentiation of human pluripotent stem cells into intestinal tissue in vitro.* Nature, 2011. **470**(7332): p. 105-109.

3. Capeling, M.M., et al., *Suspension culture promotes serosal mesothelial development in human intestinal organoids.* Cell Reports, 2022. **38**(7): p. 110379.

4. Capeling, M., et al., *Generation of small intestinal organoids for experimental intestinal physiology.* Methods Cell Biol., 2020. **159**: p. 143-174.

5. Co, J.Y., et al., *Controlling the polarity of human gastrointestinal organoids to investigate epithelial biology and infectious diseases.* Nature Protocols, 2021. **16**: p. 5171–5192.

6. Sugawara, S., et al., *Production of an aminoterminally truncated, stable type of bioactive mouse fibroblast growth factor 4 in Escherichia coli.* Journal of Bioscience and Bioengineering, 2014. **117**(5): p. 525-530.

7. Heijmans, J., et al., *ER stress causes rapid loss of intestinal epithelial stemness through activation of the unfolded protein response.* Cell Reports, 2013. **3**: p. 1128-1139.

8. Choi, K., M. Vodyanik, and I. Slukvin, *Hematopoietic differentiation and production of mature myeloid cells from human pluripotent stem cells.* Nature Protocols, 2011. **6**: p. 296–313.

9. Capeling, M., et al., *Nonadhesive Alginate Hydrogels Support Growth of Pluripotent Stem Cell-Derived Intestinal Organoids.* Stem Cell Reports, 2019. **12**(2): p. 381–394.

10. Tsai, Y.-H., et al., *LGR4 and LGR5 Function Redundantly During Human Endoderm Differentiation.* Cel Mol Gastroenterol Hepatol., 2016. **2**(5): p. 648-662.

11. Co, J.Y., et al., *Controlling Epithelial Polarity: A Human Enteroid Model for Host-Pathogen Interactions.* Cell Reports, 2019. **26**: p. 2509–2520.

12. Heijmans, J., et al., *ER stress causes rapid loss of intestinal epithelial stemness through activation of the unfolded protein response.* Cell Rep, 2013. **3**(4): p. 1128-1139.